A STUDY ON THE PREPARATION OF IONICALLY CONDUCTIVE THIN FILMS UTILIZING LOW TEMPERATURE PLASMA PROCESSES(Dissertation_全文)

AUTHOR(S):

Uchimoto, Yoshiharu

(2)

A STUDY ON THE PREPARATION OF IONICALLY CONDUCTIVE THIN FILMS UTILIZING LOW TEMPERATURE PLASMA PROCESSES

1990

YOSHIHARU UCHIMOTO

PREFACE

The present study has been carried out under the direction of Professor Zen-ichiro Takehara at the Department of Industrial Chemistry, Faculty of Engineering, Kyoto University.

The object of this study is to investigate the preparation of thin film of solid electrolyte by using a low temperature plasma process and to examine the electrochemical applications of these thin films.

The author is greatly indebted to Professor Zen-ichiro Takehara for his valuable suggestions and supervision throughout the work.

The author also would like to express his thanks to Professor Mitsunojo Ichise and Associate Professor Zempachi Ogumi for their helpful advice and discussions.

The author also is grateful to Professor Frank R. Foulkes (Department of Chemical Engineering and Applied Chemistry, University of Toronto) and Dr. Kiyoshi Kanamura for their support and encouragement. Many thanks also are due to all the members of the industrial electrochemistry laboratory for their kind encouragement and constant interest during the course of this work.

Yoshiharu Uchimoto

Yoshiharu Uchimoto

Department of Industrial Chemistry,
Faculty of Engineering,
Kyoto University
Yoshida, Sakyo-ku, Kyoto 606
JAPAN

Contents

Introduction and General Summary

Solid electrolytes, such as solid polymer electrolytes based on alkali metal salt complexes of polyethers [poly(ethylene oxide) (PEO) and poly(propylene oxide) (PPO)], ion exchange membranes, as well as yttria-stabilized zirconia (YSZ) recently have received considerable attention as potential materials for use in electrochemical applications on account of their relatively high ionic conductivities.

Since the original work of Wright [1,2] and Armand et al. [3], the ion transport properties of solid polymer electrolytes have been the focus of many studies [4-9]. Most reports of high ionic conductivity in polymers have been concerned with PEO or PPO-alkali metal salt complexes. A stoichiometric ratio of 1 mol cation to 4 mol of ethylene oxide or propylene oxide repeat unit is required for the dissociation and migration of alkali metal cation in the ionic polymer complex [1]. In early studies of solid polymer electrolytes, the fast ion transport was attributed to a intrahelical jumping process in the crystalline region of the polymer matrix [3]. However, several workers have reported that ionic transport occurs mostly in the amorphous regions of solid polymer electrolytes [10-14]. The amorphous conductivity mechanism is shown schematically in Fig. 1. The conductivity in these amorphous polymeric materials, which are generally studied above their glass transition temperatures (Tg), does not follow an Arrhenius-type equation. Instead, the Williams-Landel-Ferry (WLF) equation based on the free volume theory [15-18] is applicable;

$$\log \frac{\sigma(T)}{\sigma(Tg)} = \frac{C_1(T-Tg)}{C_2 + (T-Tg)}$$

where $\sigma(T)$ represents conductivity at temperature T, $\sigma(Tg)$ represents the conductivity at Tg, and C_1 and C_2 are con-

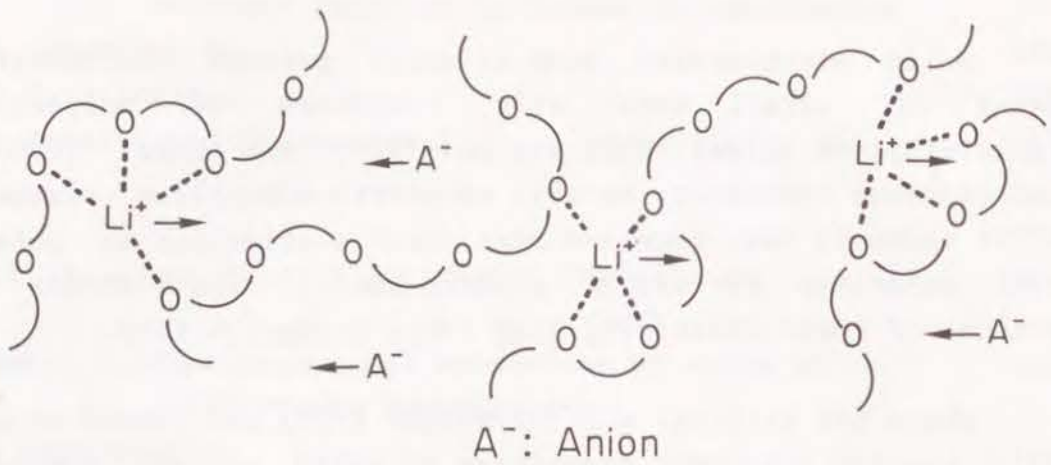

Fig. 1 Lithium ion transport within the amorphous region of PEO.

stants. The above work revealed that a high concentration of highly polar groups in the polymers which have a low Tg leads to the high ionic conductivity of these polymers.

Recently the use of thin films of solid polymer electrolytes in high-energy-density electrochemical batteries including solid-state lithium batteries has been demonstrated [19-24]. The ionic conductivities of these solid polymer electrolytes are considerably lower than those of liquid electrolytes [25] (Table 1), typical values at room temperature being in the order of 10^{-8}-10^{-6} S cm^{-1} [26]. Consequently, batteries using solid polymer electrolytes have a large internal resistance, and thus their performance at room temperature is poor. The internal resistance of the batteries must be lowered in order to improve their performance. One promising way of lowering the resistance of solid-state lithium batteries is to decrease the thickness of the polymer electrolyte.

Yttria-stabilized zirconia (YSZ) is an oxide ion conductor which has recently received a great deal of attention on account of its application to solid oxide fuel cells [27-31].

Table 1 Ionic conductivity of solid polymer electrolyte [26].

Polymer	M^+	X^-	O/M	$T_{\sigma=10^{-5}}$ (°C)	$T_{\sigma=10^{-4}}$ (°C)
PEO	Li^+	I^-	8	35	55
"	"	ClO_4^-	4.5	70	110
"	"	ClO_4^-	8	31	50
"	"	$CF_3SO_3^-$	4.5	75	120
"	"	"	8	70	100
"	"	"	14	65	85
"	Na^+	I^-	10	45	50
"	K^+	$CF_3SO_3^-$	4.5	40	70
PPO	Li^+	I^-	8	65	85
"	Li^+	$CF_3SO_3^-$	9	55	95
"	Na^+	$CF_3SO_3^-$	12	45	95

(σ in $(\Omega cm)^{-1}$)

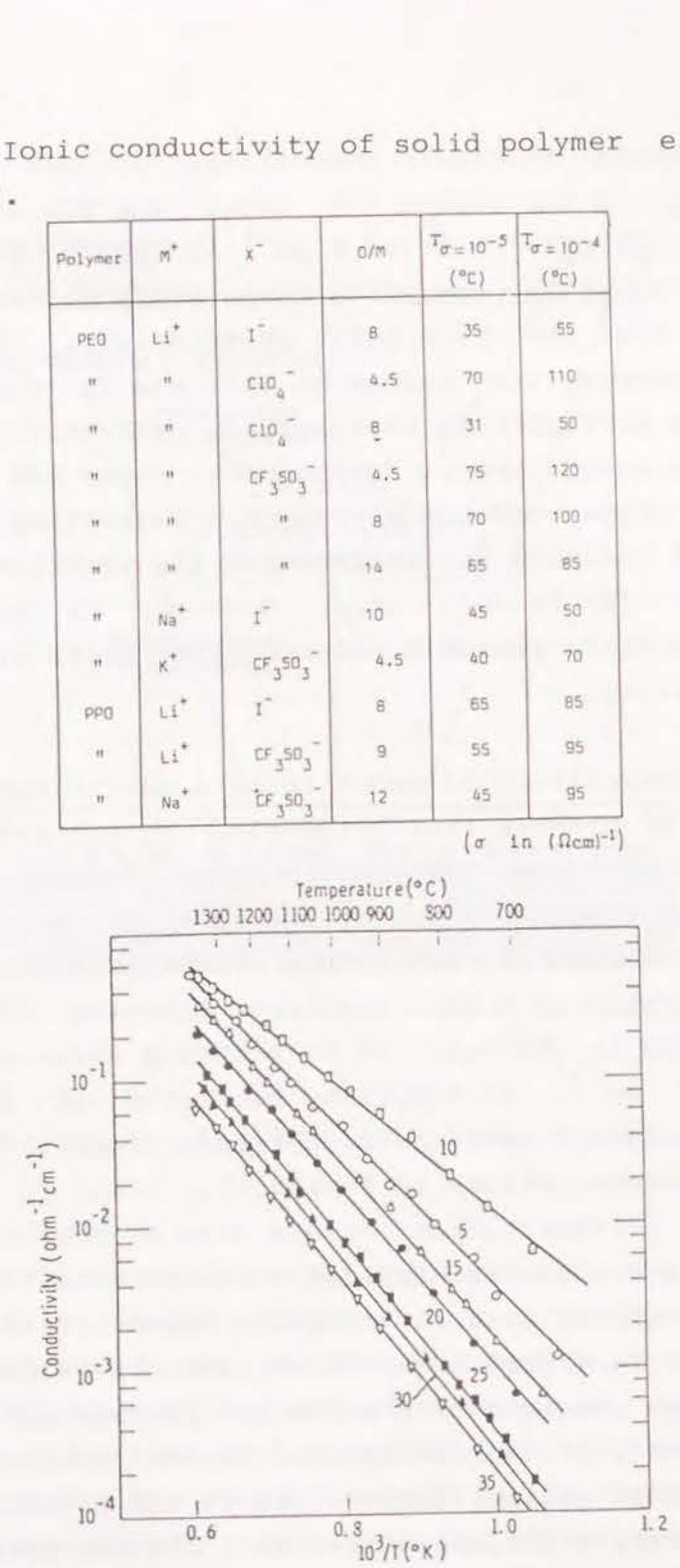

Fig. 2 Conductivity vs. reciprocal temperature for various composition in the system Y_2O_3-ZrO_2. Numbers near the curves denote mole percent Y_2O_3 [32].

Figure 2 shows the ionic conductivity of YSZ for various compositions in the system Y_2O_3-ZrO_2. The ionic conductivities are typically 10^{-2}-10^{0} S cm^{-1} at 1000 °C [32]. It is required to lower the operating temperature of the solid oxide fuel cells from the stand point of materials. Lowering the operating temperature causes an increase in resistivity of YSZ. It is difficult to increase the conductivity of YSZ by changing its composition. Furthermore, there are no practical alternative oxide conductors to date. Decreasing the YSZ film thickness is the only way to decrease its practical operating resistance. It is not easy, however, to produce thin pinhole-free films of solid polymer electrolyte or YSZ with a high reliability.

Plasma deposition is known to be a useful method for the preparation of pinhole-free ultra-thin organic and/or inorganic films [33-40]. Low temperature plasma is unique in that it can generate chemically reactive species at low temperature, due to the nonequilibrium nature of the plasma state. The plasma generated by a glow discharge possesses average electron energies in the range of 1-10 eV and electron densities of 10^{9}-10^{12} cm^{-3}. In addition, the ratio of the electron temperature (Te) to the gas temperature (Tgas) [Te/Tgas] is large, and reaches values of 10-100.

Plasma polymerization occurs when an organic vapor is injected into a glow discharge of a plasma assist gas or when plasma is generated in a pure organic vapor. This technology is known to be a useful method for the preparation of thin polymer films. Because of the low gas temperature in nonequilibrium plasma, it is possible for plasma polymerization to proceed at near ambient temperature in the presence of electrons which excite the gas molecules. The mechanism of plasma polymerization is different from that of conventional polymerization. In conventional polymerization (molecular polymerization), molecular units are linked together in the polymerization process. In contrast, plasma polymerization is characterized as an atomic polymerization. In this atomic polymerization, the starting monomer molecules are decomposed to form source elements which are used in the construction of large molecules. The overall mechanism of the plasma polymerization (competitive ablation and polymerization (CAP) mechanism) is shown in Fig. 3. The general polymerization in a glow discharge consists of both plasma-induced polymerization (molecular polymerization) and plasma-state polymerization (atomic polymerization) [41-43]. Furthermore, etching (ablation) by chemical reactions of highly energetic species also can occur in the process.

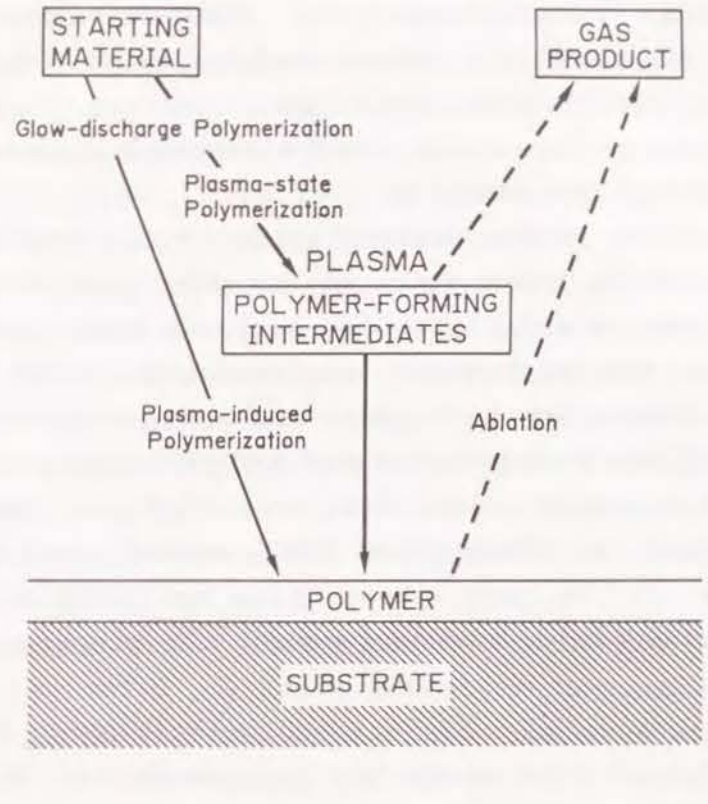

Fig. 3 Overall mechanism of plasma polymerization proposed by Yasuda and Hsu [43].

Plasma is a conductive fluid, whose charge carriers consists not only of ionic species, but also of electrons. Under certain conditions, the conductivities of low temperature plasma attain values as high as 10^{-3} S cm^{-1} [44]. Accordingly, low temperature plasmas also are candidates as conductive fluids for use in electrochemical systems, such as vapor-phase electrodeposition.

The purpose of the present study is to investigate the preparation by low temperature plasma processes of thin films of solid polymer electrolyte, ion-exchange membrane, and YSZ, for use in electrochemical applications such as lithium batteries, redox-flow batteries, and solid oxide fuel cells. The solid polymer electrolytes and ion-exchange membranes were prepared by a plasma polymerization method. A novel Vapor-Phase Electrolytic Deposition (VED) method, which involves electrolysis in the vapor-phase using low temperature plasma as a conductive fluid, was devised for the preparation of YSZ thin layers.

In Part I of this study, the preparation of thin films of solid polymer electrolyte by plasma polymerization was investigated.

In Chapter 1, the synthesis of ultra-thin polymeric layers as a host polymer, starting from octamethylcyclotetrasiloxane (OMCTS) is discussed. The polymer from OMCTS is expected to have a low glass transition temperature (Tg) and it is well known that any means of lowering the Tg favors the enhancement of the ionic conductivity of a solid polymer electrolyte [14]. The plasma polymer from OMCTS was complexed with PPO and lithium perchlorate to prepare the electrolyte film. The films formed by plasma polymerization were uniform and pinhole free. The resulting solid polymer electrolytes were about 1 μm thick and showed high ionic conductivity of the order of 10^{-6} S cm^{-1} (10 Ω cm^2: resistance per unit area of solid polymer electrolyte) at 60 °C. The conductivity depended on the content of lithium perchlorate, and its temperature dependence corresponded with the WLF equation rather than the Arrhenius equation.

In chapter 2 and 3, the preparation of thin films of solid polymer electrolyte without any plasticizer is discussed. Tris(2-methoxyethoxy)vinylsilane (TMVS) was selected as the monomer because this substance contains both the ether and siloxane group. The results of FT-IR, ^{1}H NMR, and ^{13}C NMR measurements indicated that the structure of the plasma polymer was very similar to poly(TMVS), except for the presence of a small amount of what is probably a cyclic group impurity. The glass transition temperature and ionic conductivity of the solid polymer electrolyte depended on the lithium perchlorate content, and the variation of the ionic conductivity with temperature can be describe exactly by a WLF equation. Room temperature conductivities reached value greater than 10^{-6} S cm^{-1}.

The effects of the plasma parameters on the ionic conductivity of the solid polymer electrolyte composed of plasma-polymerized TMVS-lithium perchlorate complexes are discussed in Chapter 3. FT-IR studies indicated the presence of Si-O-Si cross-linking, resulting from the decomposition of monomer, and from the ablation of deposited plasma polymer under high W/FM conditions where W is the input RF power, F is the monomer flow rate, and M is the molecular weight of the monomer. The ionic conductivity of the solid polymer electrolyte was strongly dependent on W/FM. It was found that the higher the values of W/FM, the more the Si-O-Si cross-linking reaction proceeds, leading to a concomitant decrease in the ionic conductivity of the resulting solid polymer electrolyte film.

In the solid polymer electrolyte described in Chapter 1-3, both the cation and anion are mobile. When these kinds of solid polymer electrolytes are used in electrochemical devices, the ionic conductivity measured using direct current (DC) decreases because of high polarization inside the electrolyte film, caused by the non-uniform distribution of anions and cations [45]. Therefore, thin films of solid polymer

electrolyte which had fixed sulfonic acid groups, and which were conductive only for cations were prepared. The preparation of these thin, cationically-conductive solid polymer electrolyte films is discussed in Chapter 4. Methyl benzenesulfonate was selected as the source to introduce the sulfonic acid groups. The sulfonic ester groups of the plasma polymer were transformed to lithium sulfonate groups by treatment with lithium iodide. OMCTS was selected as a monomer for the host polymer. The prepared polymer films required the addition of plasticizer to give mobility to the cations. Hybridization of this plasma polymer containing the lithium sulfonate groups with PEO resulted in the formation of a single lithium ion conductive film. The hybrid polymer electrolyte films were about 1 μm thick, pinhole-free, adherent to various substrates and showed ionic conductivities at 60 °C of the order of 10^{-6} S cm^{-1}.

In Chapter 5, the preparation of cation mobile solid polymer electrolytes, which were composed of thin films of solid polymer electrolyte having fixed carboxylic acid groups without any plasticizer is discussed. Methyl acrylate was selected as the source to introduce the carboxylic ester groups. TMVS was selected as a monomer for the host polymer. These two monomers were copolymerized in an RF glow discharge. The carboxylic ester groups introduced into the plasma polymer were transformed to lithium carboxylate groups by treatment with lithium iodide. This process gave a single lithium ion conductive film. These solid polymer electrolyte films showed ionic conductivities of the order of 10^{-8} S cm^{-1} (10^4 Ωcm^2 resistance per unit area) at room temperature. The room temperature conductivity was relatively low in comparison with the ionic conductivity values of plasma-polymerized TMVS-lithium perchlorate complex, 10^{-6} S cm^{-1}. This may be ascribed to the weak acidity of carboxylic acid and to the absence of any contribution from anion species.

In Part II, the preparation of thin film solid-state lithium batteries is discussed. The preparation of rechargeable thin film solid-state lithium batteries using the solid polymer electrolyte film prepared by plasma polymerization is discussed in Chapter 1. Since titanium disulfide is known as a desirable cathode active material for rechargeable lithium batteries [46,47], this compound was chosen as a cathode active material. A thin film of TiS_2 (10-15 μm) prepared by chemical vapor deposition (CVD) was used as the cathode. An ultra-thin film of solid polymer electrolyte (2-3 μm) prepared by hybridization of plasma polymer formed from octamethylcyclotetrasiloxane (OMCTS), PPO, and lithium perchlorate, as described in Chapter 1 of Part I, was used as the electrolyte film. The charge/discharge properties of the batteries at room temperature, and current densities of 8-40 μA cm^{-2}, were examined. The first discharge and charge reached the 90% level.

In Chapter 2, a solid polymer electrolyte film was formed by complexation of plasma-polymerized TMVS with lithium perchlorate as described in Chapter 2 of Part I. Using this electrolyte film, batteries were prepared by consecutive vapor phase processes. The battery's discharge properties at room temperature and different current densities were examined. At a low current density of 10 μA cm^{-2}, the battery showed a good performance.

In Part III the preparation of anion- and cation-exchange thin membrane by plasma polymerization is discussed. The goals of this work were to modify the cation exchange membranes to enhance their perm-selectivity, and also to prepare very thin ion exchange membranes.

In Chapter 1, the enhancement of monovalent cation perm-selectivity is discussed. Anion-exchange thin layers were prepared from 4-vinylpyridine monomer. The resulting plasma polymer layers were found to be pinhole-free and of uniform thickness (~ 0.2 μm). The thin plasma polymer layer of an

anion exchanger was deposited on the surface of the cation-exchange membrane, Nafion 117. Since the repulsion of monovalent cation by the fixed cations in the plasma polymer on the surface is weaker than that of multivalent ions, monovalent ion can be transported through the plasma polymer layer much more easily than can multivalent ions. The influence of the plasma parameters such as monomer flow rate and applied power on the plasma polymer deposition rate was investigated. The IR spectra of the plasma polymers showed the preservation of pyridine rings in the polymers. The lower the applied RF power, the greater the retention of pyridine rings was. In order to the determine the proton perm-selectivity of plasma-modified Nafion membrane, the transference number of Fe^{2+} through the membrane, t_{Fe}, was measured by using a typical two-compartment cell ($FeCl_2$-HCl/membrane/HCl) equipped with the membrane as a separator. Pretreatment of the Nafion membrane by oxygen sputtering increased its proton perm-selectivity and enhanced the adhesion of plasma polymer onto the cation exchange membrane surface. Plasma-modified Nafion membranes exhibited very high proton perm-selectivities, but at the cost of high membrane resistances. For example, membranes having t_{Fe} values of 0.00034 and 0.12 had corresponding resistances of 40 and 4.1 $\Omega\ cm^2$, respectively.

In Chapter 2, the preparation of thin fluorinated cation exchange membrane from trifluoromethanesulfonic acid and trifluorochloroethylene by plasma polymerization is described. Trifluorochloroethylene was selected as a starting material for backbone polymer. Trifluoromethanesulfonic acid and sulfur trioxide were selected as the sources of sulfonic acid groups (the fixed anion). Prepared solid polymer membranes were about 1 μm thick and exhibited ion exchange capacities. The membranes were uniform and pinhole-free in the scale of SEM observation. The film containing excess of water exhibited fairly good ionic conductivity of 5.0×10^{-5} S cm^{-1} (2.0 $\Omega\ cm^2$) at room temperature.

In Part IV, electrolysis in the vapor phase using low temperature plasma as a conductive fluid, and its application to the preparation of YSZ thin films, are discussed.

In Chapter 1, confirmation of the occurrence of the Vapor-Phase Electrolytic Deposition (VED) process, using the deposition of YSZ from $ZrCl_4$, YCl_3, and H_2O vapors on a non-porous calcia stabilized zirconia (CSZ) substrates as an example, is discussed. An RF power (13.56 MHz) of 100 W was applied to generate low temperature plasma. DC bias of 130 V was applied and the electrochemical process was impelled in the vapor-phase.

In Chapter 2, the deposition thin YSZ films on a porous CSZ substrate by VED is described. The same system as that described in Chapter 1 was used, except that a chemical vapor deposition (CVD) process was used before carrying out the VED process in order to plug up the pores of the substrate, and to cover the porous platinum electrode on the substrate with a YSZ thin layer. The deposition rate obtained with the VED process was 7 $\mu m\ h^{-1}$, which is about 4 times faster than that obtainable with a CVD-Electrochemical Vapor Deposition (EVD) process under the similar conditions. The YSZ thin film prepared by the VED process was pinhole-free and its ionic conductivity was nearly equal to that of sintered YSZ.

References

1. D. E. Fenton, J. M. Parker, and P. V. Wright, Polymer, 14, 589 (1973).
2. P. V. Wright, Br. Polym. J., 319, 137 (1975).
3. M. B. Armand, J. M. Chabagno, and M. J. Duclot, Fast Ion Transport in Solids edited by P. Vashista, J. N. Mundy, G. K. Shenoy, Elsevier, N. Y., 1979, p 131.
4. M. Watanabe, M. Kanba, H. Matsuda, K. Tsunemi, K. Mizoguchi, E. Tsuchida, and I. Shinohara, Macromol. Chem. Rapid Commun., 2, 741 (1981).
5. M. Watanabe, R. Lkekawa, K. Sanui, and N, Ogata, Macromolecules, 20, 968 (1987).
6. M. Watanabe, K. Sanui, N. Ogata, T. Kobayashi, and Z. Ohtaki, J. Appl. Phys., 57, 123 (1985).
7. K. M. Abraham and M. Alamgir, J. Electrochem. Soc., 137, 1657 (1990).
8. P. G. Bruce, J. Nowinski, F. M. Gray, and C. A. Vincent, Solid State Ionics, 38, 231 (1990).
9. A. Magistris, G. Chiodelli, K. Singh, and P. Ferloni, Solid State Ionics, 38, 235 (1990).
10. C. C. Lee and P. V. Wright, Polymer, 23, 681 (1982).
11. D. R. Payne and P. V. Wright, Polymer, 23, 690 (1982).
12. J. E. Weston and B. C. H. Steel, Solid State Ionics, 7, 75 (1982).
13. R. Dupon, B. L. Papke, M. A. Ratner, D. H. Whitmore, and D. F. Shriver, J. Am. Chem. Soc., 104, 6247 (1982).
14. M. Watanabe, M. Rikukawa, K. Sanui, N. Ogata, H. Kato, T. Kobayashi, and Z. Ohtaki, Macromolecules, 17, 2902 (1984).
15. M. L. Williams, R. F. Landel, and J. D. Ferry, J. Am. Chem. Soc., 77, 3701 (1955).
16. M. Cohen and D. Turnbull, J. Chem. Phys., 31, 1164 (1959).
17. M. Watanabe, A. Suzuki, T. Santo, K. Sanui, and N. Ogata, Macromolecules, 19, 1921 (1986).
18. J. J. Fontanella, M. C. Wintersgill, M. K. Smith, J. Semacik, and C. G. Andeen, J. Appl. Phys., 60, 2665

(1986).
19. T. A. Skotheim and O. Inganas, J. Electrochem. Soc., 132, 2116 (1985).
20. A. Hooper and J. M. North, Solid State Ionics, 9&10, 1161 (1983).
21. K. M. Abraham, M. Alamgir, and S. J. Perrotti, J. Electrochem. Soc., 135, 535 (1988).
22. M. Gauthier, D. Fauteux, G. Vassort, A. Belanger, M. Duval, P. Ricoux, J. M. Chabagno, D. Muller, P. Rigaud, M. B. Armand, and D. Deroo, J. Electrochem. Soc., 132, 1333 (1985).
23. M. Z. A. Munshi and B. B. Owens, Solid State Ionics, 38, 87 (1990).
24. M. Z. A. Munshi and B. B. Owens, Solid State Ionics, 38, 95 (1990).
25. Y. Matsuda, J. Power Sources, 20, 119 (1987).
26. M. Armand, Solid State Ionics, 9&10, 745 (1985).
27. N. J. Maskalick and C. C. Sun, J. Electrochem. Soc., 118, 1386 (1971).
28. A. O. Isenberg, Solid State Ionics, 3/4, 431 (1981).
29. W. Feduska and A. O. Isenberg, J. Power Sources, 10, 89 (1983).
30. N. J. Maskalick and D. K. McLain, J. Electrochem. Soc., 135, 6 (1988).
31. T. Inoue, T. Setoguchi, K. Eguchi, and H. Arai, Solid State Ionics, 35, 285 (1989).
32. D. W. Strickler and W. G. Carlson, J. Am. Ceram. Soc., 47, 122 (1964).
33. "Glow Discherge Process", B. Chapman, John Wiley & Sons, N. Y. (1980).
34. "Thin Film Processes", edited by J. L. Vossen and W. Kern, Academic Press, Inc., London (1978).
35. "Plasma Polymerization", M. Shen and A. T. Bell, ACS Symposium Series, Washington, D. C. (1979).
36. H. Yasuda, J. Polym. Sci., Macromol. Rev., 16, 199 (1981).
37. H. Yasuda and C. R. Wang, J. Polym. Sci., Polym. Chem.

Ed., 23, 87 (1985).
38. N. Nakagawa, H. Yoshioka, C. Kuroda, and M. Ishida, Solid State Ionics, 35, 249 (1989).
39. H. Kobayashi, M. Shen, and A. T. Bell, J. Macromol. Sci. Chem., A8, 373 (1974).
40. M. Shiloh, B. Gayer, and F. E. Brinckman, J. Electrochem. Soc., 124, 295 (1977).
41. H. Yasuda, J. Macromol. Sci., Chem., A10, 383 (1976).
42. H. U. Poll, M. Arzt, and K. H. Wickleder, Eur. Polym. J., 12, 505 (1976).
43. H. Yasuda and T. Hsu, Surf. Sci., 76, 232 (1978).
44. "Electric Plasmas: Their Natures and Uses", A. von Engel, Taylor & Francis, Ltd. London (1983).
45. N. Kabayashi, M. Uchiyama, and E. Tsuchida, Solid State Ionics, 17, 307 (1985).
46. J. R. Akridge, and H. Vourlis, Solid State Ionics, 28-30, 841 (1988).
47. K. Kanehori, K. Matsumoto, K. Miyauchi, and T. Kudo, Solid State Ionics, 9&10, 1445 (1983).

Part I. Thin Solid Polymer Electrolyte Films

Chapter 1. Hybrid Film of Plasma Polymer Formed from Octamethylcyclotetrasiloxane, Poly(propylene oxide) and Lithium Perchlorate.

1.1 Introduction

Extensive studies have recently been done on the ionic conductivity of polymer complexes formed by alkali metal salts and polyethers such as poly (ethylene oxide) (PEO) and poly-(propylene oxide) (PPO) [1-4]. Certain polymer complexes are known to exhibit ionic conductivity as high as 10^{-4}-10^{-5} S cm^{-1} at moderate temperature. These solid electrolytes have attracted strong interest due to a variety of potential applications; e.g. all solid state batteries, sensors and display devices [5-10].

Since these solid polymer electrolytes have generally lower ionic conductivity than liquid electrolyte [11], ultra-thin films are required to decrease actual film resistance of the solid polymer electrolyte. The thinner the solid polymer electrolyte, the thinner an electrochemical devices such as a battery, sensor or display device can be made. However it is not easy to prepare ultra-thin film of solid polymer electrolyte because the thinner the film the easier the generation of pin-hole becomes by conventional techniques.

Glow discharge (plasma) polymerization is a useful method to provide an ultra-thin uniform polymer layer strongly adherent on various substrates from different kind of monomers. Here, plasma polymerization technique was utilized to prepare a host polymer film for thin solid polymer electrolyte.

Starting from octamethylcyclotetrasiloxane (OMCTS), ultra-thin polymeric layers were synthesized as a host polymer by a plasma polymerization technique. Polymers containing

---

J. Electrochem. Soc., 136, 625 (1989).

a siloxane group are known to have a low glass transition temperature (Tg), which enhances ionic conductivity [12]. The plasma synthesized polymer from OMCTS was hybridized with PPO [average M.W. 4000] and $LiClO_4$ to prepare an ultra-thin solid polymer electrolyte film. These ultra-thin films were characterized by FT-IR, scanning electron microscope (SEM) and electron prove micro analyzer (EPMA). Ionic conductivity of the hybrid film was analyzed by means of complex impedance measurements.

1.2 Experimental

1.2.1 Plasma polymerization

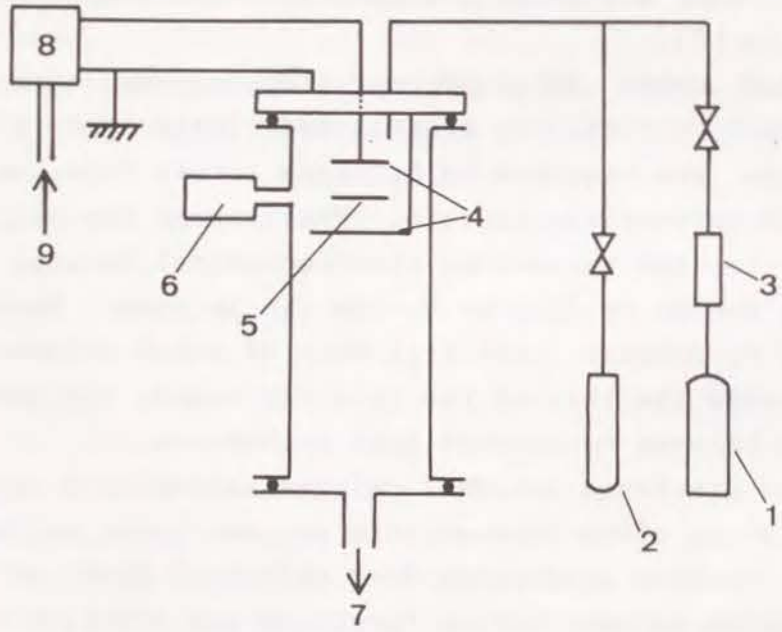

Fig. 1.1. A schmatic diagram of an apparatus for RF glow polymerization. 1: Ar, 2: monomer, 3: flow meter, 4: parallel electrodes, 5: substrate holder, 6: Pirani gauge, 7: pump, 8: matching network, 9: 13.56MHz power generator.

A schematic diagram of the apparatus used for depositing polymer films by plasma polymerization is shown in Fig. 1.1. Polymerization was performed in a capacitively coupled glass reactor of 9cm diameter and 35cm height, using stainless steel internal electrodes (28 cm^2) placed 3.5 cm apart. The system consists of a glass reactor, a monomer inlet, a Pirani gauge, an RF power supply (13.56 MHz) with an impedance matching network and a vacuum pump. Glass plates deposited with gold, stainless steel and Ni sheets were utilized as substrates. Substrates were placed between the electrodes. Argon gas [10 cm^3(STP)/min] and OMCTS vapor [2 cm^3/min] were introduced into the glass reactor. The pressure was controlled at 0.5 Torr by a needle valve. The plasma polymerization was conducted at various levels of RF power for 0.5-2 hours.

1.2.2 Materials

Octamethylcyclotetrasiloxane (OMCTS) (Shin-etsu Chem.

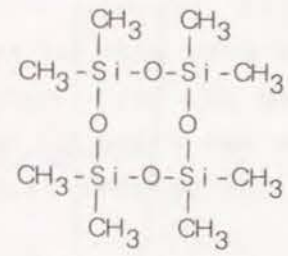

Co.), poly(propylene oxide) (PPO) (average M.W. 4000), butanol (Wako Chem. Co.) of extra pure grade were used without further purification. Anhydrous $LiClO_4$ (Wako Chem. Co.) was dried under reduced pressure (10^{-3} Torr) at 120°C for 12 h.

1.2.3 Preparation of hybrid polymer electrolyte of plasma polymer formed from OMCTS, PPO and $LiClO_4$

Most of resulting plasma polymers formed from OMCTS were about 1um thick. The polarity of polysiloxane is so low that the interaction between ions and lone pair of electrons from oxygen atoms of siloxane group does not generate a significant number of mobile ionic carriers. Therefore, the ionic conductivity of a plasma polymer formed from OMCTS complexed with

$LiClO_4$ was very low. The plasma polymer films were hybridized with PPO and $LiClO_4$ to obtain ionic conductivity. PPO has an ether group which is highly polar and is often used as a solvent for ionic compounds. Plasma polymers formed from OMCTS were soaked in butanol-PPO solution containing various concentration of $LiClO_4$ until attaining steady-state at 50 °C, then dried under reduced pressure (10^{-3} Torr) at room temperature in order to evaporate the butanol. After contact with these polymers for a few days, lithium metal kept its metallic color. This indicates the film was not active to lithium metal. Although the film was swollen by the solution during the hybridization process, the film did not peel off from the substrate. This fact unambiguously shows its good adhesion. The concentration of lithium ion in the plasma polymer was determined by utilizing an induced coupled plasma spectroscopy (ICP) instrument. Conventional inert-atmosphere techniques were adopted during the hybridization of the plasma polymer with PPO and $LiClO_4$ in order to prevent contamination by water. Impedance measurements were made on samples of the hybrid film which were prepared on gold covered stainless steel. Contact to these samples was aided by vapor-depositing a final layer of gold on top of the polymer film.

1.2.4 Measuring techniques

Alternating current impedance measurements over the frequency range $2x10^2$-$2x10^4$ Hz were made with a vector impedance meter in order to estimate the ionic conductivity of the complex film. The interfacial impedance between the complex and the electrodes was simultaneously estimated.

FT-IR measurements were performed with a Shimadzu 4100 IR spectrometer. To get IR spectra, a gold reflectance layer had been evaporated on the substrate prior to film deposition.

The rate of polymer deposition was determined by weighing the glass substrate before and after polymerization. The cross-section of the layer deposited on glass substrates was observed by SEM. The thickness of polymer layer was determined from the SEM figures. The density of plasma polymer formed from OMCTS was calculated from the thickness of cross-section of SEM figures and weight of the film.

1.3 Result and discussion

1.3.1 Characterization of plasma polymer formed from OMCTS

Polymers prepared by a plasma polymerization technique are generally insoluble in most solvents and it is difficult to determine their structure. The applied power level is

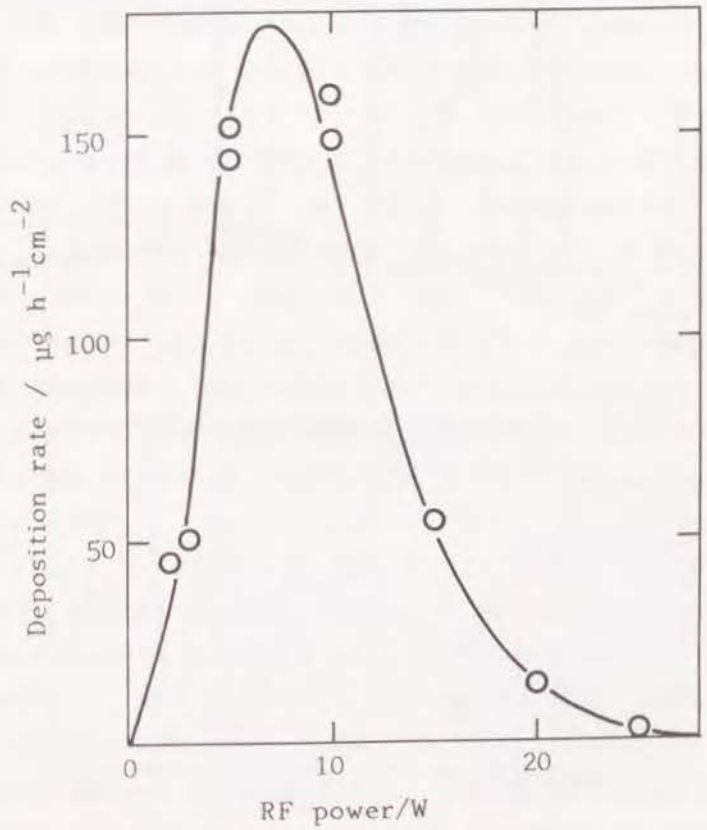

Fig. 1.2. Dependance of the deposition rate on RF power.

known to have an important influence on the structure of a plasma polymer [13,14]. The influence of power on the polymer deposition rate was first examined [flow rate of OMCTS vapor: 2 cm^3(STP)/min]. As shown in Fig. 1.2, for the low range of RF power, the deposition rate increased with increasing power, while above 10W the deposition rate decreased. This behavior is interpreted in terms of the CAP (Competitive Ablation and Polymerization) mechanism [15-17]. In this case, it is considered that the important etching species are ones from the

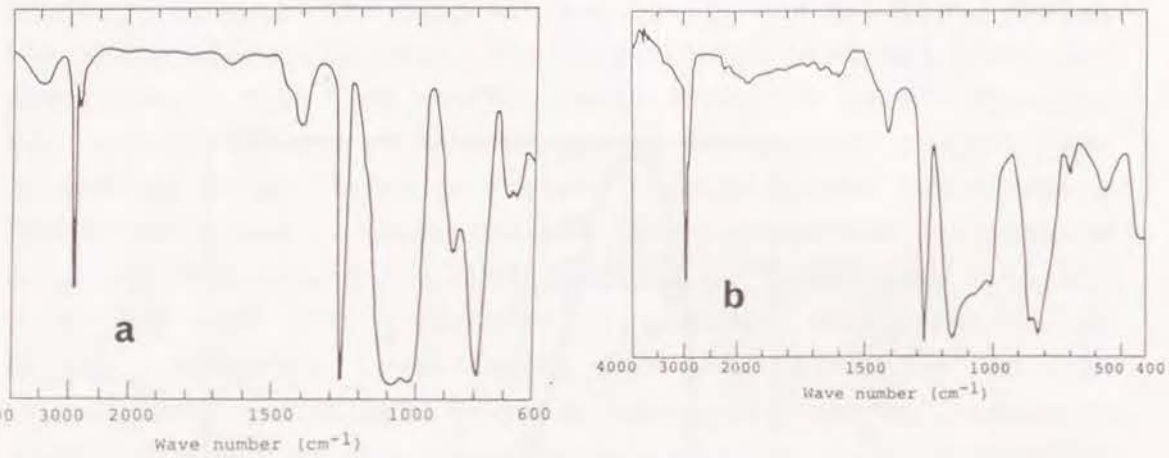

Fig. 1.3. IR spectra of polydimethylsiloxane (a), plasma polymer formed from OMCTS at 10 W (b), and 20 W (C).

Ar carrier gas. While at the lower power level, the polymerization was dominant, above 10 W the ablation process became significant. After the ablation process begins, an increase in power accelerates the ablation process, which causes the deposition rate to decrease.

The IR spectra of polydimethylsiloxane and the polymer film deposited at 10 W and 20 W are presented in Fig. 1.3. Plasma polymers formed from OMCTS at 10 W show absorptions at 2960 cm^{-1} (CH_3 stretching), 2900 cm^{-1} (CH_2 stretching), 1410 cm^{-1} (CH_3 deformation), 1259 cm^{-1} ($Si-CH_3$ sym. deformation), 1200-1000 cm^{-1} (Si-O-C, Si-O-Si stretching), 840cm^{-1} ($Si-CH_2$ sym. rocking) and 800 cm^{-1} ($Si-CH_2$ asym. rocking) [18,19]. In the spectra of both polydimethylsiloxane and plasma polymer at 10 W, there are many common absorption bands. This observation infers that the general structure of the plasma polymer at 10 W is similar to that of polydimethylsiloxane. On the other hand, some differences are found between patterns of the absorption bands of polydimethyl-siloxane and plasma polymer at 20 W. The peak strength of 2960 cm^{-1} and 1259 cm^{-1} became weak and the absorption peaks of plasma polymer at 20 W were broad. These observations suggest that methyl group elimination and Si-O-Si cross-linking reactions proceeded because of decomposition of monomer and ablation of deposited polymer due to the high applied power [20].

Figure 1.4 illustrates SEM figures of the surface and cross-section of the plasma film. Figure 1.4b clearly shows the plasma polymer is uniform and pinhole-free in the scale of SEM observation, and the film thickness was about 1.4 μm. Figure 1.4a shows that many spherical particles are formed at the surface. It was inferred that reactive species reacted with each other in the gas phase thus leading to the formation of powder particles which deposited on the substrate and grew slowly during deposition of the film [21]. The deposition of spherical particle was avoided by changing the orientation of the substrate to prevent particles formed in the vapor phase

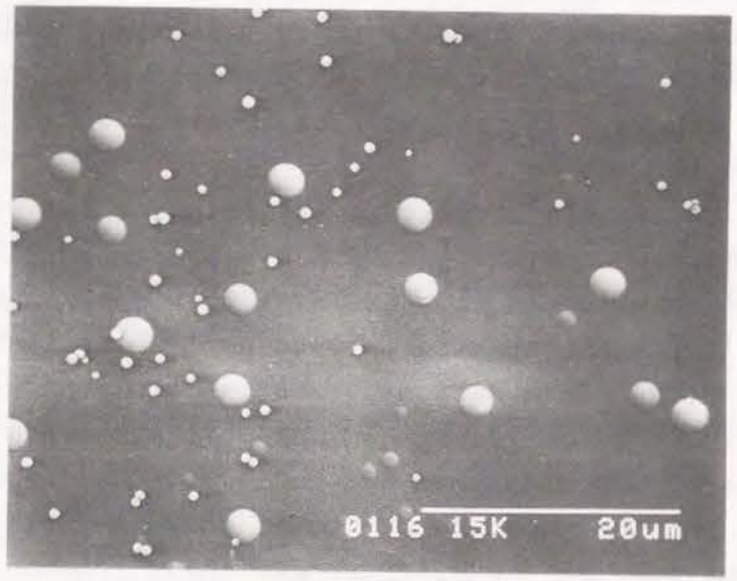

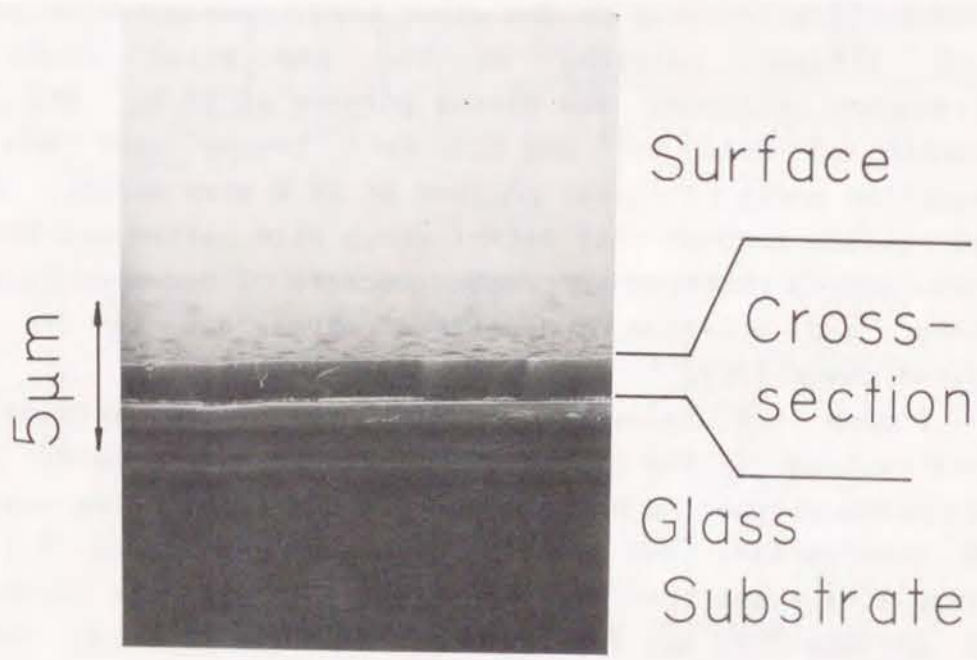

Fig. 1.4. SEM figures of surface (a) and cross-section (b) of plasma polymer.

from falling on to the substrate. The surface and cross-section of films examined in this work here was the form observed in Fig. 1.4b.

The density of films were calculated using thickness and weight of prepared plasma polymer films. The density was 1.45 g/cm^3 (in the accuracy of 5%) for different membranes prepared at 5 W. This fact supports the uniformity of the films. The value is a larger than the one for polydimethylsiloxane (1.20 g/cm^3). The difference is ascribed to the cross-linking structure of the plasma polymer.

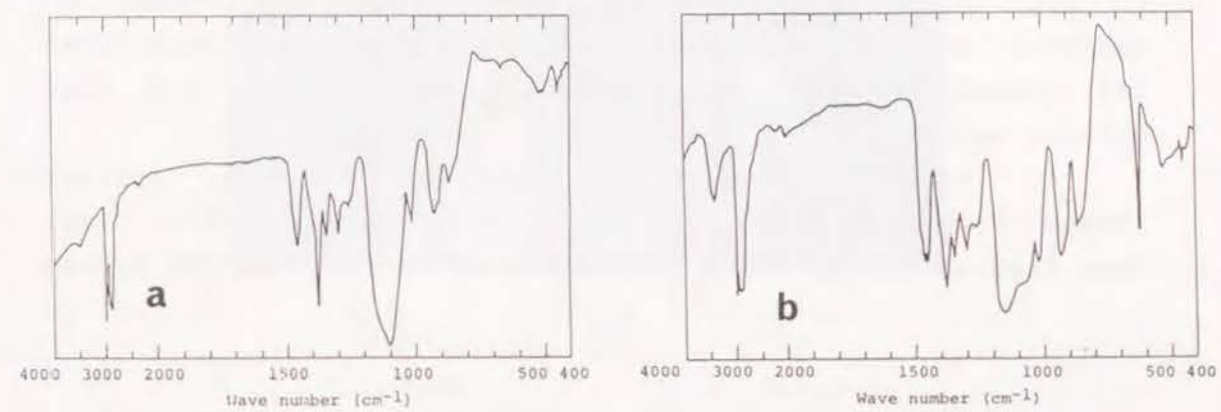

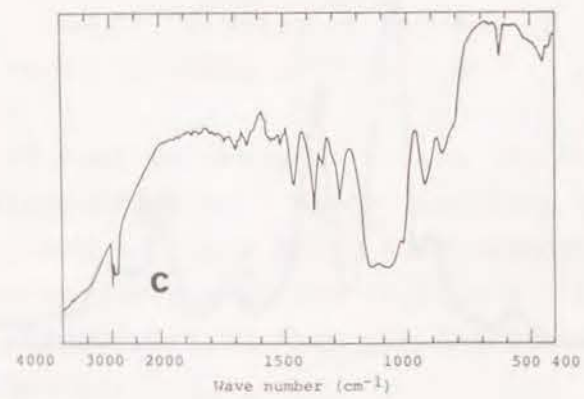

Fig. 1.5. IR spectra of PPO (a), mixture solution of PPO and $LiClO_4$ in butanol (b), and plasma polymer at 10 W after complexing with $LiClO_4$ (c).

The electrical resistance between gold layers which sandwich the plasma film was measured and the resulting large resistivity (greater than 1 M Ω) implies that the two conductive layers were not short circuited and that the plasma polymer film formed from OMCTS was pinhole-free.

The IR spectra of PPO(a), mixture solution of PPO and $LiClO_4$ in butanol(b) and hybrid polymer of plasma polymer formed from OMCTS at 10 W, PPO and $LiClO_4$ (c) are presented in Fig. 1.5. The spectrum of Fig. 1.5c showed absorption at 630 cm^{-1} which was ascribed to ClO_4^- in addition to peaks ascribed to PPO (Fig. 1.5a). On the other hand, the absorption ascribed to OH disappeared. This observation suggests that the plasma polymer contains both $LiClO_4$ and PPO and that butanol was thoroughly evaporated.

An EPMA spectrum of hybrid polymer of plasma polymer formed from OMCTS, PPO and $LiClO_4$ is presented in Fig. 1.6. This figure clearly shows the existence of ClO_4^- in the hybrid

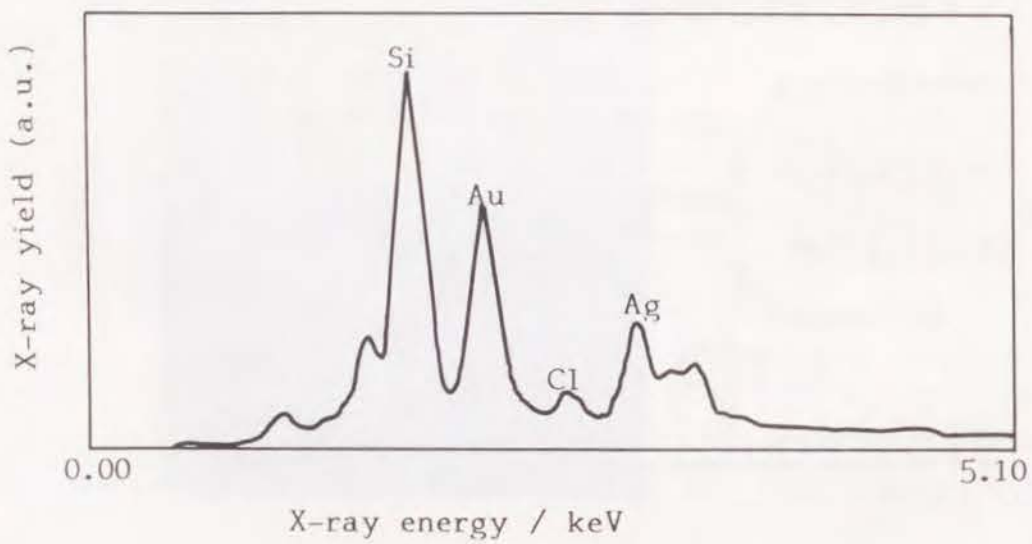

Fig. 1.6. An EPMA spectrum of hybrid polymer of plasma polymer formed from OMCTS, PPO and $LiClO_4$.

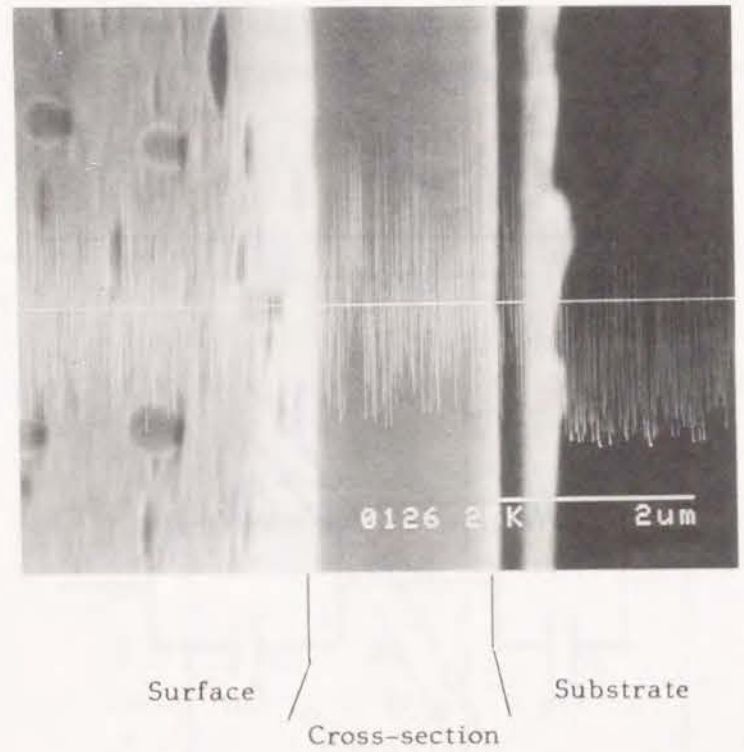

Fig. 1.7. Depth profile of Cl atom of the cross-section of hybrid polymer of Fig. 1.6.

polymer, so Li^+ must be present in the hybrid polymer to establish electroneutrality. Depth profiles of Cl in the hybrid polymer cross-sections (Fig. 1.7) indicate that Cl does not localize on the surface or the interface. From a similar measurement of the polymer surface the distribution of Cl was uniform on the surface.

1.3.2 Ionic conductivity of hybrid polymer of plasma polymer formed from OMCTS, PPO and $LiClO_4$

Figure 1.8 shows the typical complex impedance plot of Au/hybrid film of plasma polymer formed from OMCTS, PPO and

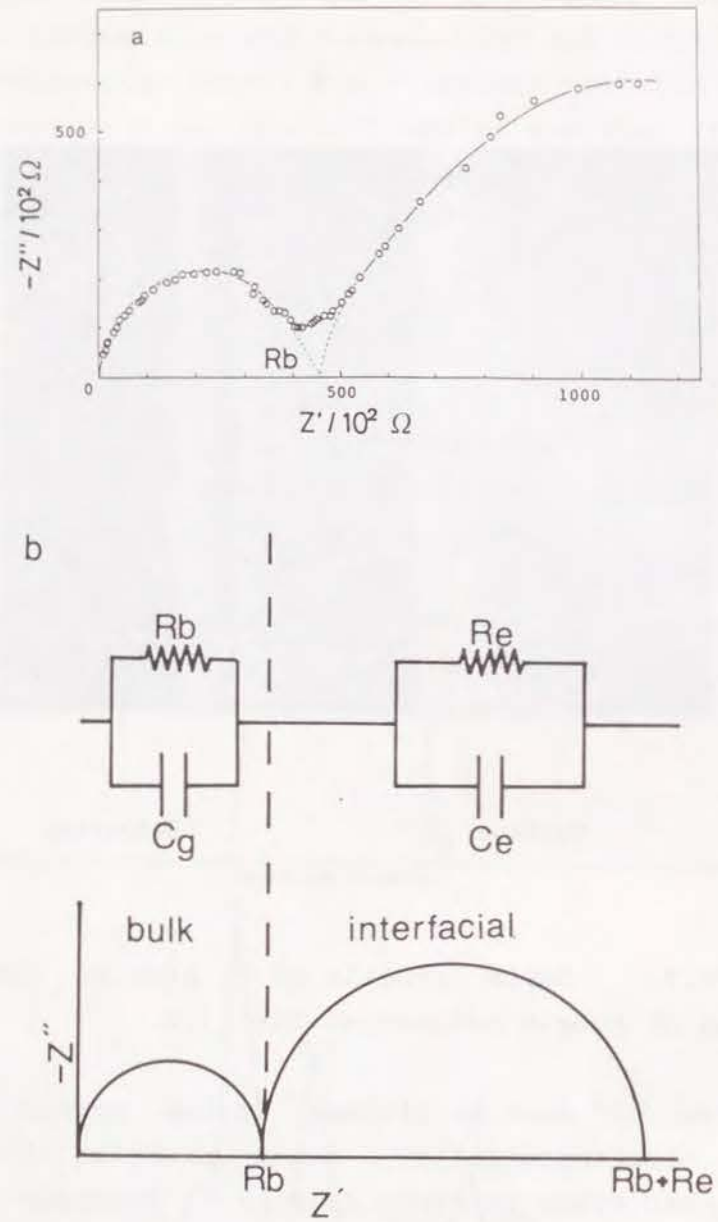

Fig. 1.8. A complex impendance plot of Au/Plasma polymer with PPO and $LiClO_4$/Au (a) and an appropriate equivalent circuit (b).

$LiClO_4$ /Au. Two arcs are distinguished. Since the electrolyte/electrode interfacial capacitance, Ce, is generally much lager than geometrical capacitance, Cg, in these polymer electrolytes, the spectra obtained are interpreted by the appropriate equivalent circuit shown in Fig. 1.8b. The first arc, for the high frequency range, is attributed to bulk

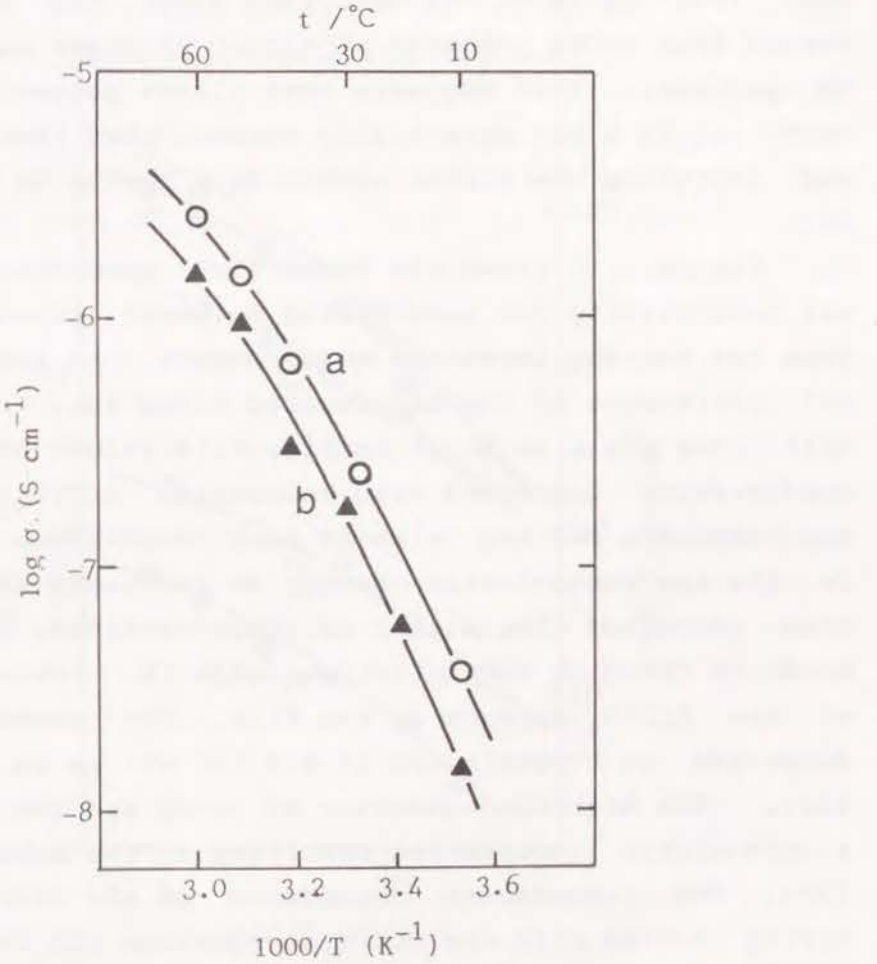

Fig. 1.9. Ionic conductivity dependence on temperature for hybrid polymer of plasma polymer formed from OMCTS (78%), PPO (20%) and $LiClO_4$ (2%). a: 5 W, b: 10 W.

electrolyte impedance. The arc was extrapolated to the Z' axis to obtain the bulk electrolyte resistance, Rb. The second arc, for the low frequency range, is attributed to electrode/electrolyte interfacial impedance.

Ionic conductivities of hybrid polymers were calculated from Rb. Values for hybrid polymers of plasma polymer at 5 W or 10 W, PPO (20%) and $LiClO_4$ (2%) are plotted vs. 1/T in Fig. 1.9. Conductivity of the hybrid polymer at 5 W is much higher than that at 10 W. As described above, the plasma polymer formed from OMCTS prepared at higher RF power gave the broader IR-spectrum. This suggests that plasma polymer formed from OMCTS at 10 W was more highly cross-linked than that at 5 W and therefore the former should have higher Tg than the latter.

Figure 1.10 shows the temperature dependence of electrical conductivity for some hybrid polymers, which was estimated from the complex impedance measurements. An apparent electrical resistance of the as-prepared films (ca. 1 μm thick) per unit area was also shown in Fig. 1.10 (right ordinate). The conductivity increased with increasing $LiClO_4$ concentration and reached a ceiling value at each temperature for 4% $LiClO_4$. In the low concentration range, an increased salt concentration increased the number of ionic carriers. On the other hand, in the high concentration range the crystallized domain of the $LiClO_4$ appears in the film. The excess $LiClO_4$ was dispersed as crystals and it did not act as an ionic carrier [22]. The high concentration of ionic species enhances the electrostatic interaction resulting in the enhancement of Tg [22]. The temperature dependence of the electrical conductivity fitted with the WLF type equation [23,24] rather than the Arrhenius equation. The activation energy estimated from the slope of the linear part of the figure tends to increase with the $LiClO_4$ concentration. This fact should be related to changes of Tg.

It is considered that the hybrid polymer electrolyte has a micro-heterogeneous structure [segregatiom to a segment of

plasma polymer formed from OMCTS and a PPO segment] and that PPO segment mainly contributes to the ionic dissociation of $LiClO_4$ [25]. This micro-heterogeneous domain was so small that this separation was not observed on SEM pictures. The segregation is often observed in the polymer containing polar groups. Perfluorinated Ionomer membrane, Nafion, is a typical

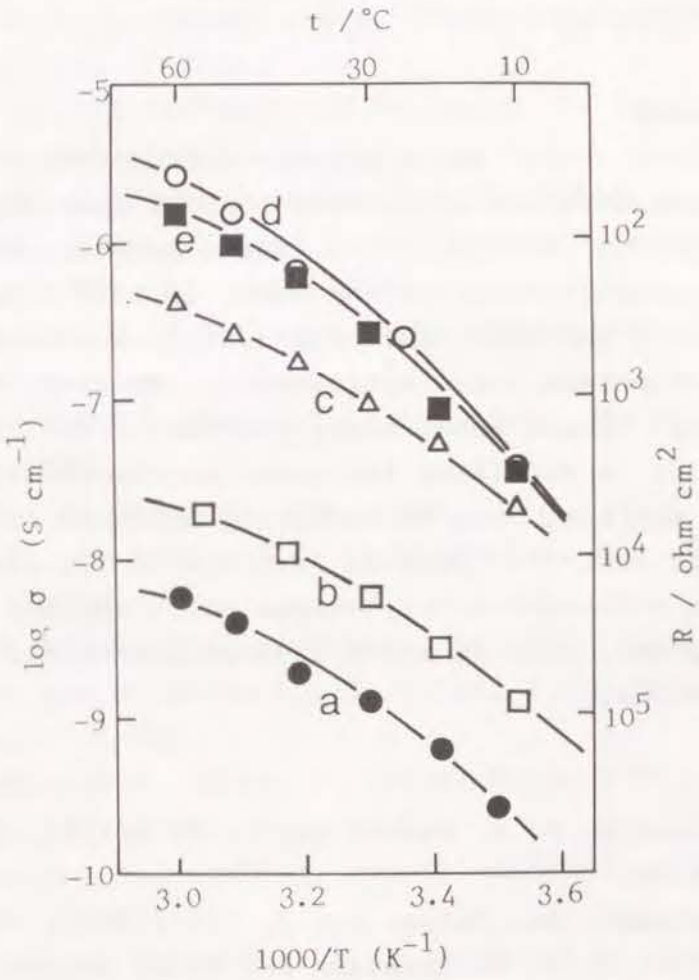

Fig. 1.10. Ionic conductivity dependence on temperature for hybrid polymer of plasma polymer formed from OMCTS, PPO (20%) and $LiClO_4$ (a: 0.2%, b: 0.6%, c: 1%, d: 2%, and e: 4%).

example. Although the micro-structure of precursor of Nafion is uniform, the saponification of it causes the microdomain phase separation in spite of the rigid structure of the perfluorinated polymer. After phase separation Nafion exhibits high ionic conductivity [26]. In the case of the present polymer film, a conduction path of the carriers similar to Nafion is expected. Conductivity of the hybrid film, plasma polymer/PPO/$LiClO_4$ (78/20/2), reached 2.6×10^{-6} S cm^{-1} (40 Ω per 1 cm^2) at 60°C.

1.4 Conclusion

An ultra thin solid polymer electrolyte film was prepared by hybridization of plasma polymer film from OMCTS with PPO and $LiClO_4$. The resulting hybrid polymers had a fairly low ionic conductivity, on the order of 10^{-6} S cm^{-1} (10 Ω per 1 cm^2) at 60°C and they could not satisfy the requirement for use as a diaphragm for electrolyzers. However, the polymer is adhesive toward substrates, pinhole free and uniform. Therefore it is promising for some electrochemical applications. For example, the conductivity obtained in the present work could meet the demands for the solid electrolyte of solid state electrochemical devices which consume very little electric power, such as solid lithium batteries, sensors, or display devices.

References

1. D. E. Fenton, J. M. Parker and P. V. Wright, Polymer, 14, 589 (1973).
2. P. V. Wright, Br. Polym. J., 7, 319 (1975).
3. M. B. Armand, J. M. Chabagno and M. J. Duclot, Fast Ion Thansport in Solids edited by P. Vashista, J. N. Mundy, G. K. Shenoy, Elsevier, N. Y., 1979, p 131.
4. M. Watanabe, M. Kanba, H. Matsuda, K. Tsunemi, K. Mizoguchi, E. Tsuchida and I. Shinohara, Makromol. Chem., Rapid Commun., 2, 741 (1981).
5. C. K. Chiang, Polymer, 22, 1454 (1981).

6. A. Hooper and J. M. North, Solid State Ionics, 9&10, 1161 (1983).
7. H. Ohno, H. Matsuda, K. Mizoguchi and E. Tsuchida, Polym. Bull., 7, 271 (1982).
8. T. Skotheim and I. Lundstrom, J. Electrochem. Soc., 129, 894 (1982).
9. M. Gauthier, D. Fauteux, G. Vassort, A. Belanger, M. Duval, P. Ricoux, J-M. Chabagno, D. Muller, P. Rigaud, M. B. Armand and D. Deroo, J. Electrochem. Soc., 132, 1333 (1985).
10. T. Nagatomo, C. Ichikawa and O. Omoto, J. Electrochem. Soc., 134, 305 (1987).
11. Y. Matsuda, J. Power Soueces, 20, 19 (1987).
12. K. Nagaoka, H. Naruse and I. Shinohara, J. Polym. Sci., Polym. Let. Ed., 22, 659 (1984).
13. H. Yasuda and T. Hirotsu, J. Appl. Polym. Sci., 21, 3139 (1977).
14. H. Yasuda and C.R. Wang, J. Polym. Sci., Polym. Chem. Ed., 23, 87 (1985).
15. H. Yasuda, J. Macromol. Sci. Chem., A10, 383 (1976).
16. H. U. Poll, M. Arzt and K. H. Wickleder, Eur. Polym. J., 12, 505 (1976).
17. H. Yasuda and T. Hse, Surf.Sci., 76, 232 (1978).
18. I. Tazima and M. Yamamoto, J. Polym. Sci., Polym. Chem. Ed., 23, 615 (1985).
19. N. Inagaki and H. Hirao, J. Polym. Sci., Part A, Polym. Chem, 24, 595 (1986).
20. T. Iijima and H. Hanafusa, Denshitsushingakkai Ronbunshi, J67-C, 88 (1984).
21. N. Niinomi, H. Kobayashi, A. T. Bell and M. Shen, J. Appl. Phys., 44, 4317 (1973).
22. K. Tsunemi, H. Ohno and E. Tsuchida, Electrochimca Acta, 28, 833 (1983).
23. M. L. Williams, R. F. Landel and J. D. Ferry, J. Am. Chem. Soc., 77, 3701 (1955).
24. M. Cohen and D. Turnbull, J. Chem. Phys., 31, 1164 (1959).

25. M. Watanabe, S. Nagano, K. Sanui and N. Ogata, J. Power Sources, 20, 327 (1987).
26. K. A. Mauritz and A. J. Hopfinger 'Modern Aspect of Electrochemistry' Vol.14, Chap.6, edited by J. O'M. Bockris, B. E. Conway and R. E. White Plenum Press. N.Y., 1987.

Chapter 2 Preparation and Characterization of Solid Polymer Electrolyte Composed of Plasma Polymerized Tris(2-methoxyethoxy)vinylsilane-$LiClO_4$ Complex

2.1 Introduction

On account of their relatively high ionic conductivities [1,2], solid polymer electrolytes based on alkali metal salts complex of polyethers [poly(ethylene oxide) and poly(propylene oxide)] recently have received considerable attention as potential materials for use in electrochemical devices, such as solid-state lithium batteries, sensors, and display devices [3-8]. The ionic conductivities of these solid polymer electrolytes are considerably lower than those of liquid electrolytes [9], typical value at room temperature being in the order of $10^{-6\sim-8}$ S cm^{-1}. Thus, in order to utilize these electrolytes in practical electrochemical devices at room temperature it is necessary to lower their ohmic resistance. This can be achieved by either increasing the specific ionic conductivity of the polymer, or by preparing the polymer in the form of an ultra-thin film.

It is well known that any means of lowering the glass transition temperature (Tg) favors the enhancement of the ionic conductivity of a solid polymer electrolyte [10]. Accordingly, among solid polymer electrolytes, polyethers containing siloxane unit complexed with alkali metal salts, such as poly(dimethylsiloxane-ethylene oxide) copolymer-lithium salt complex, are attractive, because the incorporation of a siloxane unit into a polymer generally lowers the glass transition temperature [10-14].

Plasma polymerization is known to be a useful method for the preparation of pinhole-free ultra-thin polymer film. In this Chapter, solid polymer electrolyte films having ionic

---

J. Chem. Soc., Chem. Commun., 358 (1989).
J. Electrochem. Soc., 137, 35 (1990).

conductivity comparable to that of poly(dimethylsiloxane-ethylene oxide) copolymer-alkali metal salt complexes prepared using conventional methods was prepared by the plasma polymerization method. Tris(2-methoxyethoxy)vinylsilane (TMVS) was

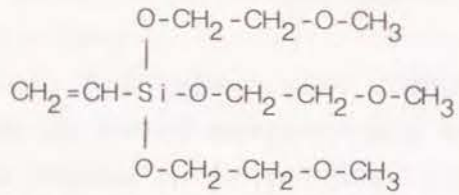

Tris(2-methoxyethoxy)vinylsilane

selected as the monomer because this substance contains both ether and the siloxane group.

The plasma-polymerized TMVS was characterized with ^{1}H NMR, ^{13}C NMR, FT-IR, and scanning electron microscopy (SEM); whereas the solid polymer electrolytes were characterized by SEM, electron probe micro analysis (EPMA), FT-IR, and differential scanning calorimetry (DSC). The ionic conductivities of the solid polymer electrolytes were determined by means of complex impedance measurements.

2.2 Experimental

2.2.1 Materials

Tris(2-methoxyethoxy)vinylsilane (TMVS) (Shin-etsu Chem. Co.), methanol (Wako Chem. Co.) of extra pure grade were used without further purification. Anhydrous $LiClO_4$ (Wako Chem. Co.) was dried under reduced pressure (10^{-3} Torr) at 60 °C for 12 h.

2.2.2 Preparation of solid polymer electrolyte [plasma polymerized TMVS-$LiClO_4$]

A schematic diagram of the process for the synthesis of the solid polymer electrolyte is shown in Fig. 1.11. First, as shown in Fig. 1.11a, a layer of plasma-polymerized TMVS of about 0.5 μm thickness was deposited on a substrate of glass

that had previously been coated with a thin layer (~200 nm) of gold by DC sputtering. Next, the substrate was removed from the plasma polymerization reactor and a thin layer of $LiClO_4$ was deposited (as described below) on its surface (Fig. 1.11b). The substrate then was again placed in the reactor and a second thin layer of plasma polymer was deposited on the $LiClO_4$ layer under the same conditions as before (Fig. 1.11c). The resulting three-layer composite was maintained at 80 °C for 24 hours under 10^{-3} Torr to enable the $LiClO_4$ to distribute throughout the plasma polymer (Fig. 1.11d). This procedure resulted in the production of an ultra-thin (~1 μm thick) film of solid polymer electrolyte, plasma polymerized TMVS-$LiClO_4$

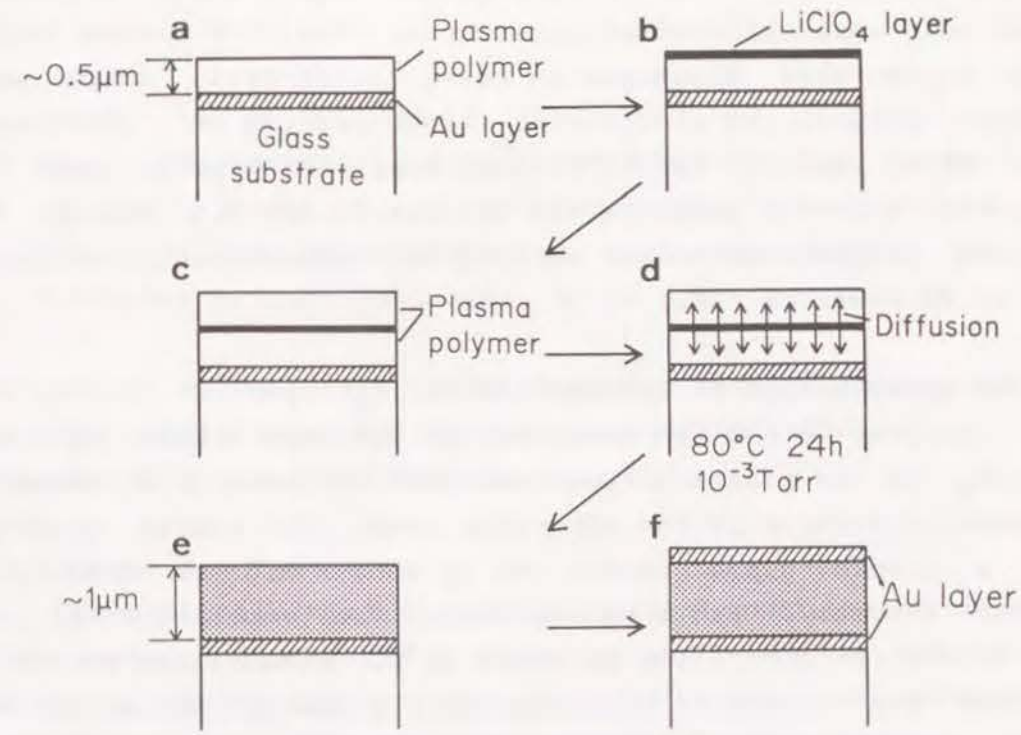

Fig. 1.11. Schematic diagram of process for synthesis of thin film of solid polymer electrolyte.

hybrid (Fig. 1.11e). As indicated in Fig. 1.11f, a second thin layer of gold was then deposited on the solid polymer electrolyte in order to carry out AC impedance measurements. The $LiClO_4$ content of the film was determined by atomic absorption spectrophotometry.

2.2.3 Plasma polymerization

The apparatus used to carry out the plasma polymerization, which has been described in detail in Chapter 1, consisted of a glass reactor equipped with capacitively coupled inner electrodes to which an alternating voltage was applied at a frequency of 13.56 MHz. The reactor was incorporated into a vacuum system consisted of a mechanical booster pump, a rotary pump, and a cold trap. The pressure in the reactor was monitored using a Pirani vacuum gauge. Glass plate deposited with gold were utilized as substrates. The thin plasma polymer films were deposited on these substrates, which were placed between two electrodes. Argon gas [10 cm^3 (STP)/min] and TMVS vapor [1 cm^3 (STP)/min] were introduced into the reactor and the pressure was maintained at 0.3 Torr. The plasma polymerization was carried out under these conditions at an RF power of 5 W.

2.2.4 Spray method of introducing $LiClO_4$ layer

A spray method was developed to lay down a thin layer of $LiClO_4$ on the plasma-polymerized TMVS. Figure 1.12 shows a schematic diagram of the apparatus used. The system consists of a tubular glass reactor (40 cm long x 3.5 cm diam.), a spray assembly, and a vacuum pump. The temperature of the substrate is controlled at about 60 °C. With values 1 and 3 closed the system is evacuated to a pressure of about 0.1 Torr. Opening valve 3 causes the air in the air reservoir 2 to be introduced into reactor 5, thereby aspirating a fine spray reservoir 4, filled with a methanolic solution containing 3% $LiClO_4$. This results in the deposition of a thin layer of $LiClO_4$ onto the substrate surface. By next closing valve 3

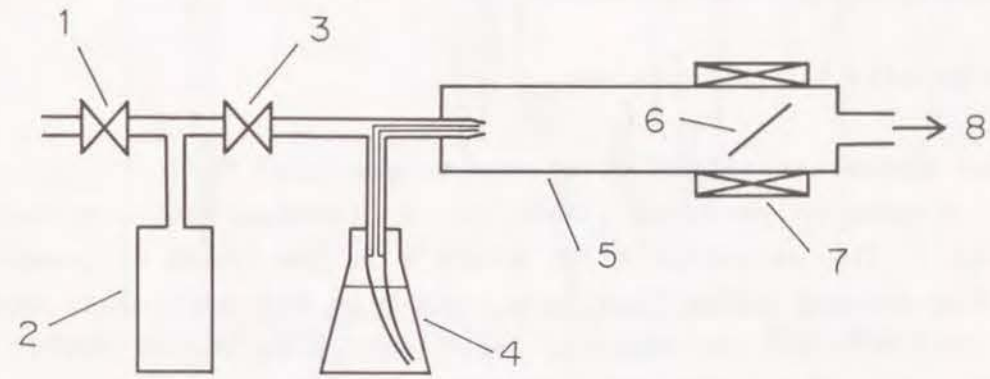

Fig. 1.12. Schematic diagram of apparatus for preparation of $LiClO_4$ layer. 1: stop valve, 2: air reservoir, 3: stop valve, 4: spray, 5: glass reactor, 6: substrate holder, 7: heater, 8: to pump.

and opening valve 1, air is reintroduced into air reservoir 2 and the cycle repeated until the deposited $LiClO_4$ layer is built up to the desired thickness.

2.2.5 Measuring Technique

Conventional inert-atmosphere (argon) handling techniques were employed during the preparation and characterization of the solid polymer electrolytes in order to prevent contamination with water. The observation that metallic lithium held in contact with the solid polymer electrolyte films for several days maintained its metallic luster indicates the water content of the solid polymer electrolyte was very low.

The ionic conductivities of the solid polymer electro-

lytes were determined from AC impedance measurements carried out over the frequency range of $2x10^2$-$2x10^4$ Hz using a vector impedance meter.

EPMA was performed with a Hitachi-Horiba EMAX-1770 electron microprobe analyzer. FT-IR spectra were obtained using a Shimadzu 4100 IR-spectrometer.

2.3 Results and discussion

2.3.1 Characterization of plasma polymerized TMVS

Plasma-polymerized TMVS is a transparent, colorless solid. The parameter W/FM, where W is the input RF power, F is the monomer molar flow rate, and M is the molecular weight of the monomer, defines the input energy of the RF power per unit mass of monomer [15,16]. Because the conditions under which the plasma polymerization was carried out were fairly mild in the case of the present study ($W/FM=2.7x10^7$ J kg^{-1}), the plasma polymers obtained are probably not highly cross-linked, as evidenced by their solubility in certain organic solvents such as acetone and dimethyl sulfoxide (DMSO). The polymers were characterized by FT-IR, ^1H NMR, and ^{13}H NMR measurements.

FT-IR spectra

Typical FT-IR spectra of TMVS and plasma-polymerized TMVS are shown in Fig. 1.13a and b, respectively. The IR spectrum of the plasma polymer is similar to that of the TMVS, except for the complete absence of the characteristic peak for the olefin group, which occurs about at 1600 cm^{-1}. Two different types of processes can occur during plasma polymerization: plasma induced polymerization or plasma-state polymerization [17]. Plasma induced polymerization (molecular polymerization) proceeds via a conventional chain propagation mechanism, which can be initiated by an ion, a radical, or a highly energetic species in the glow region. Accordingly, the plasma polymer formed from TMVS via plasma induced polymerization can

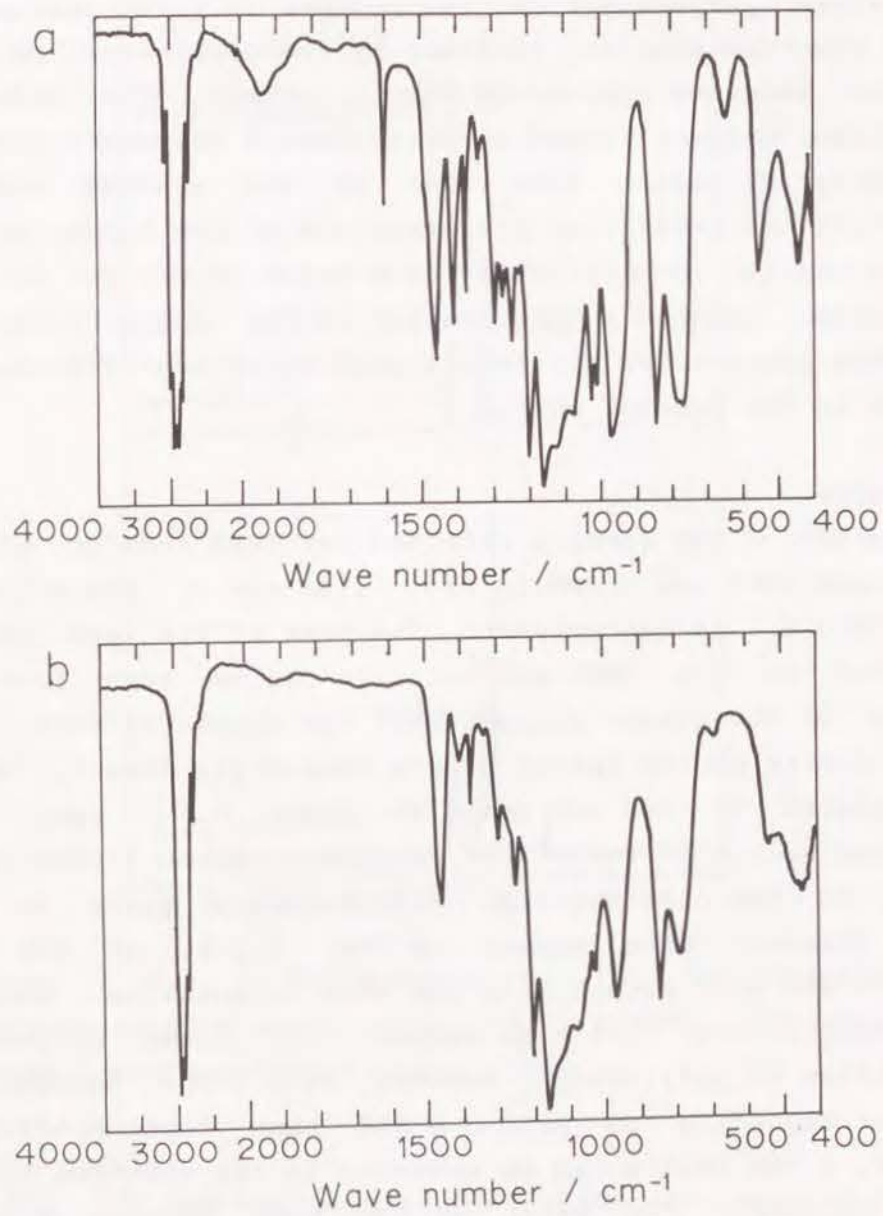

Fig. 1.13. IR spectra of (a) tris(2-methoxyethoxy)-vinylsilane, and (b) plasma polymerized tris(2-methoxyethoxy)vinylsilane.

be considered to be poly(TMVS). Conversely, in the case of plasma-state polymerization, the monomer is first decomposed to form reactive species, followed by the combination of these generated reactive species to form a polymer. The structure of a plasma polymer formed by plasma-state polymerization is drastically different from that of the staring monomer. Figure 1.13 indicates that the structure of the plasma polymer is very similar to poly(TMVS), from which it can be inferred that plasma induced polymerization is the dominant process that takes place under the fairly mild experimental conditions employed in the present work.

NMR spectra

Typical ^{1}H NMR spectra obtained for TMVS and for plasma-polymerized TMVS are shown in Fig. 1.14a and b, respectively, using DMSO-d_6 as the solvent. The peak at 2.6 ppm can be attributed to the DMSO solvent. It can be seen from the spectrum of the plasma polymer that the characteristic peaks of the olefin proton (peaks d) are completely absent, having been placed by two new peaks at about 0.5-1 ppm, which correspond to the proton of the saturated carbon formed by the opening of the olefin group. All the other peaks in Fig. 1.14a, however, also appear in Fig. 1.14b, at the same positions and with essentially the same intensities. The FT-IR spectra in Fig. 1.13 also suggest that plasma polymer is very similar to poly(TMVS). However, at 3.3 ppm, between the peak corresponding to proton b and that corresponding to proton c, a new peak e can be observed in the spectrum for the plasma polymer. The ratio of the peak heights c:b:e = 2.5:2.5:1, indicates that the magnitude of the new component is quite small. In spite of being a polymer peak, this new peak is very sharp, indicating that it can be attributed to some new, fixed construction within the polymer, as discussed below.

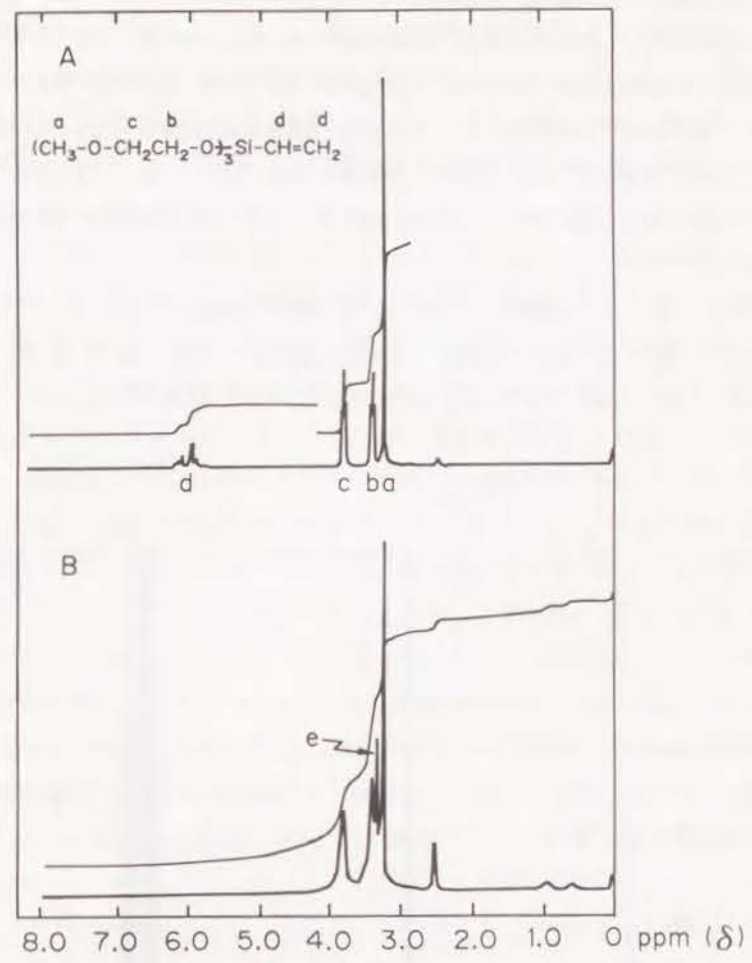

Fig. 1.14. ^{1}H NMR spectra of (A) tris(2-methoxy-ethoxy)vinylsilane, and (B) plasma polymerized tris(2-methoxyethoxy)vinylsilane.

^{13}C NMR spectra

The ^{13}C NMR spectrum of TMVS shows two peaks at 137 and 129 ppm that can be attributed to the carbons of the olefin group. These two peaks are, however, completely absent in the ^{13}C NMR spectrum of the plasma-polymerized TMVS. When a freshly prepared sample of the plasma polymer is dissolved in DMSO solvent (dissolves almost immediately), over the course of about 10 hours the presence of a small amount of diethylene glycol dimethyl ether can be detected. This indicates the

Si-O-Si cross-linking reaction has been taking place to a certain extent, probably through a solvent effect. However the ^{13}C NMR spectrum for a sample of the solid plasma polymer that was stored under an argon atmosphere for ten days was exactly the same as that obtained for a freshly prepared sample, indicating that the material is quite stable in the solid state.

Figure 1.15 shows the ^{13}C NMR spectrum of the plasma-polymerized TMVS between 25-82 ppm. Peaks f and e can be attributed to the DMSO-D_6 solvent and diethylene glycol di-

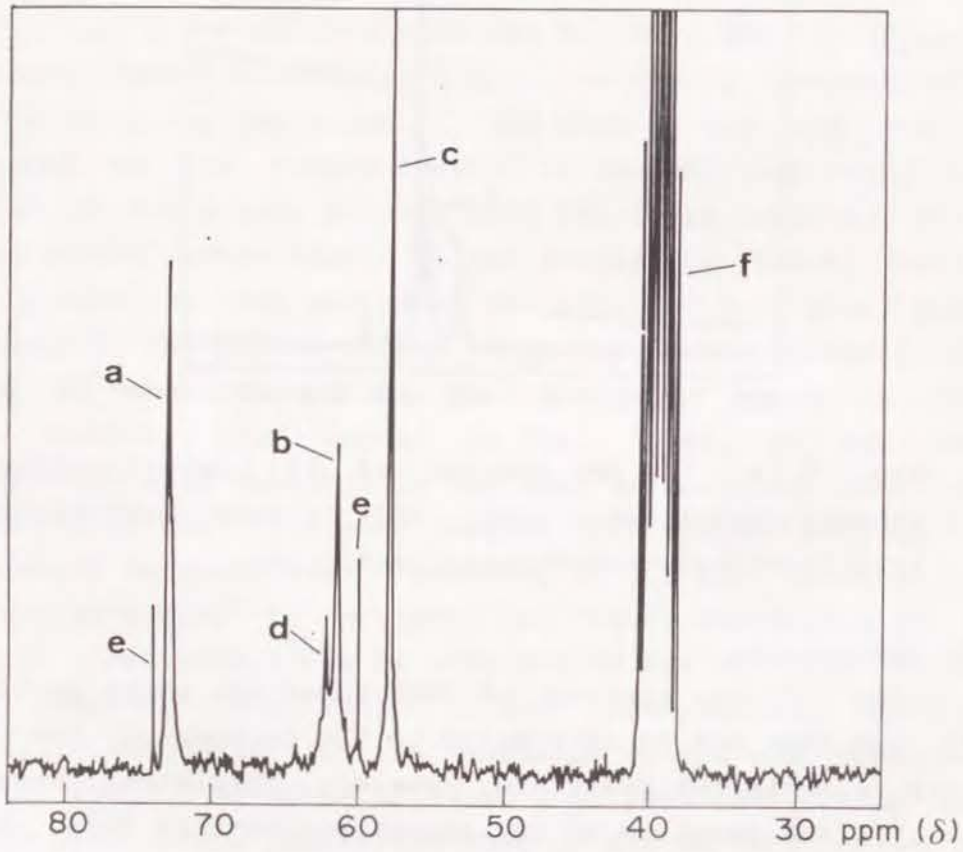

Fig. 1.15. ^{13}C NMR spectrum of plasma polymerized tris(2-methoxyethoxy)vinylsilane.

methyl ester, respectively. Peak c corresponds to the carbon of the methyl group. Peak a represents the carbon that is bounded with the proton labeled by the letter c in the molecular structure indicated in Fig. 1.14a, whereas peak b corresponds to the carbon that is bonded with the proton labeled b in the same illustration. Peak d represents the carbon that is bonded with the proton of the new peak observed in Fig. 1.14 (peak e in Fig. 1.14b). An Attached Proton Test (APT) shows that peak c corresponds to a carbon that is bonded with either one or three hydrogen atoms (i.e., $-\overset{|}{C}H$ or $-CH_3$), and that peaks a, b, c, and d all can be attributed to the $-CH_2-$ group. The shift of peak d is very similar to peak b, and as shown in Fig. 1.13, it seems that no new functional groups were formed. Thus it can be inferred that the carbon of the new peak is that of the ether group. These results seems to suggest that some cyclic grouping is formed in the plasma polymer. Two possibilities are indicated in Fig. 1.16. The peaks corresponding to the protons of the saturated carbon formed by opening the olefin group are found at a lower ppm region, and therefore are not present in the spectrum shown in Fig. 1.15.

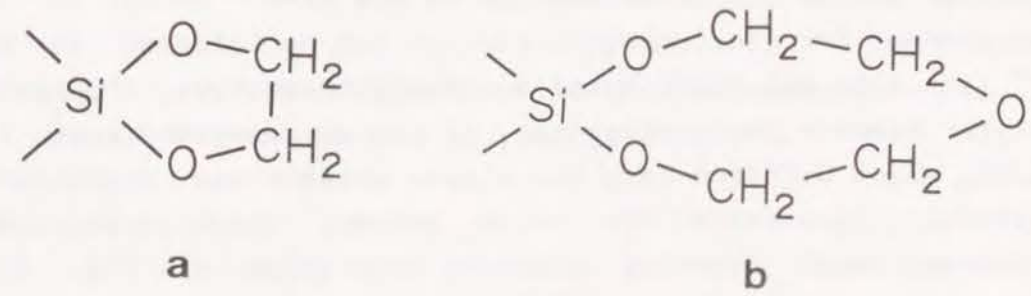

Fig. 1.16. Possible cyclic configurations occurring in plasma-polymerized tris(2-methoxyethoxy)vinylsilane.

In conclusion, the plasma polymer appears to be very similar to poly(TMVS), except for the presence of a small amount of some new grouping, probably a cyclic group. In order to achieve ionic conductivity in the polymer it is necessary that oxygen atoms of the ether groups coordinate the Li^+ ions. The presence of cyclic groups will tend to increase the rigidity of the polymer, making it more difficult for the oxygen atoms to achieve the necessary configuration for the optimal Li^+ ion complexation. Furthermore, any increase in polymer rigidity will tend to decrease segmental mobility, which also will lower the conductivity. Therefore, the formation of cyclic groups can be considered to be an undesirable side reaction which tend to lower the conductivity of the polymer. However, in the present case the amount of cyclic impurity probably is not a serious problem.

2.3.2 Characterization of the solid polymer electrolyte
[plasma polymerized TMVS-$LiClO_4$ Complex]

Electron probe micro analysis

An EPMA depth profile of the Cl in the solid polymer electrolyte is shown in Fig. 1.17. These results indicate that the distribution of Cl (as ClO_4^-) was more or less uniform across the cross-section of the film. Owing to the requirement for electroneutrality, it can be inferred that the Li^+ ion also was distributed uniformly throughout the solid polymer electrolyte. Therefore, it can be concluded that the $LiClO_4$ which diffused into the plasma polymer was distributed uniformly throughout the solid polymer electrolyte. The cross-sectional scanning electron micrograph of Fig. 1.17 shows that the solid polymer electrolyte had a thickness of about 1 μm and that at least within the scale of SEM observation, it was free from pin-holes. The fact that no short-circuiting was observed when the plasma polymer was sandwiched between two thin layer of gold for impedance measurements is further evidence that the solid polymer electrolyte film was

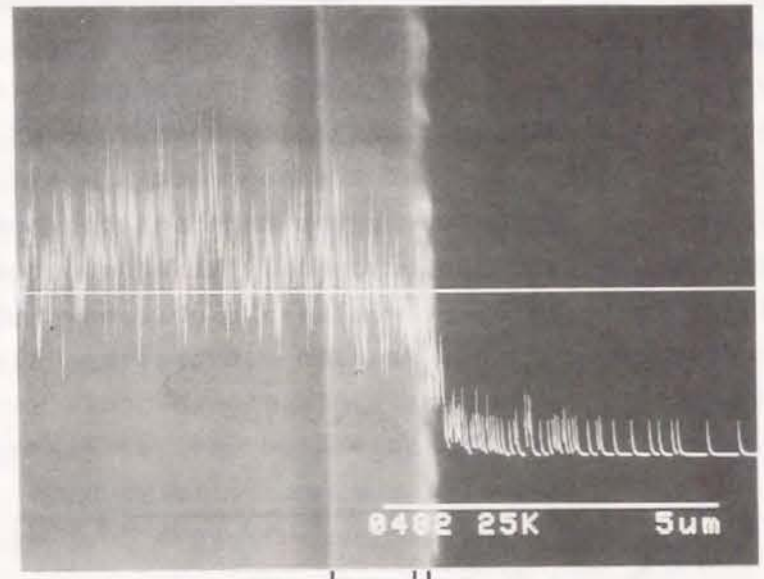

Fig. 1.17. EPMA depth profile of Cl distribution in cross-section of solid polymer electrolyte.

pinhole-free.

Differential scanning calorimetry

DSC traces obtained for the pure plasma polymer and for the solid polymer electrolytes of two different $LiClO_4$ contents are shown in Fig. 1.18. These traces were obtained using an initial heating rate of 10 °C/min. Each trace exhibits one base-line shift at the glass transition tempera-

ture. In each case the glass transition temperature (Tg) was taken as the temperature indicated by the intersection of the tangent from the base line with that from the fall line. The Tg values for pure plasma polymer, 3% $LiClO_4$ complex, 7% $LiClO_4$ complex are -91 °C, -75 °C, and -64 °C, respectively. Thus, over the range 0-7% $LiClO_4$, the glass transition temperature seems to increase almost linearly with increasing $LiClO_4$ content. This indicates that the segmental motion of the plasma polymer is suppressed by the interaction between the incorporated $LiClO_4$ and the oxygen of the ether group in the polymer [18]. Increases in the glass transition temperatures of solid polymer electrolytes with increasing alkali salt

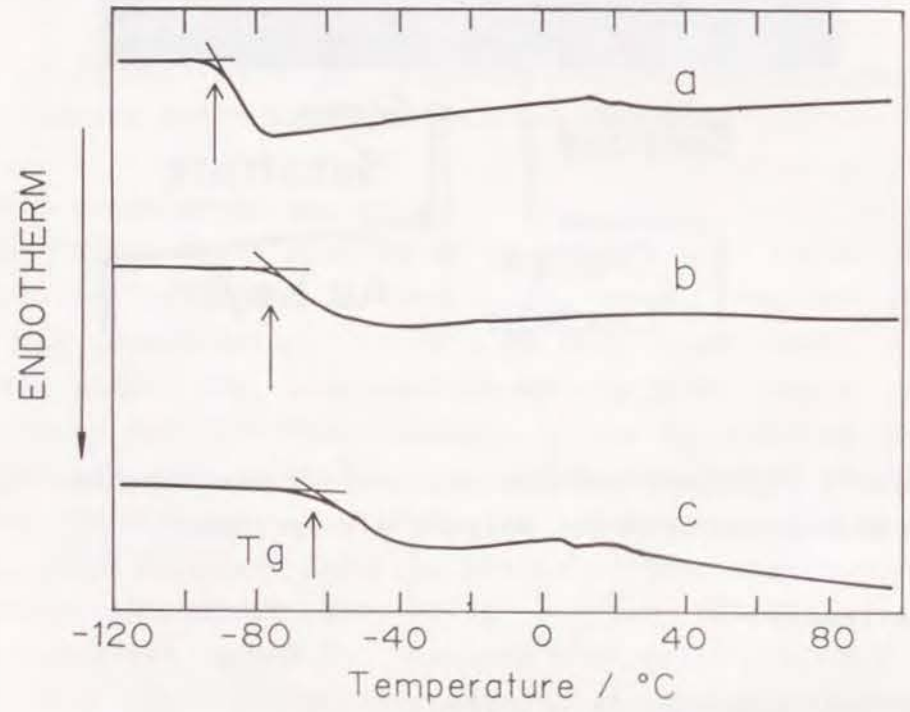

Fig. 1.18. DSC curves for (a) plasma polymerized TMVS, (b) solid polymer electrolyte containing 3wt% $LiClO_4$, and (c) solid polymer electrolyte containing 7wt% $LiClO_4$.

concentration also have been observed by other workers [18-20].

Ionic conductivity of the solid polymer electrolyte

Figure 1.19 shows a typical complex impedance plot of Au/ solid polymer electrolyte/Au. Two arcs can be distinguished. Since the electrolyte/ electrode interfacial capacitance, Ce, is generally much lager than the geometrical capacitance, Cg, the experimental complex impedance plot of Fig. 1.19a can be interpreted in terms of the equivalent circuit shown in Fig. 1.19b, for which Cg Ce. Thus the first arc, in the higher frequency range, can be attributed to the bulk electrolyte resistance. Accordingly, this arc was extrapolated to the Z' axis to obtain Rb, the bulk electrolyte resistance, from which the ionic conductivity then was calculated.

Figure 1.20 shows the variation of the ionic conductivity of the solid polymer electrolyte with temperature, at three different levels of $LiClO_4$ content. The electrical resistance per unit area, R, of the approximately 1 μm thick solid polymer electrolyte films also is indicated in the same figure on the right-hand coordinate axis. The plasma-polymerized TMVS-$LiClO_4$ complex electrolyte has conductivity values greater than 10^{-6} S cm^{-1} at room temperature. The highest conductivity of 5.6×10^{-5} S cm^{-1} (1.8 Ωcm^2) was observed at 100 °C for the formulation containing 15% $LiClO_4$. The ionic conductivities of these films are comparable with those of other highly conductive solid polymer electrolytes [18,19].

The Arrhenius plot of log vs. T^{-1} are not straight lines. This behavior often is observed for amorphous solid polymer electrolyte systems. For such systems, apparent activation energies are sometimes estimated from the linear portions of the curves. In the case of the present data, the apparent activation energy increases with increasing $LiClO_4$ content of the electrolyte. In this type of solid polymer electrolyte system, however, it is well known that the temperature dependence of the ionic conductivity is better described

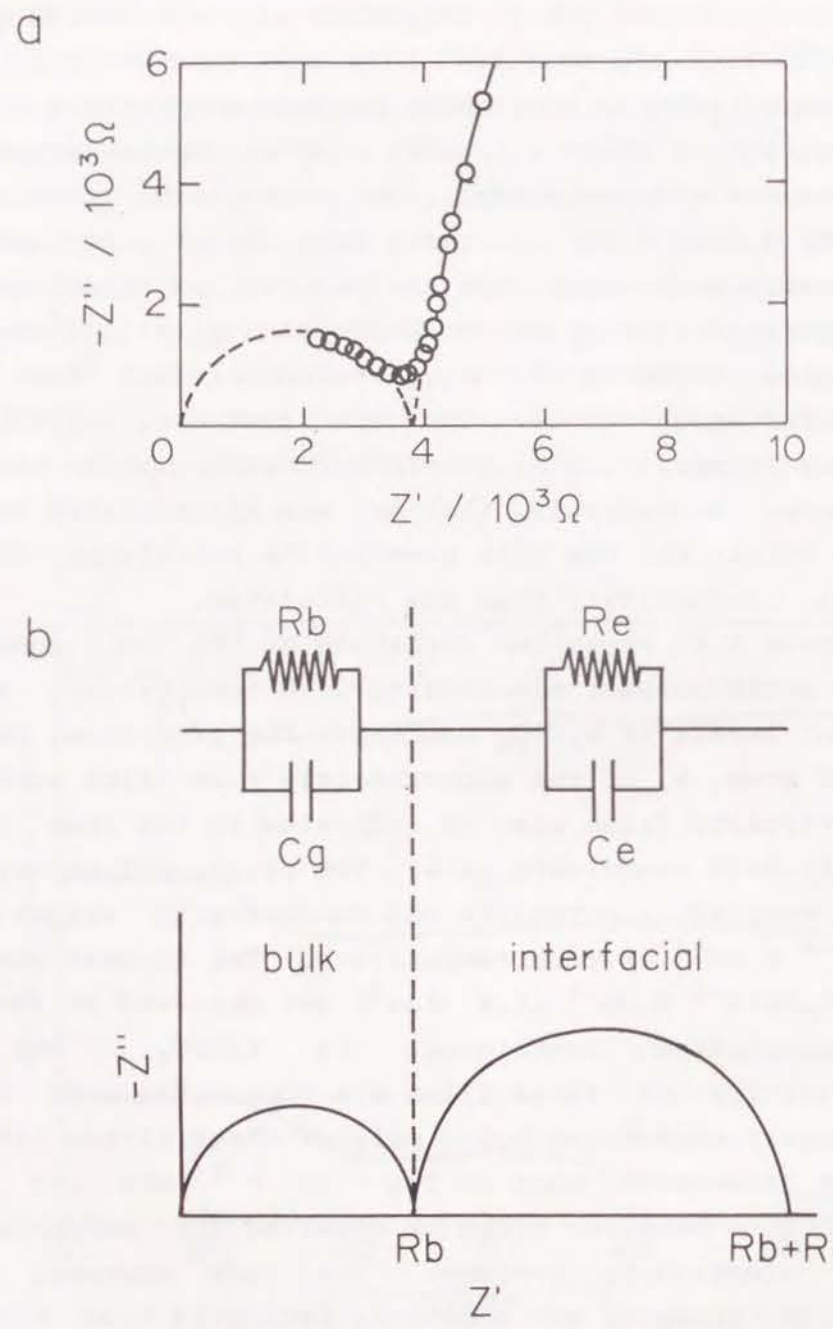

Fig. 1.19. Complex impedance measurements: (a) experimental plot for Au/ solid polymer electrolyte/Au, and (b) appropriate equivalent circuit.

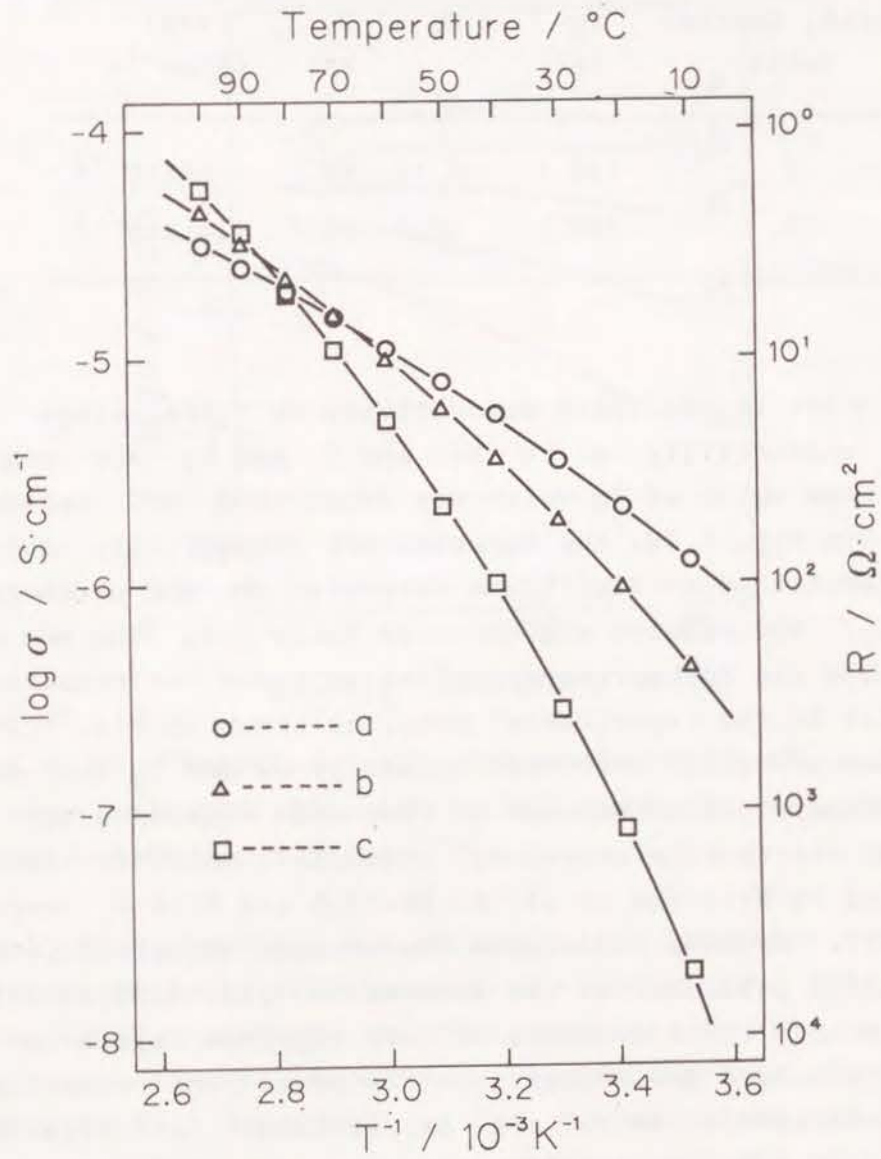

Fig. 1.20. Temperature dependence of ionic conductivity of solid polymer electrolyte containing (a) 3, (b) 7, and (c) 15 wt% $LiClO_4$.

by an equation of the WLF-type [21,22].

$$\log \frac{\sigma(T)}{\sigma(Tg)} = \frac{C_1(T-Tg)}{C_2 + (T-Tg)} \qquad [1]$$

Table 1-1 WLF parameters for solid polymer electrolytes.

$LiClO_4$ Content (wt%)	Tg (K)	C_1	C_2 (K)	σ(Tg) (S cm^{-1})
3	198.4	9.11	56.0	$3.98X10^{-12}$
7	209.1	10.5	86.1	$6.31X10^{-12}$

where σ(T) is the ionic conductivity at T (K), σ(Tg) is the ionic conductivity at Tg (K), and C_1 and C_2 are constants. Using the value of Tg value was determined DSC measurements shown in Fig. 1.18, the experimental conductivity data were computer-fitted to Eq. [1] to determine the WLF parameters, C_1 and C_2. The results are shown in Table 1-1. The use of Eq. [1] with the WLF parameters given in Table 1-1 resulted in a good fit to the experimental data, as shown in Fig. 1.20.

The so-called universal values of C_1 and C_2 that describe the temperature dependence of the ionic migration in a solid polymer electrolyte caused by segmental mobility have been reported by Williams et al. to be 17.5 and 51.6 K, respectively [21]. We have calculated the average values of C_1 and C_2 from data published in the literature [10,18,20,23-25]. In calculating these averages we have rejected values in excess of two standard deviations from the mean. The results at the 95% confidence level are as follows: $C_1=9.97\pm4.50$ and $C_2=60.5\pm30.1$ K. Thus, although our values of C_1 are somewhat lower than the universal value, and our values of C_2 somewhat higher; nevertheless, our values are in good agreement with those reported by other workers. Therefore it can be concluded from the temperature dependence of the ionic conductivity of the polymers that the conductivity correlates to the segmental mobility of the amorphous main chain.

Figure 1.21 shows the effect of the $LiClO_4$ content on the ionic conductivity at constant temperature. In all cases, for

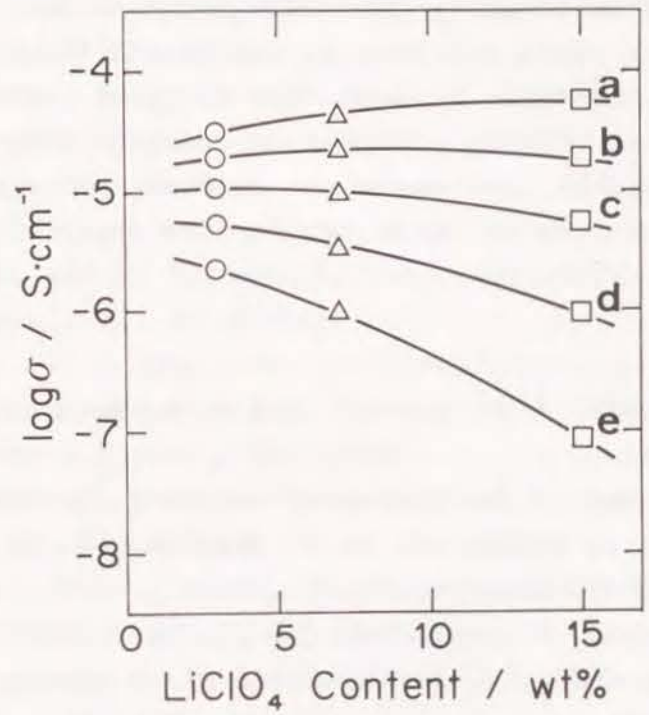

Fig. 1.21. Variation of ionic conductivity of solid polymer electrolyte with $LiClO_4$ content: (a) 100, (b)80, (c)60, (d)40, (e)20 °C.

a fixed $LiClO_4$ content, the conductivity increases approximately exponentially with increasing temperature. The effect of the $LiClO_4$ content on the conductivity at constant temperature, however, depends on the temperature. Since the conductivity is dependent on the concentration of charge carriers within the solid polymer electrolyte, the conductivity would be expected to increase with increasing $LiClO_4$ content. This is, in fact, the behavior observed at higher temperatures. However, at lower temperatures, the conductivity decreases with increasing $LiClO_4$ content. The reason for this decline is that the ionic conductivity depends not only on the concentration of carrier ions within the polymer, but also on the mobility of the individual carrier ions. The glass transition temperature of the solid polymer

electrolyte increases with increasing $LiClO_4$ content (Fig. 1.18), indicating that as the $LiClO_4$ content of the polymer is increased, the chain mobility is decreased, thereby hindering the passage of ions through the polymer network. Thus, increasing the $LiClO_4$ content increases the carrier ion concentration but decreases the carrier ion mobility. The opposing tendencies of these two factors explain the behavior shown in Fig. 1.21.

References

1. D. E. Fenton, J. M. Parker, and P. V. Wright, Polymer, 14, 589 (1973).
2. M. B. Armand, J. M. Chabagno, and M. J. Duclot, Fast Ion Transport in Solids ed. by P. Vashista, J. N. Mundy, G. K. Shenoy, Elsevier, N. Y., 1979 p. 131.
3. C. K. Chiang, Polymer commun., 22, 1454 (1981).
4. A. Hooper and J. M. North, Solid State Ionics, 9&10, 1161 (1983).
5. M. Gauthier, D. Fauteux, G. Vassort, A. Belanger, M. Duval, P. Ricoux, J. M. Chabagno, D. Muller, P. Rigaud, M. B. Armand, and D. Deroo, J. Electrochem. Soc., 132, 1333 (1985).
6. T. A. Skotheim and O. Inganas, J. Electrochem. Soc., 132, 2116 (1985).
7. K. M. Abraham, M. Alamgir, and S. J. Perrotti, J. Electrochem. Soc., 135, 535 (1988).
8. K. West, B. Zachau-Christiansen, T. Jacobsen, and S. Atlung, J. Electrochem. Soc., 132, 3061 (1985).
9. Y. Matsuda, J. Power Sources, 20, 19 (1987).
10. M. Watanabe, M. Rikukawa, K. sanui, N. Ogata, H. Kato, T. Kobayashi and Z. Ohashi, Makromolecules, 17, 2902 (1984).
11. K. Nagaoka, H. Naruse and I. Shinohara, J. Polym. Sci., Polym. Lett. Ed., 22, 659 (1984).
12. M. C. Wintersgill, J. J. Fontanella, M. K. Smith, S. G. Greenbaum, K. J. Adamic and C. G. Andeen, Polymer, 28, 633 (1987).
13. D. Fish, I. M. Khan, and J. Smid, Makromol. Chem., Rapid Commun., 7, 115 (1986).
14. K. J. Adamic, S. G. Greenbaum, M. C. Wintersgill and J. J. Fontanella, J. Appl. Phys., 60, 1342 (1986).
15. H. Yasuda and C.R. Wang, J. Polym. Sci., Polym. Chem. Ed., 23, 87 (1985).
16. M. Gazicki and H. Yasuda, J. Appl. Polym. Sci., Appl. Polym. Symp., 38, 35 (1984).
17. H. Yasuda, J. Polym. Sci., Macromol. Rev., 16, 199 (1981).
18. M. Watanabe, A. Suzuki, K. Sanui, and N. Ogata, Nippon Kagaku Kaishi, 428 (1986).
19. M. Watanabe, S. Nagano, K. Sanui, and N. Ogata, J. Power Sources, 20, 327 (1987).
20. A. Killis, J. -F. LeNest, H. Cheradame, and A. Gandini, Makromol. Chem., 183, 2835 (1982).
21. M. L. Williams, R. F. Landel, and J. D. Ferry, J. Am. Chem. Soc., 77, 3701 (1955).
22. M. Cohen and D. Turnbull, J. Chem. Phys., 31, 1164 (1959).
23. M. Watanabe, K. Sanui, and N. Ogata, J. Appl. Phys., 57, 123 (1985).
24. S. A. Greenbaum, K. J. Adamic, Y. S. Pak, M. C. Wintersgill, and J.J. Fontanella, Solid State Ionics, 28-30, 1042 (1988).
25. J. F. Lenest, H. Charadame, and A. Gandini, ibid, 28-30, 1032 (1988).

Chapter 3. Plasma-Parameter-Dependent Characteristics of Solid Polymer Electrolyte Composed of Plasma Polymerized Tris(2-methoxyethoxy)vinylsilane-$LiClO_4$ Complex

3.1 Introduction

A relatively high ionic conductivity has been reported for solid polymer electrolytes prepared by the treatment of polyethers with alkali metal salts [1,2] These solid polymer electrolytes recently have received a great deal of attention on account of their wide range of potential applications, e.g., solid state batteries, sensors, and display devices [1-5] At room temperature, however, their ionic conductivities are too low for use in electrochemical devices.

One way to solve this problem is to prepare the solid polymer electrolyte in the form of a thin film. Since plasma polymerization is an attractive method of providing uniform, ultra-thin polymer layers on various substrates [6], in Chapter 2, ultra-thin solid polymer electrolyte films was prepared by the hybridization of plasma polymerized tris(2-methoxyethoxy)vinylsilane (TMVS) with $LiClO_4$.

Plasma parameters, such as applied power, monomer flow rate, and pressure, are known to exert an important influence on the structure of the final plasma polymer [7,8]. In this Chapter, the structural changes brought about in the plasma polymer as a result of varying the plasma parameters, and, in particular, how these changes affect the ionic conductivity of the polymer was investigated.

3.2 Experimental

3.2.1 Materials

Tris(2-methoxyethoxy)vinylsilane (TMVS) (Shin-etsu Chemical Co.), methanol (Wako Chemical Co.), both of extra pure

---

Solid State Ionics, 35, 417 (1989).

grade, were used without further purification. Anhydrous lithium perchlorate (Wako Chemical Co.) was dried under reduced pressure (10^{-3} torr) at 60 °C for 12 h.

3.2.2 Plasma polymerization

The apparatus used for the plasma polymerization has been described in Chapter 1. The system consists of a glass reactor equipped with inner disk electrodes connected to an RF supply (13.56 MHz), a monomer inlet, a Pirani gauge, and a vacuum pump. Stainless steel, Ni sheets, and glass plates vapor-deposited with gold were used as substrates. The substrates were placed between the two electrodes and argon gas [10 cm^3(STP)/min] and TMVS vapor [various flow rate] were introduced into the glass reactor. The TMVS was kept at 102 C during the plasma polymerization to enhance its vapor pressure. The pressure was maintained at the desired level by controlling a main valve. Under these conditions, the RF power was turned on, and the plasma polymerization was carried out at various levels of RF power.

3.2.3 Preparation of solid polymer electrolyte [plasma polymerized TMVS-$LiClO_4$ hybrid]

First the plasma polymerized TMVS (~0.5 μm thick) was deposited on the desired substrate. Next, the substrate was removed from the reactor and sprayed with methanol containing 3% $LiClO_4$ at 60 °C to deposit a $LiClO_4$ layer. The treated substrate then was placed once more between the electrodes in the polymerization chamber and a second layer of plasma polymer (~0.5 μm thick) was deposited on the $LiClO_4$ layer under the same conditions. The resulting three-layer composite (plasma polymer-$LiClO_4$-plasma polymer) was maintained at 80 °C for 24 hours under 10^{-3} torr to permit the $LiClO_4$ to distribute uniformly throughout the plasma polymer. This treatment leads to an ultra-thin (~1 μm thick) film of solid polymer electrolyte [plasma polymerized TMVS-$LiClO_4$ hybrid]. Conventional inert-atmosphere techniques were utilized during the

preparation of the hybrid polymer in order to prevent contamination by water. The resulting film was stable, and lithium metal retained its metallic color after being in contact with the film for several days, indicating that the water content of the solid polymer electrolyte film was very low. The $LiClO_4$ content of the solid polymer electrolyte film was determined by an atomic absorption spectrophotometric measurement, which yielded a value of 3 wt% $LiClO_4$.

3.2.4 Measuring techniques

Values of the ionic conductivity of the solid polymer electrolyte were obtained from A.C. impedance measurements made using a vector impedance meter over the frequency range of $2x10^2$-$2x10^4$ Hz. The solid polymer electrolytes were sandwiched between gold layers for the purpose of making these measurements. EPMA was carried out using a Hitachi-Horiba EMAX-1770. FT-IR spectra were obtained with a Shimadzu 4100-IR-spectrometer.

3.3 Results and Discussion

3.3.1 Characterization of the plasma polymer

Plasma polymerization is known to produce a polymer that has a structure drastically different from that of the starting monomer [6]. The plasma parameters, e.g., applied power, monomer flow rate, and pressure, exert an important influence on the structure of the resulting plasma polymer. Although the conditions were fairly mild in the present work, the structure of the resultant polymers nevertheless should be dependent on these operating conditions, and it is to be expected that any changes in the structures of the polymers should result in corresponding changes in their ionic conductivities.

The effect of RF power on the polymer deposition rate was the first parameter to be examined. The effect is shown in Fig. 1.22, which shows data obtained using a monomer flow rate

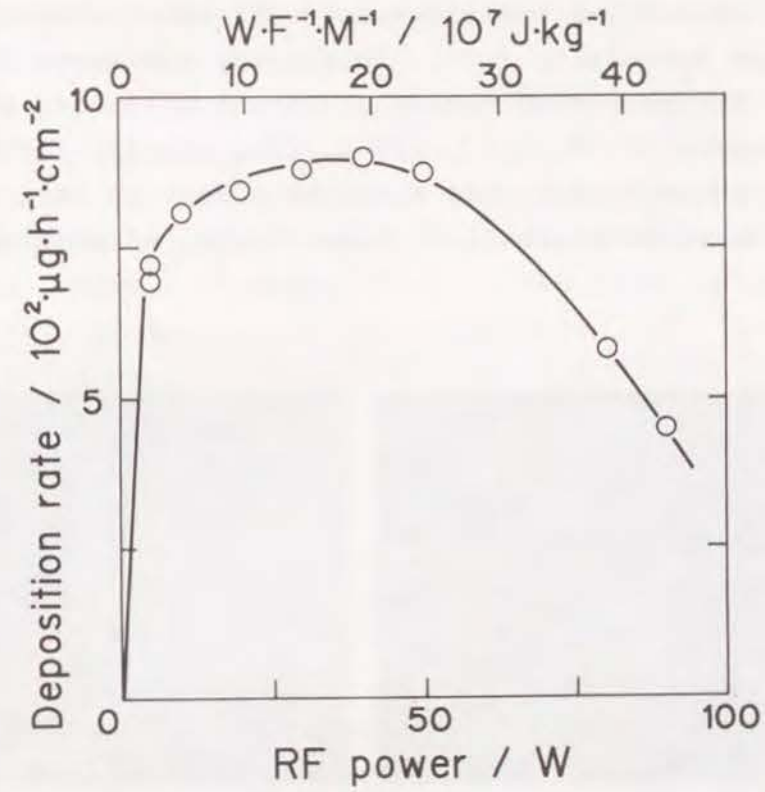

Fig. 1.22. Dependence of deposition rate on RF power. [monomer flow rate = 1 cm^3(STP)/min; pressure = 0.3 torr]

of 1 cm^3 (STP)/min and a pressure of 0.3 torr. The parameter denoted W/FM, which is indicated on the upper abscissa in Fig. 1.22, defines the input energy of the RF power per unit mass of monomer [8,9]. In this parameter, W is the input RF power, F is the flow rate of the TMVS, and M is the molecular weight of the TMVS. Various combinations of flow rates and W can be simplified using the parameter W/FM [8]. The results shown in Fig. 1.22 can be explained by the CAP (Competitive Ablation and Polymerization) mechanism [10-12]. As indicated in Fig. 1.22, at values of RF power (W/FM) lower than about 10 W, the deposition rate increases dramatically with increasing

RF power, while at powers greater than about 50W the deposition rate decreases with increasing RF power. At RF powers between 10W and 50W the power does not exert a strong influence on the deposition rate. Increasing the power leads to an increase in the concentration of reactive species up to the plateau region (10 W-50 W). In plateau region, further increments in power do not have a strong effect on the concentration of reactive species. At high powers, an ablation process

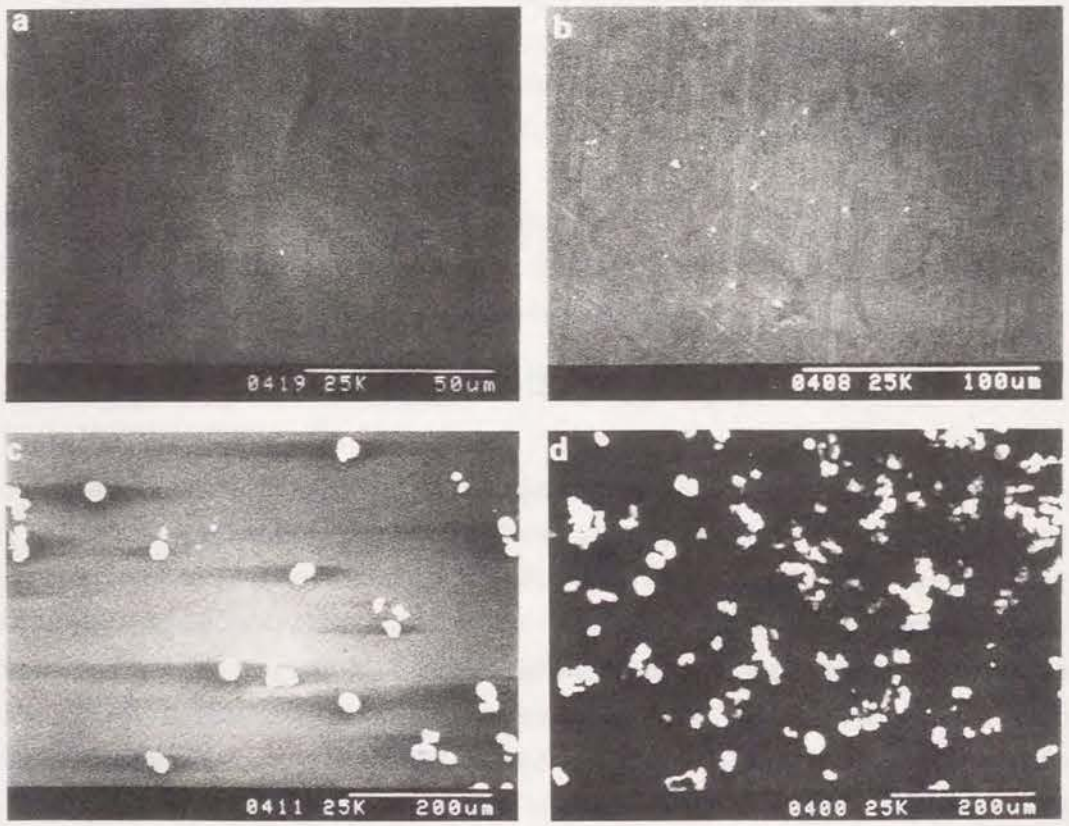

Fig.1.23. Scanning electron micrographs of surface of plasma polymer films prepared at different RF powers. [monomer flow rate = 1 cm^3(STP)/min; pressure = 0.3 torr] (a) 20 W; (b) 30 W; (c) 40 W; (d) 50 W.

takes place instead of the polymerization process. Thus, at low power levels polymerization is the dominant process, whereas above a certain power level (50 W), the ablation process becomes significant.

Figure 1.23 shows scanning electron micrographs of the surface of the plasma polymer film. In the low range of RF power (below 20 W), the surface of the plasma polymer film is planar, as shown clearly in Fig. 1.23a. Observation of the micrographs shows, however, that in the high range of RF power, many spherical particles are formed at the polymer surface, as shown in Figs. 1.23c and 1.23d, and that the extent of spherical particles formation increases with increasing RF power. From these observations it can be inferred that the activated species react with each other in the gas phase, leading to the formation of small particles [13,14]. Thus increased power enhances the gas phase reaction, which in turn leads to an increase in the amount of powder formation.

Figure 1.24 shows the IR spectra of TMVS [Fig. 1.24a] and of plasma polymers formed under three different values of W/FM [Figs. 1.24b-d]. At low values of W/FM [Fig. 1.24b] the IR spectrum of the polymer was similar to that of the TMVS, except for the complete absence of the characteristic peak for the olefin group, which occurs at about 1600 cm^{-1}. Conversely, significant differences were observed between the patterns of the absorption bands of TMVS and for the plasma polymers formed at high values of W/FM [Fig. 1.24c and d]. Except for the regions of 1050-1250 cm^{-1} (corresponding to Si-O-Si, Si-O-C stretching), at high values of W/FM the strength of all the other peaks was decreased and the absorption peaks were broadened. These observations suggest that Si-O-Si cross-linking proceeded at high values of W/FM as a result of the decomposition of monomer and of the ablation of deposited polymer due to the high applied power per unit mass of monomer.

Polymerization in a glow discharge consists of two different process, viz., plasma-induced polymerization and plas-

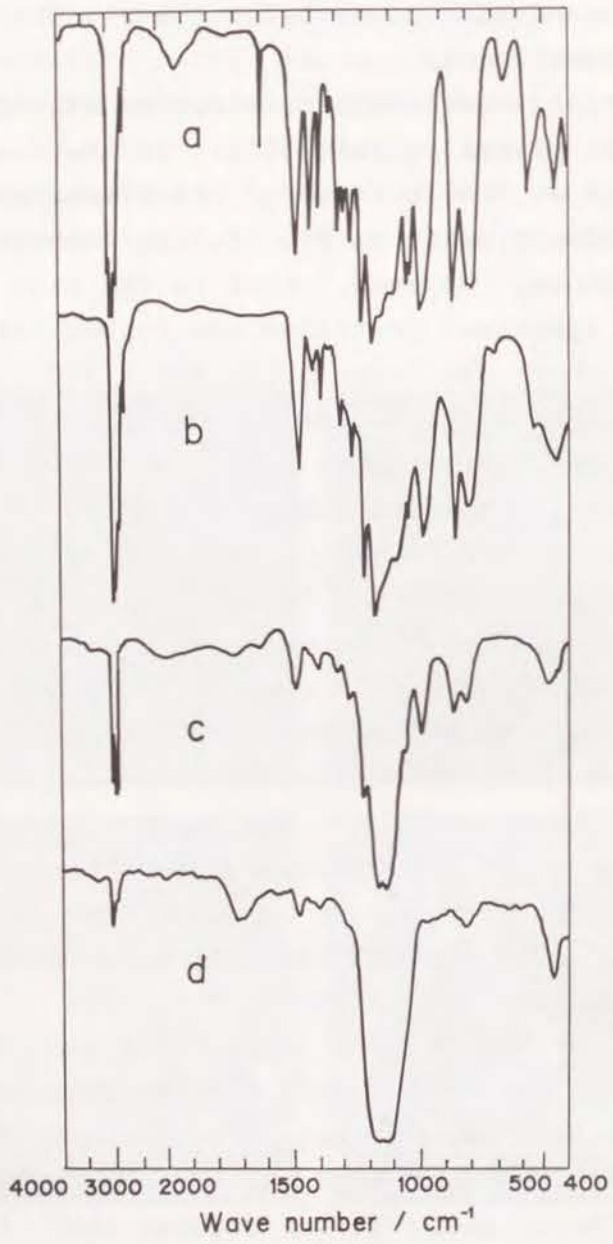

Fig. 1.24. IR spectra of tris(2-methoxyethoxy) vinylsilane (a), and its plasma polymers at W/FM values of (b) 2.4×10^7; (c) 38.3×10^7; (d) 67.1×10^7 J/kg. [pressure = 0.3 torr]

ma-state polymerization [6]. Plasma-induced polymerization (molecular polymerization) proceeds by a chain propagation mechanism [conventional polymerization mechanism]. This type of polymerization mechanism can be initiated by an ion, a radical, or a highly energetic species in the glow region. On the other hand, in the case of plasma-state polymerization (atomic polymerization), monomer is first decomposed to form reactive species, followed by a recombination of the generated reactive species to form polymer. At low values of W/FM, plasma-induced polymerization is dominant. As can be seen in Fig. 1.22, the deposition rate at 5 W is fairly high. This fact indicates that plasma-induced polymerization is dominant

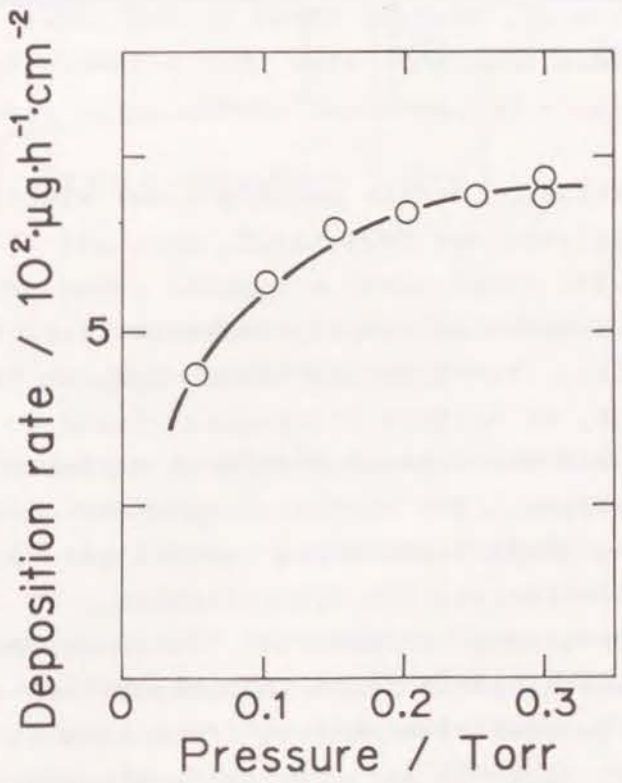

Fig. 1.25. Dependence of deposition rate on preparation pressure.
[monomer flow rate = 1 cm^3(STP)/min; RF power = 5W]

at 5 W because it is known that plasma-induced polymerization is able to proceed at even lower power levels. At high power levels, plasma-state polymerization is dominant.

Figure 1.25 illustrates the effect of pressure on the polymer deposition rate at a constant monomer flow rate of 1 cm^3 (STP)/min and RF power of 5W. It is seen that the deposition rate decreased with decreasing pressure. Since decreasing the pressure enhances electron temperature and increases electron density [10], the ablation process becomes significant at low pressure. Conversely, at a fixed value of W/FM, increasing the pressure increases both the number of reactive species and the possibility of reaction between reactive species. Polymers formed under high pressure (power: 5-10 W) were found to be soluble in organic solvents such as acetone and methyl sulfoxide, whereas those formed under low pressure were not soluble. This indicates that polymers formed at low pressure are highly branched and highly cross-linked.

3.3.2 Characterization of the solid polymer electrolyte
[plasma polymerized TMVS-$LiClO_4$ complex]

Figure 1.26, which shows a typical cross-sectional view of the solid polymer electrolyte, indicates that the film was about 1 μm thick, free from pin-holes, and, on the scale of SEM observation, of uniform thickness. Prior to making A.C. measurements, gold was deposited on both surfaces of the solid polymer electrolyte. The fact that no short circuiting was observed between these sandwiching gold layers shows that the solid polymer electrolyte was free pinholes.

EPMA observations showed that the distribution of Cl (i.e., ClO_4^-) was almost uniform throughout the cross-section of the solid polymer electrolyte. From this it can be inferred that, in order to satisfy the requirement of electroneutrality, the lithium ion also must have been uniformly distributed throughout the solid polymer electrolyte. Thus it can be concluded that the $LiClO_4$ diffuses thoroughly and uniformly into the plasma polymer.

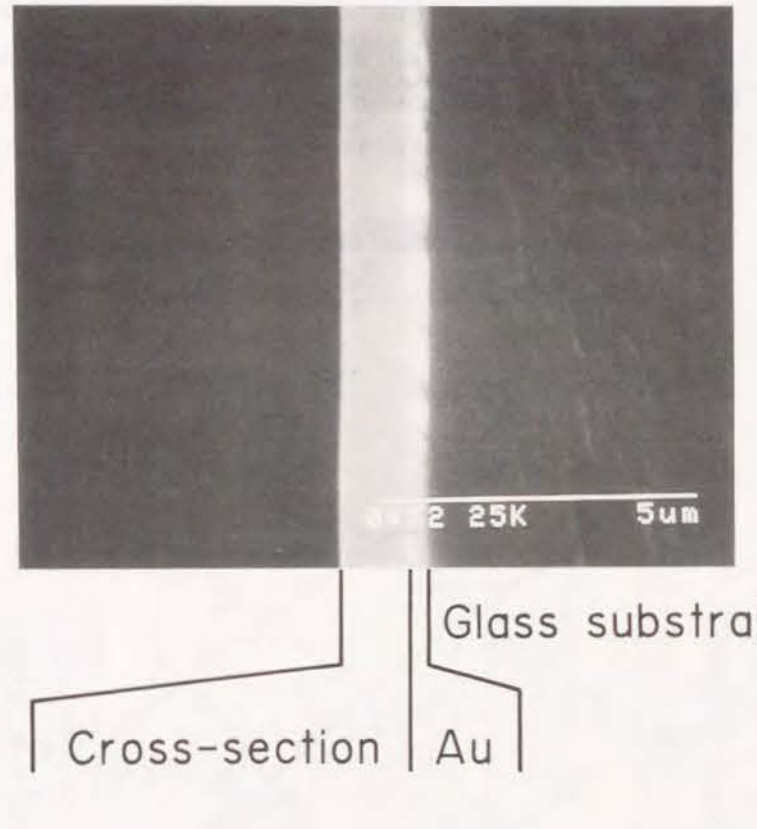

Fig. 1.26. Scanning electron micrograph of cross-section of solid polymer electrolyte.

3.3.3 Ionic conductivity of the solid polymer electrolyte

The ionic conductivity of the solid polymer electrolyte was measured by the complex impedance method using gold electrodes. Two arcs were distinguishable in the resulting complex impedance plots. In solid polymer electrolytes the capacitance of the electrolyte/ electrode interface, Ce, generally is much lager than the geometrical capacitance, Cg [15]. Therefore, the first arc, for the high frequency range, was attributed to the resistance of the bulk electrolyte, and was extrapolated to the real axis to obtain Rb, the bulk electrolyte resistance. The ionic conductivities of the solid polymer electrolytes were then calculated from these Rb

values.

The ionic conductivities of solid polymer electrolytes prepared under various pressures (at a fixed monomer flow rate of 1 cm^3 (STP)/min and RF power of 5W) are shown in Fig. 1.27 as a function of 1/T. Also indicated in Fig. 1.27 as the

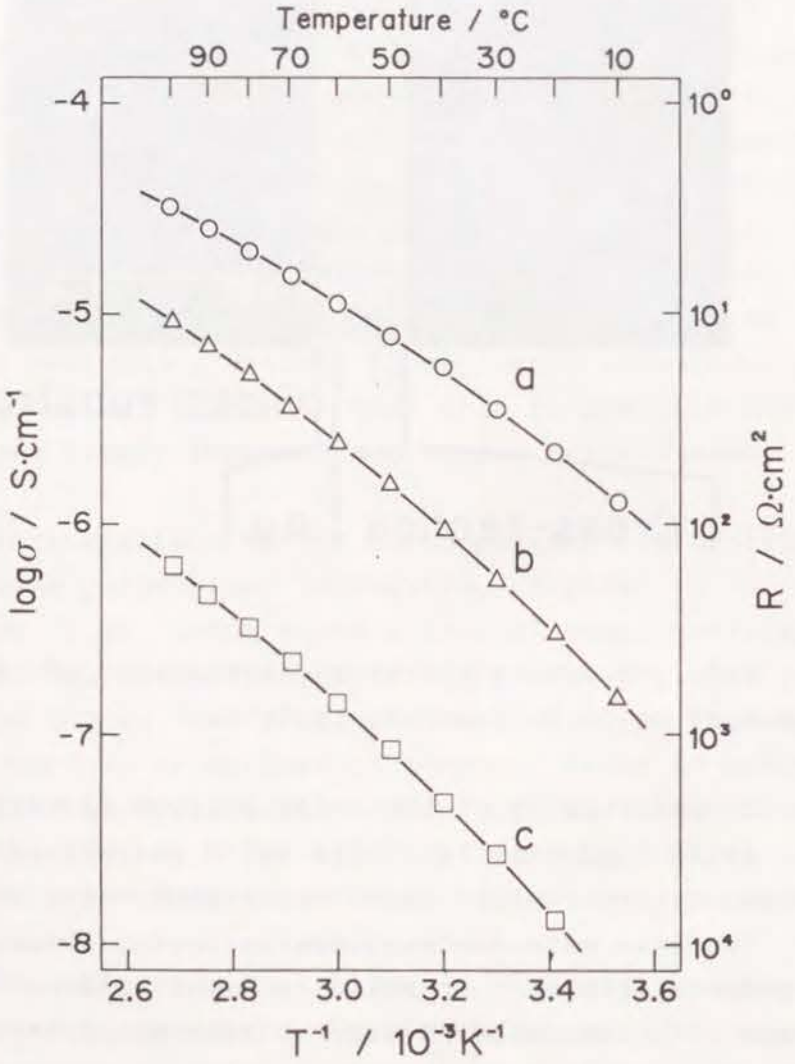

Fig. 1.27. Temperature dependence of ionic conductivity of solid polymer electrolyte prepared different pressures.
[monomer flow rate = 1 cm^3(STP)/min; RF power = 5W] (a) 0.3 torr; (b) 0.1 torr; (c) 0.05 torr.

right hand ordinate, is R, the electrical resistance per unit area of the 1 μm-thick solid polymer electrolyte film. As described in Chapter 2, the temperature dependency of the ionic conductivity of the solid polymer electrolyte correlates with the WLF equation [18,19]. At room temperature, solid

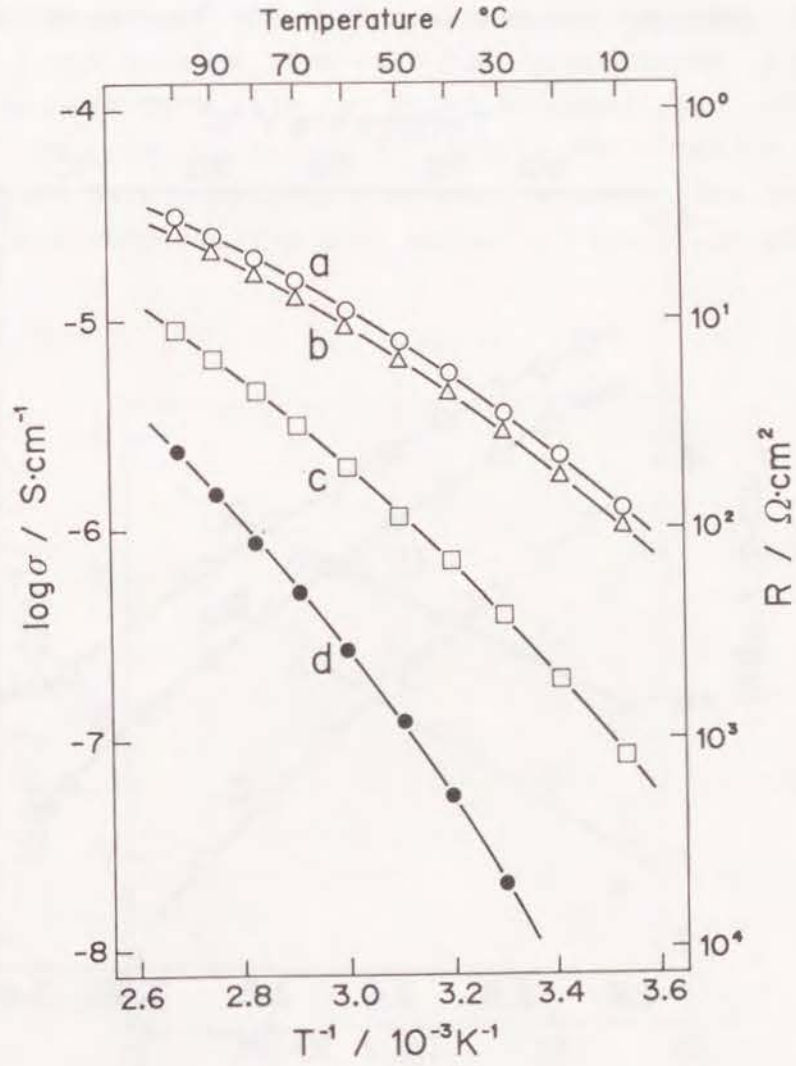

Fig. 1.28. Temperature dependence of ionic conductivity of solid polymer electrolyte prepared at different RF powers.
[monomer flow rate = 1 cm^3(STP)/min; pressure = 0.3 torr] (a) 5W; (b) 10W; (c) 20W; (d) 30W.

polymer electrolyte films prepared at a pressure of 0.3 torr exhibit conductivities of greater than 10^{-6} S cm^{-1}.

The ionic conductivity was observed to increase with increasing pressure of preparation. As described earlier, a decrease in pressure enhances the electron temperature and increases electron density, so that at low pressures the ablation process becomes significant, resulting in cross-

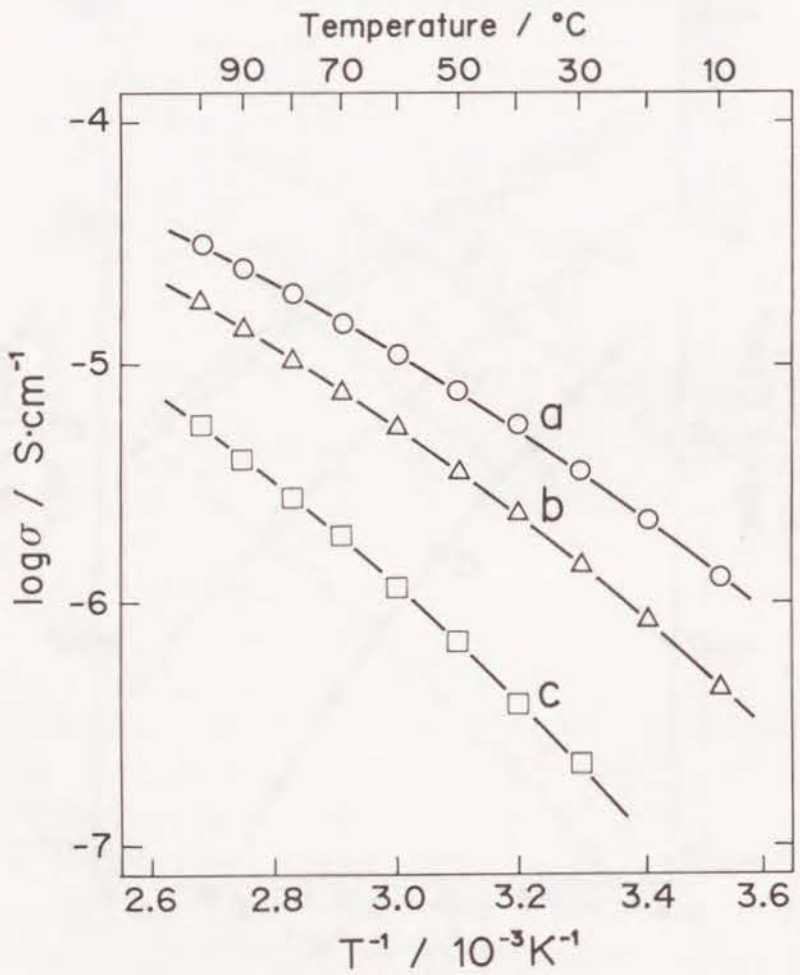

Fig. 1.29. Temperature dependence of ionic conductivity of solid polymer electrolyte prepared at different monomer flow rates.
[RF power = 5W; pressure = 0.3 torr]
(a) 1; (b) 0.5; (c) 0.2 cm^3(STP)/min.

linking. Accordingly, the glass transition temperature (Tg) of a plasma polymer prepared at a high pressure is lower than that of a plasma polymer prepared at a low pressure, leading to a higher ionic conductivity at the higher preparation pressure.

Figure 1.28 and 1.29 show the respective variation of the ionic conductivity of the solid polymer electrolyte with RF power (at fixed monomer flow rate and preparation pressure) and with monomer flow rate (at fixed RF power and operation pressure). In order to better illustrate the relative effects of the plasma parameters (RF power and monomer flow rate) on the ionic conductivity, the data shown in Figs. 1.28 and 1.29

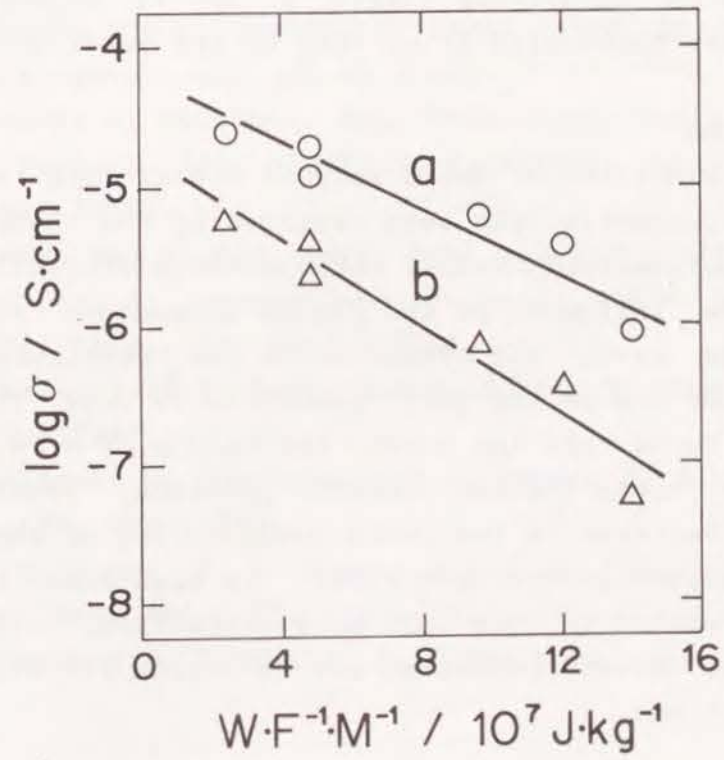

Fig. 1.30. Ionic conductivity vs. W/FM value.
[pressure 0.3 torr] (a) 80 °C; (b) 40 °C.

have been replotted in Fig. 1.30 as ionic conductivities vs. W/FM values at a constant preparation pressure of 0.3 torr. Figure 1.30 shows that ionic conductivity of the solid polymer electrolyte depends very strongly on the value of W/FM, i.e., the ionic conductivity increases exponentially as the value of W/FM decreases linearly. As discussed earlier and shown in Fig. 1.24, Si-O-Si cross-linking takes place under high W/FM conditions. Similarly, the glass transition temperature of solid polymer electrolyte prepared under high W/FM conditions is higher than that for the material prepared under low W/FM conditions. Both these facts are consistent with the observed strong decrease in conductivity with increasing values of W/FM, as shown in Fig. 1.30. Conversely, the lower the value of W/FM, the greater the ionic conductivity. However, under very low W/FM conditions ($<1\times10^{7}$ J kg^{-1}), highly viscous liquids rather than solid films form on the substrate.

3.4 Conclusion

Ultra-thin films of solid polymer electrolyte exhibiting high ionic conductivities were prepared by the hybridization of plasma polymerized tris(2-methoxyethoxy)vinylsilane with $LiClO_4$. The influence of the plasma parameters (RF power, monomer flow rate, and pressure) on the structure of the plasma polymer and on its ionic conductivity were investigated. It was found that the higher the values of W/FM, the more the Si-O-Si cross-linking reaction proceeds, leading to a concomitant decrease in the ionic conductivity of the resulting solid polymer electrolyte film. The high ionic conductivity films prepared in this work were ultra-thin, uniform, and pinhole-free. These properties are favorable for electrochemical applications.

References

1. D. E. Fenton, J. M. Parker, and P. V. Wright, Polymer, 14, 589 (1973).
2. M. B. Armand, J. M. Chabagno, and M. J. Duclot, Fast Ion Transport in Solids ed. by P. Vashista, J. N. Mundy, G. K. Shenoy, Elsevier, N.Y., 1979, p. 131.
3. M. Gauthier, D. Fauteux, G. Vassort, A. Belanger, M. Duval, P. Ricoux, J. M. Chabagno, D. Muller, P. Rigaud, M. B. Armand, and D. Deroo, J. Electrochem. Soc., 132, 1333 (1985).
4. K. M. Abraham, M. Alamgir, and S. J. Perrotti, J. Electrochem. Soc., 135, 535 (1988).
5. A. Hooper and J. M. North, Solid State Ionics, 9&10, 1161 (1983).
6. H. Yasuda, J. Polym. Sci., Macromol. Rev., 16, 199 (1981).
7. H. Yasuda and T. Hirotsu, J. Appl. Polym. Sci., 21, 3129 (1977).
8. H. Yasuda and C. R. Wang, J. Polym. Sci., Polym. Chem. Ed., 23, 87 (1985).
9. M. Gazicki and H. Yasuda, J. Appl. Polym. Sci., Appl. Polym. Symp., 38, 35 (1984).
10. H. Yasuda, J. Macromol. Sci. Chem., A10, 383 (1976).
11. H. U. Poll, M. Arzt and K. H. Wickleder, Eur. Polym. J., 12, 505 (1976).
12. H. Yasuda and T. Hse, Surf. Sci, 76, 232 (1978).
13. N. Niinoki, H. Kobayashi, A. T. Bell, and M. Schen, J. Appl. Phys., 44, 4317 (1973).
14. H. Kobayashi, A.T. Bell, and M. Schen, Macromolecules, 7, 277 (1974).
15. T. Nagatomo, C. Ichikawa, and O. Omoto, J. Electrochem. Soc., 134, 305 (1987).
16. M. L. Williams, R. F. Landel and J. D. Ferry, J. Am. Chem. Soc., 77, 3701 (1955).
17. M. Cohen and D. Turnbull, J. Chem. Phys., 31, 1164 (1959).

Chapter 4 Preparation and Characterization of Ultra-Thin Films Having Fixed Sulfonic Acid Group with Only One Mobile Species.

4.1 Introduction

Since the early investigations of solid polymer electrolyte by P. V. Wright et al. in 1973 [1] and M. B. Armand et al. in 1979 [2], efforts have been made by many workers to enhance the ionic conductivities of these electrolytes. Different kinds of solid polymer electrolytes have been studied which were formed by mixing alkali metal salts with polymers such as poly(ethylene oxide) [PEO], poly(propylene oxide) [PPO]. Among these polymers, siloxane polymers containing polar units are attractive because their glass transition temperature are generally low. A low glass transition temperature is known to be favorable for the enhancement of ionic conductivity in solid polymer electrolytes [3].

A poly(dimethylsiloxane-ethylene oxide) [poly(DMS-EO)] copolymer is an example of a material with a low glass transition temperature, and solid polymer electrolyte has been prepared from this polymer and alkali metal salts [4-7].

Since the conductivity of the film is low, its practical resistance can be lowered by decreasing the film thickness. However, it is not easy to prepare thin pinhole-free polymer films using conventional techniques. Plasma polymerization is a useful method of preparing such thin films. As described in Chapter 1, solid polymer electrolyte films was prepared by the hybridization of plasma-polymerized octamethylcyclotetrasiloxane (OMCTS) with poly(propylene oxide) and $LiClO_4$.

In most of the solid polymer electrolytes reported, both the cation and anion are mobile. When these kind of solid

---

Chemistry Letters, 1811 (1988).
J. Electrochem. Soc., 137, 29(1990).

polymer electrolytes are used in electrochemical devices, the DC ionic conductivity decreases because of high electric resistance due to the non-uniform distribution of anion and cation [8]. To improve this situation, a few polymer electrolytes with only one mobile species have been reported [8-10]. The present study focuses on the preparation of solid polymer electrolyte films sustained by single lithium ion species.

Many studies on plasma polymerization have been reported, including the preparation of siloxane polymers. However, it is difficult to introduce a sulfonic group bonded to a polymer chain using this method. Sulfonic acid groups are usually introduced by a chemical treatment after a plasma process. However, some problems may occur during this chemical treatment, including decomposition of the host polymer. In this Chapter, a sulfonic group was introduced into the siloxane polymer during the plasma polymerization process itself. The sulfonic group was first introduced as an ether by the addition of gas containing sulfonic ester group. The sulfonic ester group was then converted to a lithium salt by a reaction with lithium iodide.

$$-SO_3R + LiI \longrightarrow -SO_3^-Li^+ + RI$$

Methyl benzenesulfonate or methyl methanesulfonate was selected as the source to introduce the sulfonic ester group. OMCTS was selected as a monomer for the host polymer. The prepared plasma polymers were characterized by ESCA, FT-IR, SEM and an electron probe micro analyzer (EPMA). The plasma polymers containing lithium sulfonate were next hybridized with PEO (average M.W. 300) to form an ultra-thin film containing single mobile lithium ions.

4.2 Experimental

4.2.1 Materials

Octamethylcyclotetrasiloxane (OMCTS) (Shin-etsu Chem. Co.), poly(ethylene oxide) (PEO) (average M.W. 300), methyl methanesulfonate, methyl benzenesulfonate, butanol, propylene carbonate (Wako Chem. Co.) of extra pure grade were used without further purification. Anhydrous lithium iodide (Wako Chem. Co.) was dried under reduced pressure of 10^{-3} Torr at 60 ℃ for 12 hours.

4.2.2 Plasma polymerization

The apparatus used for the plasma polymerization has been described in Chapter 1. It consists of glass reaction chamber (9 cm diameter and 35 cm height) equipped with capacitively coupled inner electrodes which are connected to an RF power supply (13.56MHz) with an impedance matching network. The reaction chamber is fitted with two monomer inlets, a Pirani gauge and is connected to a vacuum pump system via an main valve. Glass plates deposited with gold, stainless steel and Ni sheets were utilized as the substrates. Substrates were placed between the electrodes. Argon gas [10 cm^3(STP)/min], OMCTS vapor [2 cm^3 (STP)/min] and methyl methanesulfonate or methyl benzenesulfonate vapor [various flow rates] were introduced into the glass reactor. The pressure in the reaction chamber was maintained at 0.05 Torr by controlling a main valve. After setting the gas pressure, the RF power was turned on, and the plasma polymerization was carried out at various power levels of RF power for 0.5-1 hour. The resulting plasma polymer deposits were about 1 μm thick.

4.2.3 Formation of sulfonic acid group

Polymer films deposited on substrates were soaked in sat. LiI/propylene carbonate solution at 50 ℃ for 30 min. After soaking, the films were washed with propylene carbonate to remove away the excess LiI and alkyl iodide from the films.

These treated films then were dried under reduced pressure (10^{-3} Torr) at 50 ℃ for 12 hours in order to evaporate the propylene carbonate.

4.2.4 Preparation of hybrid polymer electrolyte film

Since a siloxane group has low polarity, ionic compounds do not dissolve well in polysiloxane. Therefore, the ionic conductivity of the plasma polymer film after treatment with LiI is low and is undetectable by AC method. In order to enhance the ionic conductivity, a film treated with LiI was hybridized with PEO (averaged M.W. 300). Conventional inert atmosphere techniques were used during the following preparation of the hybrid polymer in order to prevent contamination by water. The film treated with LiI was soaked in a PEO-butanol mixture solution for 1 hour at 30 ℃. Since the PEO content of the plasma polymer did not change after 30 min, it is assumed that steady state was attained by 1 hour. After this treatment the film was dried under reduced pressure (10^{-3} Torr) at room temperature for 12 hours in order to evaporate the butanol. The above treatment gives an ultra-thin (~1 μm thick) hybrid polymer electrolyte film.

Lithium metal kept its metallic luster after several days in direct contact of the hybrid film. This observation indicates that the water content of the hybrid film was very low. Lithium ion concentration was determined by atomic absorption spectrophotometry. The PEO content was estimated from the weight change of the polymer before and after the hybridization step. Gold layer was deposited onto this polymer electrolyte for impedance measurements.

4.2.5 Measuring techniques

Alternating current impedance measurements were made over the frequency range $2x10^2$-$2x10^4$ Hz with a vector impedance meter.

The cross-section of the film deposited on a glass substrate was observed by SEM. The thickness of the film was

estimated from SEM figures. Electron probe micro analysis (EPMA) were performed with a Hitachi-Horiba EMAX-1770. FT-IR spectra were obtained using a multirefluction method using a Shimadzu 4100-IR-Spectrometer.

4.3 Results and discussion

4.3.1 Characterization of plasma polymer

The RF power input energy per unit mass of monomer is defined by the parameter W/FM, where W is an input RF power, F is a monomer flow rate, and M is the molar mass of the monomer. The values of these plasma preparation parameters are given in Table 1-2.

The Plasma polymers were colorless. The IR spectra of the plasma polymers formed from OMCTS and methyl benzenesulfonate and from OMCTS and methyl methanesulfonate are shown in Fig. 1.31(a) and (b), respectively. The EPMA spectra of these two polymers suggested that the polymers had same Si-to-S ratio. Reference to the IR spectra of Fig. 1.31 and to Table

Table 1-2. Plasma polymer preparation parameters

	Monomer	
	Methyl Benzenesulfonate	Methyl Methanesulfonate
W (watts)	20	10
F (mol/s)	7.44×10^{-7}	1.49×10^{-6}
M (kg/mol)	0.172	0.110
W/FM (J/kg)	1.6×10^{8}	6.1×10^{7}

1-3 shows that the two polymers exhibit many absorption bands in common.

The polymer of Fig. 1.31(a) exhibits absorption peaks at 3050 cm^{-1}, 1600 cm^{-1}, 1490 cm^{-1}, 1480 cm^{-1}, 1450 cm^{-1}, 1360 cm^{-1} and 1180 cm^{-1}. These peaks are not observed

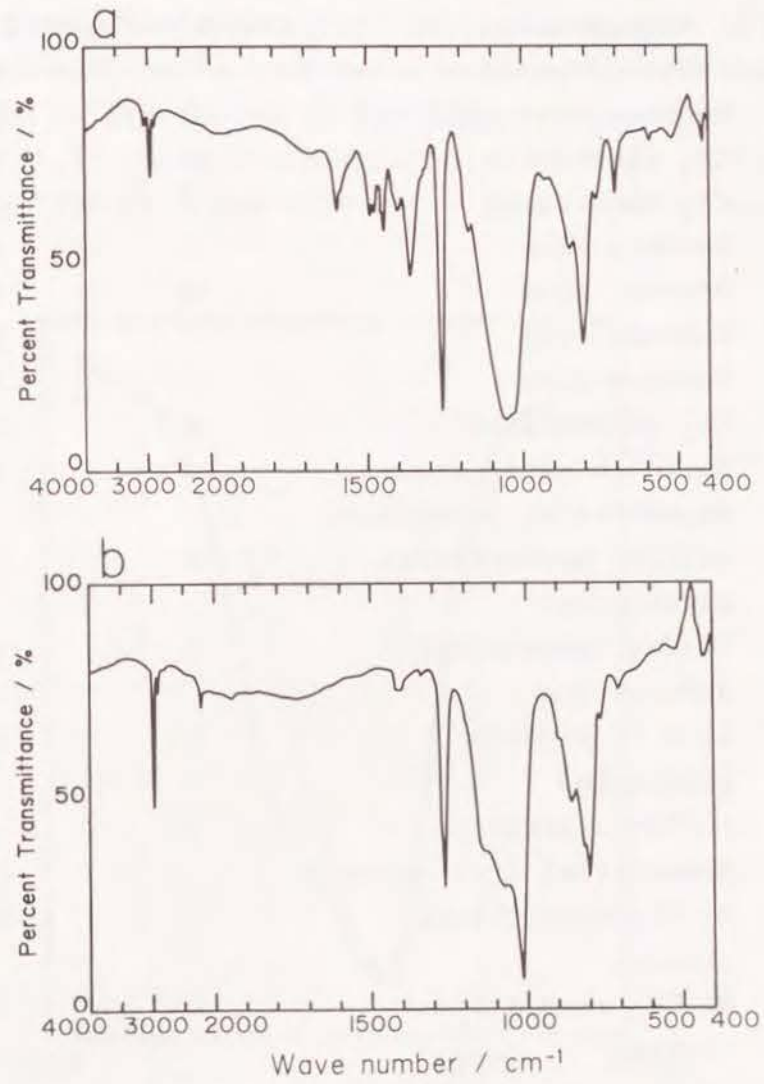

Fig. 1.31. IR spectra of plasma polymers.
(a)polymer formed from OMCTS [1.49×10^{-6} mol/sec] and methyl benzenesulfonate [7.44×10^{-7} mol/sec],
(b)polymer formed from OMCTS [1.49×10^{-6} mol/sec] and methyl methanesulfonate [1.49×10^{-6} mol/sec].

Table 1-3. Features of IR spectra of plasma polymers
(O = present, X = absent)

λ^{-1} (cm^{-1})	Assignment	Plasma polymer		
		OMCTS/MBS[a]	OMCTS/MMS[b]	OMCTS[c]
3050	Benzene ring	O	X	X
2960	CH_3 stretching	O	O	O
2900	CH_2 stretching	O	O	O
1600	Benzene ring	O	X	X
1490	Benzene ring	O	X	X
1480	Benzene ring	O	X	X
1450	Benzene ring	O	X	X
1410	CH_3 deformation	O	O	O
1360	Sulfonic ester group asymmetrical stretching	O	X	X
1275	sulfone asymmetrical stretching	X	O	X
1260	Si-CH_3 symmetrical deformation	O	O	O
1200-1100	Si-O-C, Si-O-Si stretching	O	O	O
1180	Sulfonic ester symmetrical stretching	O	X	X
840	Si-CH_2 symmetrical rocking	O	O	O
800	Si-CH_2 asymmetrical rocking	O	O	O

a:Plasma polymer formed from OMCTS and methyl benzenesulfonate
b:Plasma polymer formed from OMCTS and methyl methanesulfonate
c:Plasma polymer formed from OMCTS

in the IR spectrum of the plasma polymer formed from OMCTS. The two peaks at 1360 cm^{-1} and 1180 cm^{-1}, which are assigned, respectively, to asymmetrical and symmetrical stretching vibration modes of sulfonic ester group, are not observed in Fig. 1.31(b). This suggests that the plasma polymer prepared from methyl benzenesulfonate contains sulfonic ester group while that prepared from methyl methanesulfonate does not. The peaks at 3050 cm^{-1}, 1600 cm^{-1}, 1490 cm^{-1}, 1480 cm^{-1} and 1450 cm^{-1} can be attributed to the benzene ring [15].

Figure 1.32 shows a magnified part of Fig. 1.31(a) and (b) between 1300 cm^{-1} and 1230 cm^{-1}. The common absorption

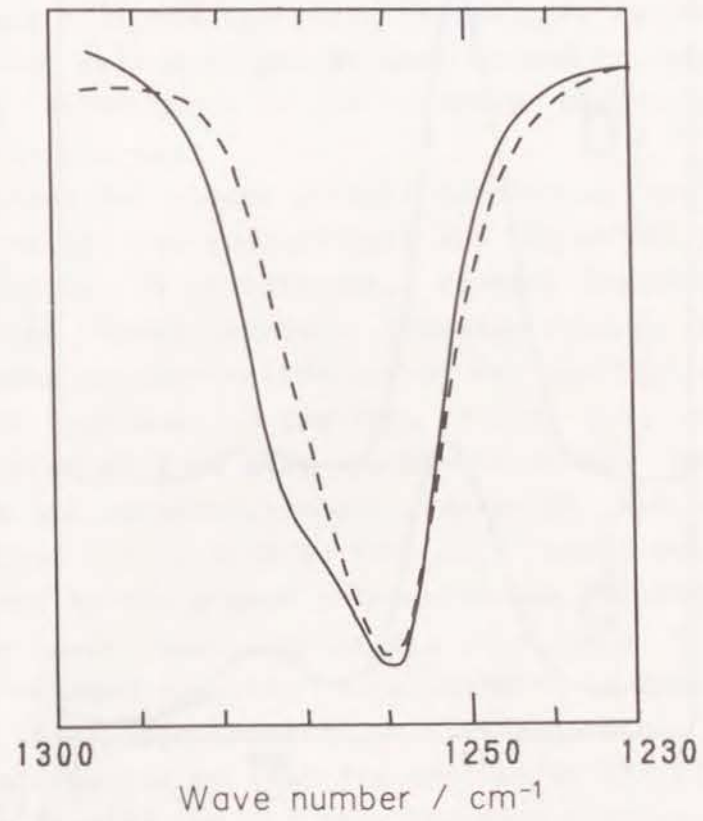

Fig. 1.32. IR spectra between 1300-1230 cm^{-1}.
Broken line: plasma polymer of Fig. 1.31(a),
Solid line: plasma polymer of Fig. 1.31(b).

peak at 1260 cm^{-1} is assigned to Si-CH_3 symmetrical deformation. The polymer prepared from methyl methanesulfonate (solid line) shows a new absorption peaks at 1275 cm^{-1}. This peak could be assigned to asymmetrical stretching vibration of the sulfone (-SO_2-) group. This result, together with the absence of sulfonic ester absorption bands at 1360 cm^{-1} and 1180 cm^{-1}, suggests that the plasma polymer prepared from methyl methanesulfonate contains sulfone groups instead of sulfonic ester group. This is further supported by Fig.

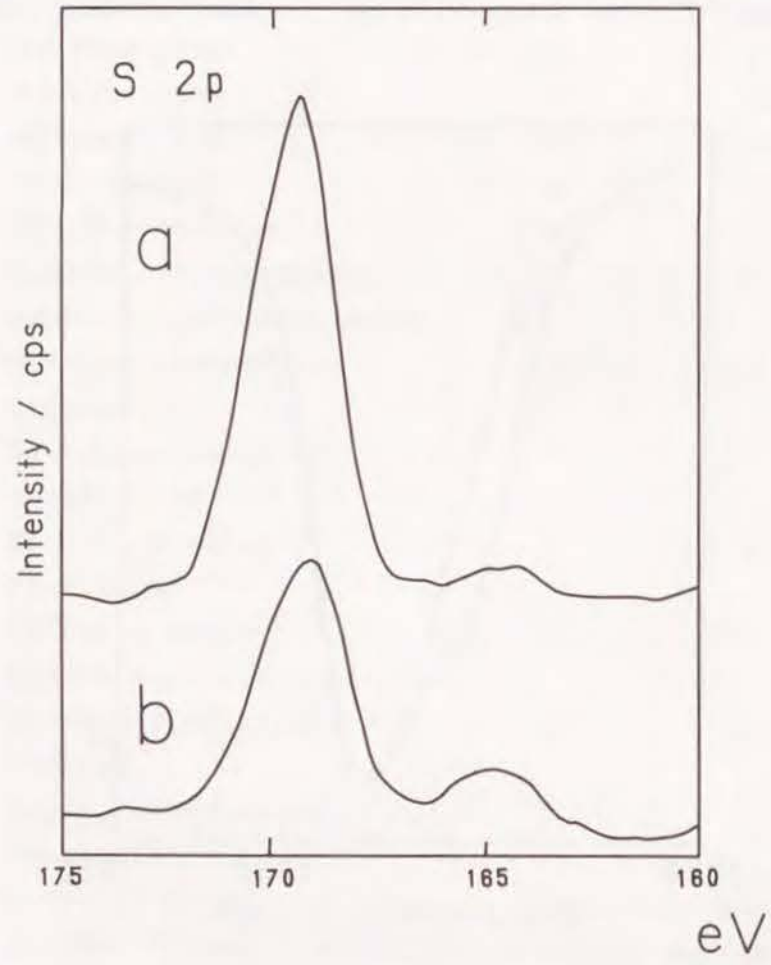

Fig. 1.33. ESCA S_{2p} spectra of plasma polymers. (a)plasma polymer of Fig. 1.31(a), (b)plasma polymer of Fig. 1.31(b).

1.33(a) and (b), which show the respective ESCA S_{2p} spectra of the polymer of Fig. 1.31 (a) and (b). The peak at 169.3 eV for the polymer prepared from methyl benzenesulfonate can be assigned to the sulfonic ester group [16], while the peak at 169.0 eV for the plasma polymer prepared from methyl methanesulfonate can be assigned to the sulfone group [16]. The common weak peak at about 164.5 eV probably corresponds to the sulfoxide (-SO-) group [16,17]. The foregoing results suggest that the plasma polymer formed from methyl benzenesulfonate contains sulfonic ester groups and may contain a small quantity of sulfoxide, the plasma polymer formed from methyl methanesulfonate contains sulfone groups and a somewhat lager quantity of sulfoxide. In spite of the relatively low plasma input energies utilized (low W/FM values), it is inferred that the sulfone and sulfoxide groups were formed by decomposition of sulfonic ester group in the monomers during the plasma polymerization process.

The reason the plasma polymer functional group differs between the methyl benzenesulfonate and the methyl methanesulfonate reactions is of interest. Because reactive species exist at a high concentration in the glow region, the reaction path in plasma polymerization cannot be exactly determined. The reactive species in the glow region can, however, be partially inferred from mass spectra of methyl benzenesulfonate and methyl methanesulfonate. Although radical species and/or radical anions such as $[\Phi SO_3CH_3]^-$ might well play an important role in the plasma polymerization process, unfortunately, our mass spectrometer was only able to determine positively charged species. Nevertheless, in spite of this limitation, mass spectrometry is a very useful method for obtaining information on reactive species in the glow region.

Figure 1.34(a) and (b) show the mass spectra of methyl benzenesulfonate and methyl methanesulfonate, respectively. Ionization was effected by electron bombardment at 10, 15, 20 eV. The average electron temperature under the glow discharge used in this study was less than 10 eV [18]. Therefore, the

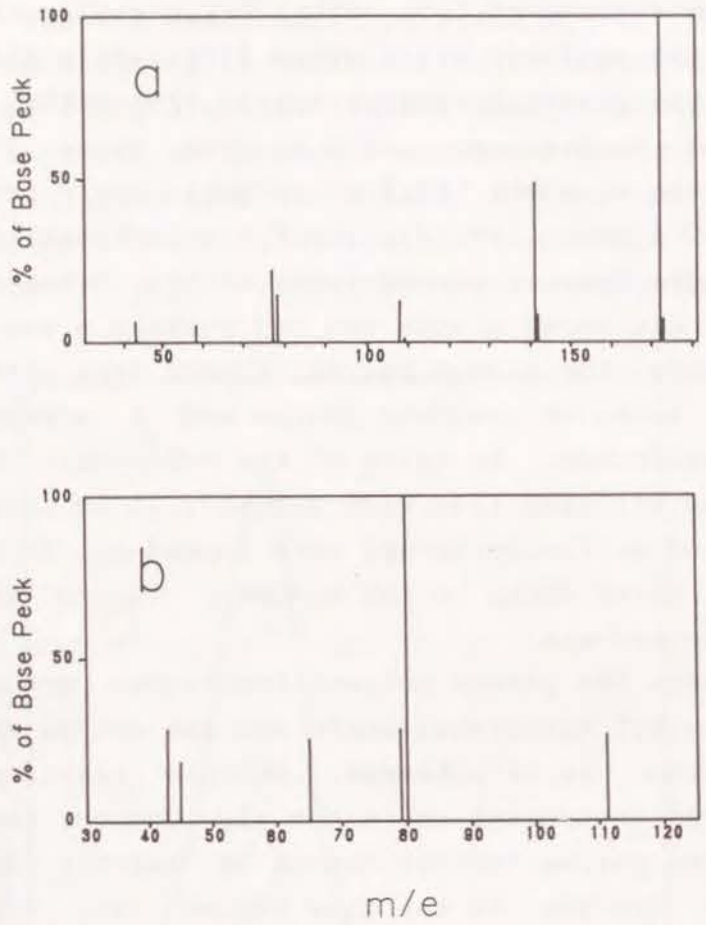

Fig. 1.34. Mass spectra of monomers (electron temperature: 10 eV).
(a)methyl benzenesulfonate,
(b)methyl methanesulfonate.

fragmentation at 10 eV should be similar to that under the glow discharge conditions. The mass spectrum of methyl benzenesulfonate at 10 eV has a main peak at m/e = 172, which is the parent peak. A similar spectrum is obtained at 15eV, but the spectrum at 20eV is different. At 20 eV the parent peak becomes smaller and the peak at m/e = 77 becomes lager because fragmentation proceeds more extensively than at the lower

energy levels. The species at m/e = 172 (denoted by a in the accompanying reaction scheme) is one of the main active ionic species under the present plasma polymerization conditions. The reaction of this species with other monomer (e.g., with OMCTS) yields a polymer containing sulfonic ester groups. Sulfonic ester group can be introduced by aromatic substitution, which results in the fixation of benzenesulfonic ester group to the polymer chain. At high electron temperatures such as 20 eV, decomposition of the parent species proceeds extensively.

The mass spectrum of methyl methanesulfonate at 10 eV (Fig. 1.34 b) indicates that a peak at m/e = 80 is the main peak. The structure of the species of m/e = 80 is indicated as (b) in the reaction scheme [19]. Reaction of this species with other monomers (e.g., OMCTS) yields a polymer containing sulfone group. This is in accordance with the results of the

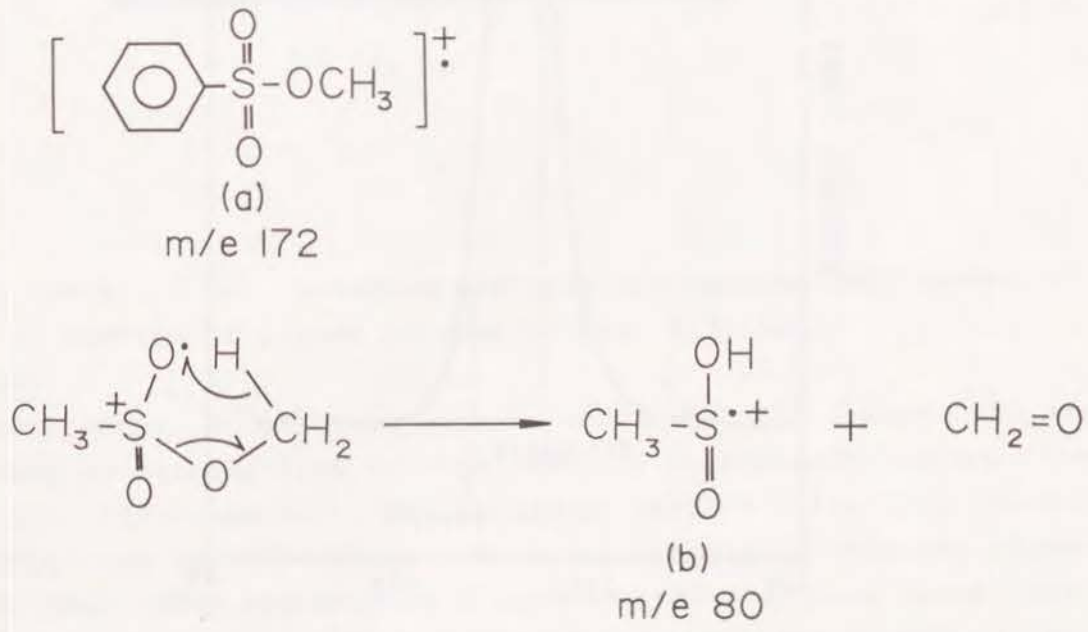

Reaction scheme showing ionic species generated during plasma polymerization.

IR spectra (Fig. 1.31 and 1.32) and of the ESCA S_{2p} spectra (Fig. 1.33).

Figure 1.35 shows the ESCA Si_{2p} spectrum of the polymer of Fig. 1.31(a). The spectrum for the polymer of Fig. 1.31(b) was almost identical. The value of the chemical shift of the Si_{2p} peak is not similar to that of poly(dimethylsiloxane) but rather to that of a silicate. This suggests that the Si-O-Si cross-linking reaction proceeded extensively.

Figure 1.36 shows a scanning electron micrograph of the cross-section of a plasma polymer formed from methyl benzene-

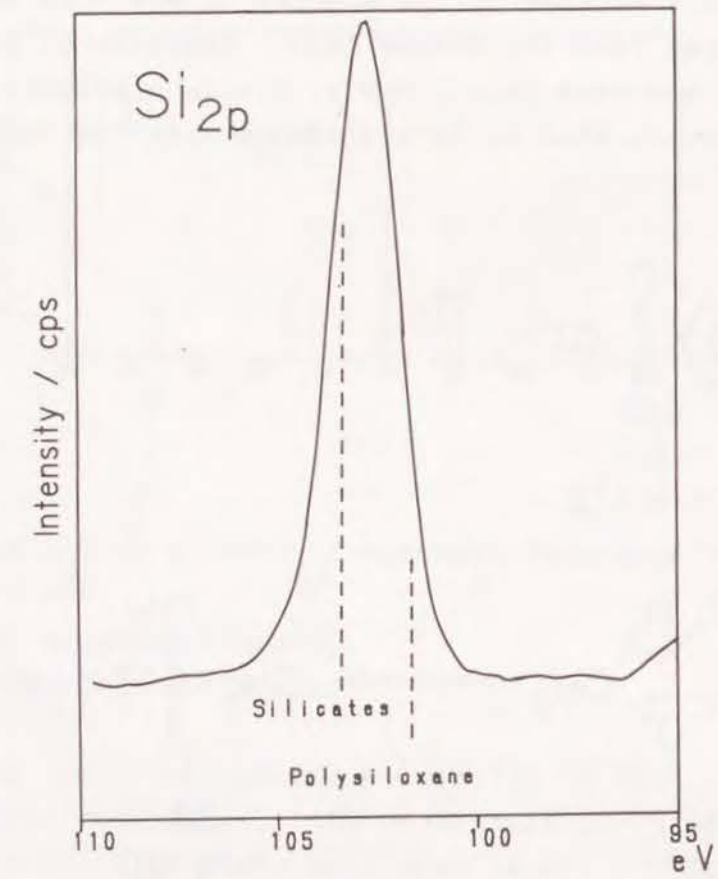

Fig. 1.35. ESCA Si_{2p} spectrum of plasma polymer of Fig. 1.31(a).

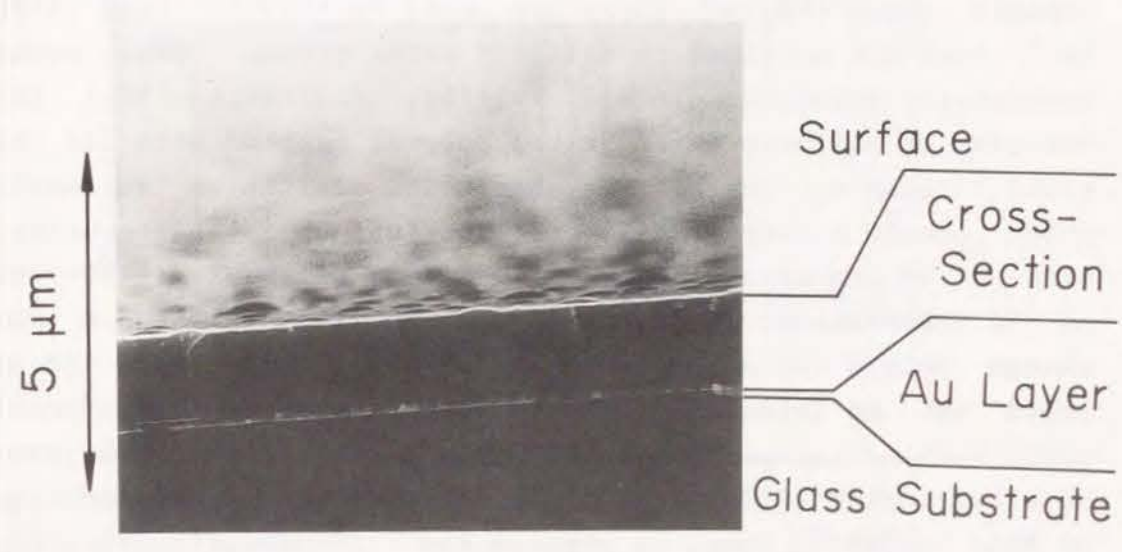

Fig. 1.36. Scanning electron micrographs of cross-section of plasma polymer of Fig. 1.31(a).

sulfonate. This figure clearly shows that the plasma polymer film is pinhole-free on this scale of observation. Also, the film thickness (~1.3 µm) is almost uniform with only slight roughness on the surface. Gold was evaporated onto the plasma polymer film prepared on a gold-covered stainless steel substrate. The electrical resistance between the two gold layers was in excess of 1 MΩ , implying that the two gold layers were not short circuited, i.e., that the plasma polymer film was pinhole-free.

4.3.2 Transformation to lithium sulfonate group

The plasma polymer films were treated with saturated LiI/ propylene carbonate solution to yield lithium sulfonate groups. Figure 1.37 shows the IR spectra of the plasma polymer from methyl benzenesulfonate before [Fig. 1.37(a)] and after [Fig. 1.37(b)] the treatment with LiI. Figure 1.37(a) clearly shows the two absorption peaks at 1360 cm^{-1} and 1180 cm^{-1} that are ascribed to sulfonic ester group. These peaks completely disappear in Fig. 1.37(b), indicating that the reaction of sulfonic ester in the polymer reacted with LiI to yield lithium sulfonate. The absorption of lithium sulfonate which should appear at 1175 cm^{-1} and 1055 cm^{-1} [15] overlaps with a strong absorption of Si-O-C and Si-O-Si (1180-1000 cm^{-1}). EPMA observation showed that the Si/S ratio did not change before and after treatment with LiI, and that iodine could not be detected. This indicates that the sulfonate group remains in the plasma polymer. Moreover, the absorption of alkyl iodide (600-580 cm^{-1}) is not observed in the spectrum of Fig. 1.37(b). Thus, it appears the lithium sulfonate group is fixed to the backbone chain of the polymer.

The polymer treated with LiI was soaked in aqueous 0.5 M CsOH for about 30 min and thoroughly washed with distilled water. The sample was covered with a thin layer of Ag to prevent it from charging up during EPMA measurements. The resulting EPMA spectrum (Fig. 1.38) shows the existence of Cs in the plasma polymer, indicating that the plasma polymer behaves as an ion-exchanger. In order to confirm that the strong basic CsOH did not cleavage the siloxane bonds to form a SiOCs salts, a plasma polymer formed from OMCTS, which did not contain sulfonic acid group, also was soaked in 0.5M aq. CsOH for about 30 min and washed thoroughly with water. After this treatment, no Cs was detected in the polymer film by EPMA, indicating that any siloxane bond cleavage reaction either is very slow or does not occur.

The ratio of sulfur contributing to ion-exchange vs. total sulfur contained in the plasma polymer was roughly estimated

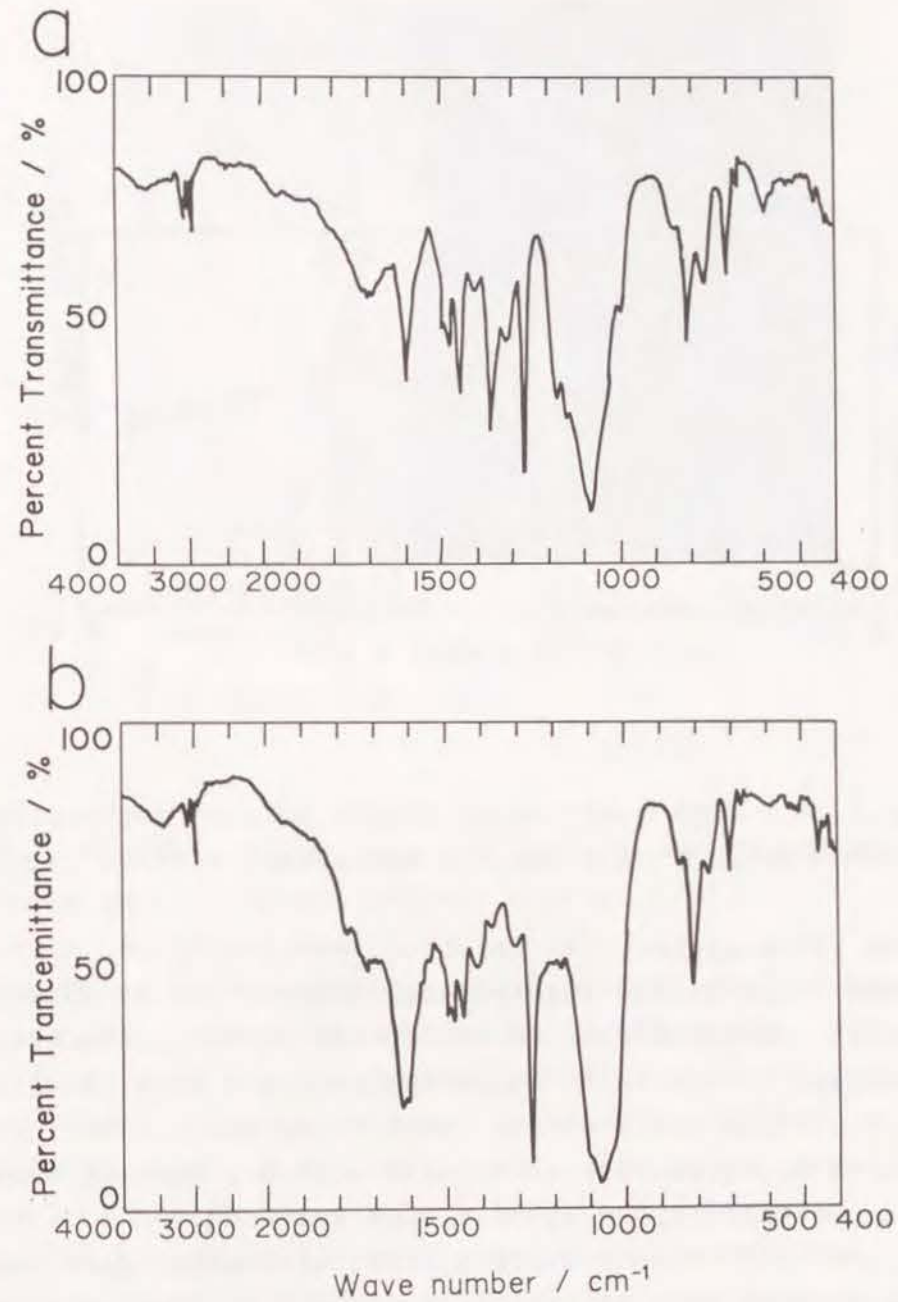

Fig. 1.37. IR spectra of plasma polymer formed from OMCTS [1.49×10^{-6} mol/sec] and methyl benzene sulfonate [8.99×10^{-7} mol/sec].
(a)before treatment with LiI, (b)after treatment with LiI.

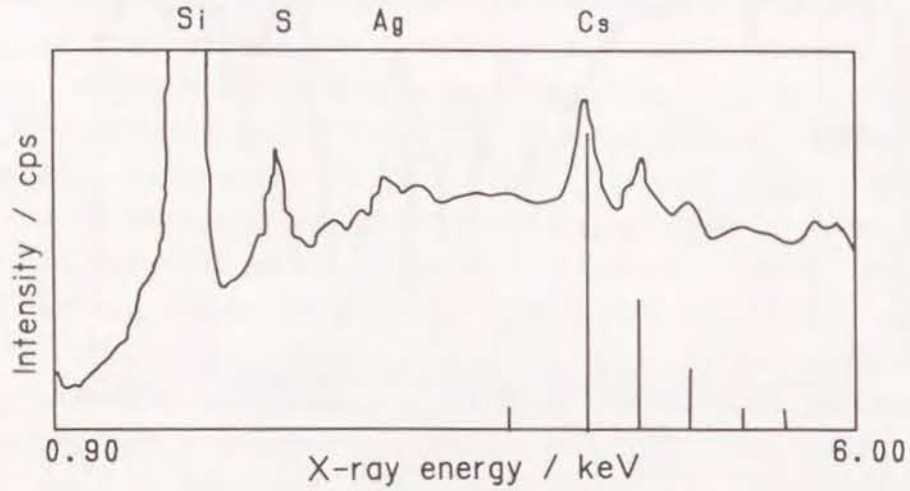

Fig. 1.38. EPMA spectrum of plasma polymer containing sulfonic acid group after ion-exchanging with Cs^+.

from the S/Cs ratio. The relative sensitivity of S/Cs was determined using Nafion incorporated with Cs^+ as a reference. The results indicated that 90-95% of the sulfur contributes to ion-exchange. This is in agreement with the ESCA analytical data of Fig. 1.33 (a). On the other hand, the plasma polymer from methyl methanesulfonate treated with LiI did not show any ion-exchange capacity in aqueous CsOH solution.

Figure 1.39 shows a depth profile of the Cs distribution in the plasma polymer of Fig. 1.38. The distribution of Cs is almost uniform throughout the cross-section of the polymer; therefore the sulfonic acid group distributes itself uniformly in the polymer film in order to satisfy the requirement for electroneutrality. Figure 1.39 also shows that the plasma polymers is still pinhole-free and is unchanged in thickness (about 1.3 μm) after the above-described chemical treatment.

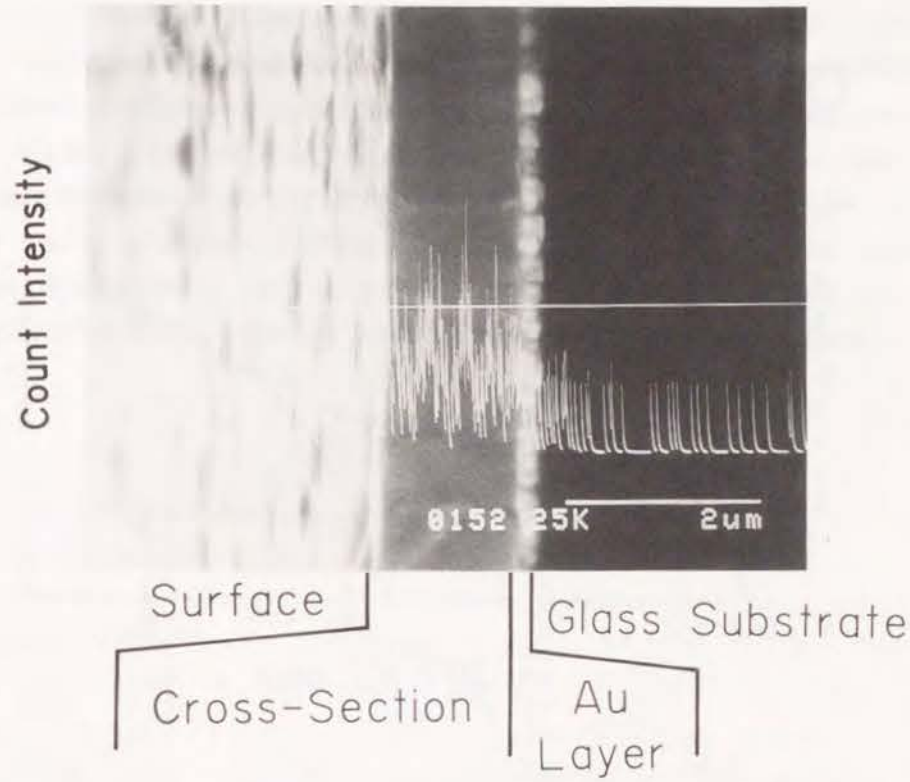

Fig. 1.39. Depth profile of Cs distribution of cross-section of the polymer of Fig. 1.38.

4.3.3 Lithium ion conductivity of hybrid polymer [plasma polymer containing lithium sulfonate group - PEO]

Figure 1.40 shows a typical complex impedance plot of Au/hybrid film [plasma polymer containing lithium sulfonate group-PEO(average M.W. 300)] /Au. Two arcs were distinguished. Since the electrolyte/electrode interfacial capacitance, Ce, is generally much lager than geometrical capacitance, Cg, in these polymer electrolytes, the spectra obtained are interpreted by the appropriate equivalent circuit shown in Fig. 1.40(b). The first arc, for the high frequency range, is attributed to a bulk electrolyte impedance. The arc was extrapolated to the Z' axis to obtain a bulk electrolyte resistance, Rb. The second arc, for the low frequency range, is attributed to an electrode/electrolyte interfacial impedance.

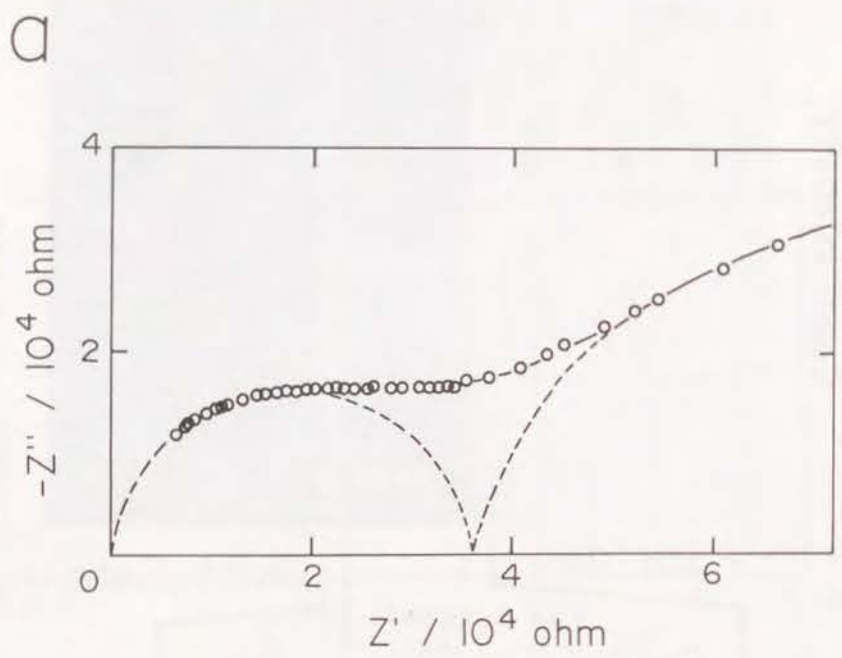

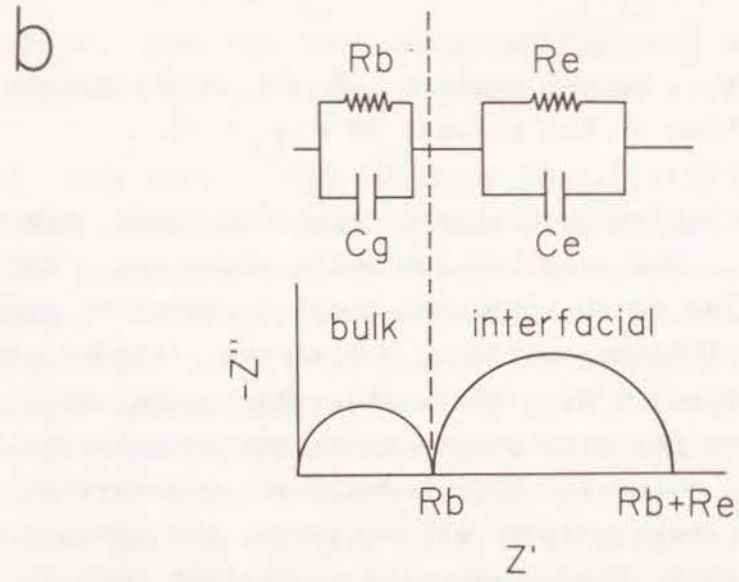

Fig. 1.40. A complex impedance plot of Au/hybrid polymer of plasma polymer containing lithium sulfonate group and PEO/Au (a) and appropriate equivalent circuit (b).

The lithium ion conductivities of the hybrid polymers were calculated from the values of Rb. The conductivities (left-hand ordinate) and the resistance per unit area of 1 um thick films (right-hand ordinate) for the hybrid polymers [plasma polymers which contain Li^+ (0.3%) or Li^+(0.1%) - PEO (10%)] are plotted against 1/T in Fig. 1.41. The lithium sulfonate content in the plasma polymers was changed by controlling the flow rate of methyl benzenesulfonate vapor. The

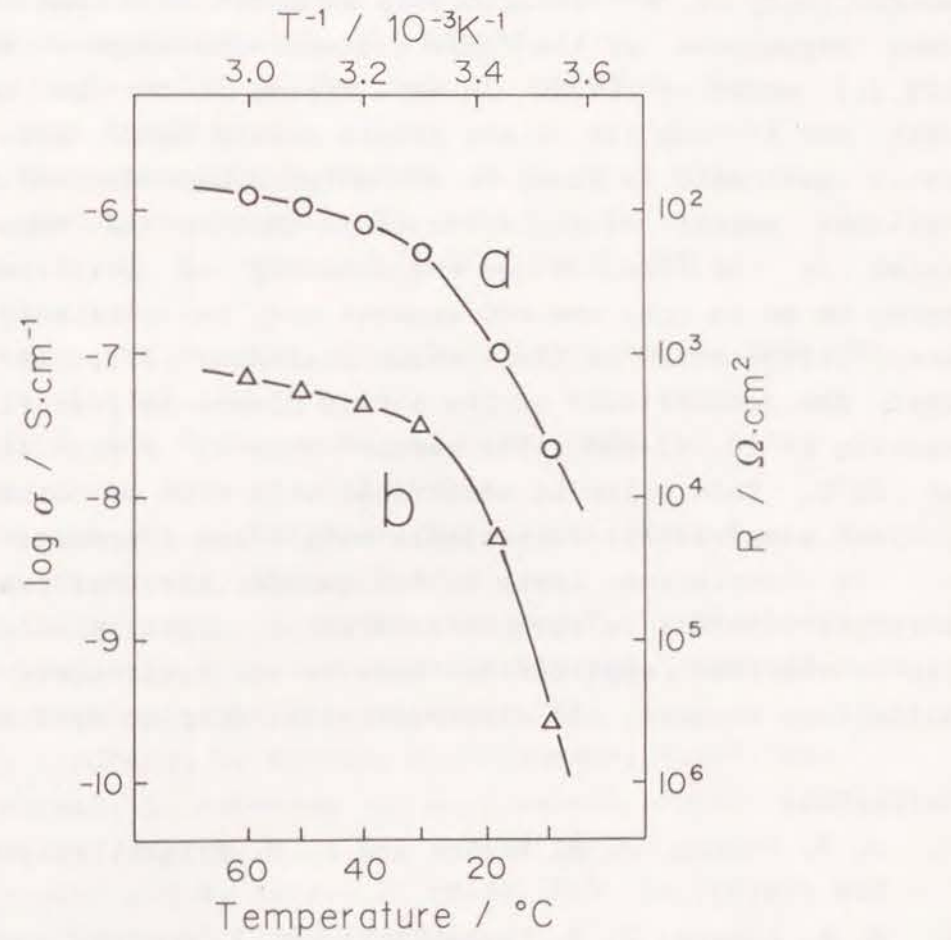

Fig. 1.41. Temperature dependence of ionic conductivities of hybridized plasma polymers.
(a)polymer containing 0.3% Li^+ + 10% PEO.
(b)polymer containing 0.1% Li^+ + 10% PEO.

conductivity of PEO/butanol-treated polymer which has not been reacted with LiI is very low (less than 10^{-11} S cm^{-1} at room temperature), therefore it can be inferred that the measured conductivity is not due to the introduction of H^+ ions into the polymer by the treatment with PEO/butanol. It is seen that the ionic conductivity of the polymer increases with an increase in Li^{+1} ion content, since a high Li^+ ion concentration leads to an increase in the number of ionic charge carrier. Although there is an apparent change in the slope of the conductivity vs. T^{-1} relationship at about 30 °C, the temperature dependence of the ionic conductivity obeys a WLF type [20,21] equation [22]. In this system it can be concluded that the lithium ion is the single mobile ionic species because sulfonate is fixed to the polymer backbone and no significant amount of any other ionic species is expected to exist in the film. Since the polarity of polysiloxane is known to be so low, the PEO segment must be contribute to the ionic dissociation of the lithium sulfonate [23]. It is noted that the conductivity of the hybrid plasma polymer film containing Li^+(0.3%)-PEO (10%) reaches 1.3×10^{-6} S cm^{-1} (80 Ωcm^2) at 60 °C. This value is comparable with that of other solid polymer electrolytes with single mobile ionic species [8-10].

In conclusion, these hybrid polymer electrolytes, which strongly adherent to various substrates, appear promising for electrochemical applications such as all solid-state lithium batteries, sensors, and electrochemical display devices.

References

1. D. E. Fenton, J. M. Parker and P. V. Wright, Polymer, 14, 589 (1973).
2. M. B. Armand, J. M. Chabagno and M. J. Duclot, Fast Ion Transport in Solids edited by P. Vashista, J. N. Mundy, G. K. Shenoy, Elesevier, N.Y., 1979, p. 131.
3. M. Watanabe, M. Rikukawa, K. Sanui, N. Ogata, H. Kato, T. Kobayashi and Z. Ohashi, Makromolecules, 17, 2902 (1984).

4. K. Nagaoka, H. Naruse and I. Shinohara, J. Polym. Sci., Polym. Lett. Ed., 22, 659 (1984).
5. M. C. Wintersgill, J. J. Fontanella, M. K. Smith, S. G. Greenbaum, K. J. Adamic and C. G. Andeen, Polymer, 28, 633 (1987).
6. D. Fish, I. M. Khan and J. Smid, Makromol. Chem., Rapid Commun., 7, 115 (1986).
7. K. J. Adamic, S. G. Greenbaum, M. C. Wintersgill and J. J. Fontanella, J. Appl. Phys., 60, 1342 (1986).
8. N. Kobayashi, M. Uchiyama and E. Tsuchida, Solid State Ionics, 17, 307 (1985).
9. L. C. Hardy and D. F. Shriver, J. Am. Chem. Soc., 107, 3823 (1985).
10. D. J. Bannister, G. R. Davies, I. M. Ward and J. E. Nclntyre, Polymer, 25, 1291 (1984).
11. H. Yasuda, C. E. Lamaze, J. Appl. Polym. Sci., 15, 2277 (1971).
12. H. Yasuda, T. Hirotsu, J. Polym. Sci., Polym. Chem. Ed., 16, 743 (1978).
13. I. Tazima and M. Yamamoto, J. Poly. Sci., Polym. Chem. Ed., 23, 615 (1985).
14. N. Inagaki and H. Hirao, J. Polym. Sci. Part A, Polym. Chem., 24, 595 (1986).
15. R. M. Silverstein, G. C. Bassler and T. C. Morril, 'Spectrometric Identification of Organic Compounds, Forth Edition' John Wiley & Sons, 1981.
16. B. J. Lindberg, K. Hamrin, G. Johansson, U. Gelius, A. Fahlman, C. Nordling and K. Siegbahn, Physica Scripta, 1, 286 (1970).
17. N. Inagaki and H. Hirao, J. Polym. Sci. Part A, Polym. Chem., 25, 1803 (1987).
18. D. B. Graves and K. F. Jensen, IEEE Transaction on Plasma Sci., PS-14, 78 (1986).
19. W. E. Truce, R. W. Campbell and G. D. Madding, J. Org. Chem., 32, 308 (1967).
20. M. L. Williams, R. F. Randel and J. D. Ferry,

J. Am. Chem. Soc., 77, 3701 (1955).
21. M. Cohen and D. Turnbull, J. Chem. Phys., 31, 1164 (1959).
22. N. Kobayashi, H. Ohno and E. Tuchida, Nippon Kagaku Kaishi, 441 (1986).
23. M. Watanabe, S. Nagano, K. Sanui and N. Ogata, J. Power Soueces, 20, 327 (1987).

Chapter 5 Preparation and Characterization of Solid Polymer Electrolyte Having Fixed Carboxylic Acid Groups with Single Mobile Species

5.1 Introduction

Extensive studies have recently done on the ionic conductivity of solid polymer electrolytes prepared by the treatment of polyethers with alkali metal salts [1,2]. The ionic conductivities of these solid polymer electrolyte are considerably lower than those of liquid electrolytes. Because of the difficulty in decreasing the specific resistivities, it is necessary instead to make use of these materials in the form of ultra-thin films. In previous Chapters, the preparation of ultra-thin solid polymer electrolyte utilizing plasma polymerization technique was described.

In most of the solid polymer electrolytes reported, both the cation and anion are mobile. When these solid polymer electrolyte are used in electrochemical devices, the DC conductivity decreases because of high resistance due to the non-uniform distribution of anions and cations [3]. Several solid polymer electrolytes with only one mobile species have been reported previously [3-5]. The present study focuses on the preparation of solid polymer electrolyte films sustained by single lithium ion species without any plasticizer by all vapor-phase preparation. Tris(2-methoxyethoxy)vinylsilane (TMVS) was selected as one of the monomer because this substance contains both the ether group and the siloxane group. In this Chapter, a carboxylic acid group was fixed into the plasma-polymerized TMVS polymer chain during the plasma polymerization process. The carboxylic acid group was first introduced as an ester by the addition of gas containing the carboxylic ester group. The carboxylic ester group was then converted to a lithium carboxylate group by reaction with

---

Solid State Ionics, 40/41, 624 (1990).

lithium iodide [6,7]:

$$-\underset{\underset{O}{\|}}{C}-O-CH_3 + LiI \longrightarrow -\underset{\underset{O}{\|}}{CO^-Li^+} + CH_3I$$

The formed iodomethane (bp. 41-43 °C) was removed by evaporation.

5.2 Experimental

5.2.1 Materials

Methyl acrylate, methanol (Wako Chemical Co.), tris(2-methoxyethoxy)vinylsilane (TMVS) (Shin-etsu Chemical Co.), of extra pure grade, were used without further purification. Anhydrous lithium iodide (Wako Chemical Co.) was dried under reduced pressure (10^{-3} Torr) at 60 °C for 12 hours.

5.2.2 Plasma polymerization

The apparatus used for the plasma polymerization has been described in Chapter 1. Polymerization was performed in a capacitively coupled glass reactor, using stainless steel internal electrodes. The substrate were placed between the two electrodes and argon gas [10 cm^3(STP)/min], TMVS vapor [1 cm^3(STP)/min] and methyl acrylate vapor [various flow rate] were introduced into the reactor. The pressure was maintained at 0.3 Torr by controlling a main valve. under these conditions, the RF power (13.56 MHz) was carried out at 5W.

5.2.3 Preparation of solid polymer electrolyte [Conversion from carboxylic ester to lithium carboxylate]

A schematic diagram of the process for the synthesis of the solid polymer electrolyte is shown in Fig. 1.42. First, as shown in Fig. 1.42a, a plasma polymer formed from TMVS and methyl acrylate (about 0.5 μm thick) was deposited on the desired substrate. Next, the treated substrate was removed from the plasma polymerization reactor and a thin layer of

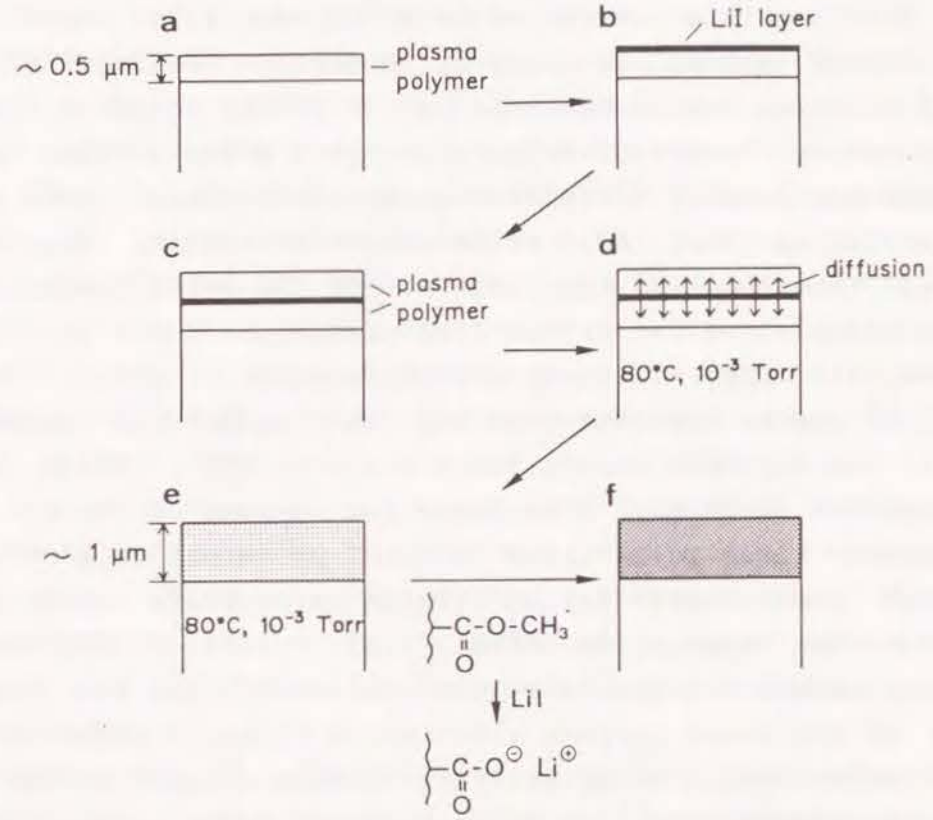

Fig. 1.42. Schematic diagram of process for synthesis of thin film of solid polymer electrolyte having lithium carboxylate group with single lithium ion conductive film.

lithium iodide was deposited by using a spray method on its surface [Fig. 1.42b]. The substrate then was again placed in the plasma polymerization reactor and a second thin layer of plasma polymer was deposited on the lithium iodide layer under the same condition as before [Fig. 1.42c]. The resulting three-layer composite (plasma polymer-lithium iodide-plasma polymer) was maintained at 80 °C for 24 hours under 10^{-3} Torr to permit the lithium iodide to distribute uniformly throughout the plasma polymer [Fig. 1.42d]. In this condition, the

carboxylic ester group was converted to a lithium carboxylate by reaction with lithium iodide [Fig. 1.42e].

The complete conversion from the carboxylic ester group to lithium carboxylate group is impossible because the unreacted lithium iodide remained in the plasma polymer. Therefore, about 30-40% of carboxylic ester group in the plasma polymer was convert to lithium carboxylate group. EPMA observation shows that the lithium iodide diffusion [Fig. 1.42d stage] takes only within 10 min. On the other hand, FT-IR observation shows conversion from carboxylic ester to lithium carboxylate [Fig. 1.42e stage] takes about 6 hours. Therefore, it can be regarded that the reaction between carboxylic ester and lithium iodide takes place after lithium iodide distribute uniformly throughout the plasma polymer. This treatment leads to an ultra-thin (~1 μm thick) film of solid polymer electrolyte having lithium carboxylate with single lithium ion conductive film [Fig. 1.42f]. Conventional inert-atmosphere techniques were utilized during the preparation of the solid polymer electrolyte films in order to prevent contamination by water. The lithium content of the solid polymer electrolyte film was determined by an atomic absorption spectrophotometric measurement. The iodide content of the solid polymer electrolyte film was determined by EPMA measurement and spectrophotometric measurement as starch-iodine-chromogen [8].

5.2.4 Measuring techniques

The ionic conductivities of the solid polymer electrolytes were determined from AC impedance measurements carried out over frequency range of $2x10^2$-$2x10^4$ Hz using a vector impedance meter.

EPMA was performed with a Hitachi-Horiba Model EMAX-1770 electron microprobe analyzer. FT-IR were using a Shimadzu Model 4100 IR-spectrometer.

5.3 Results and discussion

5.3.1 Characterization of the solid polymer electrolyte

Typical FT-IR spectra of TMVS, plasma polymer formed from TMVS and methyl acrylate [Fig. 1.42a stage] and plasma polymer reacted with lithium iodide [Fig. 1.42f stage] are shown in Figs. 1.43a, 1.43b and 1.43c, respectively. The IR spectra of the plasma polymer before reaction with lithium iodide is similar to that of the TMVS, except for the addition of the characteristics peak of C=O stretching vibration of carboxylic ester (1734 cm^{-1}) and C-O-C stretching vibration (1337 cm^{-1}), and the complete absence of the characteristics peak for the olefin group (1599 cm^{-1}). These facts indicate that the structure of the plasma polymer formed from TMVS and methyl acrylate is very similar to poly(TMVS) having fixed carboxylic ester group, from which it can be interfered that plasma-induced polymerization is the dominant process that takes place fairly mild experimental conditions employed in the present work.

Appearance of a characteristics peak of CO_2^- stretching vibration of carboxylic acid (1619 cm^{-1}) and decreasing of peak strength of carboxylic ester group (1734 and 1337 cm^{-1}) are shown in Fig. 1.43c. Moreover, the absorption of alkyl iodide (600-580 cm^{-1}) is not observed in the spectrum of Fig. 1.43c. EPMA measurement and spectrophotometric measurement of iodostarch reaction showed that the solid polymer electrolyte of Fig. 1.43c did not contain iodine in the range of these analysis. These facts indicate that the conversion from the carboxylic ester group to lithium carboxylate group takes place in the plasma polymer and that the lithium carboxylate group is fixed to the backbone chain of the polymer.

5.3.2 Lithium ion conductivity of the solid polymer electro lyte having lithium carboxylate group

Figure 1.44 shows the variation of the ionic conductivity of the solid polymer electrolyte with temperature, at differ-

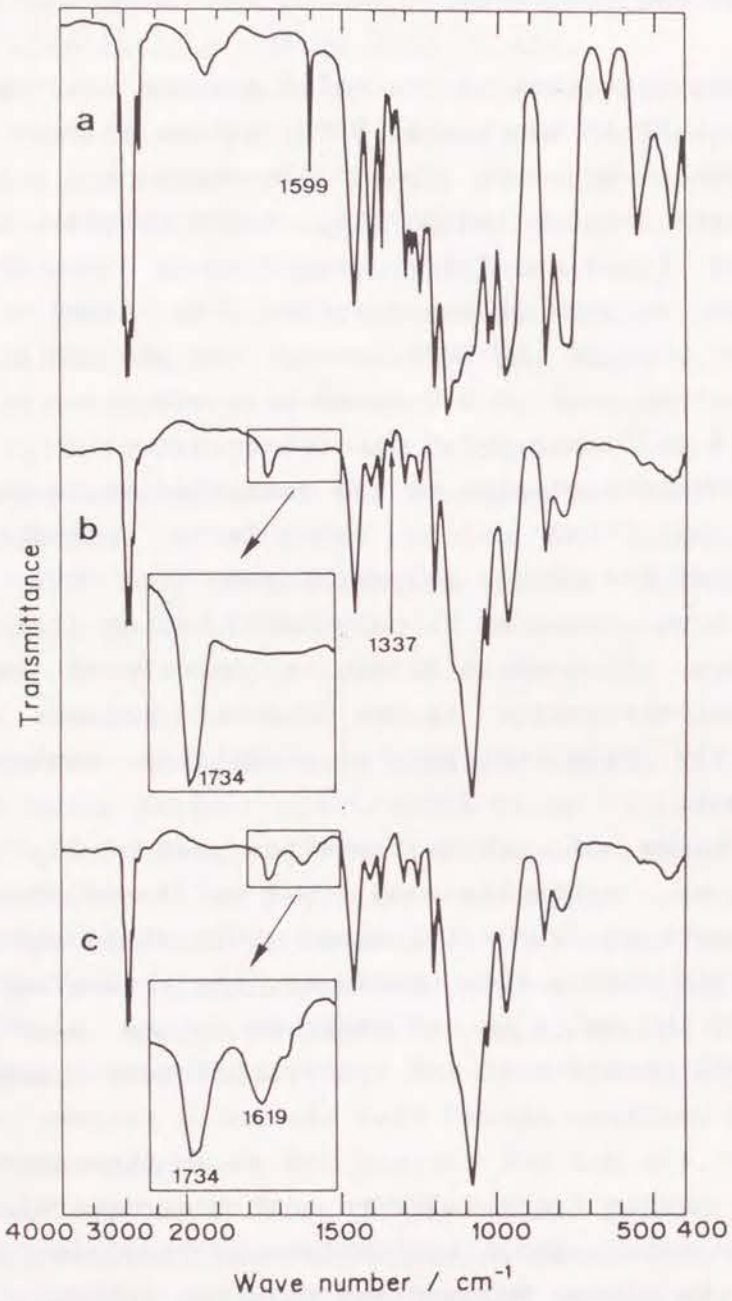

Fig. 1.43. IR spectra of tris(2-methoxyethoxy) vinylsilane [TMVS] (a), plasma polymer formed from TMVS [1 cm^3(STP)/min] and methyl acrylate [0.4 cm^3(STP)/min] (b), and the plasma polymer of (b) after treated with LiI (c).
[pressure = 0.3 Torr, RF power = 5 W]

ent levels of Li^+ content. The electrical resistance per unit area of the approximately 1 μm-thick solid polymer electrolyte films also is indicate indicated in the same figure on the right-hand coordinate axis. The solid polymer electrolyte with single mobile species has conductivity values greater than 10^{-8} S cm^{-1} at room temperature. As described in Chapter 2 and 3, the room temperature conductivity was relatively low

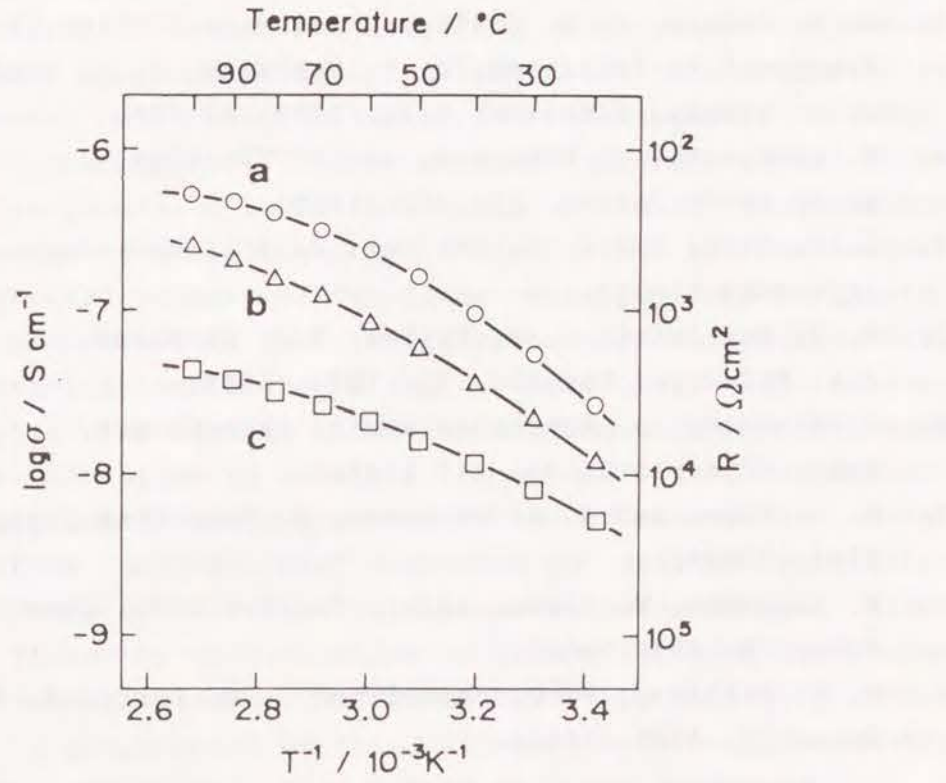

Fig. 1.44. Temperature dependence of ionic conductivities of solid polymer electrolytes having fixed carboxylic acid group.
(a) solid polymer electrolyte containing 0.4% Li^+
(b) solid polymer electrolyte containing 0.2% Li^+
(c) solid polymer electrolyte containing 0.1% Li^+

in comparison with ionic conductivity of plasma-polymerized TMVS-$LiClO_4$ complex of 10^{-6} S cm^{-1}. Such reason is considered that a weak acidity of carboxylic acid and that a absence of contribution of anion species. The temperature dependence of the conductivity was fitted the WLF type equation [9] rather than the Arrhenius equation.

References

1. D. E. Fenton, J. M. Parker, and P. V. Wright, Polymer, 14, 589 (1973).
2. M. B. Armand, J. M. Chabagno, and M. J. Duclot, Fast Ion Transport in Solids ed. by P. Vashista, J. N. Mundy, G. K. Shenoy, Elsevier, N.Y., 1979, p. 131.
3. N. Kobayashi, M. Uchiyama, and E. Tsuchida, Solid State Ionics, 17, 307 (1985).
4. L. C. Hardy and D. F. Shriver, J. Am. Chem. Soc., 107, 3823 (1985).
5. D. J. Bannister, G. R. Davies, I.M. Ward and J.E. McIntyre, Polymer, 25, 1291 (1984).
6. F. Elsinger, J. Schreiber and A. Eschenmoser, Helv. Chim. Acta, 43, 113 (1960).
7. W. L. Meyer and A. S. Levinson, J. Org. Chem., 28, 2184 (1963).
8. K. Sugawara, T. Koyama and K. Terada, Bull. Chem. Soc. Jpn., 28, 494 (1955).
9. M. L. Williams, R. F. Landel and J. D. Ferry, J. Am. Chem. Soc., 77, 3701 (1955).

Part II. Thin Solid-State Lithium Batteries

Chapter 1 Thin All-Solid-State Lithium Batteries Utilizing Solid Polymer Electrolyte Prepared by Plasma Polymerization

1.1 Introduction

Solid polymer electrolytes prepared by mixing of poly(ethylene oxide)(PEO) as well as poly(propylene oxide)(PPO) with alkali metal salts have attracted considerable attention due to their application to all-solid-state lithium batteries [1-3]. Ionic conductivity of reported solid polymer electrolytes is typically $10^{-6\sim-8}$ S/cm at room temperature, and these values are generally lower than those of liquid electrolytes [4]. Because of their low ionic conductivity, lithium batteries using solid polymer electrolytes generally does not exhibit good properties in both utilization and charge/discharge characteristics until around 100°C. Therefore, solid polymer electrolytes for lithium batteries are required to decrease thickness in order to attain a low actual film resistance. Plasma polymerization is a useful method to provide an ultra-thin uniform polymer layer deposited on various substrates [5]. In Chapter 1 of Part I, ultra-thin solid polymer electrolyte films by hybridization of plasma polymerized octamethylcyclotetrasiloxane (OMCTS) with PPO and $LiClO_4$. In this Chapter, a preparation of thin all-solid-state rechargeable lithium batteries using this hybrid film was described.

1.2 Experimental

The apparatus used for the plasma polymerization consists of a glass reactor (9 cm diameter and 35 cm height) equipped

---

J. Electrochem. Soc., 135, 2649 (1988).
J. Power Sources, 26, 457 (1989).

with capacitively coupled inner electrodes (6 cm diameter) connected with an RF power supply (13.56 MHz). A TiS_2 film deposited on borosilicate glass was utilized as a substrate, which was placed between the electrodes. Argon gas [10 cm^3 (STP)/min] and OMCTS [2 cm^3 (STP)/min] were introduced into the glass reactor. The pressure was maintained at 0.5 Torr by controlling a throttle valve connecting to a vacuum pump. At this point, the RF power at 5 W was turned on. The plasma polymer films deposited on the substrate were soaked in butanol-PPO [M.W. 4,000]-$LiClO_4$ solution for more than 1 h to attain equilibrium [9], and then dried at 80 °C under vacuum (10^{-3} Torr) for 24 h to remove butanol and water. The concentration of lithium ion in a plasma polymer-PPO mixture was determined by atomic absorption spectrophotometry. The ionic conductivity of the hybrid polymer electrolyte (plasma polymer-PPO-$LiClO_4$) was estimated by an AC impedance measurement with a vector impedance measurement over the frequency range $2x10^2$-$2x10^4$ Hz.

Thin film of TiS_2 for the cathode active material was deposited by a low pressure chemical vapor deposition (CVD) technique from a mixture of $TiCl_4$ and H_2S diluted with argon as the source gas. A film prepared by this method is nearly stoichiometric TiS_2 films which had predominant (110) orientation [10]. All-solid-state lithium batteries were constructed with the hybrid polymer electrolyte (2-3 μm) deposited on TiS_2 CVD cathode (10-15 μm) and a Li foil anode.

1.3 Results and Discussion

The characterization of the plasma polymer is not easy. Its IR spectrum of plasma polymer formed from OMCTS suggests that the basic structure of the plasma polymer was similar to that of poly(dimethylsiloxane). SEM observation indicated that the plasma polymer was uniform and pinhole-free.

Figure 2.1 shows the temperature dependence of the ionic conductivity of the hybrid polymer electrolyte [plasma polymer/PPO/ $LiClO_4$=78/20/2wt%]. An actual electrical resistance of the hybrid films (1 μm thick) per unit area is also shown in Fig. 2.1 at right ordinate. The temperature dependence of ionic conductivity exhibit the WLF-type [6,7] dependence rather than the Arrhenius-type one. Conductivity of hybrid polymer electrolyte reached $2.6x10^{-6}$ S/cm (40 Ω per 1 cm^2) at 60 °C. As described in Chapter 1 of Part I, the hybrid polymer electrolyte is considered to have a micro-heterogeneous structure [plasma polymerized OMCTS segment-PPO segment] and PPO segment mainly contributes to the ionic dissociation of $LiClO_4$.

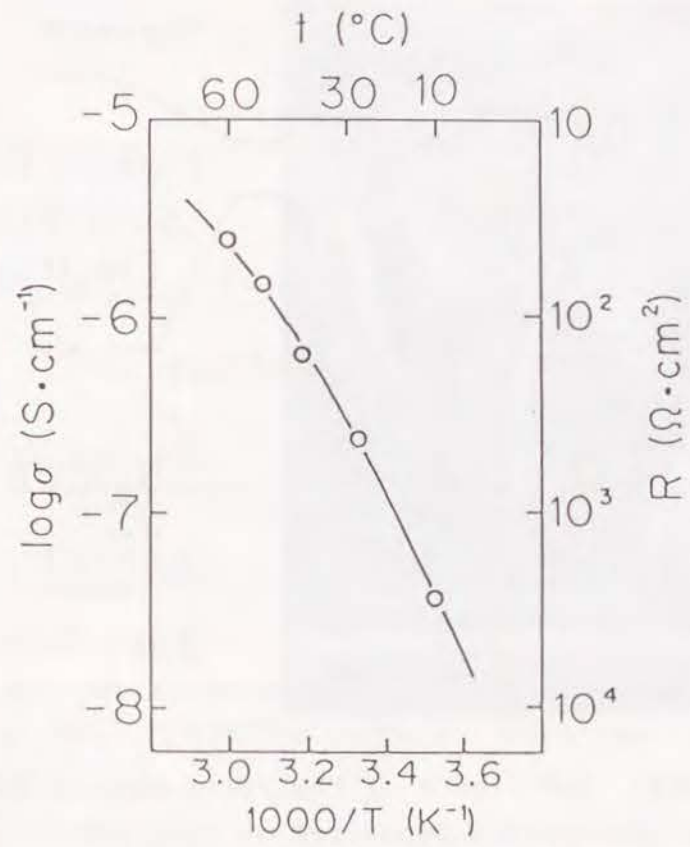

Fig. 2.1. Ionic conductivity dependence of the hybrid film on temperature, which contains PPO(20wt%) and $LiClO_4$ (2wt%).

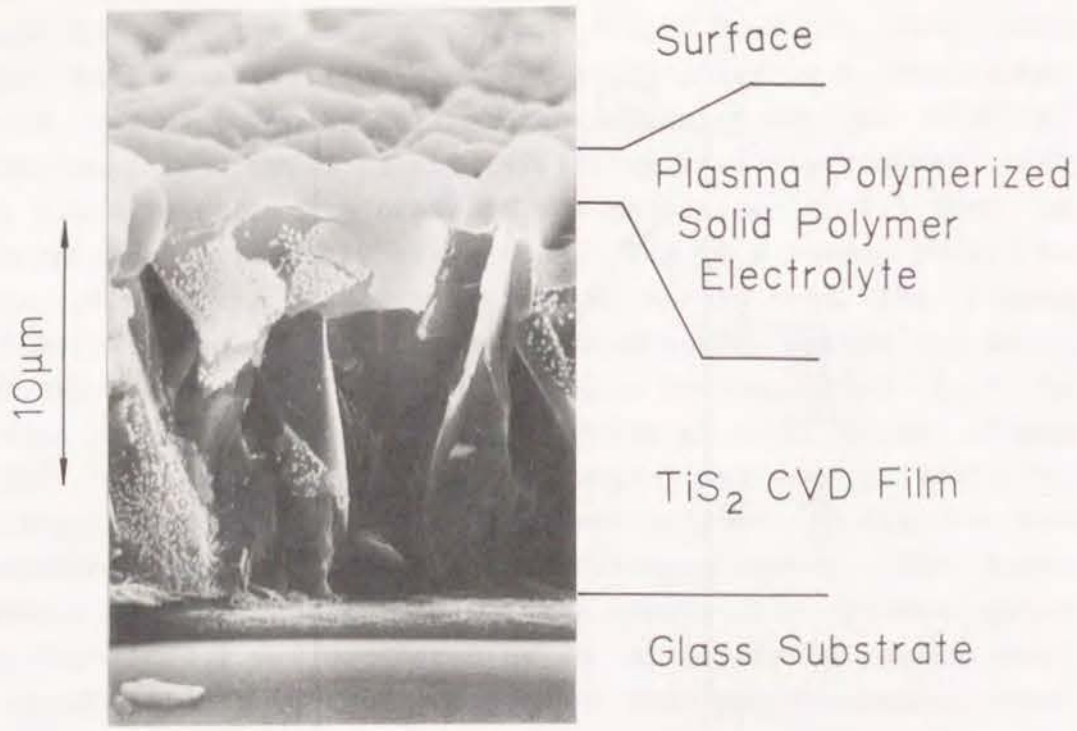

Fig. 2.2. SEM figure of the cross-section of hybrid polymer electrolyte deposited on TiS_2 CVD film.

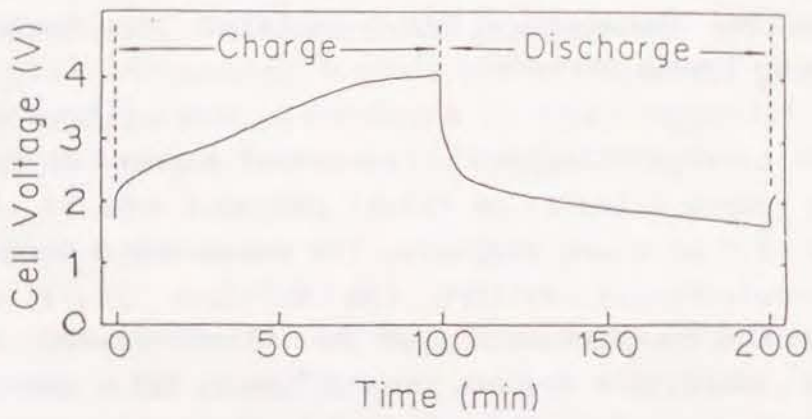

Fig. 2.3. Charge/discharge cycle for all-solid- state lithium battery at room temperature.
Discharge current: 16 $\mu A/cm^2$
Charge current : 16 $\mu A/cm^2$

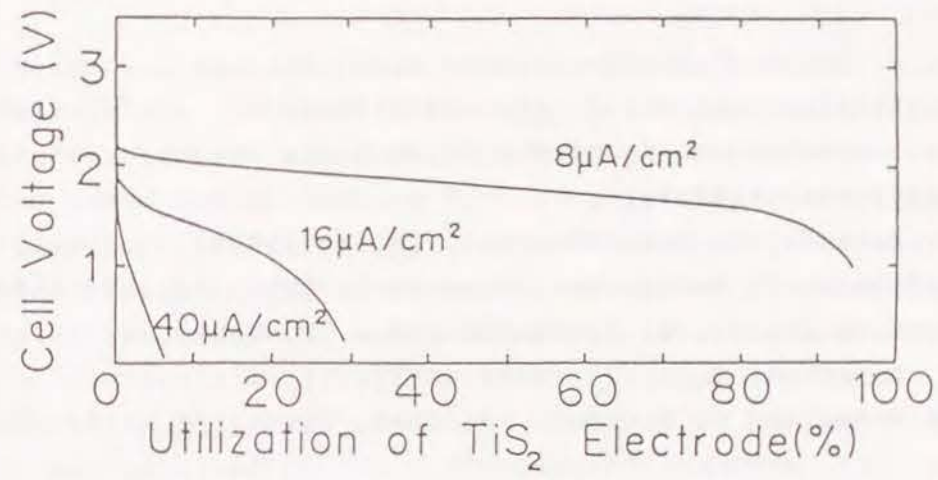

Fig. 2.4. Utilization of all-solid-state lithium batteries vs. discharge current densities at room temperature.

Figure 2.2 illustrates SEM figure of the cross-section of hybrid polymer electrolyte deposited on a TiS_2 CVD film. The figure shows that TiS_2 CVD film is about 15 μm and a hybrid polymer electrolyte layer is about 2 μm. The hybrid polymer electrolyte is pin-hole free, and covers TiS_2 film completely.

In Fig. 2.3, the charge-discharge curve of the battery is shown. The cell was cycled at 16 $\mu A/cm^2$. The fairly good rechargeability of the battery is confirmed by Fig. 2.3, which internal resistance of this batteries is fairly large. It is inferred that solid polymer electrolyte does not closely contact with lithium electrode. The first discharge performance of cells at various current density at room temperature are given in Fig. 2.4. At a low current density of 8 $\mu A/cm^2$, the discharge curve plateau extend to 85% of utilization of TiS_2 (to $LiTiS_2$).

References

1. M. Gauthier, D. Fauteux, G. Vassort, A. Belanger, M. Duval, P. Ricoux, J. M. Chabagno, D. Muller, P. Rigaud, M. B. Armand and D. Deroo, J. Electrochem. Soc., 132, 1333 (1985).
2. K. M. Abraham, M. Alamgir and S. J. Perrotti, J. Electrochem. Soc., 135, 535 (1988).
3. A. Hooper and J. M. North, Solid State Ionics, 9&10, 1161 (1983).
4. Y. Matsuda, J. Power Sources, 20, 19 (1987).
5. H.Yasuda, J. Polym. Sci., Macromol. Rev., 16, 199 (1981).
6. M. L. Williams, R. F. Randel and J. D. Ferry, J. Am. Chem. Soc., 77, 3701 (1955).
7. M. Cohen and D. Turnbull, J. Chem. Phys., 31, 1164 (1959).

Chapter 2 Thin Film Solid-State Lithium Batteries Prepared by Consecutive Vapor-Phase Processes

2.1 Introduction

Recently, a significant amount of work has been devoted to solid-state lithium batteries utilizing solid polymer electrolytes which are made from polymer complexes formed by lithium salts and polyethers such as poly(ethylene oxide) and poly(propylene oxide) [1-6]. At room temperature, however, the ionic conductivity of these solid polymer electrolytes is typically two orders of magnitude lower than those of organic liquid electrolytes [7]. Therefore, some of the major problems found in batteries utilizing their solid polymer electrolytes are ascribed to the difficulty of lowering the actual resistance of the solid polymer electrolyte. Because of the difficulty in decreasing their specific resistivities, it is necessary instead to make the solid polymer electrolytes very

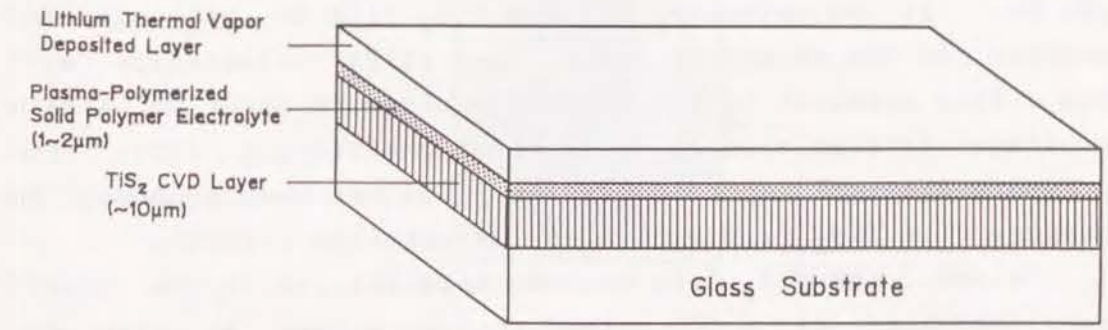

Fig. 2.5. A schematic view of the thin film solid-state lithium battery.

J. Chem. Soc., Chem. Commun., 1673 (1989).
Submitted for publication to J. Elecrtrochem. Soc.

thin. Plasma polymerization is an attractive method to provide uniform, ultra-thin polymer layers on various substrates [8].

In previous chapters, the preparation of such solid polymer electrolyte films by this method was discussed. Here, the fabrication of thin film solid-state lithium batteries using the polymer electrolyte film prepared by the plasma polymerization technique was described. The structure of the all solid-state lithium battery is schematically shown in Fig. 2.5. The interface between the solid polymer electrolyte and electrodes which affect the discharge performance of the solid-state battery was investigated.

2.2 Experimental

2.2.1 Preparation of Thin Solid-State Lithium Battery

A schematic diagram of the process for preparing the thin film solid-state lithium batteries is shown in Fig. 2.6. We chose TiS_2 as a cathode active material, since it is known to be a desirable cathode active materials for a lithium battery [9,10]. It is necessary for the TiS_2 film to be thin and uniform in its thickness and to have (110) orientation with its c-axis parallel to the substrate plane in order to attain a large lithium chemical diffusion coefficient [11]. Low pressure chemical vapor deposition (CVD) has been proposed to prepare thin TiS_2 film with (110) orientation [10,12].

First, the TiS_2 film cathode material (10-15 μm thick) was deposited by a CVD method through a mask to give the pattern shown in Fig. 2.6(a) (7 mm width) on the borosilicate glass substrate. Next, the solid polymer electrolyte (1-2 μm thick) was deposited on top of the TiS_2 CVD layer (Fig. 2.6(b)). Finally, a lithium layer (various thicknesses, 7 mm width) was deposited on top of the solid polymer electrolyte layer using a thermal vapor-deposition technique (Fig. 2.6(c)). An effective surface area for the solid-state lithium battery is 49 mm^2.

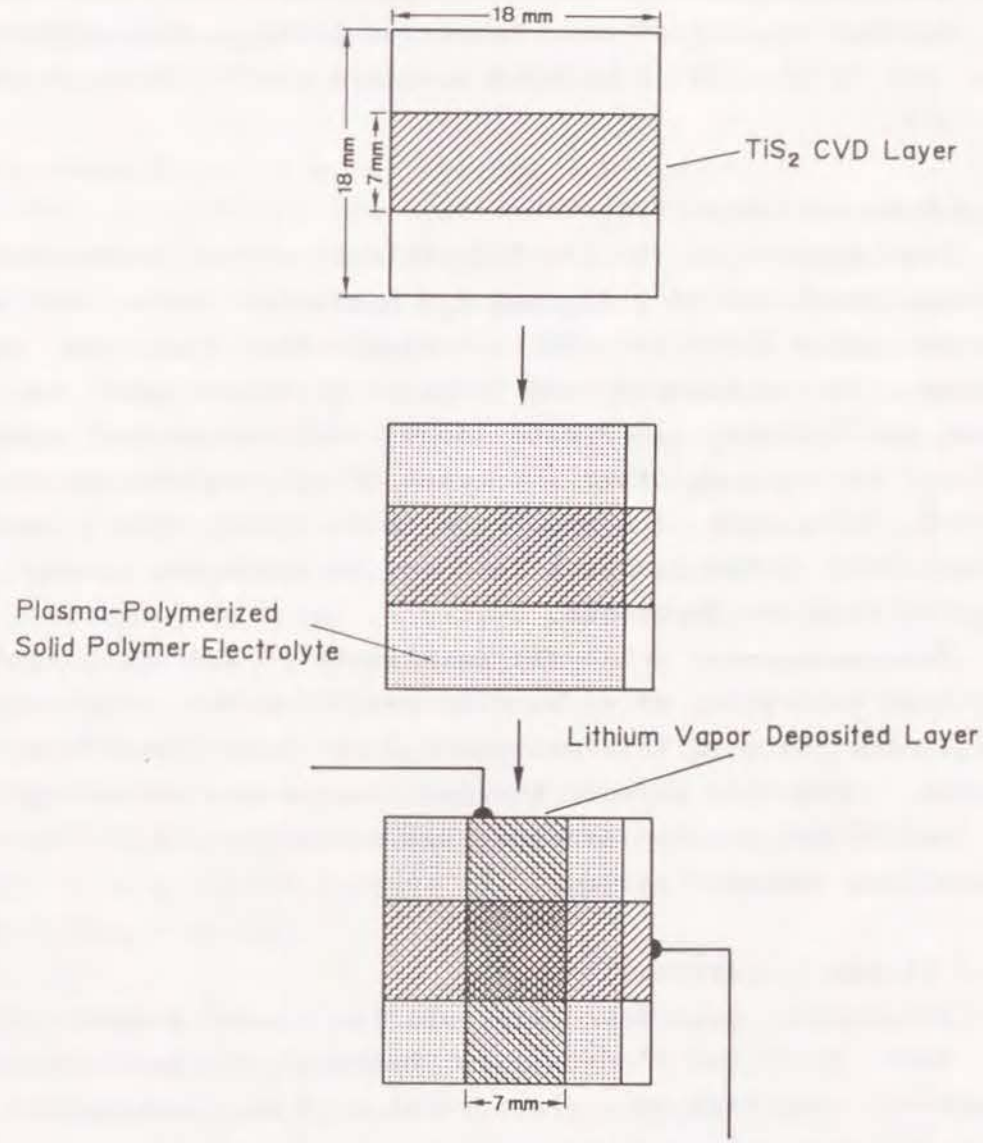

Fig. 2.6. A process for preparation of the thin film solid-state lithium battery.

2.2.2 Materials

Tris(2-methoxyethoxy)vinylsilane (TMVS) and trimethylsilanol (Shinetsu Chemical Co., extra pure grade), methanol, ethanol, and butanol (Wako Chemical Co., guaranteed reagent grade), $TiCl_4$ (Wako Chemical Co., chemical grade), 1-

butyllithium (1.6 mol dm^{-3} hexane solution) (Kanto Chemical Co.) and borosilicate glass (Iwaki glass Co.) were used without further purification. Anhydrous $LiClO_4$ (Wako Chemical Co.) was dried under a reduced pressure of 10^{-3} Torr at 60 °C for 12 h.

2.2.3 Preparation of TiS_2 CVD Film

The production of the TiS_2 thin film was carried out through reaction of $TiCl_4$ and H_2S mixtures in a cold-wall reactor using a thermal CVD technique. The stainless steel reactor (14 cm diameter and 21 cm height) consisted of two source-gas inlets, a Pirani gauge, and a pumping system. Heating was accomplished by means of a resistance heater mounted underneath the substrate table (63.6 cm^2). On the borosilicate glass plates placed on the substrate table, the TiS_2 CVD film was deposited.

The substrate table was maintained at 430 °C. Ar was saturated with $TiCl_4$ at 20 °C. The resulting gas contained 1% $TiCl_4$. A mixture of this gas and H_2S was introduced into the reactor. The flow rate of the gas mixture was maintained at 200 cm^3(STP)/min. The pressure was maintained at 5 Torr by controlling the main valve.

2.2.4 Plasma Polymerization

The apparatus used to carry out the plasma polymerization has been described in detail in Chapter 1 of Part I. The apparatus consisted of a glass reactor (9 cm diameter and 35 cm height) equipped with capacitively-coupled inner electrodes (each area of 28.3 cm^2 and electrode gap of 3.5 cm) to which an alternating voltage was applied at a frequency of 13.56 MHz, a monomer inlet, and vacuum system consisting of a mechanical booster pump, a rotary pump, and a cold trap. The pressure in the reactor was monitored using a Pirani gauge. Ar gas (10 cm^3 (STP)/min) and TMVS vapor (1 cm^3 (STP)/min) were introduced into the reactor. The pressure was maintained at 0.3 Torr by controlling a main valve. After setting conditions, the RF power of 5 W was turned on, and the plasma polymerization was carried out. The thin plasma polymer film was deposited on the substrate, which was placed between two electrodes. The deposition rate is about 6 μm h^{-1}.

2.2.5 Preparation of Solid Polymer Electrolyte

The process for the synthesis of the thin solid polymer electrolyte film has been described in detail in Chapter 2 of Part I. After depositing a plasma-polymerized TMVS layer of about 0.5 μm thickness on a substrate, the substrate was removed from the plasma polymerization reactor and deposited with a thin layer of $LiClO_4$ layer by spraying methanol solution containing 3% $LiClO_4$ on its surface at about 60 °C. The system of the spray method is evacuated to a pressure of about 0.1 Torr. The substrate then was again placed in the reactor and a second thin layer of plasma polymer layer was deposited on top of the $LiClO_4$ layer using the same procedure as for the first layer. The resulting three-layer composite was then maintained at 80 °C for 24h under 10^{-3} Torr to enable the $LiClO_4$ to distribute uniformly throughout the plasma polymer layer. This procedure resulted in the production of an 1 μm thick film of solid polymer electrolyte, plasma polymerized TMVS-$LiClO_4$ complex.

2.2.6 Preparation of lithium alkoxides and lithium alkylsilanolate as reference compounds

1-butyllithium were reacted with excess amount of methanol, ethanol, butanol, and trimethylsilanol in hexane at room temperature and lithium methoxide, lithium ethoxide, lithium butoxide, and lithium trimethylsilanolate, were synthesized respectively. The excess of the alcohol or silanolate and hexane used as the solvent were evaporated at room temperature under 10^{-3} Torr. The resulting lithium alkoxides and lithium alkylsilanolate were white powders.

2.2.7 FT-IR Measurement

First, a layer of plasma polymer formed from TMVS of about 50-70 nm thickness was deposited on a KBr plate. Next, a thin layer of lithium metal was deposited on the plasma polymer layer. The substrate then was maintained at 80 °C for 5 h under Ar atmosphere for the lithium with the plasma polymer to react.

A schematic view of an apparatus for FT-IR measurement of the product of the reaction between plasma polymer and lithium is shown in Fig. 2.7.

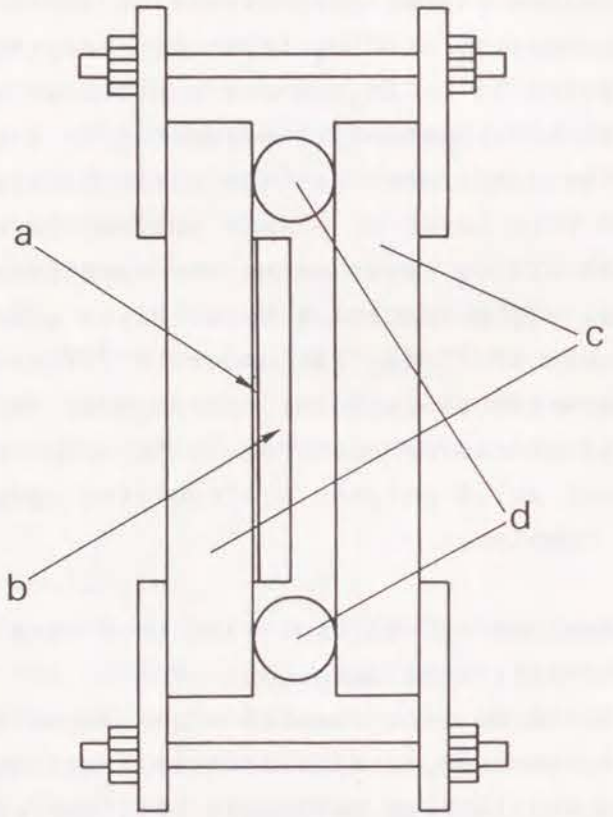

Fig. 2.7. A schematic view of an apparatus for FT-IR measurement of the reaction product between plasma polymer formed from tris(2-methoxyethoxy)vinylsilane and lithium.
a: unreacted plasma polymer layer, b: product of the reaction between the plasma polymer and lithium, c: KBr plate, d: O-ring

2.2.8 Measuring Techniques

Conventional inert-atmosphere (argon) handling techniques were employed during the preparation and characterization of the thin solid-state lithium batteries in order to prevent contamination with water. Electron probe micro analysis (EPMA) was performed with a Hitachi-Horiba EMAX-1770.

2.3 Results and Discussion

2.3.1 Thin TiS_2 Films Prepared by CVD

Stoichiometry of the CVD films was estimated by EPMA measurement. Figure 2.8 shows the influence of source gas composition ($H_2S/TiCl_4$) on the stoichiometry of deposited $Ti_{1+x}S_2$ film by CVD. The x value of the $Ti_{1+x}S_2$ increases with decreasing a ratio of H_2S to $TiCl_4$.

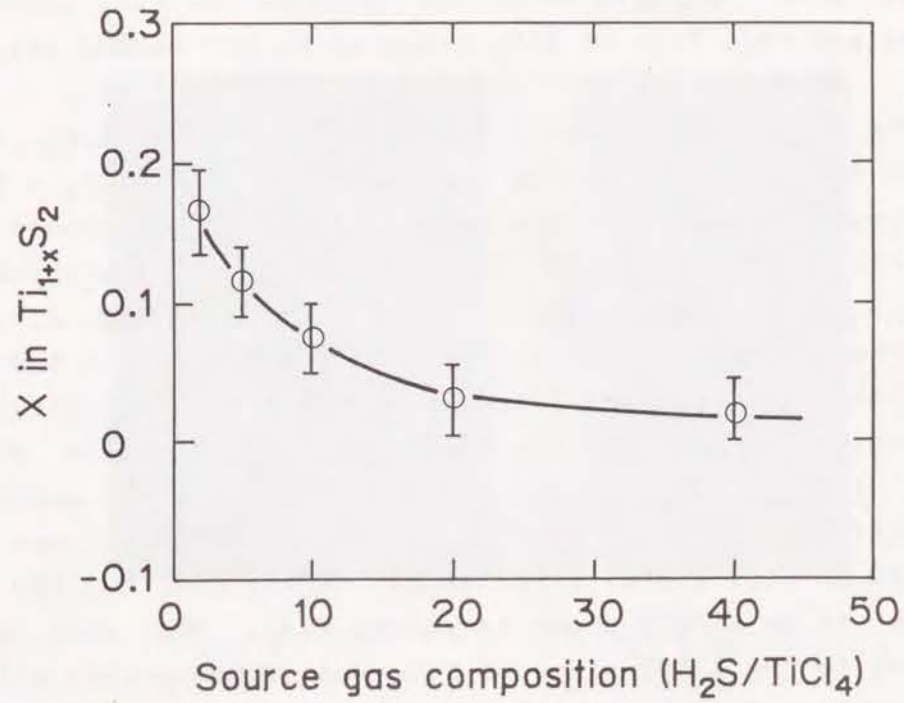

Fig. 2.8. Influence of the source gas composition ($H_2S/TiCl_4$) on the stoichiometry of deposited $Ti_{1+x}S_2$ films.

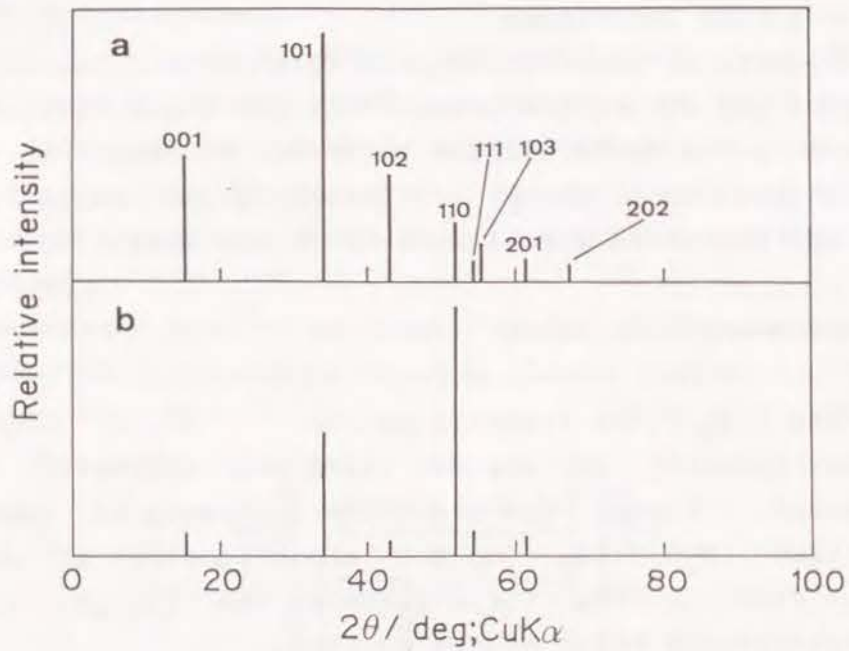

Fig. 2.9. X-ray diffraction patterns for TiS_2 (ASTM) (a) and thin film of TiS_2 prepared by CVD method (b).

The X-ray diffraction patterns for hexagonal TiS_2 (ASTM) (a) and for the thin film of TiS_2 formed at $H_2S/TiCl_4$ = 20 (b) are shown in Fig. 2.9. The result of Fig. 2.8 showed that the thin TiS_2 film of Fig. 2.9(b) was nearly stoichiometric ($Ti_{1.03}S_2$). The larger the value of x value of Fig. 2.8, the lower the lithium chemical diffusion coefficient in the TiS_2 is, which influences the performance of the battery [10]. The diffraction pattern for the CVD film shows six peaks at the (001), (101), (102), (110), (111), and (201) TiS_2 positions. All diffraction peaks in Fig. 2.9(b) (for sample) are also observed in Fig. 2.9(a) (from ASTM). Therefore, the CVD film appears to be single-phase hexagonal TiS_2. The peak corresponding to the (110) plane of TiS_2 was stronger than all the other peaks. This indicates that the thin TiS_2 film prepared by the CVD method has a remarkable orientation of the crystallographic c-axis parallel to the substrate plane as compared to nonoriented hexagonal TiS_2 of Fig. 2.9(a). Film adhesion

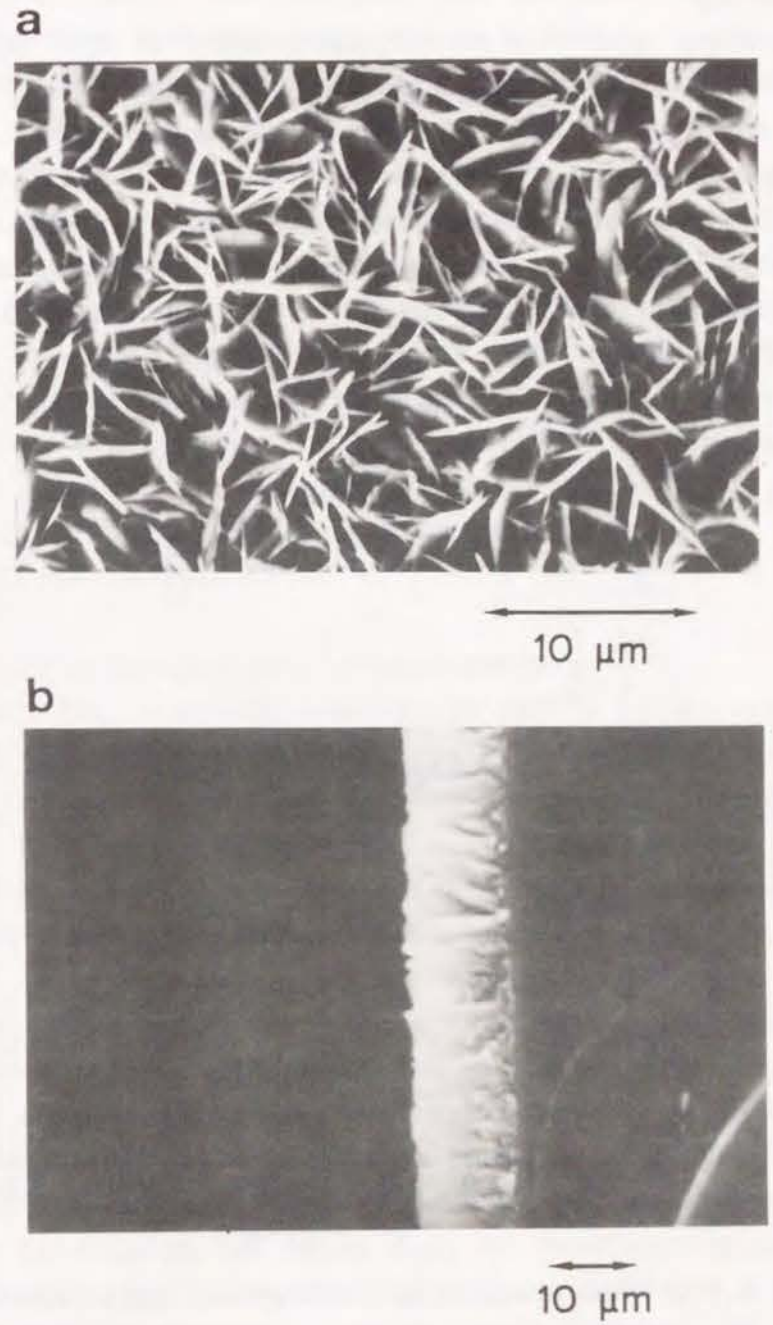

Fig. 2.10. Scanning electron micrographs of thin film of TiS_2 prepared by CVD method of Fig. 2.9 (b). (a) surface, (b)cross-section

to the glass substrate decreased with increasing a ratio of H_2S to $TiCl_4$.

Scanning electron micrographs (SEM) of the surface and the fracture cross-sections of the thin TiS_2 film corresponding to the TiS_2 of Fig. 2.9(b) are shown in Fig. 2.10(a) and (b) respectively. The films were made of small (5-10 μm), narrow plate-like crystallites that grew perpendicularly to the substrate plane. The same structure has been observed by other workers for TiS_2 prepared by CVD method [10,12]. The cross-sectional SEM of Fig. 2.10(b) indicate the film is about 12 μm thick and, on the scale of SEM observation, of uniform in thickness.

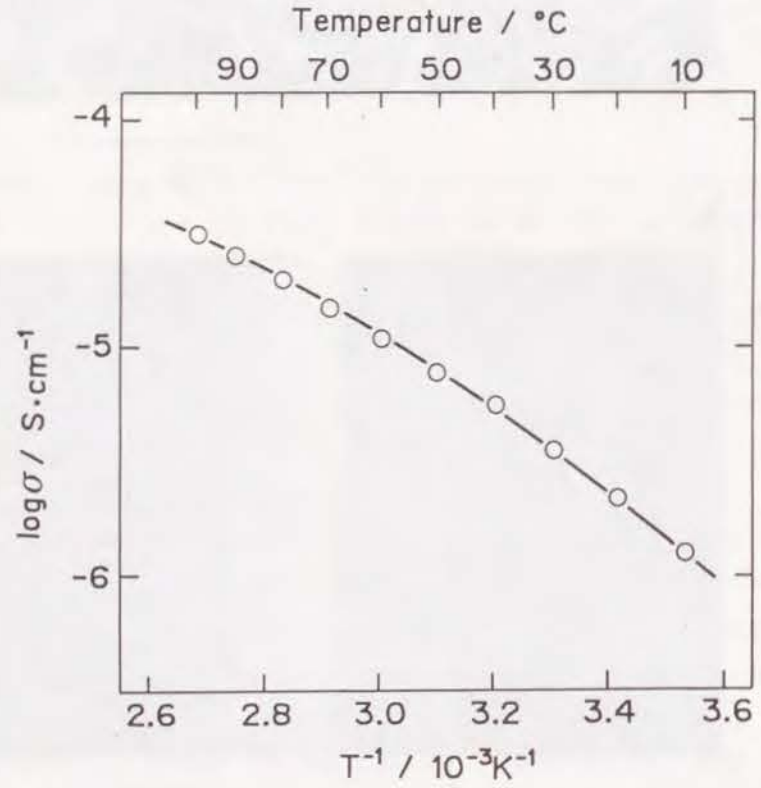

Fig. 2.11. Temperature dependence of ionic conductivity of solid polymer electrolytes prepared by the complexation of plasma-polymerized tris(2-methoxyethoxy)vinylsilane (monomer flow rate = 1 cm^3(STP) /min; RF power= 5 W; pressure= 0.3 Torr) with 3 wt% lithium perchlorate.

2.3.2 Solid Polymer Electrolyte by Plasma Polymerization

The thin film electrolyte was prepared as described above. The film was transparent and colorless solid. FT-IR spectrum of the plasma-polymerized film showed the polymer was similar to that of bulk TMVS, except for the complete absence of the characteristic absorption peak of the olefin group at 1600 cm^{-1}. This indicates the plasma-polymerized TMVS is very similar to poly(TMVS).

Figure 2.11 shows the variation of the conductivity of the solid polymer electrolyte with temperature. The solid polymer electrolyte (plasma-polymerized TMVS-$LiClO_4$ complex) has conductivity values greater than 10^{-6} S cm^{-1} at room temperature. The variation with temperature is typical of ionic conductivity and can be described by using an equation of the WLF type equation [13,14].

2.3.3 Thin Film Solid-state Lithium Battery

A scanning electron micrograph of the fracture cross-section of a undischarged thin film solid-state lithium battery is shown in Fig. 2.12. An EPMA depth profile signal for Si in the battery is also shown in the same figure. The Si distribution results from the solid polymer electrolyte and glass substrate. The figure shows that the TiS_2 CVD film of Fig. 2.9 (b) (~12 μm thick) is covered with the plasma-polymerized solid polymer electrolyte (~1.5 μm thick) and lithium layer (~1.5 μm thick). The solid polymer electrolyte seems to penetrate into the TiS_2 layer although the penetration depth is small. The shape of the TiS_2 is not altered by the deposition of the solid polymer electrolyte. An excess of lithium was deposited, so that the quantity of lithium would not have an influence on the discharge performance of the battery.

The first discharge of cells at different current densities at room temperature (15-20°C) are shown in Fig. 2.13. At a low current density of 10 μA/cm^2, this battery had high utilization. The cells seems to have fairly high internal

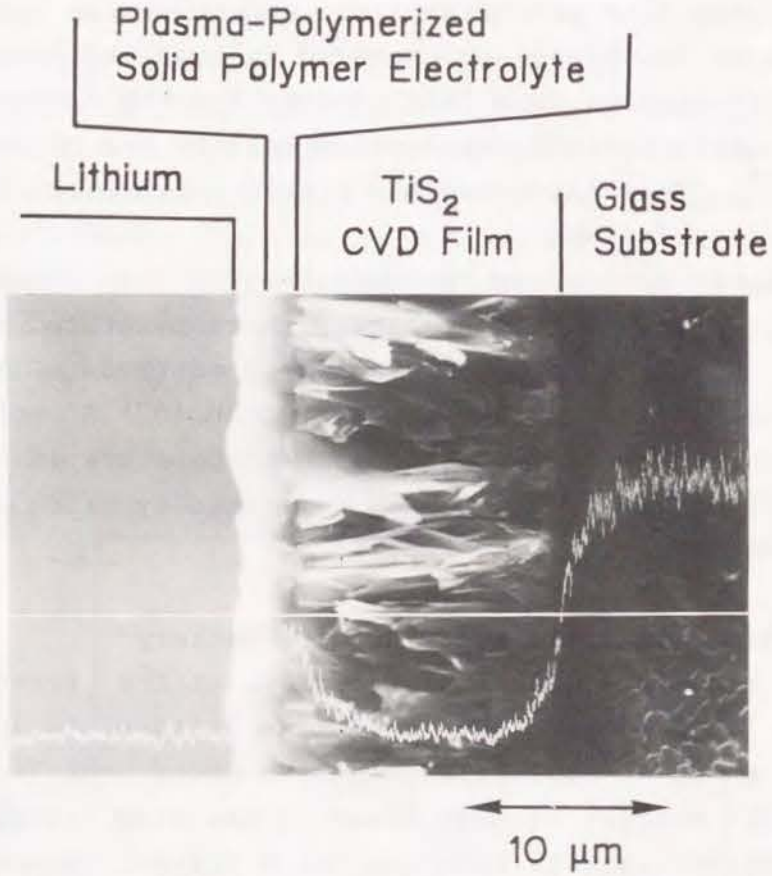

Fig. 2.12. A scanning electron micrograph of the cross-section of a thin film solid-state lithium battery and Si X-ray line.

resistance from the appearance of the discharge curve. The discharge performance of the cells at room temperature is low compared with reported solid-state lithium batteries using conventional solid polymer electrolyte operating above 100 °C [1-4]. The thickness of the solid polymer electrolyte of these reported solid-state lithium batteries are about 10^2 μm which is two orders of magnitude thicker than that of the present battery. Ionic conductivities of solid polymer electrolytes at 100 °C is generally about two orders of magnitude higher than that at room temperature [15,16]. Therefore,

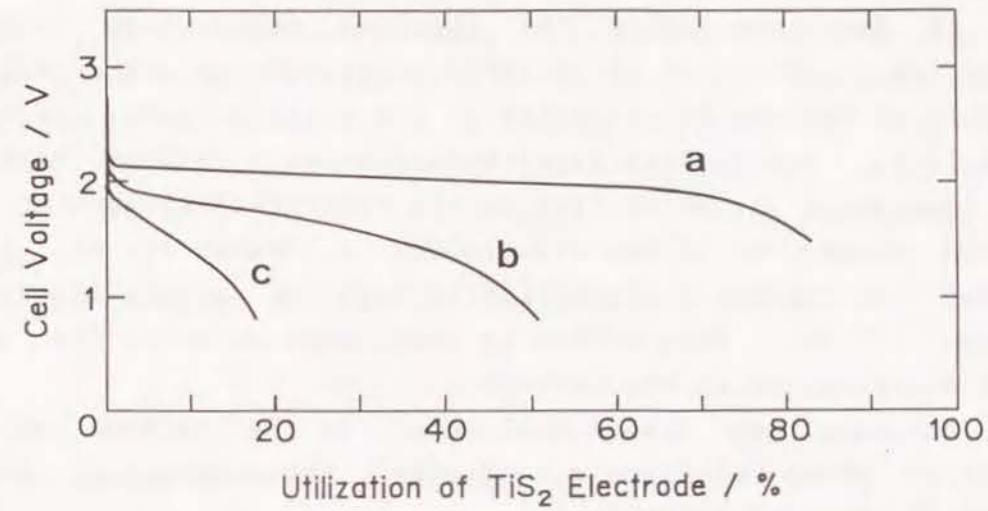

Fig. 2.13. Utilization curves of thin film solid-state lithium batteries at different discharge current densities at room temperature.
a: 10 μA/cm^2, b: 20 μA/cm^2, c: 40 μA/cm^2

practical resistance values of solid polymer electrolyte are almost equal for both the reported batteries operating at 100 °C and the battery of present study operating at room temperature.

The solid-state lithium batteries operating at about 100 °C were fabricated using composite cathode [mixture of cathode active material and solid polymer electrolyte] [1-4]. Thus, the surface area of cathode active material contacting with solid polymer electrolyte is different between the battery operating at about 100 °C and that of the present battery. Therefore, the low discharge performance of the present study may be due to the interfacial resistance between the electrolyte and lithium and/or to the overpotential between the electrolyte and cathode active material.

2.3.4 Interface between Solid Polymer Electrolyte and Cathode Active Material

As describes above, the reported solid-state lithium batteries operating at about 100°C comprised composite cathode mixture of cathode active material and solid polymer electrolyte [1-4]. The current distribution in such cathode mixture is considered to be similar to the current distribution in porous electrodes or bed electrodes. J. Newman et. al. have solved the current distribution in such of porous-electrode system [17-19]. This method is applicable to solve the current distribution in the battery.

Assuming one dimensional model, in the cathode active material phase [electronic conductor], the movement of electrons is governed by Ohm's law

$$i_1 = - \sigma \frac{d\Phi_1}{dx} \qquad (1)$$

where i_1 is the current density in a cathode active material phase in A cm^{-2}; σ is the effective conductivity of cathode active material in S cm^{-1}; Φ_1 is potential (subscription 1 means an cathode active material phase); and x is distance through the one-dimensional composite cathode. The σ can be estimated from the conductivity σ_o of the cathode active material of TiS_2.

$$\sigma = (1-\epsilon)^{1.5} \sigma_o \qquad (2)$$

where σ_o is 1×10^3 S cm^{-1} [20].

Similarly, Ohm's law governs the variation of potential in the solid polymer electrolyte [ionic conductor] in the composite cathode.

$$i_2 = - \kappa \frac{d\Phi_2}{dx} \qquad (3)$$

$$\kappa = \epsilon^{1.5} \kappa_o \qquad (4)$$

where i_2 is the current density in a pore electrolyte phase in A cm^{-1}; and κ is the effective conductivity of the pore electrolyte in S cm^{-1}; and κ_o is the conductivity of the pore electrolyte. Conductivity κ_o of the solid polymer electrolyte at 100°C is 5×10^{-3} S cm^{-1} (subscription 2 means an electrolyte phase).

For constant current discharge of I A cm^{-2},

$$I = i_1 + i_2 \qquad (5)$$

The following boundary conditions are valid.

$$\text{At } x = 0,\ i_2 = I,\ i_1 = 0,\ \Phi_2 = 0.$$
$$\text{At } x = L,\ i_2 = 0.$$

where L is the thickness of one-dimensional composite cathode; 100 μm.

In the case of this type of lithium battery, the overpotential is considered to be small. Therefore, this problem may be solved for a linear polarization equation.

$$\frac{di_2}{dx} = c(\Phi_1 - \Phi_2)$$

where c is a constant. The equation are solved as follows.

$$\frac{dj}{dx} = \frac{\upsilon \kappa}{(\kappa + \sigma)\sinh} \left[\frac{\sigma}{\kappa} \cosh \upsilon (1-y) + \cosh \upsilon y \right] \qquad (6)$$

where $j = i_1 I^{-1}$, $y = x L^{-1}$, $\upsilon = \sqrt{\delta}$, $\delta = L I \beta \left(\frac{1}{\kappa} + \frac{1}{\sigma} \right)$,

$$\beta = 0.5 \frac{F}{RT}$$

The resulting discharge current distributions in composite cathode for linear polarization at different discharge current densities are shown in Fig. 2.14. Under the low discharge current density of 1 mA cm^{-2}, the current distribution is almost uniform in the composite cathode. This fact indicates that not only the surface of the cathode active material at the interface between the solid polymer electrolyte and the composite cathode (at x = 0) but also the whole surface area of active material in the composite cathode contributes the discharge.

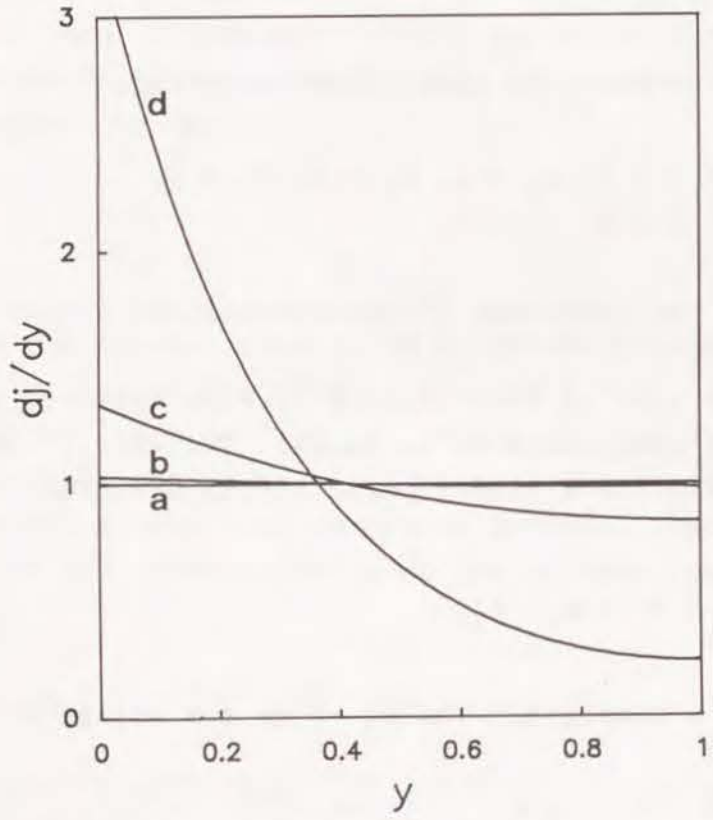

Fig. 2.14. Discharge current distributions in composite cathode for linear polarization at different discharge current densities of a: 10^{-4}, b: 10^{-3}, c: 10^{-2}, d: 10^{-1} A cm^{-2}.
ϵ = 0.5, $\kappa_e = 5 \times 10^{-3}$ S cm^{-1}, $\sigma_e = 10^3$ S cm^{-1}
thickness of composite cathode: 100 μm

Total surface area of spherical active material of 10 μm diameter in average in the composite cathode of 100 μm thickness is 30.2 cm^2 per unit apparent surface area. Because TiS_2 is layered compound, shape of TiS_2 particle is not sphere but narrow plate. For narrow plate like mica, Carman surface shape factor, which means ratio surface area of spherical particle of unit volume/surface area of practical particle of unit volume, is about 0.3 [21]. Therefore, the surface area which contact with solid polymer electrolyte in composite cathode is larger than 30.2 cm^2. The chemical diffusion coefficient of lithium in TiS_2 having (110) orientation, whose c-axis is perpendicular to the flux is 2×10^{-8} cm^2 s^{-1} and the value is 4-5 orders of magnitude lager than that in TiS_2 whose c-axis is parallel to the flux of lithium [22]. The majority of the TiS_2 surface in the composite cathode is cleavage plane and this plane is disadvantageous for diffusion of lithium. Therefore, Carman surface shape factor of 0.3 would be compensated by this disadvantageous surface exposure of TiS_2 particles. The highest apparent discharge current density to obtain 80% utilization is 1 mA cm^2 for the battery using composite cathode operating at 100 °C [1], and this value is two orders of magnitude larger than that for the batteries of present study (10 μA cm^{-2}). The effective surface area of the cathode is only 30 times larger than that of present study even at the highest estimate. As shown in Fig. 2.12, in the case of present battery, the electrolyte can penetrate into some depth of the TiS_2 layer and therefore the real surface area must be larger than the apparent surface area. The surface area ratio of the reported batteries to the present battery must be smaller than the estimated value, 30. From this estimation, the low discharge performance can not be ascribed solely to the overpotential between the electrolyte and cathode active material but also should be ascribed to the interfacial resistance between the electrolyte and lithium. The difference temperature of two systems is about 80 °C. This difference had to cause the electrode kinetics of discharge

reaction on the cathode and anode. This influence was neglected in the present treatment owing to the difficulty of its estimation, while it may give a large contribution to the performance.

2.3.5 Interface between Solid Polymer Electrolyte and Lithium Anode

Many workers reported that a film formed on the lithium surface by reaction of the lithium and electrolyte between lithium and liquid electrolyte [23-27]. The interface layer, which is slightly conductive for lithium ion, behaves as a passivation film during discharge of lithium batteries. Identification of the surface films formed on lithium in various organic solvents were reported by D. Aurbach et. al. [28-31]. For example, lithium alkoxides are formed on lithium surface by reaction of ether solvent, e.g., diethoxyethane and tetrahydrofuran, with lithium [29].

FT-IR transmission spectra of lithium alkoxides by KBr tablet method as reference compounds are shown in Fig. 2.15. The spectra of lithium methoxide (Fig. 2.15a), lithium ethoxide (Fig. 2.15b), and lithium butoxide (Fig. 2.15c) are in good agreement with the literature [28,29]. FT-IR transmission spectra of same material of Fig. 2.15 by nujol mull method are shown in Fig. 2.16. The IR spectra of Fig. 2.16 exhibit absorption peaks of 2950, 2925, 2855, 1460, 1380, 725 cm^{-1} which can be attributed to the nujol. The IR spectra of Fig. 2.16 are very similar to that of Fig. 2.15, except for the LiO stretching vibrations which occur at about 600-400 cm^{-1}. In KBr tablet method the lithium alkoxides contacted with KBr and may react with KBr resulting in the formation of potassium alkoxides and LiBr. The contribution of absorption from these compounds interferes and obscure the absorption of the alkoxides (Li-O stretching) at a low wave number region. In order to escape this interference the nujol mull method was also utilized. Peak assignments for FT-IR spectra of lithium alkoxides were performed using that of nujol mull method,

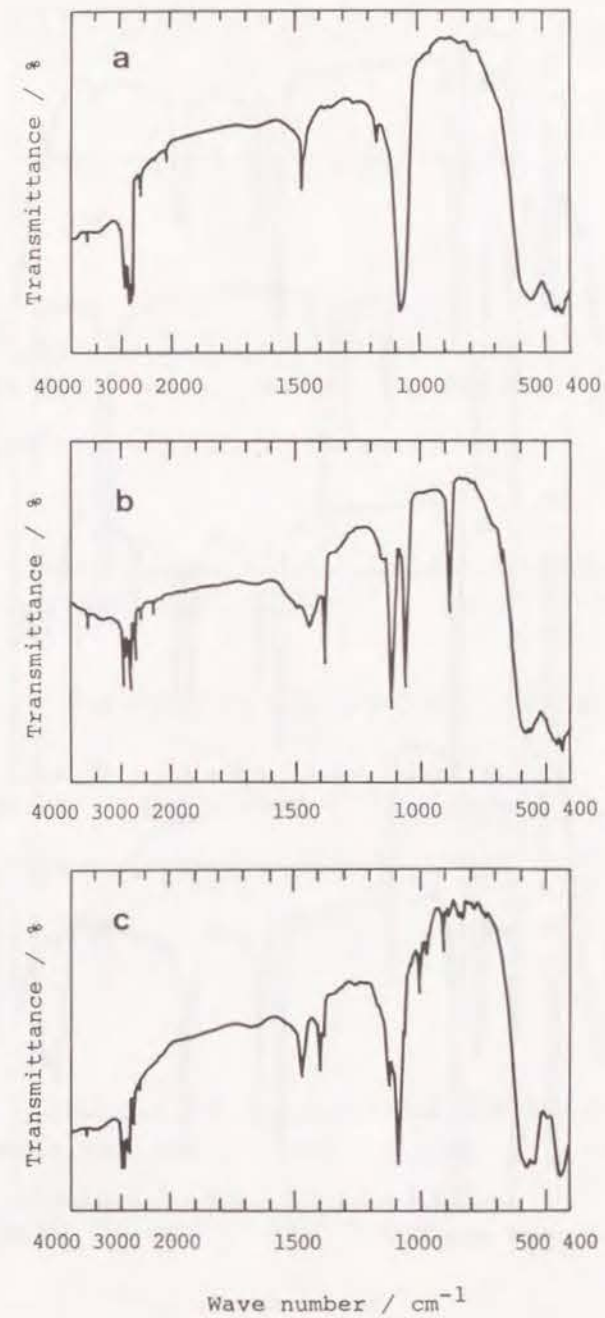

Fig. 2.15. FT-IR transmission spectra of (a) lithium methoxide, (b) lithium ethoxide, (c) lithium butoxide by KBr tablet method.

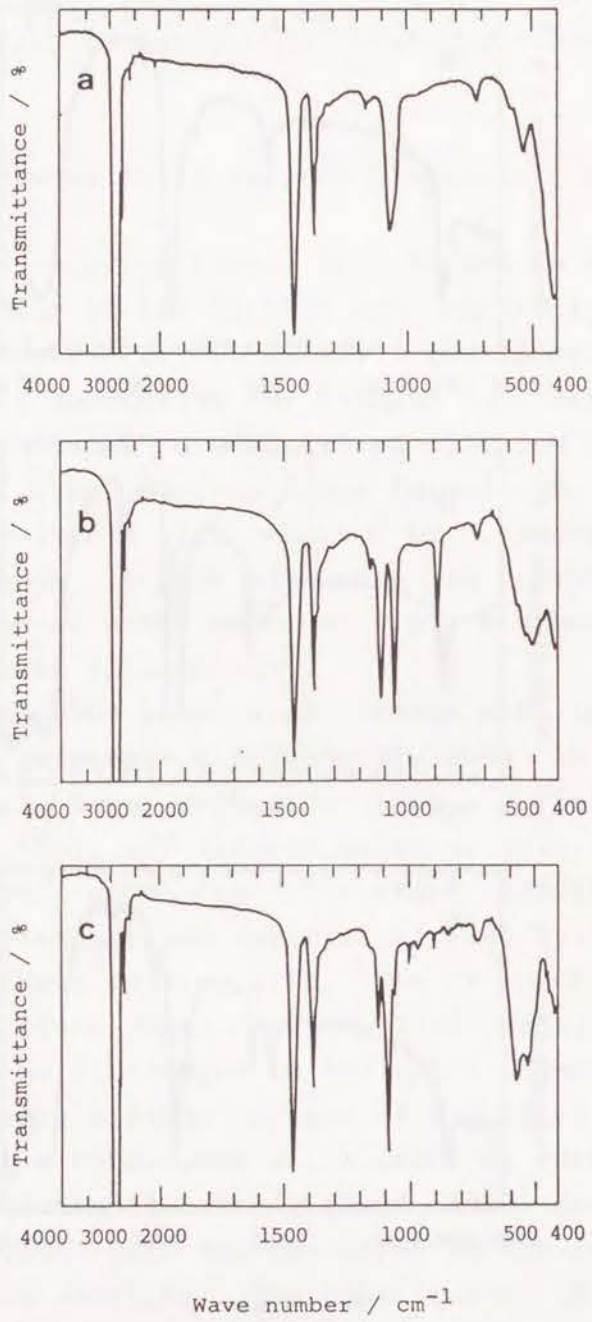

Fig. 2.16. FT-IR transmission spectra of (a) lithium methoxide, (b) lithium ethoxide, (c) lithium butoxide by nujol mull method.

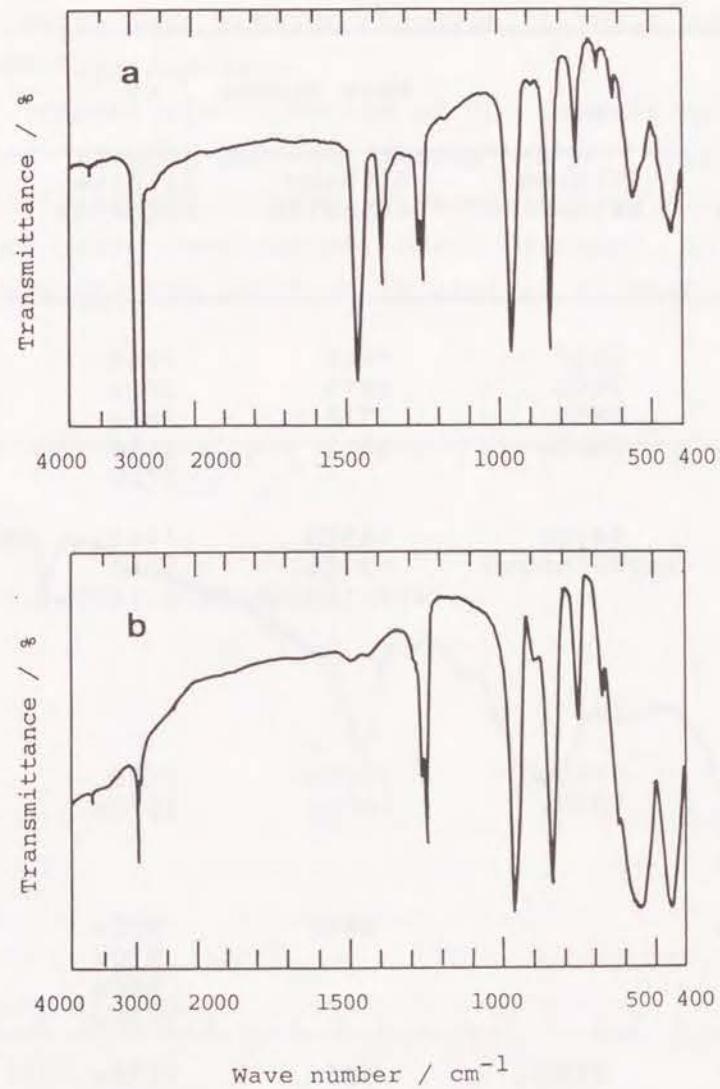

Fig. 2.17. FT-IR transmission spectra of lithium trimethylsilanolate by (a) nujol mull method and (b) KBr tablet method.

Table 2.1. Main peak assignments for FT-IR spectra of lithium methoxide, lithium ethoxide, lithium butoxide and lithium trimethylsilanolate.

Band description	Wave number / cm^{-1}			
	lithium methoxide	lithium ethoxide	lithium butoxide	lithium trimethyl-silanolate
CH stretch	2930 2850 2800 2600w	2960 2810 2710 2610	2960 2920 2870 2810 2720	2955 2900
CH bend	1470m 1400-1500wb	1450m 1390m 1400-1600wb	1460 1360 1400-1600wb	1500m 1440m 1300-1500wb
CH_3 bend				1260s 1240s 835s
CO stretch	1160w 1075s	1120s 1060s	1120 1080s	
SiO stretch				955s
CH_2 stretch		885s	995w 970w 900w 835w	745m
LiO stretch	535 415s	535 505 420	575s 530s 420	560 430

s: strong, m: medium, w: weak, b: broad

except for peaks at 3500-2500, 1500-1300, 750-700 cm^{-1} because of overlap with absorption of nujol. FT-IR transmission spectra of lithium trimethylsilanolate by (a) nujol mull method and (b) KBr tablet method are shown in Fig. 2.17.

Table 2.1 shows main peak assignments for FT-IR spectra of lithium methoxide, lithium ethoxide, lithium butoxide and lithium trimethylsilanolate.

FT-IR transmission spectrum of the product of the reaction between plasma polymer formed from tris(2-methoxy-ethoxy)vinylsilane and lithium is shown in Fig. 2.18. However the peak of the spectrum is broad because of its high molecular weight, the spectrum is similar to that of lithium

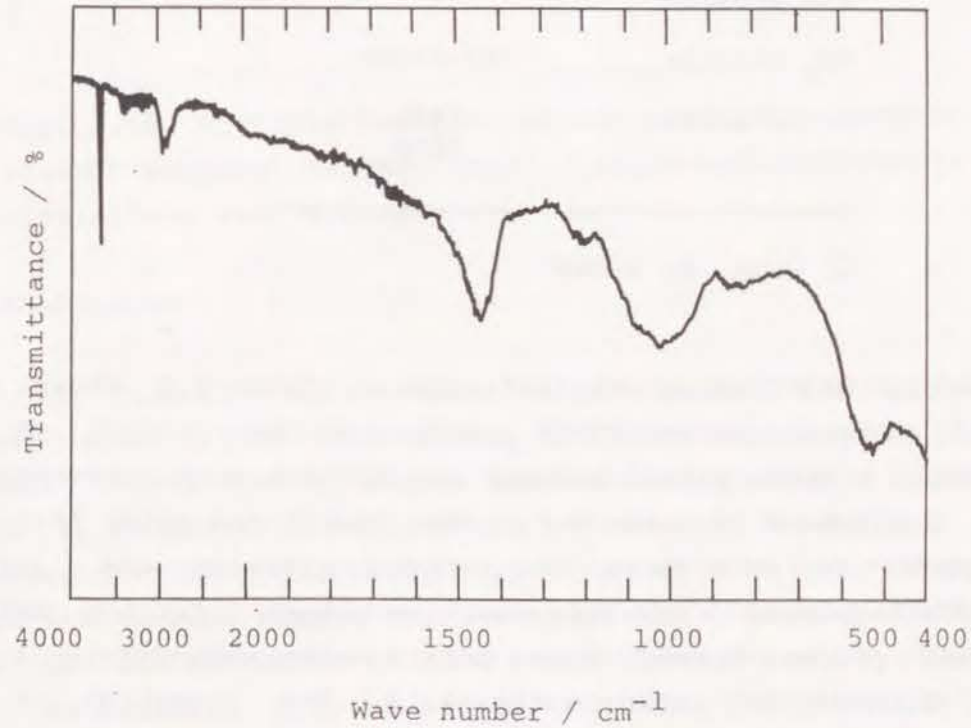

Fig. 2.18. FT-IR transmission spectrum of the product of the reaction between plasma polymer formed from tris(2-methoxyethoxy)vinylsilane and lithium.

Table 2.2. Main peak assignments for FT-IR spectrum of the product of the reaction between plasma polymer formed from tris(2-methoxyethoxy)vinylsilane and lithium.

Band description	Wave number / cm^{-1} product
CH stretch	2900
CH bend	1400-1500b
CO stretch SiO stretch	900-1100b
CH_2 stretch	750-900wb
LiO stretch	540b 400b

w: weak, b: broad

alkoxide and lithium alkylsilanolate. Table 2.2 shows main peak assignments for FT-IR spectrum of the product of the reaction between plasma polymer and lithium with reference to the assignment of Table 2.1. This result indicates that the product is a mixture of lithium alkoxide and lithium alkylsilanolate. Possible reaction scheme occurring between plasma polymer formed from tris(2-methoxyethoxy)vinylsilane and lithium is shown in Fig. 2.19. The formation of the alkoxides and the silanolates at the interface between plasma polymer electrolyte and lithium would enhances the resistance at the interface; the compounds would enhance the interfacial resistance of the thin film lithium battery.

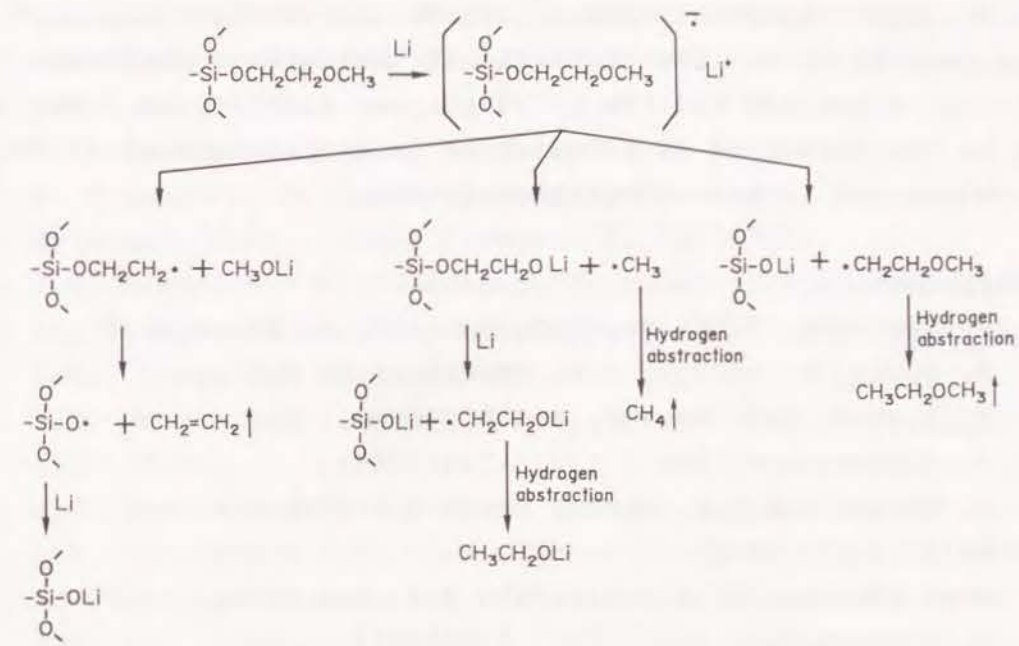

Fig. 2.19. Possible reaction scheme occurring between plasma polymer formed from tris(2-methoxyethoxy)-vinylsilane and lithium.

2.4 Conclusion

The thin film solid-state lithium batteries were fabricated using a thin film of TiS_2 CVD cathode, a thin solid polymer electrolyte by plasma polymerization, and a lithium anode by consecutive vapor-phase processes. The battery was examined for their discharge properties at room temperature at different current densities. Although the discharge performance of the batteries at room temperature was low compared with solid-state lithium batteries using composite cathode above 100 ℃, at a low current density of 10 $\mu A/cm^2$, the battery showed a high performance. The low discharge performance of the batteries is ascribed both to the interfacial resistance between the electrolyte and lithium and to be overpotential between the electrolyte and cathode active material. The

overpotential was caused by the narrower contact area between solid polymer electrolyte and cathode active material. FT-IR measurements show the interfacial resistance between the lithium electrode and the solid polymer electrolyte film was due to the formation of a resistive layer (mixture of lithium alkoxides and lithium alkylsilanolates).

References

1. M. Gauthier, D. Fauteux, G. Vassort, A. Belanger, M. Duval, P. Ricoux, J-M. Chabagno, D. Muller, P. Rigaud, M.B. Armand, and D. Deroo, J. Electrochem. Soc., 132, 1333(1985).
2. A. Hooper and J.M. North, Solid State Ionics, 9&10, 1611(1983).
3. K.M. Abraham, M. Alamgir, and S.J. Perrotti, J. Electrochem. Soc., 135, 535(1988).
4. F. Bonino, M. Ottaviani, B. Scrosati, and G. Pistoia, J. Electrochem. Soc., 135, 12(1988).
5. K. West, B. Zachau-Christiansen, T. Jacobsen, and S. Atlung, J. Electrochem. Soc., 132, 3041(1985).
6. P. Novak, O. Inganas, and R. Bjorklund, J. Electrochem. Soc., 134, 1341(1987).
7. Y. Matsuda, J. Power Sources, 20, 19(1987).
8. H. Yasuda, J. Polym. Sci., Macromol. Rev., 16, 199(1981).
9. J.R. Akridge, and H. Vourlis, Solid State Ionics, 28-30, 841(1988).
10. K. Kanehori, K. Matsumoto, K. Miyauchi, and T. Kudo, Solid State Ionics, 9&10, 1445(1983).
11. M.S. Wittingham, Prog. Solid State Chem., 12, 41(1978).
12. K. Kanehori, F. Kirino, Y. Ito, K. Miyauchi, and T. Kudo, J. Electrochem. Soc., 136, 1265(1989).
13. M.L. Williams, R.F. Landel, and J.D. Ferry, J. Am. Chem. Soc., 77, 3701(1955).
14. M. Cohen and D. Turnbull, J. Chem. Phys., 31, 1164(1959).

15. M.B. Armand, J.M. Chabagno, and M.J. Duclot, "Fast Ion Transport in Solids", P. Vashista, J.N. Mundy, and G.K. Shenoy, Editors, p. 131, Elsevier Pub. Co., New York (1979).
16. M. Watanabe, M. Kanba, H. Matsuda, K. Tsunemi, K. Mizoguchi, E. Tsuchida, and I. Shinohara, Makromol. Chem., Rapid Commun., 2, 741(1981).
17. J.S. Newman and W. Tidemann, "Advanced in Electrochemistry and Electrochemical Engineering", Vol. 11, John Wiley & Sons, Inc., New York, (1978).
18. J.S. Newman and C.W. Tobias, J. Electrochem. Soc., 109, 1183(1962).
19. J.S. Newman and W. Tidemann, AIChE J., 21, 25(1975).
20. L.E. Conroy and K.C. Park, Inorganic Chem., 7, 459(1968).
21. K. Okada and Y. Sometani, "Chemical Engineering", Kyoritu Pub. Inc., Tokyo, (1965).
22. D.A. Winn, J.M. Shemilt, and B.C.H. Steele, Mat. Res. Bull., 11, 559(1976).
23. Y. Geronov and R.H. Muller, J. Electrochem. Soc., 132, 285(1985).
24. A.N. Dey, Thin Solid Films, 43, 131(1977).
25. E. Peled, J. Electrochem. Soc., 126, 2047(1979).
26. I. Yoshimatsu, T. Hirai, and J. Yamaki, J. Electrochem. Soc., 135, 2422(1988).
27. C.D. Desjardins, G.K. MacLean, and H. Sharifian, J. Electrochem. Soc., 136, 345(1989).
28. D. Aurbach, M.L. Daroux, P.W. Faguy, and E. Yeager, J. Electrochem. Soc., 134, 1611(1987).
29. D. Aurbach, M.L. Daroux, P.W. Faguy, and E. Yeager, J. Electrochem. Soc., 135, 1863(1988).
30. D. Aurbach, J. Electrochem. Soc., 136, 906(1989).
31. D. Aurbach, J. Electrochem. Soc., 136, 1606(1989).

Part III. Thin Ion-exchanger Films

Chapter 1 H^+ ion Perm-Selective Membrane from Nafion for Redox-Flow Battery

1.1 Introduction

Ion-exchange membranes have been used in a variety of electrochemical applications, including, among others, water electrolyzers [1,2], sensors [3,4], and redox-flow batteries [5,6]. Although such membranes have a high selectivity of counter-ions over co-ions, their selectivity among different counter-ions is generally low. The range of applications for ion-exchange membranes would be extended if such membranes had a higher selectivity among counter-ions. For example, the performance of a redox-flow battery is strongly dependent on the separator perm-selectivity among ions of the same polarity. Thus, the development of the Iron-Chromium redox-flow battery would be greatly aided by the availability of a cation exchange membrane having a high proton perm-selectivity [6]. This battery usually consists of two solutions divided by a separator. Each solution contains redox cations (e.g., Fe^{2+}/Fe^{3+}, Cr^{2+}/Cr^{3+}), protons and anions. The transport of the redox ions through the separator decreases the cell efficiency and cyclicity. Although an anion exchange membrane might be suitable as a barrier against the redox cations, its electrical resistance is generally too high compared to that of conventional cation exchange membranes. Furthermore, some anionic complex ions containing the redox species may permeate through anion exchange membranes. Cation exchange membranes, on the other hand, generally exhibit lower electrical resistance, but are readily permeated by the redox cations.

J. Electrochem. Soc., 136, 1247 (1989).
Chemistry Letters, 513 (1990).
J. Electrochem. Soc., 137, 1430 (1990).

In this Chapter, the enhancement of the proton perm-selectivity of a cation exchange membrane via the modification of the cation exchange membrane was investigated.

The principle of the enhanced proton perm-selectivity is shown schematically in Fig. 3.1, using an HCl-$FeCl_2$ solution, which is representative of the half-cell of an Iron-Chromium redox-flow battery. A thin plasma polymer layer (PPL) of an anion exchanger is deposited on the surface of the cation exchange membrane. On account of electrostatic repulsion from the fixed anionic groups in the cation exchange membrane, Cl^- ions cannot be transported through the membrane. Simi-

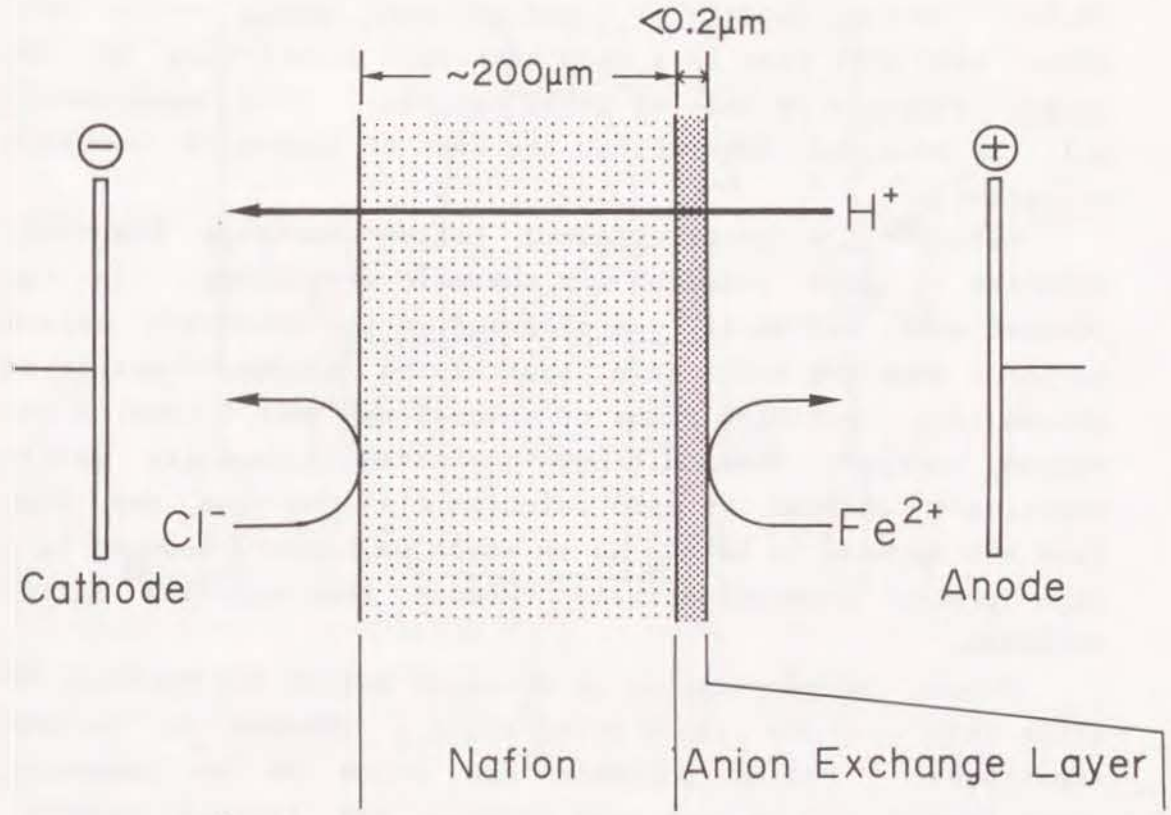

Fig. 3.1. Principle of the enhancement of H^+ ion perm-selectivity through a cation exchange membrane.

larly, the transport of H^+ ions and Fe^{2+} ions also is suppressed by the electrostatic repulsion from the fixed cationic groups in the thin plasma polymer layer on the surface of the cation exchange membrane. However since the repulsion of H^+ ions by the fixed cations in the PPL is weaker than that of Fe^{2+} ions, protons can be transported through the PPL much more easily than can Fe^{2+} ions. This relatively weaker repulsion of protons through the thin layer can be attributed to proton jumping and/or activated transport through the hydrogen-bonding networks in the anion exchanger [7,8]. Indeed, this preferential proton transfer in the thin film can be ascribed to the same mechanism that accounts for the anomalously high conductivities in simple aqueous acid solution [9,10]. A high density of fixed cationic groups in the thin layer will give rise to a high transport selectivity of the proton relative to that of other cations. This enhancement will be achieved, however, at the cost of increased membrane resistivity.

Nafion®*, a perfluorinated cation exchange membrane, exhibits a high chemical and thermal stability. In the present work, Nafion 117 was selected as the substrate cation exchange membrane and a thin layer having nitrogen-containing groups (e.g., pyridine rings or amines) was then formed on the Nafion surface. These nitrogen-containing groups are easily positively charged in acid solution [11], so that the thin film can be made to behave as an anion exchanger, leading to a high proton perm-selectivity through the modified Nafion membrane.

Plasma polymerization is a useful method for forming an ultra-thin uniform layer which tightly adheres to various substrates. Plasma polymers are known to be generally cross-linked and to have high chemical and thermal stabili-

---

* "Nafion" is a registered trade mark of the Du Pont de Nemours and Co., Inc.

ties. Moreover, the extreme thinness of the PPL makes it possible to keep the resistance of the plasma-modified Nafion relatively low. For these reasons plasma polymerization was selected as the method for forming an ultra-thin layer of an anion exchanger on Nafion.

1.2 Experimental

Plasma Polymerization

As shown in Fig. 3.2, the plasma polymerization system consisted of a tubular glass reactor (9 cm diameter, 35 cm

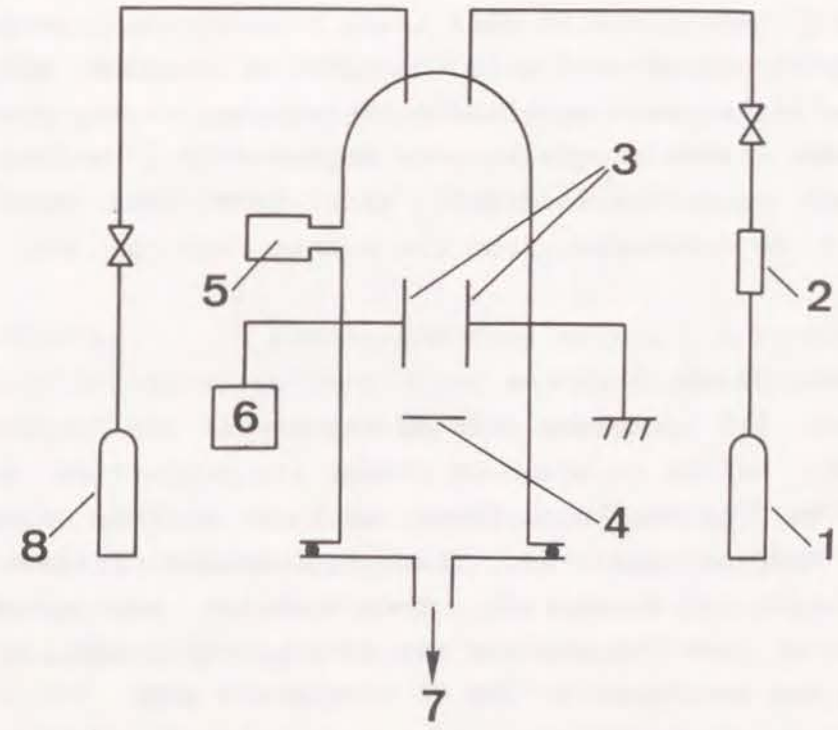

Fig. 3.2. Schematic diagram of plasma reactor.
1, Ar; 2, flow meter; 3, parallel electrodes;
4, substrate holder; 5, Pirani gauge; 6, power source;
7, pump; 8, source gas.

height) equipped with a pair of stainless steel SUS-304 inner disk electrodes (28 cm^2, 4 cm electrode gap), two gas inlet lines, a Pirani gauge, a power supply connected with an impedance matching network, and a vacuum pumping system. The reactor was evacuated to a pressure lower than 1 Pa before starting the polymerization. Ammonia [12], triethylamine (TEA), and 4-vinylpyridine (4-VP) [13] were examined as the materials used to form the thin layer of anion exchanger. The monomer vapor and a plasma assist gas (Ar, 10 cm^3(STP)/min) were introduced separately from the top of the glass reactor. While maintaining a constant flow of the gases, the reactor was pumped and maintained at 66.5 Pa by controlling a throttle valve connected to the vacuum pump. Then, plasma polymerization was initiated by applying AF (Audio Frequency, 10 kHz) or RF (Radio Frequency, 13.56 MHz) power between the electrodes. Glass plates coated with gold (hereinafter denoted Au/glass) and Nafion sheets were utilized as substrates. The substrate was placed either in the in-glow region (i.e., between the electrodes) or in the (nominal) "after-glow" (see discussion below), 2 cm downstream from the bottom edge of the electrodes.

Pretreatment of the Membrane

Nafion 117 membrane (178 μm thickness) was chosen for this study. Nafion is known to change its properties depending on the treatment conditions, such as boiling time and solution compositions [14]. This pretreatment followed the one by Yeager and Steck [15]. Then membrane was maintained under 1 Pa at room temperature for 24 hours to evaporate water after boiling treatment in the H^+ form for 1 hour.

Properties of the plasma polymer

The surface and cross-sectional morphology of the plasma layer formed on Au/glass was observed with a scanning electron microscope (SEM) (Hitachi model S-510). The deposition rate of the plasma layer (μg cm^{-2} h^{-1}) was determined from the weight difference of Au/glass before and after polymerization.

The plasma membranes were characterized by FT-IR spectrometry (Shimadzu FTIR-4100), using a reflection method.

The ohmic resistance of the plasma-modified Nafion was measured as follows: The membrane was inserted as a separator (area exposed to solution, 3.14 cm^2) between two compartments of a glass cell without any treatment after plasma polymerization. Each compartment was filled with 1.0M HCl. A movable Luggin capillary, connected to a Ag/AgCl reference electrode, was inserted into each compartment. By moving the edges of the capillary tips, the solution ohmic drop profile could be measured under constant current electrolysis conditions (10 mA). The ohmic voltage drop across the membrane (and hence, the ohmic resistance of the membrane) was obtained by extrapolating the voltage profile to the position of the separator surfaces.

The perm-selectivity of the plasma-modified Nafion was evaluated from the transference number of the Fe^{2+} ion (t_{Fe}) in the H^+-Fe^{2+} system. A total charge of 100 C was passed at a constant current of 10 mA (12.8 mA/cm^2) through the system:

0.5M $FeCl_2$ +1.0M HCl(anolyte)	plasma-modified Nafion (plasma layer contacting the anolyte)	2.0M HCl (catholyte)

After the electrolysis, the total amount of Fe^{2+} in the catholyte was measured by absorption spectrometry using o-phenanthroline [16] to evaluate the amount of Fe^{2+} transported through the plasma-modified Nafion. Values of t_{Fe} were calculated from the amount of Fe^{2+} transported and the total charge passed during the electrolysis.

1.3 Results and Discussion

Comparison of monomers for the modification of Nafion

Anion exchange membrane usually have nitrogen-containing functional groups (e.g., amines or pyridine rings), which are quaternarized to ammonium cations. High concentrations of such functional groups increase the anion exchange capacity of the membranes. Accordingly, ammonia and TEA were selected to introduce amino groups in the plasma layer, and 4-VP was selected to introduce pyridine rings. The properties of the plasma polymer also may be influenced by the frequency of the applied power. For the work reported in this section, AF power was applied to polymerization a thin layer of anion exchanger.

Table 3.1. Transference numbers of Fe^{2+}(t_{Fe}) through plasma-treated Nafion® 117 membranes(1)

	Conditions			
	Pressure (Pa)	Plasma Power (W,AF)	Time in Plasma(min)	t_{Fe}
Nafion 117	--	--	--	0.59
Nafion 117+$(CH_3CH_2)_3N$	67	50	10	0.11
Nafion 117+NH_3	67	200	60	0.10
Nafion117+4-VP(2)	7	50	30	0.00048
Nafion 117+4-VP+Ar	7	50	10	0.00034

(1) Plasma polymerization carried out in in-glow region

(2) 4-vinylpyridine

The values of t_{Fe} through Nafion, plasma-treated using ammonia, TEA, and 4-VP are summarized in Table 3.1. All samples were treated in the in-glow region of the reactor. Although the plasma conditions employed during each experiment were not precisely the same; the results in Table 3.1 show that, of the three monomer compounds studied, the plasma layer of 4-VP suppressed the transport of the Fe^{2+} ion the best. The suppression by 4-VP was more effective than that by ammonia or TEA by at least two orders of magnitude. Therefore, based on these results, 4-VP was adopted as the monomer for the work described in the remainder of the present communication.

It was observed, however, that the membrane resistances were unacceptably high (on the order of 30~40 Ωcm^2) for all cases in which the substrate was set in the in-glow region. Since both the substrate and the polymer surface were subjected to repeated attack by the activated species in the in-glow region, it can be inferred that functional groups in the Nafion surface and in the deposited polymer layer were destroyed and that the plasma polymer was highly cross-linked, thereby increasing the resistance of the membrane. Therefore, for the work reported in the following sections the substrates were set in the "after-glow" region in order to keep the membrane resistances as low as possible. Furthermore, since AF power is known to impart a higher energy than RF power to activated species in plasma [17], and this favors increased resistance, RF power was subsequently selected instead of AF power for the polymerization process.

Effects of some polymerization parameters on rate of plasma polymerization

The mechanisms of plasma polymerization are not yet fully understood, and their elucidation is difficult. Although the complexity of the reaction path and the multi-dependency of the polymerization rate on the plasma conditions give rise to experimental difficulties, at the same time these also impart flexibility in designing the surface-modifying layer on the Nafion. In order to enhance the perm-selectivity of the proton according to the principle outlined in Fig. 3.1, it is necessary to form on the Nafion surface a thin anion exchange layer having a high ion-exchange capacity. Since little is known about the plasma polymerization of monomers containing functional groups [18], the dependence of the deposition rate on the monomer flow rate and on the magnitude of the applied RF power was investigated using 4-VP as monomer. The substrates were set in the "after-glow" region in order to prevent the monomer and deposited polymer from decomposing from direct exposure to the plasma.

The dependence of the monomer deposition rate on the applied RF power was examined at a 4-VP flow rate of 5 cm^3 (STP)/min and pressure of 66.5 pa. As shown in Fig. 3.3, at applied RF powers below about 30 W, the deposition rate increased sharply with increasing power. This is the type of behavior expected to occur in the after glow region, where an increase in plasma power gives rise to an increase in the concentration of active species, which in turn leads to higher polymer deposition rates. Conversely, beyond 30~40 W, the deposition rate decreased as the power increased. This behavior probably indicates that at higher power the plasma region begins to extend to the after-glow region, so that the after-glow region in effect becomes similar to the in-glow region since it now contains plasma. When plasma is present, the Competitive Ablation and Polymerization (CAP) mechanism [19-22] can be used to explain the behavior shown in Fig. 3.3. In the plasma region, the monomer is activated to radicals and

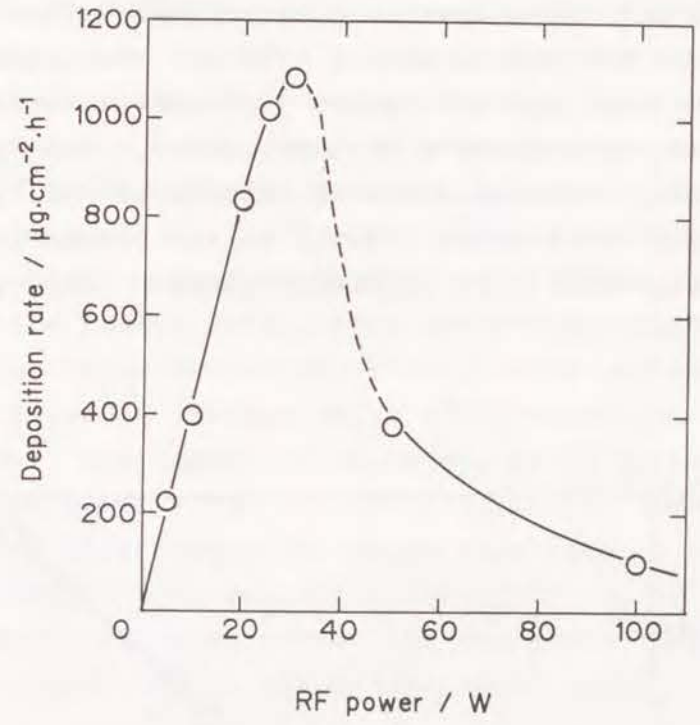

Fig. 3.3. Effect of RF power on deposition rate of plasma polymer deposited in "after-glow" region from 4-vinylpyridine.
Pressure = 67 Pa; Ar flow rate = 10 cm^3(STP)/min;
4-vinylpyridine flow rate = 5 cm^3(STP)/min.

ions which react to form polymer [23,24]. These species are not necessarily the same as those that are formed in the after-glow region. The excitation energy of the plasma is high and the excited species can possess high energy. Under these conditions two different types of polymerization can take place. The first, a polymerization process similar to conventional chain propagation, proceeds at the olefinic double bond of the 4-VP. This radical polymerization is triggered by radical species formed by plasma activation.

This type of polymerization process is called "plasma-induced polymerization". With the second type of polymerization, the collision of activated species causes combination processes that occur in the plasma state. These processes lead to polymer formation, and are termed "plasma-state polymerization". With plasma-state polymerization, the polymer is formed by the repeated stepwise reactions of initiation, propagation and termination [19]. As the plasma-state polymerization proceeds, the activated species may attack the

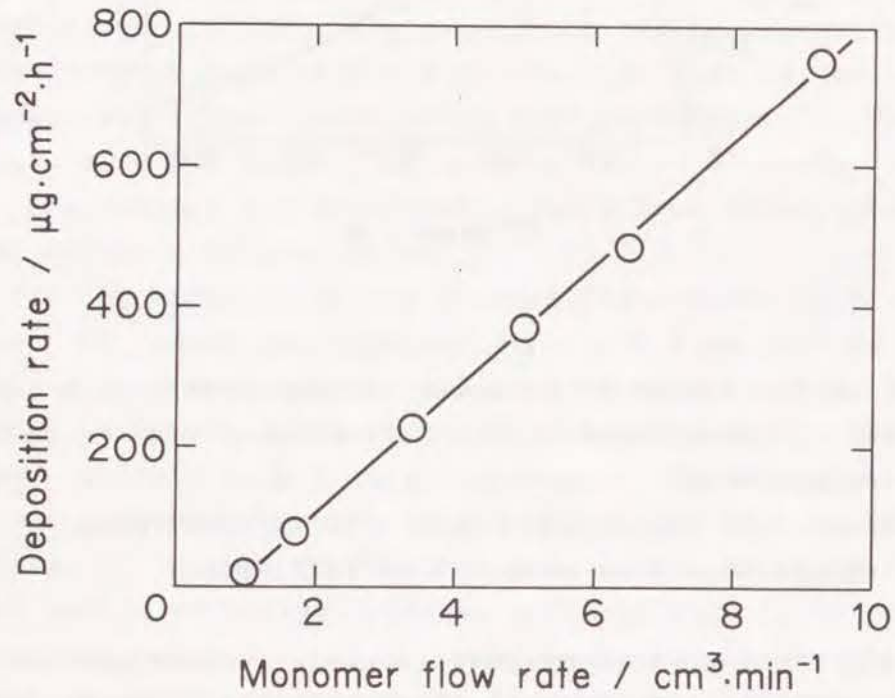

Fig. 3.4. Effect of monomer flow rate on deposition rate of plasma polymer deposited in "after-glow" region from 4-vinylpyridine.
Pressure = 67 Pa; Ar flow rate = 10 cm^3(STP)/min;
RF power = 50 W.

growing polymer layer. This attack can decompose the polymer, extend the cross-linking of the polymer, or cause the elimination of deposited polymer (ablation process). These polymerization and ablation processes proceed competitively, and the overall plasma polymerization rate is dependent on the plasma conditions. At lower RF powers, the polymerization process is dominant and the polymerization rate increases with increasing RF power. Conversely, above a certain level of RF power, the ablation process becomes significant. By further increasing the power, this latter process gradually begins to exert a major influence on the overall rate of the polymerization, and beyond a certain value of RF power (39 40 W in the present case), the deposition rate begins to decrease with increasing RF power [25].

Fig. 3.4 illustrates the deposition rate at 50 W RF power as a function of 4-VP monomer flow rate. Under the conditions employed it is seen that the deposition rate is almost directly proportional to the monomer flow rate.

IR spectroscopic characterization of 4-VP plasma polymer

Scanning electron micrographs indicated that the plasma layer was pinhole-free and of uniform thickness. From the values of the observed thickness and the weight change of the substrate before and after the polymerization, it was estimated that the density of the plasma polymer was on the order of 1.3 g/cm^3. This value is greater than that of polystyrene-like polymers, which have densities of about 1.0 g/cm^3 [26]. The difference can be ascribed largely to the cross-linking of the plasma polymer. Fig. 3.5(a) and 5(b) show the IR spectra of the plasma polymers obtained in the "after-glow" region at 10 W and 50 W RF power, respectively. Both spectra exhibit absorption peaks at 3340 cm^{-1} (N-H vibration) and at 2240 cm^{-1} (C≡N vibration), which indicates that cleavage of pyridine rings in the 4-VP took place during the plasma polymerization process. The four characteristic peaks ascribed to the pyridine ring at 1600 cm^{-1}~1400 cm^{-1} are sharp at 10 W, but

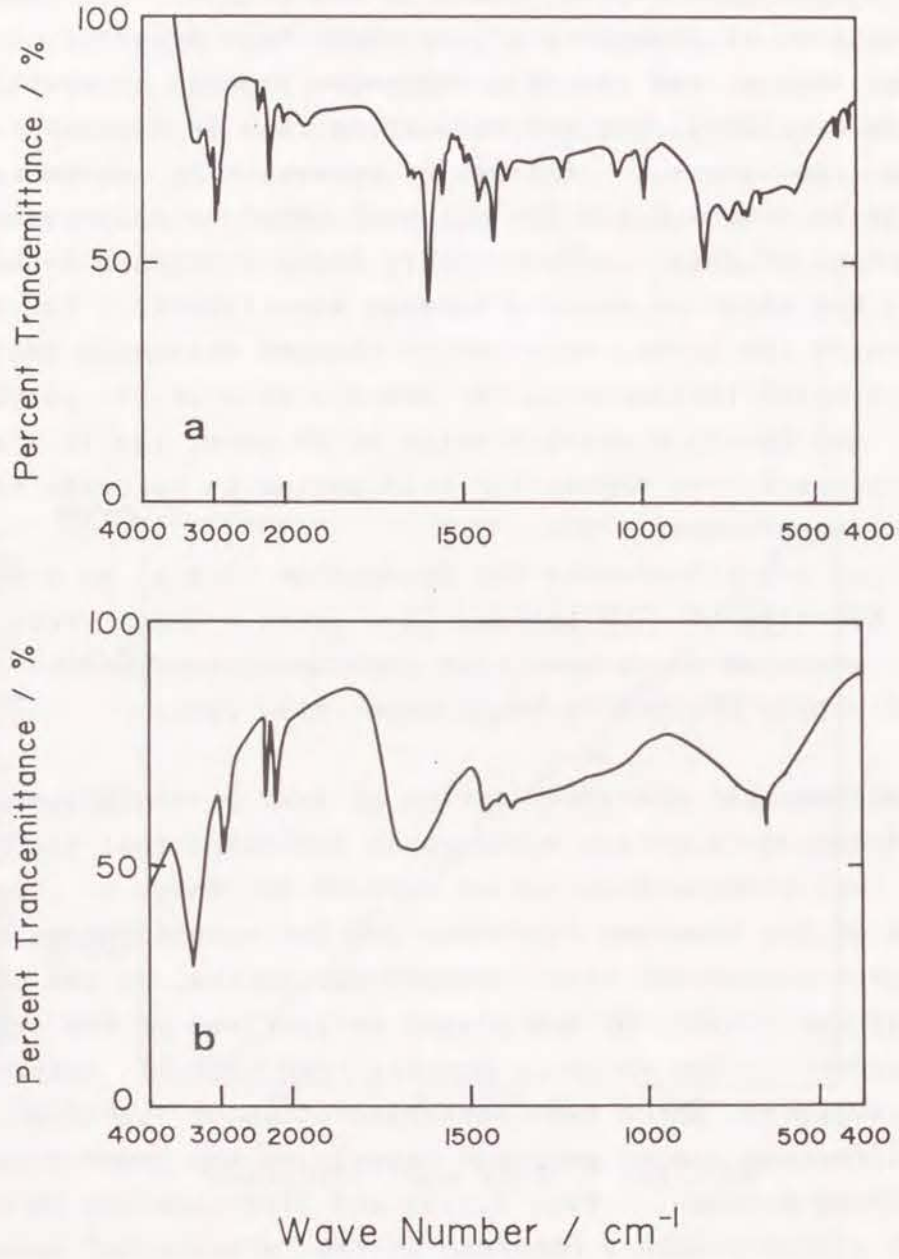

Fig. 3.5. IR spectra of plasma polymer films deposited in "after-glow" region from 4- vinylpyridine at (a) 10 W RF power, (b) 50 W RF power.
Pressure = 67 Pa; Ar flow rate = 10 cm^3(STP)/min;
4-VP flow rate = 5 cm^3(STP)/min.

obscure at 50 W. Furthermore, all the peaks of the film at 50 W are broad. These observations indicate that the extent of pyridine ring cleavage (ablation) increases with increasing RF power, which is consistent with the CAP mechanism referred to in the previous section.

Effect of oxygen sputtering

Nafion, a perfluorinated polymer, has a low surface energy, and the adhesion of plasma polymer film to the Nafion surface is so weak that the plasma layer, especially when prepared under mild conditions (i.e., at low RF power and in

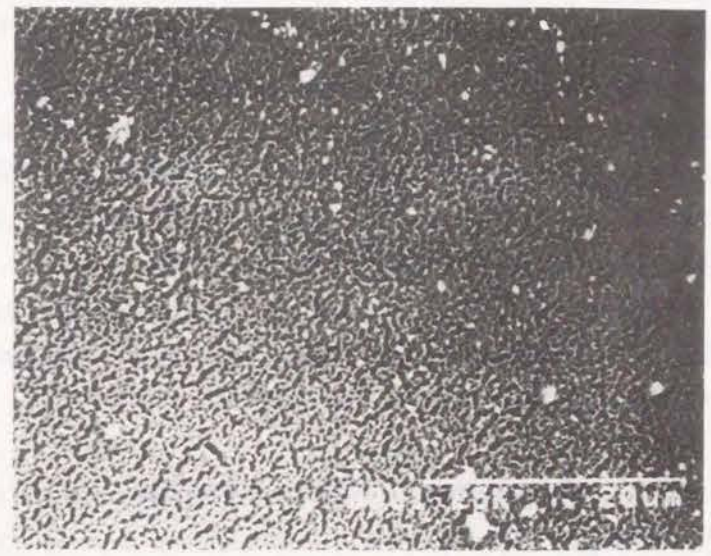

Fig. 3.6. Scanning electron micrograph of the Nafion surface after O_2 sputtering.
Oxygen sputtering pre-treatment for 5 min in oxygen plasma at oxygen flow rate = 10 cm^3(STP)/min; pressure = 6.55 Pa, and RF Power = 50 W.

the after-glow region), is apt to peel off from the Nafion surface during electrolysis. Under more severe plasma polymerization conditions, the adhesion improves, but at the cost of pyridine ring decomposition. In order to increase the adhesion without causing extensive damage to the 4-VP monomer, the Nafion surface was pre-treated by oxygen plasma sputtering prior to polymerization. A Nafion sheet was fixed to an RF electrode and sputtered with oxygen plasma at a flow rate of 10 cm^3(STP)/min, 6.55 Pa pressure, and 50 W RF power. After this treatment, a plasma layer of approximately 0.2 μm thickness was deposited on the sheet in the after-glow region. The resulting deposited layer adhered tightly to the Nafion and did not delaminate when the membrane was used for the previously described electrolysis procedure to determine t_{Fe}. Fig. 3.6 shows the scanning electron micrograph of the Nafion surface after O_2 sputtering. This figure showed a surface roughening on the oxygen-sputtered Nafion. The Nafion surface before sputteing is flat and no observable contrast was detected. Although there was little difference in the IR spectrum of the Nafion before and after sputtering, it can be interred that the tighter adhesion was the result of better mechanical anchoring (though surface roughening) and of enhancement of the surface energy by the introduction of oxygen-containing groups into the Nafion surface.

Perm-selectivity of oxygen-sputtered Nafion modified by 4-VP plasma polymerization

The transference number of Fe^{2+} through Nafion modified with 4-VP following oxygen sputtering is summarized in Fig. 3.7, together with the corresponding membrane resistances. In general, it was found that t_{Fe} for Nafion sputtered with oxygen plasma was significantly lower than that for untreated Nafion (0.27 vs. 0.59), and that increasing the sputtering time increased the membrane resistance but did not appreciably affect t_{Fe}. Accordingly, for each case shown in Fig. 3.7, the Nafion was sputtered for 1 min before plasma polymeriza-

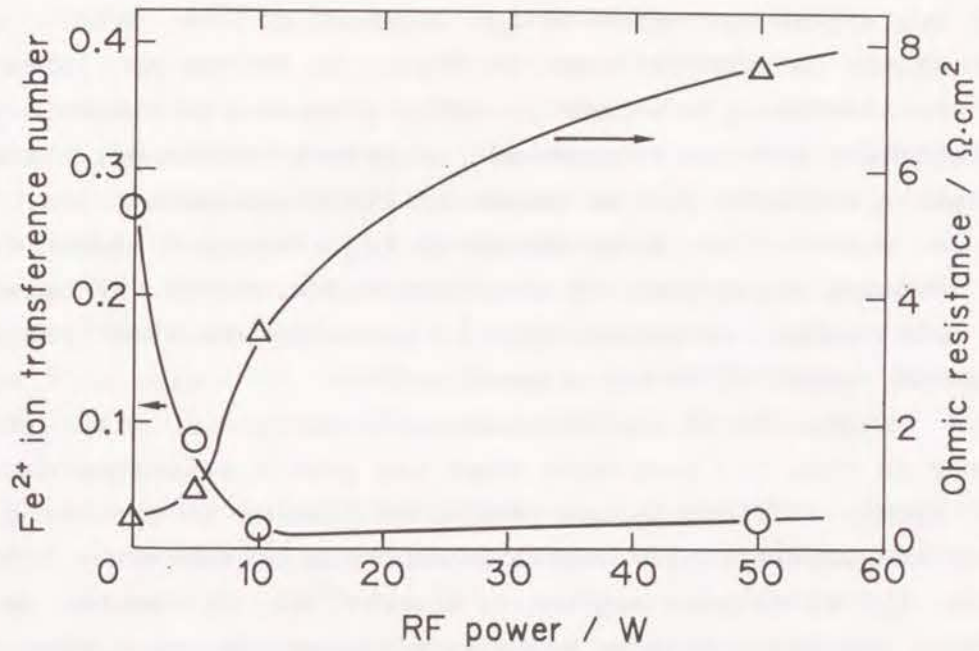

Fig. 3.7. Variation of t_{Fe} and membrane resistance with RF power for 4-VP plasma-modified Nafion 117 membranes pre-treated by oxygen sputtering.
Oxygen sputtering pre-treatment for 1 min in oxygen plasma at oxygen flow rate = 10 cm^3(STP)/ min; pressure = 6.55 Pa, and RF Power = 50 W. Plasma polymerization carried out for 5 min in after-glow region at pressure = 67 Pa; Ar flow rate = 10 cm^3(STP)/min; 4-VP flow rate = 5 cm^3 (STP)/min. Average thickness of plasma polymer layer 0.22 μm. Membrane resistances measured in 1.0 M HCl as described in text.

tion.

The data plotted in Fig. 3.7 show that when the oxygen-sputtered Nafion was modified by 4-VP plasma polymerization, t_{Fe} was lowered even further. For example, Nafion modified by plasma polymerization at an RF power of 10 W exhibited a value of t_{Fe} that was almost twenty times smaller than the t_{Fe} value for oxygen-sputtered Nafion alone (0.015 vs. 0.27). In view of the IR spectra shown in Fig. 3.5, it can be inferred that the introduction of the pyridine ring in the plasma layer is important for the enhancement of perm-selectivity, likely through an increase in the number of fixed cationic sites.

In contrast to the behavior of t_{Fe}, Fig. 3.7 shows that the membrane resistance increased with increasing RF power. This resistance increase also is probably related to the increased number of fixed cationic sites.

A comparison of the data shown in Table 3.1 with those plotted in Fig. 3.7 indicates that the proton selectivities of 4-VP plasma-modified Nafion membranes treated in the in-glow region are significantly higher than those of membranes treated in the after-glow region. However, as discussed in a previous section, in-glow treatment causes decomposition of the starting monomer and results in a high degree of polymer cross-linking, which leads to unacceptably high resistance values.

1.4 Conclusion

Ultra-thin layers of nitrogen-containing groups were prepared by plasma treatment using ammonia, TEA, and 4-VP. Nafion 117 membranes that were modified with plasma polymer layers obtained by using 4-VP as monomer and argon as carrier gas were able to suppress the transport of Fe^{2+} ion by at least two orders of magnitude more effectively than Nafion treated using ammonia or TEA. Accordingly, 4-VP was selected as the monomer of choice. The deposition rate of 4-VP plasma polymer increased with increasing applied RF power, attaining a maximum value at an RF power of about 30 W, beyond which the deposition rate decreased with increasing RF power. The deposition rate was almost directly proportional to the monomer flow rate over the flow rate range of 1~10 cm^3 (STP)/ min. The thin layers obtained were pinhole-free and of uniform thickness.

When the Nafion was plasma-modified in the in-glow region, the resulting plasma-modified membranes exhibited very low values of Fe^{2+} ion transference number (t_{Fe} 0.0003); however, the membrane resistances were unacceptably high (30 ~ 40 Ωcm^2). Accordingly, all subsequent plasma polymerization was carried out in the "after-glow" region.

Oxygen sputtering the Nafion surface prior to plasma modification was found not only to be an effective surface pretreatment for obtaining a tightly adherent plasma polymer layer, but also to significantly lower t_{Fe}. The values of t_{Fe} for oxygen-sputtered membranes could be further lowered by more than an order of magnitude by plasma modification using 4-VP as the monomer, suggesting that the presence of the pyridine ring in the plasma polymer layer strongly influences the perm-selectivity of modified Nafion membranes. Unfortunately, the increase in membrane resistance brought about by oxygen sputtering and plasma modification is a problem that still remains to be solved.

References

1. R. S. Yeo, J. McBreen, G. Kissel, F. Klesa, and S. Srinivasan, J. Appl. Electrochem., 10, 741 (1980).
2. J. L. Weisinger and R. R. Russel, J. Electrochem. Soc., 125, 1482 (1978).
3. A. B. Laconti and H. J. Marget, J. Electrochem. Soc., 118, 506 (1971).
4. N. Oyama, T. Osaka, and T. Okajima, Anal. Chem., 54, 979 (1986).
5. H. Ohya, K. Emori, T. Ohto, Y. Negishi, and K. Matsumoto, Denki Kagaku, 53, 462 (1985).
6. K. Nozaki, H. Kaneko, A. Negishi, and T. Ozawa, Denki Kagaku, 51, 189 (1983).
7. K. A. Mauritz and C. L. Gray, Macromolecules, 16, 1279 (1983).
8. S. R. Lowry and K. A. Mauritz, J. Am. Chem. Soc., 102, 4665 (1980).
9. M. Eigen, Angew. Chem., 75, 489 (1963).
10. D. A. Lown and H. R. Thirsk, Trans. Faraday Soc., 67, 132 (1971).
11. N. Inagaki, Thin Solid Films, 118, 225 (1984).
12. R. K. Sadhir, Z. N. Sanjana, and H. E. Saders, J. Appl. Polym. Sci., Appl. Polym. Symp., 42, 27 (1988).
13. H. Ohya, T. Ohto, T. Sawamura, H. Honda, K. Matsumoto, and Y. Negishi, Denki Kagaku, 56, 34 (1988).
14. W.G. Grot, G.E. Munn, and D.N. Walmsley, Paper 154 presented at The Electrochemical Society Meeting, Houston, TX, May 7-11, 1972.
15. A. Steck and H. L. Yeager, Anal. Chem., 52, 1215 (1980).
16. Nippon Bunseki Kagaku Binran(Handbook of Analytical Chemistry), Maruzen, Tokyo, 1971, p. 99.
17. B. Chapman, Glow Discharge Processes, John Wiley and Sons, New York, 1980, Chap. 5.
18. J. Sakata and M. Wada, J. Appl. Polym. Sci., 35, 875 (1988).
19. H. Yasuda, J. Macromol. Sci. Chem., A10, 383 (1976).

20. H. U. Poll, M. Arzt, and K. H. Wickleader, Eur. Polym. J., 12, 505 (1976).
21. H. Yasuda and T. Hsu, Surf. Sci., 76, 232 (1978).
22. H. Yasuda, J. Polym. Sci., Macr. Rev., 16, 119 (1981).
23. K. Kobayashi, M. Shen, and A. T. Bell, J. Macromol. Sci. Chem., A8, 373 (1974).
24. J. M. Tibbet, R. Jensen, A. T. Bell, and M. Shen, Macromolecules, 10, 647 (1977).
25. M. Gazicki and H. Yasuda, J. Appl. Polym. Sci., 38, 35 (1984).
26. Nippon Bunseki Kagaku Binran (Handbook of Analytical Chemistry), Maruzen, Tokyo (1971), p.1065.

Chapter 2 A New Ultra-thin Fluorinatedsulfonic Acid Membranes Prepared by Plasma Polymerization

2.1 Introduction

Extensive studies have recently been done on ion-exchange membranes, which have been used in a variety of applications, including fuel cells [1], batteries [2], electrolyzers for water [3] and organic syntheses [4], sensors [5]. Especially, fluorinated cation exchange membrane, such as Nafion® [6], having good chemical and thermal stabilities has been used in a variety of electrochemical processes. However, existing fluorinated cation exchange membrane including Nafion are phase separated and can be represented by a three-phase model with hydrophobic amorphous and crystalline regions and hydrophilic ionic domain because of their non-cross-linking structure [7]. The ionic conductivity of commercially available fluorinated cation exchange membrane is lower than that of cross-linked hydrocarbon cation exchange membrane because of low ion exchange capacity. Preparation of cross-linked fluorinated cation exchange membrane will surely lead a improvement of property of the membrane including perm-selectivity and conductivity.

Plasma polymerization is a useful method to deposit ultra-thin, uniform polymer films on various substrates and, in previous Chapters, details of the preparation and application of a number of ionically conductive polymer films prepared using this technique was presented. Membranes prepared by this method are known to be generally highly cross-linked, and the membranes have a superior chemical and thermal stability. Therefore the introduction of ionic group into the fluorinated plasma polymer layer would give the cross-linked fluorinated ion-exchanger film. This communication reports on the preparation of ultra-thin cross-linked fluorinated sulfonic acid membranes utilizing plasma polymerization method.

J. Electrochem. Soc., 137, 3319 (1990).

2.2 Experimental

Figure 3.8 schematically shows the apparatus for the plasma polymerization, which consists of a glass reactor equipped with capacitively coupled inner electrodes (6 cm diameter) connected to an RF supply (13.56 MHz), three monomer inlets, a Pirani gauge, and a vacuum pump. Trifluorochloroethylene (TFCE) was selected as a monomer for backbone polymer. Trifluoromethanesulfonic acid (TMSA) was selected as a

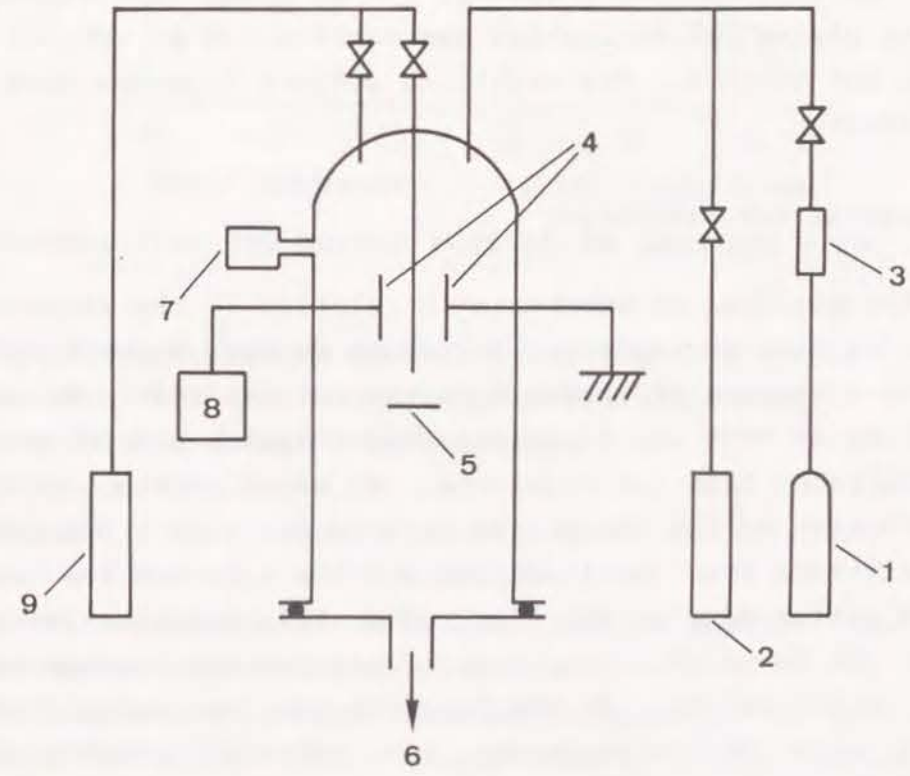

Fig. 3.8. A schematic diagram of an apparatus for plasma polymerization.
1, Ar; 2, TFCE; 3, flow meter; 4, parallel electrodes; 5, substrate; 6, pump; 7, Pirani gauge; 8, matching network; 9, TMSA.

source to introduce the sulfonic acid group. The end of the inlet of TMSA was located either in the top of the glass reactor or in the (nominal) "after glow ", 1 cm downstream from the bottom edge of the electrodes. Glass plates deposited with gold, and stainless steel sheets were utilized as the substrates, whose position was changeable. Argon gas was admitted from the top of the reactor, and the substrate surface was exposed to the argon plasma for 10 min in order to remove water adsorbed on the surface. After the system was evacuated to 10^{-3} Torr, the TFCE gas [10 cm^3(STP)/min] and the TMSA vapor [various flow rate] were introduced into the reactor. The pressure in the reactor was maintained at 0.5 Torr. After setting the gas pressure, the RF power was turned on, and the plasma polymerization was carried out at various power levels for 0.5-1 h. The resulting polymer deposits were about 1 μm thick.

2.3 Results and Discussion

The position of substrate in relation to the electrode is known to have an important influence on the deposition rate and the structure of produced plasma polymer [8]. The deposition rate of TFCE was first measured changing the position of a substrate from the electrode. As shown in Fig. 3.9, the distribution of the deposition rate is not simply dependent on the distance from the electrode and the rate had the maximum at the bottom edge of the electrode. This behavior is interpreted in terms of a competitive ablation and polymerization (CAP) mechanism [9]. At the upstream in-glow region from the bottom edge of the electrode, the ablation process became significant because the excited species which have energy high enough to cause the ablation exist at a high concentration. On the other hand, at the downstream from the bottom edge of the electrode, e.g., in "after-glow region", active species loose their energy by collision during traversing in the space between the bottom edge of the electrode and the substrate.

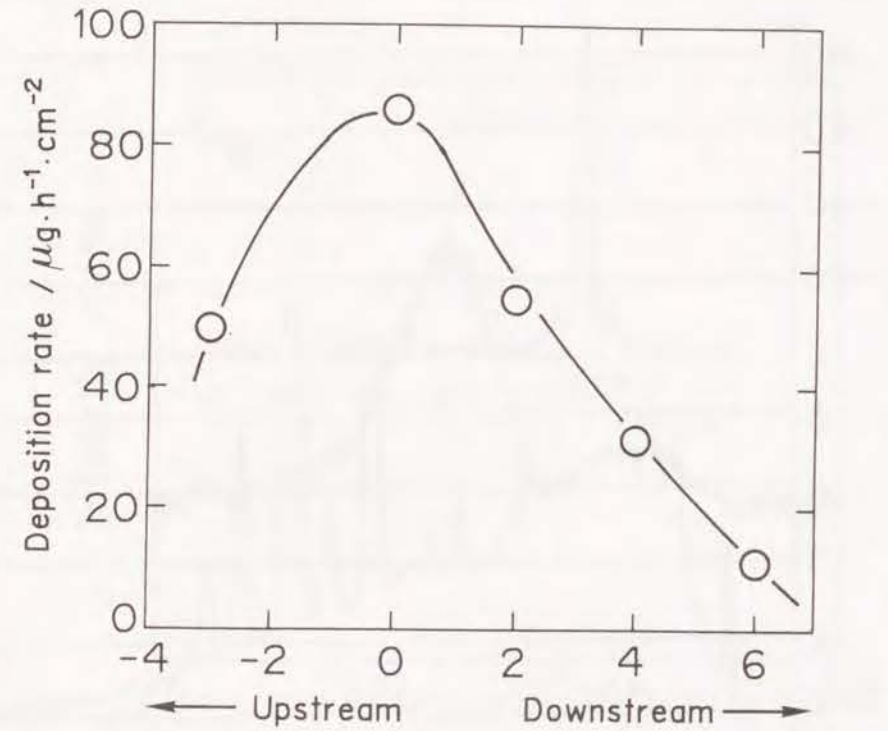

Fig. 3.9. Dependence of the deposition rate on the distance from the bottom edge of the electrode.
Flow rate of TFCE: 10 cm^3(STP)/min
RF power: 25 W
Polymerization pressure: 0.5 Torr

Therefore the concentration of the reactive species decreased and the deposition rate decreased.

As described above, TMSA was selected as a source to introduce the sulfonic acid group. During plasma polymerization, substrates were placed at 2 cm downstream of the bottom edge of the electrode. The plasma polymer from TFCE and TMSA introduced at "after glow" region [Polymer A] was soaked in aqueous 0.5M CsOH solution for 30 min and thoroughly washed with distilled water. The EPMA spectrum (Fig. 3.10) of the resulting plasma polymer showed the existence of Cs in the

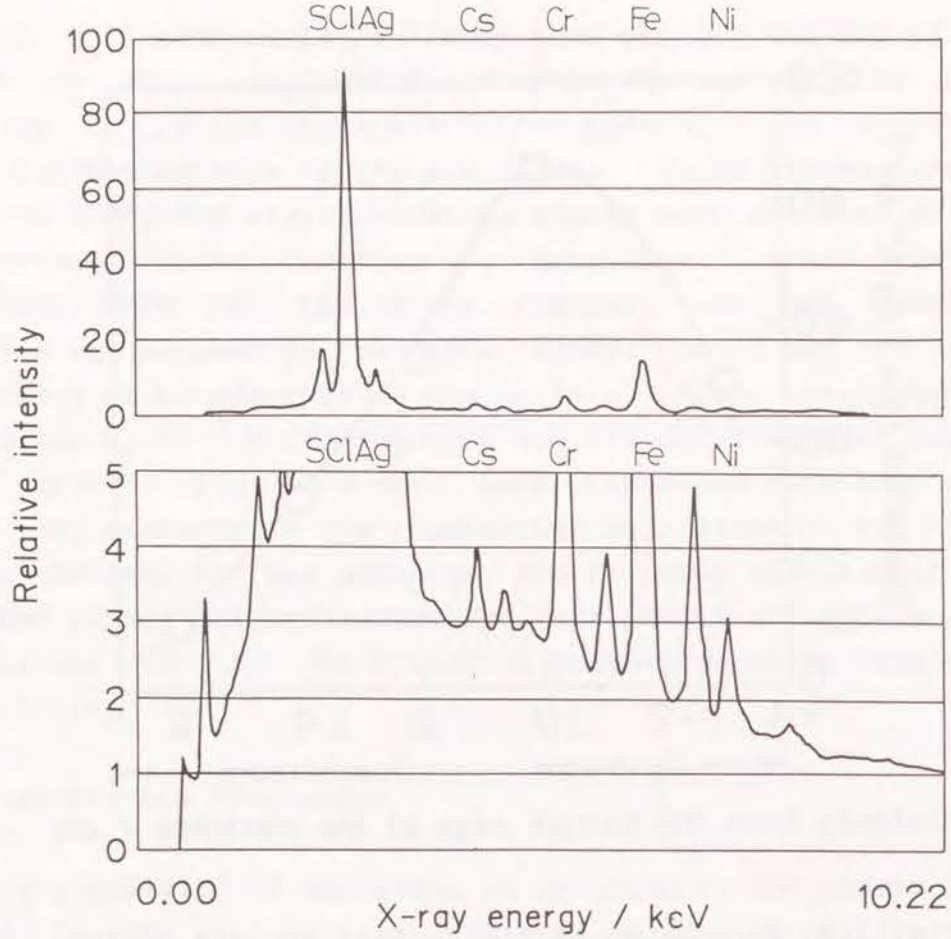

Fig. 3.10. EPMA spectra of plasma polymer containing sulfonic acid group after ion exchanging with Cs^+.
Polymerization condition:
Flow rate of TFCE: 10 cm^3(STP)/min
Flow rate of TMSA: 2 cm^3(STP)/min
RF power: 40 W
Polymerization pressure: 0.5 Torr

plasma polymer, indicating that the plasma polymer behaved as an ion exchanger. On the other hand, the plasma polymer from TFCE and TMSA introduced at the top of the glass reactor [Polymer B] did not show any ion exchange capacity in aqueous CsOH solution.

ESCA S_{2p} spectrum of the Polymer A was shown in Fig. 3.11. The peak at 169 eV can be assigned to the sulfonic acid

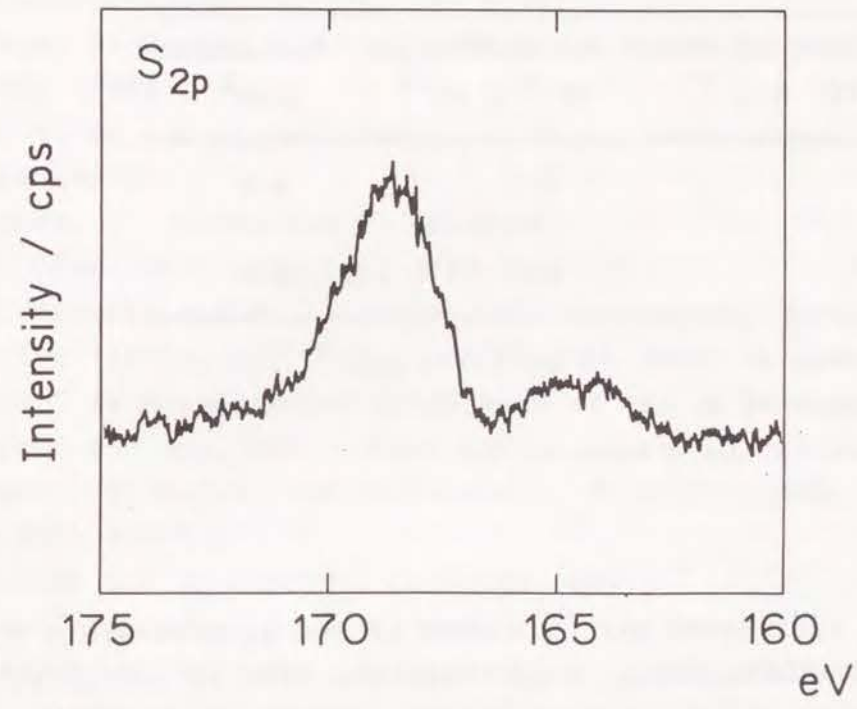

Fig. 3.11. ESCA S_{2p} spectrum of plasma polymer of Fig. 3.10.

group, while the small peak at 164 eV probably corresponds to the sulfone group [10], which was formed by the decomposition of sulfonic acid group of the TMSA during plasma polymerization process. This result indicates that the sulfonic acid group was fixed into the plasma polymer backbone of Polymer A. On the other hand, ESCA S_{2p} spectrum of the Polymer B showed only the peak at 164 eV. This fact indicate that the TMSA was decomposed in glow region.

The cross-sectional SEM figure of the Polymer A shows that the polymer film was about 1 μm thick and pinhole-free in the scale of SEM observation. The ionic conductivity of the Polymer A was estimated by an AC impedance measurement. Table 3.2 shows the ionic conductivity of the Polymer A. The mem-

Table 3.2. Ionic conductivities and membrane resistance of plasma polymers

Flow rate of TMSA/ $cm^3(STP)\ min^{-1}$	Conductivity/ $10^{-5}\ S\ cm^{-1}$	Resistance/ $\Omega\,cm^2$
2	2.5	4.0
4	5.0	2.0

Flow rate of TFCE: 10 $cm^3(STP)\ min^{-1}$
RF power: 40 W
Polymerization pressure: 0.5 Torr

brane resistance per unit area of the approximately 1 μm thick fluorinatedsulfonic acid membrane also is indicate. It is seen that the ionic conductivity of the polymer increases with an increase in the flow rate of the TMSA, since the large flow rate leads to an increase in sulfonic acid group content in the membrane. The fluorinated sulfonic acid membrane in wet condition has conductivity values greater than $10^{-5}\ S\ cm^{-1}$ at room temperature.

The ionic conductivity of the membrane is still lower than the ion-exchange membrane on the market. However, the resistance of the membrane is comparable with that of commercial available ion-exchange membrane. The membrane is adhesive toward substrates, pinhole-free, and uniform thickness. Therefore, this plasma polymerization method is promising for the preparation of practical fluorinated ion exchange membrane of cross-linked structure.

References

1. W. Paik, T. E. Springer, and S. Sriniversan, J. Electrochem. Soc., 136, 644 (1989).
2. H. Ohya, K. Emori, T. Ohto, and Y. Negishi, Denki Kagaku, 53, 462 (1985).
3. P. W. T. Lu and S. Srinivasan, J. Appl. Electrochem., 9, 269 (1979).
4. Z. Ogumi, T. Mizoe, and Z. Takehara, Bull. Chem. Soc. Jpn., 61, 4183 (1988).
5. A. B. Laconti and H. J. Marget, J. Electrochem. Soc., 118, 506 (1971).
6. "Nafion" is a registered trade mark of the Du Pont de Nemours and Co., Inc.
7. Z. Ogumi, T. Kuroe, and Z. Takehara, J. Electrochem. Soc., 132, 2601 (1985).
8. H. Yasuda and T. Hirotsu, J. Polym. Sci., Polym. Chem. Ed., 16, 229 (1978).
9. H. Yasuda, J. Macromol. Sci. Chem., A10, 383 (1976).
10. B. J. Lindberg, K. Hamrin, G. Johansson, U. Gelius, A. Fahlman, C. Nordling, and K. Siegbahn, Phys. Scr., 1, 286 (1970).

Part IV. Vapor-Phase Electrolytic Deposition

Chapter 1 Electrochemical Deposition of Oxides at Oxide/Plasma Interfaces

1.1 Introduction

The great majority of electrochemical reactions are carried out using liquid electrolytes, such as aqueous solutions, nonaqueous solutions or molten salts, although solid electrolyte also have recently gained increasing importance. Gaseous plasma also recently has been suggested as a candidate for use in electrochemical system [1,2]. Electrodeposition from the vapor phase has potential use in the preparation of thin films for semiconductors, oxide super conductors, fuel cells, etc. However, the use of plasma as a medium for conducting electrochemical investigation is difficult, since the charge carriers in plasma consist not only of ionic species, but also of electrons, and as a result, electronic conduction could occur at the interface between a plasma and a solid electrode.

The three main types of stable plasma are hot plasma, arc plasma and glow discharge plasma (also known as low-temperature of nonequilibrium plasma). the temperature of hot plasma (more than a few million degrees) is too high for the investigation of chemical reactions. Previous studies utilizing plasma in electrochemical studies have used the powered electrode in arc plasma as the site of electrochemical reaction [1,2]. However, the temperature of electrodes on which arc discharge occurs is known to become very high, making them difficult to use as stage for chemical reactions. With glow discharge plasma, while the temperature of the powered electrode is much lower, the electrode is attacked by accelerated cations, leading to emission of electrons, as well as cathode

---

Submitted for publication to J. Electrochem. Soc.

fall formation. Thus, in this study, in order to eliminate the complexities associated with using a powered electrode to conduct chemical reactions, a third electrode was introduced into the plasma as a stage for conducting electrochemical reactions. The introduction of a separate working electrode also allows the potential of the working electrode to be controlled independent of the plasma parameters. A glow discharge plasma was used in the present work because of its relatively low temperature, compared with arc-discharge plasma. Under certain conditions, the conductivity of glow discharge plasma can be as high as 10^{-3} S cm^{-1} [3]. The novel Vapor-phase Electrolytic Deposition (VED) process was demonstrated using the electrolytic deposition of an ionically-conductive oxide (yttria-stabilized zirconia, YSZ) at an oxide/plasma interface.

1.2 Theoretical Considerations

In the bulk of glow discharge plasma, charge is mainly carried by electrons, due to their high mobility (the electron temperature exceeds 10,000°C) relative to ionic species (which attain temperatures of several hundred degrees at most). The ionic species, which are generated by an electron collision and by Penning dissociation by excited species, serve to maintain macroscopic electroneutrality in the bulk plasma. However, owing to the difference in mobilities of electrons and ions, an ion sheath is formed in the interfacial region between a glow discharge plasma and a substance inserted in the plasma, and the inserted substance becomes negatively biased relative to the potential of the bulk plasma [4]. In this ion sheath, the flux of ions (mostly cations) is equal to that of the electrons.

1.2.1 Vapor Phase Electrolytic Deposition (VED)

If two electronic conductors (electrodes) are inserted into plasma and a DC bias is spanned between them, the poten-

tial drop in the ion sheath on the negatively-biased electrode increases, and an electron sheath is then formed on the positively-biased electrode [4]. The fourth electrode serves as a counter electrode to apply a DC voltage on the third electrode.

The system is shown in Fig. 4.1. The sheathes formed on the biased electrodes (Fig. 4.1a) are analogous to double layers formed on electrodes in electrolyte solutions (Fig. 4.1b), although the sheathes are much thicker than double layers. The different thickness can be attributed to differences in the numbers and mobilities of the charge carriers in the

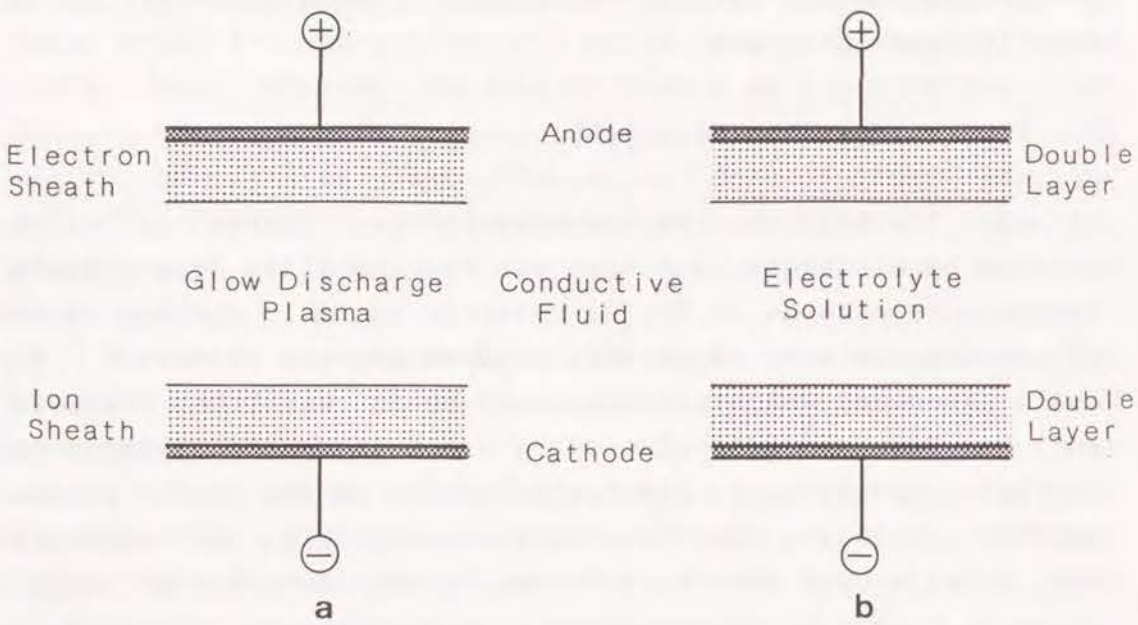

Fig. 4.1. Comparison of (a) vapor-phase electrolytic deposition system using a glow discharge plasma as the conductive medium with (b) conventional electrolyte deposition system. (The system for generation of the glow discharge plasma is not shown.)

respective system [5]. Since the density of charged species in plasma is very low due to a low ionization ratio, the plasma is comparable to a dilute electrolyte-solution system.

Cations are transported and accelerated toward the negatively biased electrode under the potential field prevailing the sheath, as is often the case with electrodes for plasma generation. When the cations have a high energy (potential or kinetic energy), they etch the electrode surface ("etching" phenomena). When their energy is low (low kinetic energy), they may react with species existing on the electrode surface to form other chemical species. When this process proceeds continuously, the charge carried by the cations to the surface must be neutralized by some reaction or process, or else charge accumulation would occur. In vapor-phase electrolytic deposition (VED), the charge carried by the cations is compensated for by transfer of electrons from the negatively-biased electrode (which is supplied with electrons from the DC power supply) to the incoming cationic species.

$$L^+ + e \longrightarrow L \qquad (1)$$

where L^+ represents the cations reaching the electrode, and L represents the electrodeposited product. Heat generation may also occur in reaction (1). This process is analogous to the electrochemical reduction of cations in an electrolyte solution system.

The electron donated by the negatively-biased electrode also may react with the neutral species in the plasma which are either in their ground state or in their excited state.

$$MA + e \longrightarrow MA^- \ (\longrightarrow M + A^-) \qquad (2)$$

where MA and MA^- represent a neutral metal compound gas in the plasma and the corresponding anion, respectively. This reaction releases anions (MA^- or A^-), and is analogous to the electrochemical reduction of neutral species in electrolyte

solutions. When reaction (1) and (2) take place on the negatively-biased electrode, a DC current flows through the DC bias circuit, and charge must be carried through the plasma, including the ion and electron sheaths.

The phenomena described above are analogous to those that are thought to occur on Langmuir probes used for plasma diagnostics [3]. However, studies using Langmuir probes have concentrated on the positively-biased probe, with the goal of obtaining information about electrons in the plasma. Furthermore, since deposition on the probe introduces ambiguities into the measurements, care is taken to prevent such deposition from occurring in studies using Langmuir probes.

There are situations in which VED will not occur. For example, if the potential of the negatively-biased electrode exceeds the work function of electrode material, electrons will be emitted from the electrode, and conduction will be almost entirely by electronic migration. Another example of a situation in which VED will not occur is if the electrodeposited product is an insulator. In such a case, the bias potential will be nullified by the insulating layer, and the electrodeposition process will cease.

1.2.2 Vapor-Phase Electrolytic Deposition of Oxides at Plasma/Oxide Interfaces

An oxide (ionic conductor)/Plasma interface is shown schematically in Fig. 4.2. While most of the discussion in the preceding section also applies to interfaces between plasma and ionic conductor, instead of reactions (1) and (2), reactions such as reactions (3) and (4) may take place between the ionic conductor (B in Fig. 4.2) and the plasma (C in Fig. 4.2):

$$bL^{+} + B^{b-} \longrightarrow L_bB \qquad (3)$$

$$MA + B^{b-} \longrightarrow MB + A^{b-} \qquad (4)$$
$$\text{or} \qquad \longrightarrow M + AB^{b-}$$

where B^{b-} represents charge-carrying ions in the ionic conductor. However, electron transfer reactions such as reactions (1) and (2) also must take place at the interface between the ionic conductor (B in Fig. 4.2) and the negatively-biased electrode in the DC circuit (A in Fig. 4.2). Reactions (3) and (4) are analogous to reactions occurring at the interface between two immiscible electrolyte solutions when the charge carriers are different in the two phases [5]. The ionic conductor/plasma interface also different from a metal/plasma interface in that a potential field can exist in the oxide layer. This potential field aids the transport of ionic species (e.g., reactant B^{b-} in Eqs. (3) and (4)) through the

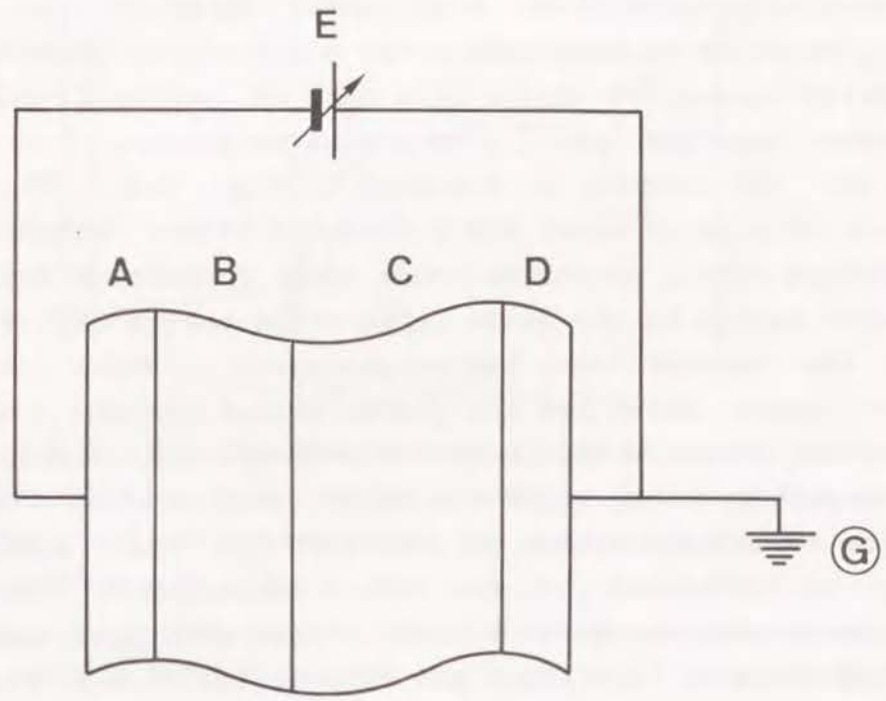

Fig. 4.2. Model of the electrode/oxide/plasma interface: A. negatively-biased electrode; B. ionically-conductive oxide; C. glow-discharge plasma; D. counter electrode for DC bias; E. DC power supply. (Electrodes for plasma generation are not shown.)

oxide layer to the oxide/plasma interface. While the plasma is not directly influenced by the potential field in the oxide layer, it is affected by the potential at the oxide/plasma interface.

The incorporation of a solid ionic conductor (e.g., oxide layer) between an electronic conductor (eg., metal) and a plasma facilitates the occurrence of VED. When an electronic conductor is used as the negatively-biased electrode, an electronic current flows through the external DC circuit (electrochemical leak current), because the leaked electrons carry most of the charge in the plasma, due to their high mobility. This electrochemical leak current makes it difficult to conduct electrochemical processes in plasmas using electronically-conductive electrodes. Thus, in the present study, we chose to demonstrate the electrolytic deposition of ionically-conductive oxide film onto an ionically-conductive substrate inserted into a glow discharge plasma.

The VED system is depicted in Fig. 4.3. The system consist of a metal anode and a porous platinum cathode, which is covered with a nonporous oxide layer conductive for O^{2-} on the side facing to the anode. The oxide-coated cathode separate the reactor into two compartments. Argon and metal halide gases, which are the plasma assist gas and the metal source for oxide deposition, respectively, are introduced into the compartment into which the oxide layer and the anode face. A glow discharge plasma is generated in this compartment. Water is introduced into the second compartment, into which the porous platinum cathode faces. When a DC bias voltage is applied between the anode and cathode (which are placed in glow discharge plasma) from the external DC supply, a potential profile like that shown in Fig 3b is formed. Due to this applied voltage, H_2O is reduced to form oxide ions and hydrogen:

$$H_2O + 2e \longrightarrow H_2 + O^{2-} \qquad (5)$$

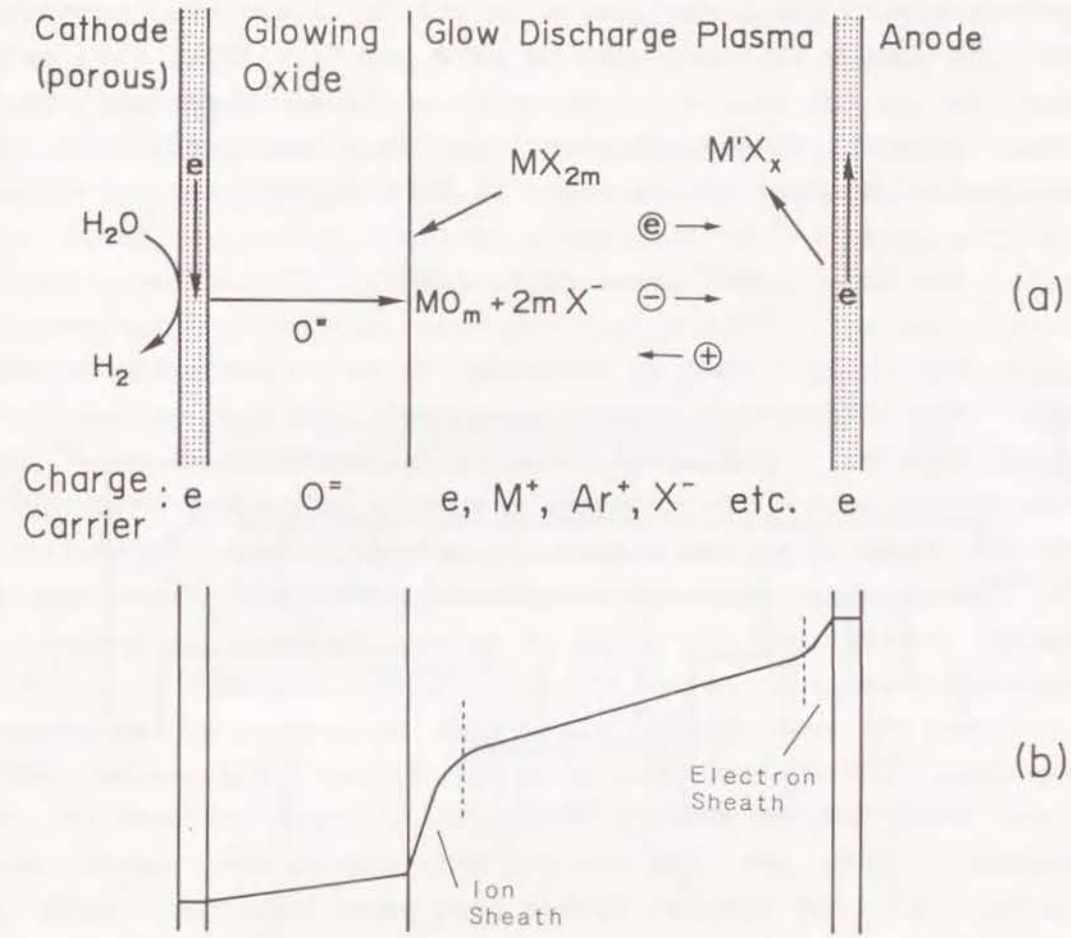

Fig. 4.3. (a) Reaction scheme of oxide growth in a system using a glow discharge plasma as the conductive medium and (b) schematic of the potential profile of the system.
MX_{2m} = source gas (metal halide) for oxide formation;
MO_m = oxide conducting for oxide anion; X = halogen;
M and M' = metals.

The oxide ions produced at the cathode migrate through the oxide layer toward the outer surface under driving force of the electric field generated by the applied DC bias. The oxide surface is negatively biased relative to the bulk plasma, due to the formation of an ion sheath. The DC bias must overcome this potential in order for oxide anions to be trans-

ported toward the oxide/plasma interface; i.e., the potential of the porous platinum must be more negative than the value due to the ion sheath on the oxide surface. When the oxide ions reach the solid/plasma interface, they react at the surface with metal halide vapor to form oxide:

$$MX_{2m} + mO^{2-} \longrightarrow MO_m + 2mX^- \qquad (6)$$

Since the oxide formed by reaction (6) is an oxide-ion conductor, the deposition process continues, and the oxide grows continuously. The X^- ions released by reaction (6) move into the plasma bulk. Electrolytic oxidation processes must occur at the anode or in the plasma, to prevent charge accumulation in the plasma. The anodic reaction may be the formation of metal halides of the anode material, halogen formation or perhaps others.

In the bulk plasma, the charge is carried by electrons, cations, and anions, including the X^- ions produced by reaction (6). In the present study, since argon was used as the plasma assist gas, the cations existing in the plasma were mainly Ar^+ but cations formed from metal halides, such as MX_{2m}^+ MX_{2m-n}^+, M^+ and others also may have been present. In the case of plasma containing (highly electronegative) halides, electron attachment to the halide also may occur [6], yielding anions like MX_{2m}^-. Although cations and anions thus formed also would contribute to conduction in the plasma bulk, their contribution to the overall conductivity would be small.

In the present study, the vapor-phase electrodeposition process was demonstrated by depositing yttria-stabilized zirconia (YSZ, an oxide-ion conductor) from YCl_3 and $ZrCl_4$, using radio-frequency (RF) plasma as the electrolyte. In this system, the reaction corresponding to reaction (6) are:

$$ZrCl_4 + 2O^{2-} \longrightarrow ZrO_2 + 4Cl^- \qquad (7)$$

and

$$2YCl_3 + 3O^{2-} \longrightarrow Y_2O_3 + 6Cl^- \qquad (8)$$

1.3 Experimental

1.3.1 Apparatus

The Apparatus used for deposition of YSZ films is schematically shown in Fig. 4.4. The reactor was constructed of two tubes, an external quartz glass tube ("5" in Fig. 4.4) and an alumina tube ("6" in Fig. 4.4). The vapor phase YSZ electrodeposition and the corresponding cathode reaction (water

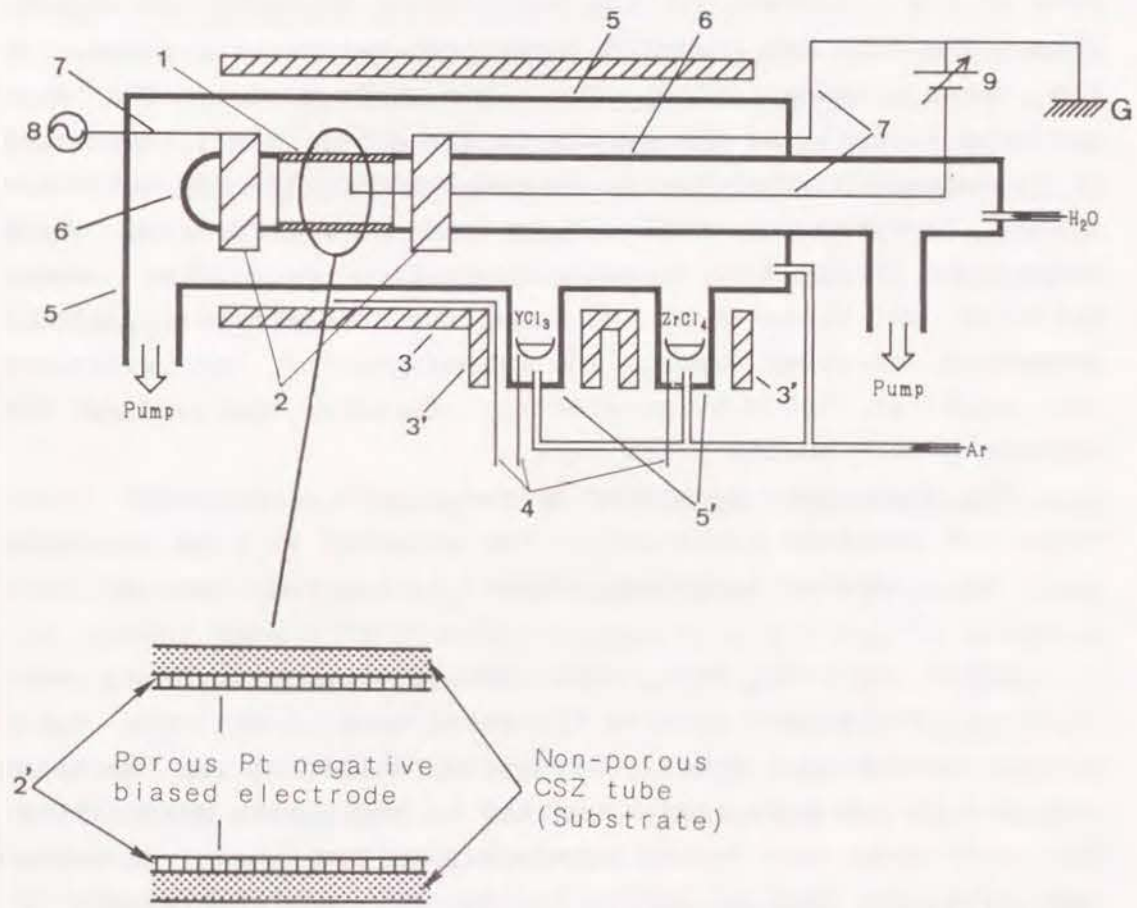

Fig. 4.4. Schematic of an apparatus for vapor phase oxide deposition. 1. CSZ substrate; 2. Pt ring electrodes; 2'. porous Pt electrode deposited on the CSZ substrate; 3. main furnace; 3'. small furnaces; 4. thermocouples; 5. quartz glass tube; 5'. side arms of quartz tube; 6. alumina tube; 7. Pt lead; 8. RF power supply; 9. DC power supply.

reduction) were conducted in separate compartments. The alumina tube formed an inner compartment where water reduction was carried out, and the space between the alumna tube and the quartz tube formed an outer compartment for vapor phase oxide electrodeposition. These two compartments were exhausted separately by two rotary pumps.

A nonporous calcia-stabilized zirconia (CSZ) tube (Nippon Kagaku Togyo Co., Ltd., 10 mm O.D., 2 mm wall thickness) was used as the substrate for the vapor-phase electrolytic deposition. The tube was inserted (cemented) between two pieces of the inner alumina tubing. The outer surface of the CSZ tube was used directly as the substrate for oxide electrodeposion. It is noteworthy that the large thickness of the CSZ substrate likely rendered any contribution from Electrochemical Vapor Deposition (EVD) [7,8] to oxide deposition negligible. Porous platinum was sintered on the inner surface for the cathodic reduction of water vapor. The temperature of the substrate was kept at 1100 °C by an electric furnace surrounding the outside of the quartz glass tube.

The plasma was generated by two platinum rings (RF electrode and grounded electrode). The grounded Pt ring was also used as a counter electrode (anode) to complete the DC bias circuit.

Anhydrous $ZrCl_4$ (Wako Pure Chemicals) and anhydrous YCl_3 (Aldrich 99.9%) was used as the metal sources for the oxide electrodeposition process. Crucibles containing the chloride were set in two side arms connected to the quartz glass tube. The side arms were heated separately by two small furnaces: the $ZrCl_4$ was kept at 280 °C, and the YCl_3 was kept at 790 °C. The resulting metal chloride vapor was carried by Ar gas (99.9%, 20 cm^3(STP) min^{-1}) and introduced into the outer compartment, over the outside surface of the CSZ substrate.

Water for the cathode reaction was supplied to the inner compartment by bubbling Ar gas (5 cm^3(STP) min^{-1}) through a thermostated humidifier kept at 30 °C.

1.3.2 Procedure for VED

The electrolysis procedure was as follows: the pressure in the outer compartment was set at 1.5 Torr. After the gas pressure had stabilized, the RF power (13.5 MHz, 100 W) was turned on, and a DC bias of 130 V was applied between the porous platinum electrode and the grounded platinum ring electrode. The deposition was carried out for 1-2 h.

13.3. Analytical Procedures

The YSZ films formed by VED were examined by SEM (Hitachi model S-51), Electron probe microanalysis (EPMA) (Horiba model EMAX-1770), ESCA (Shimadzu model ESCA-850) and X-ray diffraction (Shimadzu XD-5A). Yttrium contents in the deposited films were calculated from results of EPMA and ESCA measurements. Film thickness were determined from SEM micrographs of film cross-sections.

1.4 Results and Discussion

1.4.1 Electrolysis Using Glow-Discharge (Low-temperature) Plasma

As shown in Fig. 4.5, upon application of 130 V DC bias, the current density initially dropped from 7 mA cm^{-2} to about 2 mA cm^{-2} within 20 min, and then remained almost constant (very slow decrease with time). The low current densities, obtained despite the high applied voltage, can be attributed to the high resistance of the bulk plasma and the ion sheath formed at the oxide-plasma interface.

The high plasma resistance likely resulted from a reduction of the electron density due to the combination with electronegative species such as halogens (e.g., chlorine)[6]. Such electronic combination with substance in the plasma decreases the electron density in the plasma. The conductivity of a plasma, σ, can be approximated by Eq. (9):

$$\sigma = eNu \qquad (9)$$

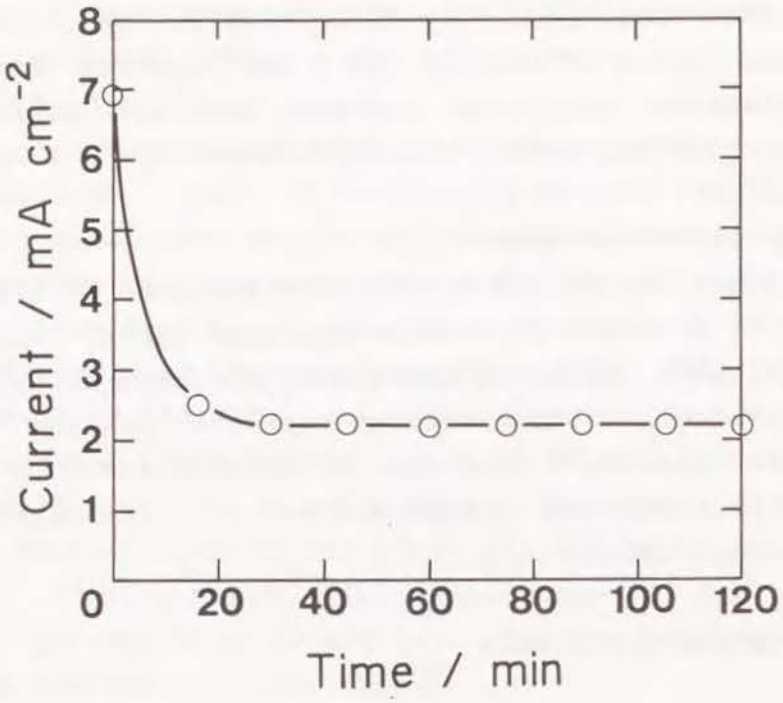

Fig. 4.5. Variation of current density with time. VED reactor conditions: pressure of the outer compartment of the reactor = 1.5 Torr; RF power = 100 W; DC voltage = 130 V; substrate temperature = 1100 °C; temperature of $ZrCl_4$ source = 280 °C; temperature of YCl_3 source = 790 °C; temperature of H_2O source = 30 °C.

where n is the electron density, u is the electron mobility and e is the electronic charge, 1.60219×10^{-19} C. According to Eq. (9), the conductivity of bulk plasma is approximately proportional to the electron density. Ionic species account for relatively little of the conductivity of plasma because of their low mobility [4]. In the discharge of electronegative gas, for example, Cl_2, BCl_3, etc., negative ions are formed by combination with slow (low kinetic energy) electrons [6,7].

The formation of negative ions is dependent on the extent and time of electron energy relaxation, and therefore on the plasma parameters, such as frequency and pressure. For plasma generated using Cl_2 gas, and the same RF frequency used in this study (13.56 MHz), the anion density has been reported to be 10 times larger than the electron density[6]. Since the plasma used in the present work was generated using electronegative gases ($ZrCl_4$ and YCl_3), significant anion formation likely occurred, resulting in a high plasma resistance.

1.4.2 Deposition of Thin YSZ Layers by VED

A YSZ layer formed after 2 h of VED at 130 V was analyzed by EPMA (elemental analysis). The EPMA spectrum for electrodeposited YSZ is shown in Fig. 4.6. The spectrum shows strong yttrium K_α and K_β peaks, while only a small calcium K_α peak (from the CSZ substrate) is visible. These results show that the CSZ substrate was covered by a yttrium-containing film. As a basis for comparison, another run was carried out under the same condition, without applying the DC bias. The yttrium peaks in the EPMA spectrum were negligible for this latter run without DC bias. These two sets of results indicate that deposition of yttrium occurred only when a DC bias was applied. Furthermore, the fact that yttrium was not deposited without a DC bias implies that deposition by Electrochemical Vapor Deposition (EVD) [8-10] was negligible, since EVD requires no DC bias. Under the conditions used in the present work, the rate-controlling step of the EVD process is electron transport in the stabilized zirconia, and thus the rate of EVD was inversely proportional to the thickness of the stabilized zirconia [11]. As a result, the large thickness of the CSZ substrate used in this study likely rendered the driving force for EVD negligible, and consequently, the Vapor-phase Electrolytic Deposition process likely occurred exclusive of any contribution from EVD.

As further confirmation of the occurrence of VED, the relative amount of yttrium deposited on the substrate were

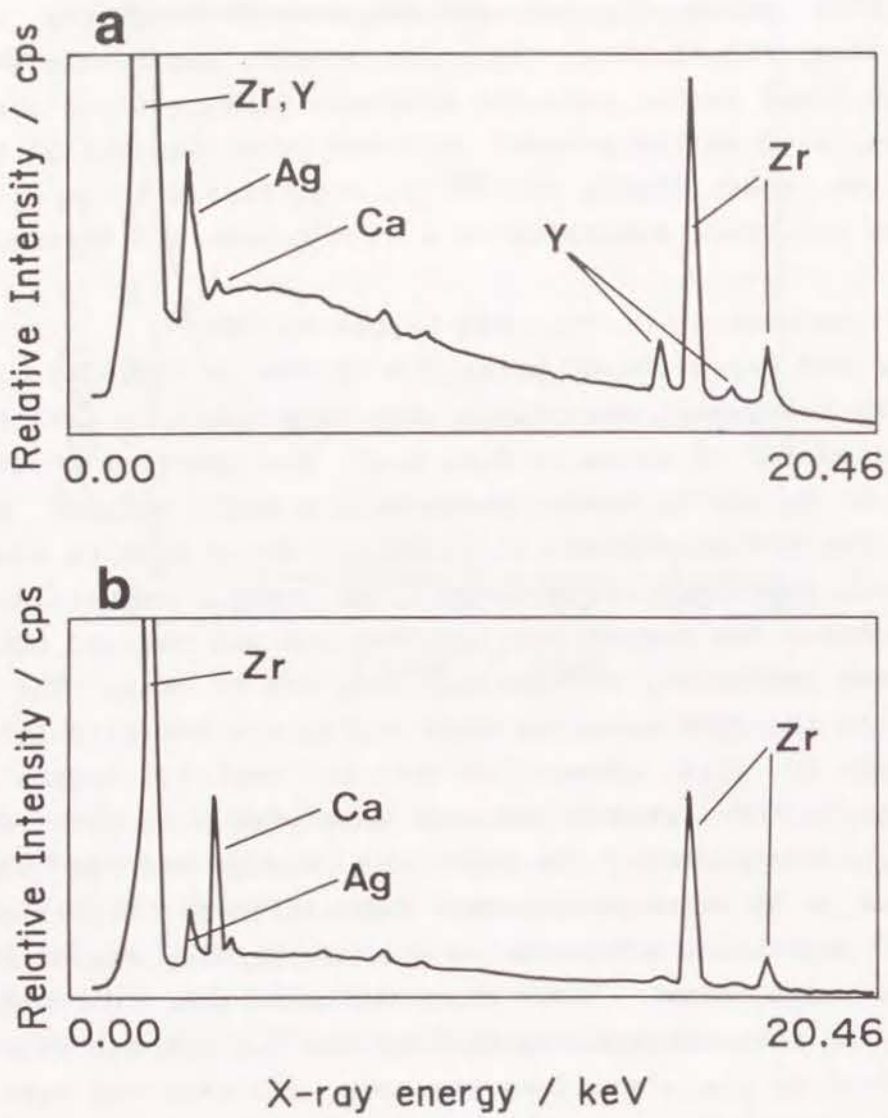

Fig. 4.6. EPMA spectra of a substrate after VED (a) with DC bias of 130 V, and (b) without DC bias.

compared with those expected from the current distribution in the reactor. Since the porous platinum electrode and the counter electrode were positioned at right angles to one another in the VED reactor, the current distribution was asymmetric, as in conventional liquid-electrolyte electrolyzers. Furthermore, since the conductivity of glow discharge plasma is much smaller than that of conventional liquid electrolytes (the conductivity of a glow discharge plasma of hydrogen has been reported as 6 mS cm^{-1} [3]), the ohmic resistance between the counter (grounded) electrode and the substrate likely was significantly higher at positions father from the counter electrode. Consequently, the current at the CSZ substrate likely decreased with increasing distance from the counter electrode. If the current flowing in the reactor corresponds to the Faradaic VED process, then the distribution in the current should have resulted in a corresponding distribution of the deposition rate; the father from the counter electrode, the slower the rate of deposition should have been [12]. Accordingly, as a measure of the deposition rate, the yttrium content of a film formed by VED was analyzed by ESCA. The average yttrium content of the half of the sample closest to the counter electrode was twice as high as that of the half of the sample farthest from the counter electrode. These results indicate that the currents flowing at the substrate corresponding to the vapor-phase electrolytic deposition of YSZ.

1.4.3 Characterization of YSZ Film

The X-ray diffraction pattern of the deposited film (Fig. 4.7) corresponds to that of cubic zirconia. However, in every peak of the X-ray diffraction pattern, a shoulder or splitting was observed. The X-ray diffraction pattern of YSZ is similar to that of CSZ, except that it shifts to a slightly lower angle [13]. Thus, the X-ray diffraction pattern of the deposited film corresponds to that expected for a thin layer if cubic YSZ on a CSZ substrate.

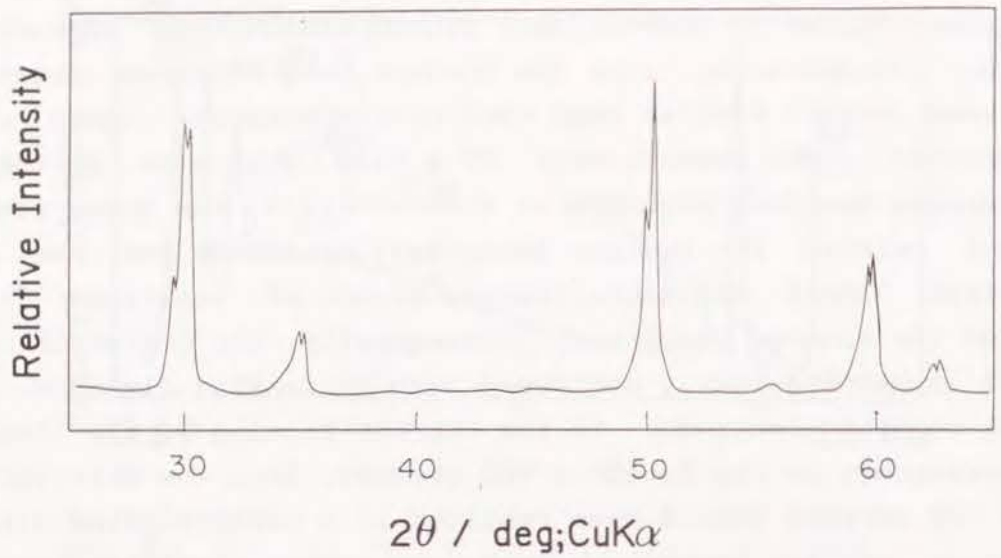

Fig. 4.7. X-ray diffraction pattern of the substrate of Fig. 4.6(a).

Depth profile of calcium and yttrium obtained by EPMA are shown in Fig. 4.8. Figure 4.8 shows that calcium was not present in the deposited film. Since the distributions of the peaks for both yttrium and calcium were fairly sharp at the film/substrate interface, it can be concluded that the YSZ film was not formed by exchange of calcium from the CSZ substrate with yttrium. This conclusion also is supported by the X-ray diffraction measurements, since the peaks of the X-ray spectrum were not broadened after VED, but were separated into two or had a shoulder.

A scanning electron micrograph of the fracture cross section of the deposited film is shown in Fig. 4.9. In the scale of SEM observation, the film is smooth and pinhole-free. A film of about 3 μm thickness was deposited on the CSZ sub-

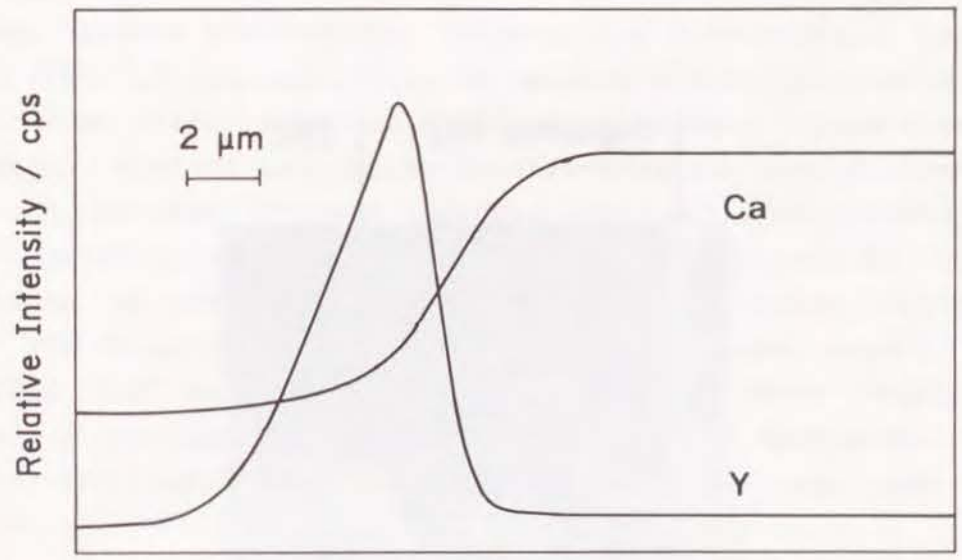

Fig. 4.8. Depth profile of Ca and Y in the YSZ film deposited on CSZ substrate.

strate. The current efficiency for the deposition was calculated from this apparent average thickness and the charge passed, assuming that the zirconium formation proceeded via a four-electron process. The current efficiency thus calculated was 40%. Two possible reasons for this low current efficiency are etching of the growing film by exposure to the plasma, and electronic conduction through the growing YSZ layer.

1.4.4 Anodic Reactions in the VED Process

Since an ionic conduction was incorporated into the DC circuit, some anodic reactions had to take place in order to form a closed circuit of external DC bias. Most probably, oxidation of the anode metal resulting in metal chloride formation, and chlorine production took place on the anode.

Fig. 4.9. SEM micrograph of fracture cross-section of YSZ thin film on CSZ.

However, since plasma is conductive toward electrons, it is conceivable that the anodic reactions could take place in the bulk plasma (e.g., chlorine formation) and/or on the counter electrode.

1.5 Conclusion

It has been confirmed that an electrolytic reaction can be made to occur at a solid electrode placed in a glow discharge plasma electrolyte. Vapor-phase Electrolytic Deposition (VED) of YSZ induced by an applied electrochemical motive force took place at the solid/plasma interface. Such electrochemical systems using glow discharge plasma are of interest not only because of their numerous potential applications, but also because of their importance to the theoretical understanding of electrified interfaces. The operating variables for VED (bias voltage and external current) are easily controlled for vapor-phase processes, such as those which are widely-investigated for the preparation of functional thin films for semiconductors, oxide superconductors, and fuel cells.

References

1. K. Kawabuchi, and S. Magari, J. Appl. Phys., 50, 6222 (1979).
2. A. K. Vijh, "Modern Aspect of Electrochemistry" Vol. 17 Chap. 1, edited by J. O'M. Bockris, B. E. Conway, and R. E. White, Plenum, New York, (1986).
3. A. von Engel, "Electric Plasmas: Their Nature and Use", Taylor & Francis, Ltd., London, (1983).
4. B. Chapman, "Glow Discharge Processes" Chap. 3, John Wiley & Sons, New York, (1980).
5. Z. Samec, V. Merecek, J. Koryta, and M. W. Khalil, J. Electrochem. Soc., 83, 393 (1977).
6. R. A. Gottscho and C. E. Gaeb, IEEE Trans. Plasma Sci., PS-14, 92 (1986).
7. G. L. Rogotf, J. M. Kramer, and R. B. Piejale, IEEE Trans. Plasma Sci., PS-14, 103 (1986).
8. A. O. Isemberg, ECS Symp., Electrode Materials, Processes Energy conversion and Storage, 77-6, 572 (1977).
9. M. F. Carolan, and J. N. Michaels, Solid State Inics,

25, 207 (1987).
10. U. B. Pal and S. C. Singhal, This Journal, 137, 2937 (1990).
11. W. H. Rhodes and R. E. Carter, J. Amer. Ceram. Soc., 49. 244 (1966).
12. J. Newman, "Electrochemical System" Chap. 21, Prentice-Hall, Englewood Cliffs, N. J. (1973).
13. Joint Committee on Power Diffraction Standards.

Chapter 2 Preparation of Thin Yttria Stabilized Zirconia Films by Vapor-Phase Electrolytic Deposition

2.1 Introduction

The fabrication of thin layers of ionically conductive oxides such as stabilized zirconia is important for the successful development of an electrolyte for various electrochemical devices, such as solid oxide fuel cells (SOFCs) [1,2], sensors [3], and steam electrolyzers [4]. The ionic conductivity of stabilized zirconia is typically 10^{-2}-10^{0} S cm^{-1} at 1000 °C. For its practical application in electrochemical devices as an electrolyte, it is necessary to decrease its practical operating resistance. Thin films will meet this requirement. It is not easy, however, to form a thin pinhole-free (gas tight) stabilized zirconia film with a high reliability, and a number of technologies have been devised and investigated to produce such thin films. These include CVD [5-7], plasma-spraying [8,9], RF-sputtering [10,11], and electrochemical vapor deposition (EVD) [12,13]. However, each of these technologies has difficulties: pore and void formation in the deposited film, slow deposition rate, damage on the substrate, and others.

In this Chapter, we report on the application of a new technology, Vapor-phase Electrolytic Deposition (VED), for the preparation of gas tight thin films of ionically conductive oxides [yttria-stabilized zirconia (YSZ)] on a porous substrate. The principle of VED, which has been described in detail in a previous chapter, is an electrolysis using low temperature plasma as a conductive fluid.

The VED technology resembles the EVD method. Figure 4.10 shows the principles of EVD and VED. In EVD (Fig. 4.10a), the driving force is dependent of the difference in the oxygen activity at the two gaseous phases which contact the growing

---

submitted for publication to J. Electrochem. Soc.

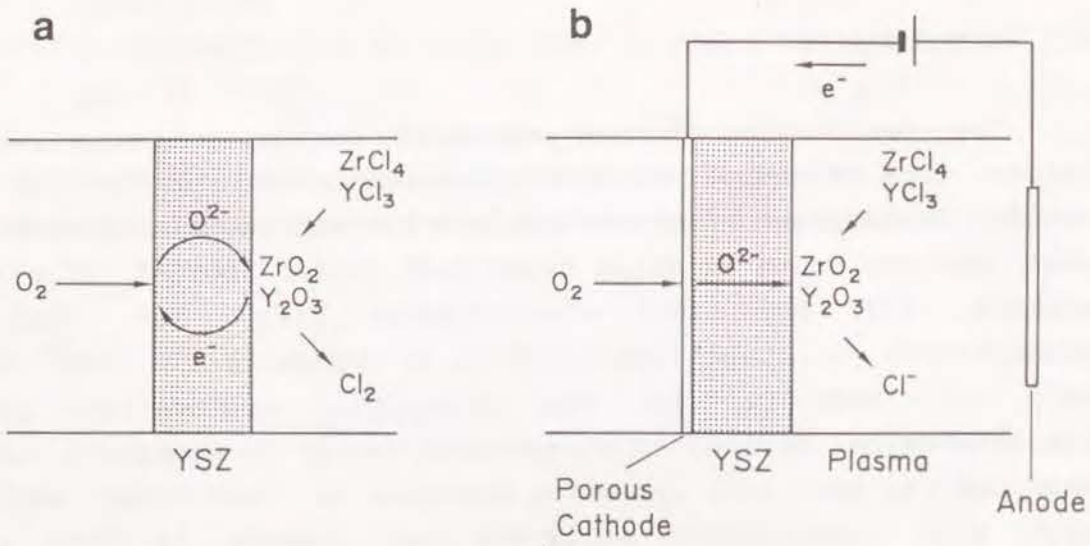

Fig. 4.10. Principles of Electrochemical Vapor Deposition (EVD) and Vapor-Phase Electrolytic Deposition (VED).

YSZ film [12,13]. This difference in oxygen activity causes a potential field , which accelerate the transport of oxide ion, O^{2-}, through the growing oxide. This movement disturbs the electro-neutrality in the oxide and leads to a charge distribution. To keep charge neutrality inside the YSZ layer, electrons must move in the reverse direction against the unfavorable potential field to maintain the oxide growth. At steady state, the magnitude of these two fluxes in opposite directions has to be equal. Therefore, in the EVD process, the deposition rate is determined by an electron flux in the oxide layer, and it is difficult to control the deposition rate.

In addition to electron and oxide ion, metal cation and positive holes may contribute to the electric conduction. In

the case of high oxygen partial pressure, positive holes (h) are produced according to Eq. (1) [14]:

$$O_2 + 2V\ddot{o} = Oo + 4h \qquad (1)$$

where $V\ddot{o}$ is the oxygen vacancy. In the system adopted in this work, the oxygen partial pressure is relatively low, so it is inferred that only a minor contribution is made by positive hole conduction. On the other hand, electron conduction appears in the low oxygen partial pressure region according to [14]:

$$2Oo = O_2 + 2V\ddot{o} + 4e \qquad (2)$$

However, since the transference number of the electron is still low under the conditions of low oxygen partial pressure, electron conduction is the rate limiting step in the EVD process [15].

Furthermore cations may contribute to the conduction in the oxide. The diffusion coefficients of metal cations are 10^5 times smaller than that of the oxide anion at 2000 °C [16]. At 1000 °C, the difference becomes much larger, so the transport of metal cation is not important.

On the other hand, in the VED (Fig. 4.10b), electron transport through the growing film is not required and the driving force for the oxide ion transport, i.e., the potential field throughout the growing oxide, is supplied by an applied DC bias voltage. Furthermore, under limited electron transport conditions, the growth rate of the oxide layer may be enhanced. The DC current density will give the magnitude of the oxide ion (O^{2-}) flux through the oxide film, which corresponds to the deposition rate of the oxide layer. If electron conduction takes place in the same direction to some extent, the current efficiency will decrease.

However, in the VED, the reactor becomes more complicated than that for EVD, and sputtering of the growing film might

take place due to high energy particles formed in the plasma.

2.2 Experimental

2.2.1 Materials

Anhydrous $ZrCl_4$ (Wako Chemical Company, extra pure grade) and anhydrous YCl_3 (Aldrich Chemical Company, extra pure grade) were used without further purification. Porous calcia-stabilized zirconia (CSZ) tube (Nippon Kagaku Togyo Co., Ltd, 3 mm thickness, 13 mm outside diameter, 3 cm length, 28% porosity) was used as a substrate. Platinum paste (Tokuriki Chemical Laboratory, No. 8103) was used for deposition of the porous platinum electrode on the porous CSZ substrate.

2.2.2 Vapor-Phase Electrolytic Deposition (VED)

The apparatus used for the VED has been described in a previous chapter. Since a porous CSZ tube deposited with a porous platinum electrode on its outer surface was used as a substrate in this report, the apparatus was slightly modified for attachment of the porous substrate. A schematic diagram of the part of apparatus for depositing YSZ film by VED is shown in Fig. 4.11. The reactor was constructed of two tubes, which were evaculated separately to prevent the source gases from mixing. The $ZrCl_4$ and YCl_3 vapors were introduced in the outer quartz tube. The source chlorides, $ZrCl_4$ and YCl_3, were heated separately at fixed temperatures of 280 °C and 820 °C, respectively. Ar gas (50 cm^3(STP)/min) was introduced in the outer quartz tube as a carrier gas of the source chlorides. Ar gas (10 cm^3(STP)/min) saturated with H_2O at 10 °C was introduced in the inner alumina tube. The reactor chamber containing the substrate, which was cemented into the middle of the alumina tube, was maintained at 1100 °C.

RF power (13.56 MHz) was applied between two inner electrodes (E1 and E2, E2 is a grounded electrode) to generate low temperature plasma. This low temperature plasma behaves as a conductive fluid. Between the grounded electrode (E2) and the

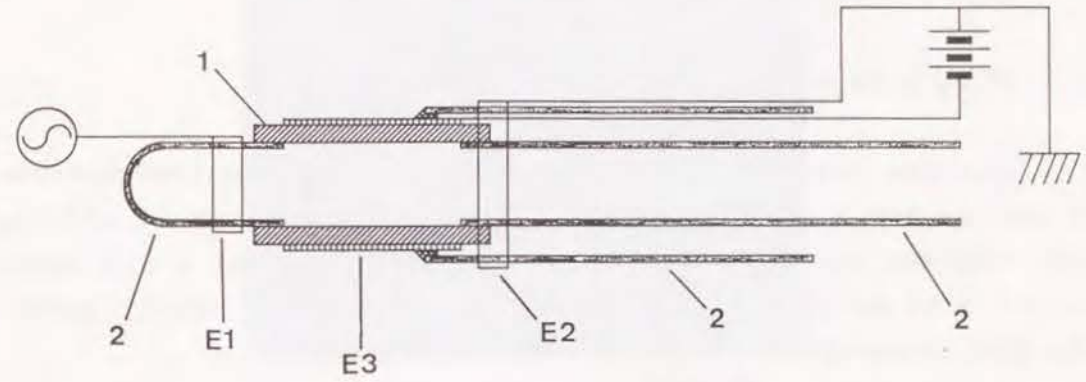

Fig. 4.11. A Schematic diagram of the pats of apparatus for VED method using porous CSZ tube as a substrate.
1, porous CSZ tube; E1, RF electrode; E2, grounded electrode (anode for DC); E3, porous platinum electrode (cathode for DC); 2, alumina tubes.

porous platinum electrode deposited on the porous CSZ substrate (E3), DC bias was applied to drive the electrochemical processes in the vapor phase. In this case, conductivity between E2 and E3 was sustained by the low temperature plasma.

When the porous platinum electrode deposited on the porous CSZ substrate was not covered with the YSZ layer, the DC current between E2 and E3 was carried mainly by electrons in the plasma; as a result, the YSZ layer did not grow. It was necessary, preceding to application of the dc voltage, to cover the porous electrode (E3) with an electronically non-conductive film for the film growth by the VED process.

As the first step, a CVD process was carried out without the application of RF power and DC bias in order to close the

pores of E3 and to cover it with a YSZ layer. In the CVD process, $ZrCl_4$ and YCl_3 were directly contacted with H_2O, reacting (Eq. 3 and 4) to form YSZ film:

$$ZrCl_4 + 2H_2O = ZrO_2 + 4HCl \quad (3)$$

$$YCl_3 + 3H_2O = Y_2O_3 + 6HCl \quad (4)$$

For the next step, RF power of 100 W was supplied between E1 and E2 and a DC bias of 65 V was applied between E2 and E3. The VED was carried out under these conditions at a pressure of 2.5 Torr in the outer compartment in order to easily generate low temperature plasma.

2.2.3 Measuring techniques

The ionic conductivities of the YSZ films were determined from AC impedance measurements carried out using a vector impedance meter. A thin layer of platinum was deposited on the YSZ thin film in order to carry out AC impedance measurements. The surface and fracture cross-section of the YSZ film were observed by scanning electron microscope (Hitachi S-51).

X-ray diffraction measurements were performed with a Shimadzu model XD-5A.

2.3 Results and Discussion

2.3.1 Preparation of YSZ thin film by CVD process

The CVD process was carried out at various pressures in the outer compartment, without RF power and DC bias. The pressure in the outer compartment was changed and the surface of the porous platinum electrode (E3) was examined by SEM.

Figure 4.12 shows scanning electron micrographs of the surface of (a) the porous CSZ substrate deposited with the porous platinum electrode and (b) the product after 2 h at 2 Torr in the outer compartment. Observation of the micrograph of Fig. 4.12(b) reveals that the surface is still porous and

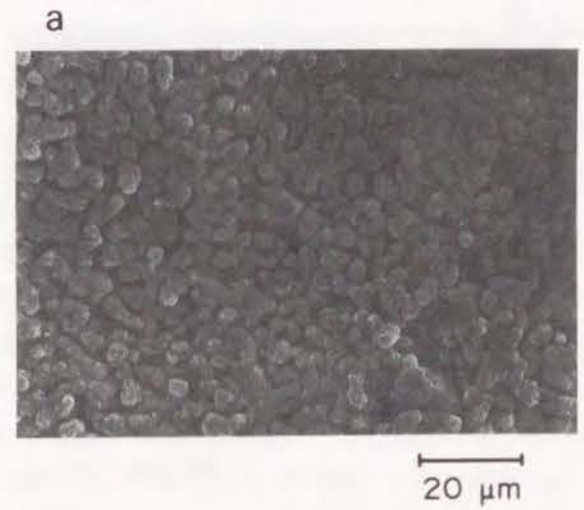

Fig. 4.12. Scanning electron micrographs of surface of (a) porous CSZ substrate deposited with platinum and (b) the substrate after CVD process at 2 Torr in outer compartment for 2 h.

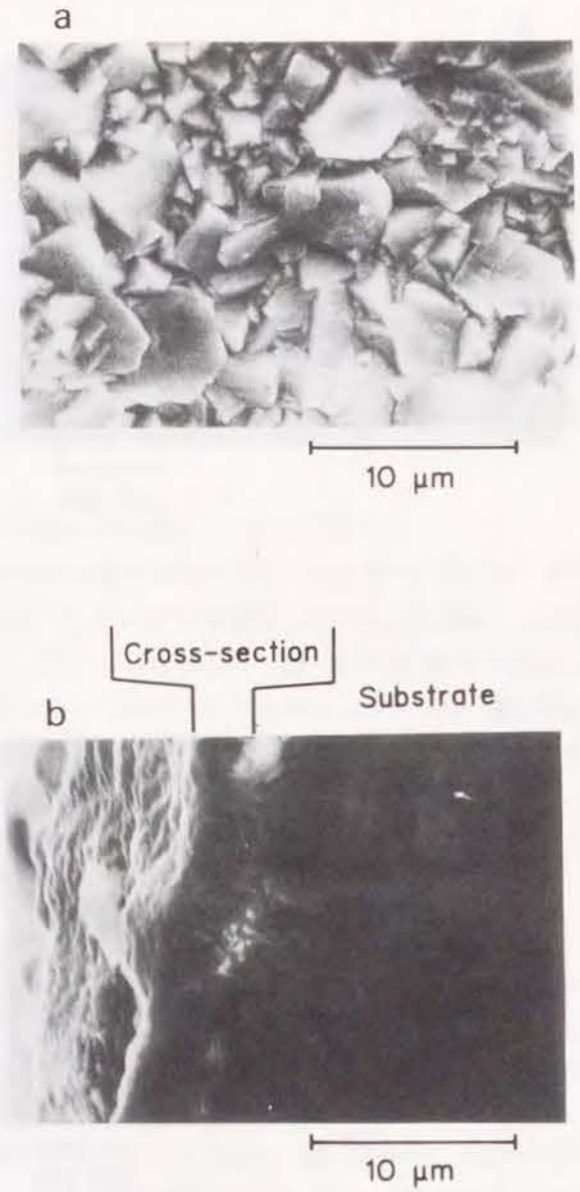

Fig. 4.13. Scanning electron micrographs of (a) surface and (b) fracture cross-section of porous CSZ substrate deposited with platinum after CVD process at 5 Torr in outer compartment for 2 h.

that the base porous platinum electrode was not covered completely by YSZ. In the lower range of pressure (below 1.5 Torr) CVD product was not observed.

In the CVD process, the pressure difference on either side of the substrate is very important. When the inner pressure of the substrate was very high, no deposition of porous film was obtained. It is necessary to keep the pressure difference to almost zero in the CVD process.

Fig. 4.13 shows the scanning electron micrographs of the surface and fracture cross-section of YSZ film prepared by the CVD method after 2 h at 5 torr in the outer compartment. Under these conditions, the pressure difference between the inner and outer side of the porous substrate was small and a YSZ film was deposited on the outer surface of the substrate, because H_2O diffuses in the pores of the substrate faster than chloride [13]. In the $ZrCl_4$-YCl_3-H_2O system under atmospheric pressure using quartz glass as substrates, YSZ films prepared by CVD have an orientation in which the (100) plane is parallel to the surface of the substrate [6]. From the micrographical view of the surface, the crystal did not show any preferential orientation and the Pt electrode was covered well by the YSZ layer. This was also confirmed by X-ray diffraction.

Without a DC bias, deposition by an EVD process had to take part in the film growth. Since the film thickness was about 3 µm, therefore, the deposition rate of the YSZ film by CVD-EVD process was 1.5 µm h^{-1} under the operating conditions used.

2.3.2 Preparation of thin YSZ film by VED process

YSZ films were prepared using the VED method. First, the Pt electrode was covered with a YSZ film by a CVD-EVD process at 5 Torr in the outer compartment as described above. Next DC voltage was applied between electrodes E2 and E3 and the YSZ film grown using VED under RF plasma generation at 100 W. For this step the pressure was reduced to 2.5 Torr because the RF plasma was not stable at 5 Torr.

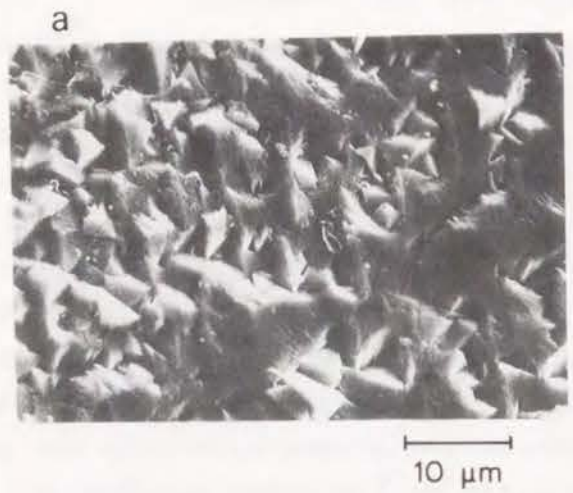

Fig. 4.14. Scanning electron micrographs of (a) surface and (b) fracture cross-section of porous CSZ substrate deposited with platinum after VED process (Zr X-ray Line).

Scanning electron micrographs of the YSZ film deposited by successive CVD-EVD (1 h) and VED (1.5 h) processes are shown in Fig. 4.14. The surface morphology was not very different from those obtained using CVD-EVD process. However, it appears that the surface of Fig. 4.14 is smoother than that of Fig. 4.13. The grain size was about 5 μm. From the cross-sectional view, the film thickness was shown to be about 12 μm. Therefore, the deposition rate by the VED process was 7 μm h^{-1}. As described above, the deposition rate of YSZ film using CVD-EVD under these conditions was 1.5 μm h^{-1}. These facts indicate that the deposition rate using VED is about 4 times faster than that obtained using CVD-EVD under the present conditions.

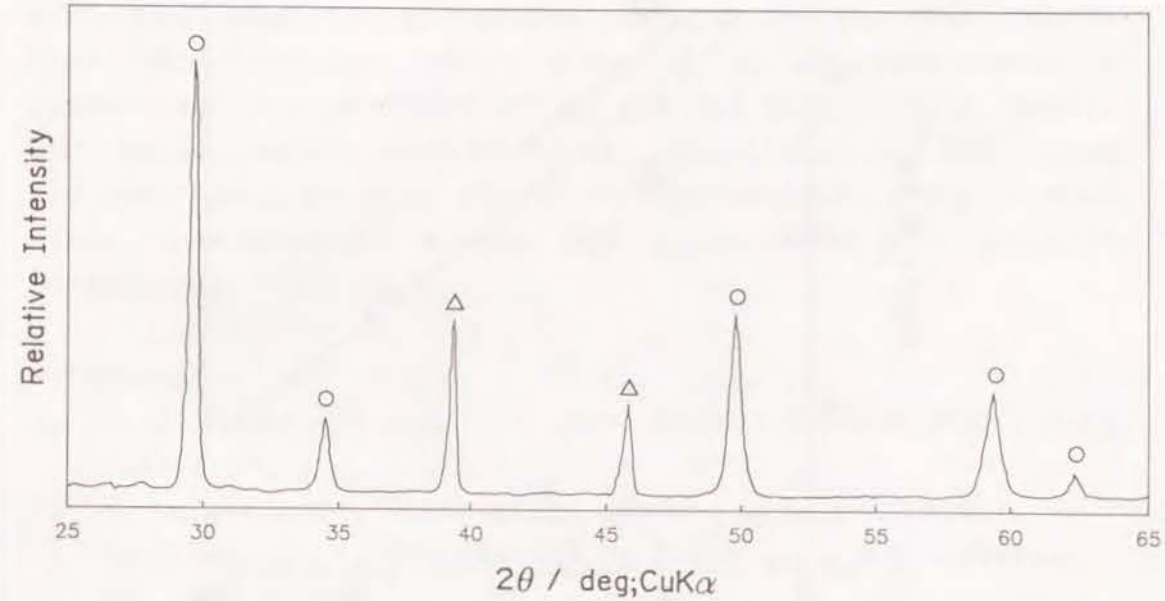

Fig. 4.15. X-ray diffraction of porous CSZ substrate deposited with platinum after VED process.
○: stabilized zirconia
△: platinum

Fig. 4.15 shows the X-ray diffraction pattern of the deposited film. The X-ray diffraction pattern of cubic zirconia and Pt porous electrode were identified. Due to the large thickness of the porous platinum layer (about 30 μm), the X-ray diffraction peak of the porous CSZ substrate tube was not detected. This indicates that the thin film prepared by the VED method is yttria-stabilized zirconia. Furthermore, ESCA spectra showed that the YSZ contained about 7-9% Y_2O_3.

Fig. 4.16 shows plots of the conductivity of the YSZ film against temperature, for (a), a film prepared by the VED method, and (b) for a sintered YSZ pellet (b) [17]. The

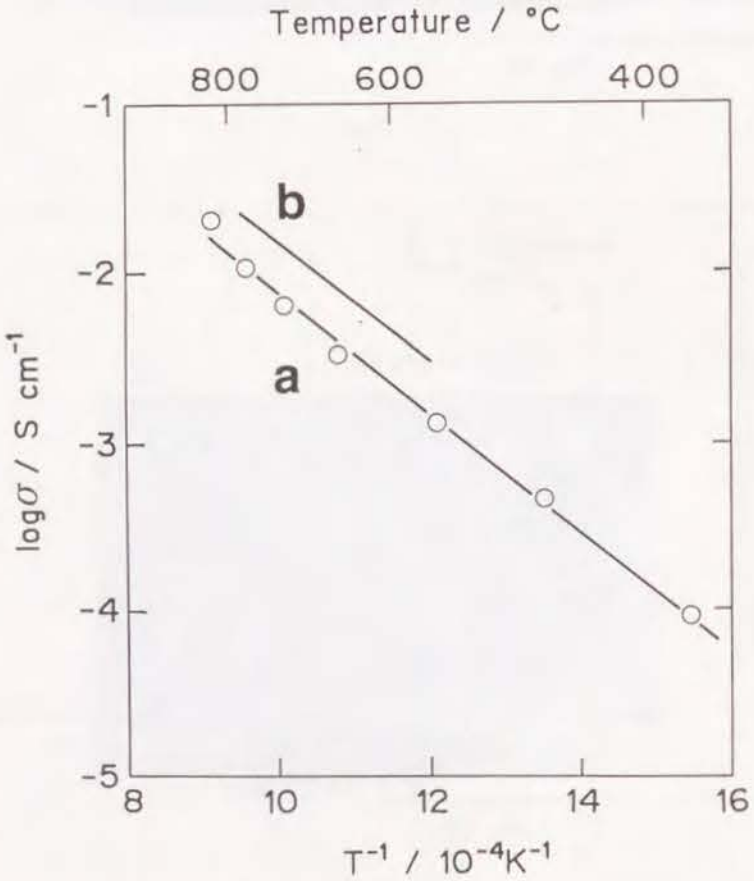

Fig. 4.16. Temperature dependence of conductivity of YSZ film.
a: YSZ thin film prepared by VED method,
b: YSZ (7 mol% Y_2O_3) by Ref. 17.

conductivities were calculated from the ohmic resistance without correcting for the ohmic drop at the electrode and of the lead wire. The conductivity values were very close to those of the sintered pellet. From the slope of the plot, the activation energy was calculated to be 19.3 kcal/mol.

Gas (Ar) leak was examined by applying a pressure difference of 500 mm H_2O between the inside and outside the YSZ thin film. No gas leakage was detected using our equipment, which has an estimated detection limit 10^{-12}-10^{-13} m^2 s^{-1} Pa^{-1}. This indicates that the YSZ thin film was pinhole-free.

2.4 Conclusion

The VED method was found to be capable of preparing thin YSZ films. The deposited films were pinhole-free and exhibited good electrochemical characteristics. The deposition rate was low, but is expected to be accelerated by optimizing the operating conditions and the reactor design. VED is a promising method for the preparation of YSZ films, and this technique also should be applicable to other systems where the products during the preparation are ionically conductive.

References

1. N. J. Maskalick and C. C. Sun, J. Electrochem. Soc., 118, 1386 (1971).
2. A. O. Isenberg, Solid State Ionics, 3/4, 431 (1981).
3. Y. Miyahara, K. Tsukada and H. Miyagi, J. Appl. Phys., 63, 2431 (1988).
4. E. J. L. Schouler, M. Kleitz, E. Forest, E. Fernandez, and P. Fabry, Solid State Ionics, 5, 559 (1981).
5. J. Minet, F. Langlais and R. Naslain, J. Less-Common Metals, 132, 273 (1987).
6. H. Yamane and T. Hirai, J. Crystal Growth, 94, 880 (1989).
7. Y. Takahashi, T. Kawae, M. Nasu, J. Crystal Growth,

74, 409 (1986).
8. G. Chiodelli, A. Magistris, M. Scagliotti, and F. Parmigiani, J. Material Science, 23, 1159 (1988).
9. M. Scagliotti, F. Parmigiani, G. Samoggia, G. Lanzi, and D. Richon, J. Material Science, 23, 3764 (1988).
10. A. Negishi, K. Nozaki and T. Ozawa, Solid State Ionics, 3/4, 443 (1981).
11. N. Nakagawa, H. Yoshioka, C. Kuroda and M. Ishida, Solid State Ionics, 35, 249 (1989).
12. I. O. Isemberg, ECS Symp. Electrode Materials, Processes Energy Conver. Storage, 77-6, 572, 1977.
13. M. F. Carolan and J. N. Michaels, Solid State Ionics, 25, 207 (1987).
14. M. Jayaratna, M. Yoshimura, and S. Sohmiya, J. Material Sci., 22, 2011 (1987).
15. U. B. Pal and S. C. Singhal, Proceeding of the First International Symposium on SOFC, 89-11, 41, 1989.
16. W. H. Rhodes and R. E. Carter, J. Am. Ceram. Soc., 49, 244 (1966).
17. J. M. Dixon, L. D. Lagrange, U. Merten, C. F. Miller and J. T. Porter, J. Electrochem. Soc., 110, 276 (1963).

Publication List

Part of this thesis have been published on the following journals;

(1) A New Ultra-thin Film of Solid Polymer Electrolyte Prepared by Plasma Polymerization.
Z. Ogumi, Y. Uchimoto, and Z. Takehara,
Chemistry Letters, 1811 (1988).

(2) Thin All-Solid-State Lithium Batteries Utilizing Solid Polymer Electrolyte Prepared by Plasma Polymerization.
Z. Ogumi, Y. Uchimoto, Z. Takehara, and Y. Kanamori,
J. Electrochem. Soc., 135, 2649 (1988).

(3) Hybrid Film of Plasma Polymer Formed From Octamethyl-cyclotetrasiloxane, Poly(propylene oxide), and Lithium Perchlorate.
Z. Ogumi, Y. Uchimoto, and Z. Takehara,
J. Electrochem. Soc., 136, 625 (1989).

(4) A Novel Thin Film of a Solid Polymer Electrolyte composed of Plasma-Polymerized Tris(2-methoxyethoxy)vinylsilane-$LiClO_4$ Hybrid.
Z. Ogumi, Y. Uchimoto, and Z. Takehara,
J. Chem. Soc., Chem. Commun., 358 (1989).

(5) Enhancement of Proton Selectivity of Cation Exchange Membrane by Plasma Modification.
Z. Ogumi, Y. Uchimoto, M. Tsujikawa, and Z. Takehara,
J. Electrochem. Soc., 136, 1247 (1989).

(6) Plasma-Parameter-Dependent Characteristics of Solid Polymer Electrolytes Composed of Plasma-Polymerized Tris(2-methoxyethoxy)vinylsilane-Lithium Perchlorate Hybrids.
Y. Uchimoto, Z. Ogumi, and Z. Takehara,
Solid State Ionics, 35, 417 (1989).

(7) Preparation of Ultra-thin Solid-state Lithium Batteries utilizing a Plasma-polymerized Solid Polymer Electrolyte.
Z. Ogumi, Y. Uchimoto, Z. Takehara, and Y. Kanamori,
J. Chem. Soc., Chem. Commun., 1673 (1989).

(8) All-Solid-State Lithium Batteries.
Z. Ogumi, Y. Uchimoto, and Z. Takehara,
J. Power Sources, 26, 457 (1989).

(9) Preparation and Characterization of Ultrathin Films Having Fixed Sulfonic Acid Groups with One Mobile Species.
Z. Ogumi, Y. Uchimoto, Z. Takehara, and F.R. Foulkes,
J. Electrochem. Soc., 137, 29 (1990).

(10) Preparation and Characterization of Solid Polymer Electrolyte Composed of Plasma-Polymerized Tris-(2-methoxyethoxy)vinylsilane-$LiClO_4$ Complex.
Y. Uchimoto, Z. Ogumi, Z. Takehara, and F.R. Foulkes,
J. Electrochem. Soc., 137, 35 (1990).

(11) A Novel Thin Film of Anion Exchanger Prepared by Plasma Polymerization.
Z. Ogumi, Y. Uchimoto, M. Tsujikawa, and Z. Takehara,
Chemistry Letters, 1990, 513 (1990).

(12) H^+ Ion Perm-Selective Membrane from Nafion for Redox-Flow Battery.
Z. Ogumi, Y. Uchimoto, M. Tsujikawa, Z. Takehara, and F.R. Foulkes,
J. Electrochem. Soc., 137, 1430 (1990).

(13) A New Ultra-thin Fluorinated Cation-Exchange Film Prepared by Plasma Polymerization.
Z. Ogumi, Y. Uchimoto, and Z. Takehara,
J. Electrochem. Soc., 137, 3319 (1990).

(14) Preparation and Characterization of Solid Polymer Electrolyte Having Fixed Carboxylic Acid Groups with Single Mobile Species.
Y. Uchimoto, Z. Ogumi, and Z. Takehara,
Solid State Ionics, 40/41, 624 (1990).

(15) Thin Film Solid-State Lithium Batteries Prepared by Consecutive Vapor-Phase Processes.
Z. Takehara, Z. Ogumi, Y. Uchimoto, and Y. Kanamori,
Submitted for publication to J. Electrochem. Soc.

(16) Electrochemical Deposition of Oxides at Oxide/Plasma Interfaces.
Z. Ogumi, Y. Tsuji, Y. Uchimoto, and Z. Takehara,
Submitted for publication to J. Electrochem. Soc.

(17) Preparation of Thin Yttria Stabilized Zirconia Films by Vapor-Phase Electrolytic Deposition.
Z. Ogumi, Y. Tsuji, Y. Uchimoto, and Z. Takehara,
Submitted for publication to J. Electrochem. Soc.